

Vision, cortical maps and neuronal plasticity in Bassoon and PSD-95 mutant mice.

Dissertation

for the award of the degree

“Doctor rerum naturalium”

of the Georg-August-Universität Göttingen

within the doctoral program Sensory and Motor Neuroscience

of the Göttingen Graduate School for Neurosciences, Biophysics, and Molecular
Biosciences (GGNB)

of the Georg-August University School of Science (GAUSS)

submitted by

Bianka Götze

from Lichtenstein/Sachsen, Germany

Göttingen 2013

Examination board:

Prof. Dr. Siegrid Löwel (First Reviewer)

Systems Neuroscience Group
Johann-Friedrich-Blumenbach-Institut für Zoologie und Anthropologie
Bernstein Focus for Neurotechnology
Georg-August-Universität, Göttingen

Prof. Dr. Tobias Moser (Second Reviewer)

Abteilung Hals-Nasen-Ohrenheilkunde
Universitätsmedizin Göttingen

Dr. Oliver Schlüter

Molekulare Neurobiologie
European Neuroscience Institute, Göttingen

Prof. Dr. André Fiala

Molekulare Neurobiologie des Verhaltens
Johann-Friedrich-Blumenbach-Institut für Zoologie und Anthropologie
Georg-August-Universität, Göttingen

Prof. Dr. Tim Gollisch

Abteilung Augenheilkunde
Universitätsmedizin Göttingen

Prof. Dr. Andreas Stumpner

Zelluläre Neurobiologie
Johann-Friedrich-Blumenbach-Institut für Zoologie und Anthropologie
Georg-August-Universität, Göttingen

Declaration of originality:

I hereby declare that this doctoral thesis is my own work and has been written independently, with no other sources and aids than quoted within texts, references and acknowledgements.

Göttingen, 26th February 2013

.....

Bianka Götze

Table of contents

Abstract	3
1. Introduction.....	5
1.1 Visual pathway.....	5
1.2 Ocular dominance	7
1.3 Neuronal plasticity	9
1.4 Synapses	15
1.4.1 Chemical synapses.....	15
1.4.2 The presynaptic protein Bassoon	17
1.4.3 The postsynaptic protein PSD-95	23
1.5 Aims.....	27
2. Materials and methods	28
2.1 Animals	28
2.1.1 Bassoon	28
2.1.2 PSD-95	28
2.2 Monocular deprivation	29
2.3 Treatment with diazepam	29
2.4 Quantification of visual capabilities.....	30
2.4.1 Virtual-reality optomotor system.....	30
2.4.2 Visual water task.....	32
2.5 Surgical preparations for optical imaging	33
2.6 Optical imaging of intrinsic signals	34
2.7 Visual stimuli.....	35
2.8 Data Analysis.....	37
2.8.1 Maximum response and map quality	37
2.8.2 Ocular dominance index	39
2.9 Immunohistochemistry	40
2.9.1 Parvalbumin (PV), the potassium voltage-gated channel Kv3.1b and brain derived neurotrophic factor (BDNF)	40
2.9.2 Microscopy and analyses	42
2.10 Chemicals.....	45
2.11 Solutions	47

2.12 Statistical analyses	48
3.A Results of Bassoon mutant mice	49
3.1 Visual acuity	49
3.1.1 Virtual-reality optomotor system	49
3.1.2 Visual water task	51
3.2 Contrast sensitivity	51
3.3 Temporal resolution	53
3.4 Development of visual function	54
3.4.1 Visual acuity	54
3.4.2 Contrast sensitivity	57
3.5 Enhancement of vision after monocular deprivation	59
3.5.1 Visual acuity	59
3.5.2 Contrast sensitivity	61
3.6 Optical imaging of intrinsic signals	65
3.6.1 Maximum response and map scatter	65
3.6.2 Visual acuity and contrast sensitivity	73
3.6.3 Ocular dominance index	77
3.7 Immunohistochemistry	89
3.7.1 Parvalbumin (PV)	89
3.7.2 Kv3.1b	92
3.7.3 Brain-derived neurotropic factor (BDNF)	93
3.B Results of PSD-95 KO mice	96
3.8 Visual acuity	96
3.8.1 Virtual-reality optomotor system	96
3.8.2 Visual water task	97
3.9 Contrast sensitivity	98
3.10 Enhancement of vision after monocular deprivation	99
3.10.1 Visual acuity	99
3.10.2 Contrast sensitivity	102
3.11 Optical imaging of intrinsic signals	107
3.11.1 Maximum response and map scatter	107
3.11.2 Ocular dominance	111
4. Discussion	126
4.1 Robust visual performance of Bsn ^{-/-} mice	126

4.2 Impaired OD plasticity in adult Bsn ^{-/-} mice	130
4.3 Impaired interocular plasticity in Bsn ^{-/-} mice.....	134
4.4 Normal visual capabilities of PSD-95 KO mice	134
4.5 Juvenile-like OD plasticity for life in PSD-95 KO mice	136
4.6 Similar interocular plasticity in PSD-95 KO mice	138
5. References	140
6. Abbreviations	153
Acknowledgements	157
Curriculum Vitae.....	158

Abstract

Bassoon mutant mice (Bsn^{-/-}) display a striking loss of synaptic ribbons in photoreceptor terminals, which impairs signal transduction through the retina (Altrock *et al.*, 2003; Specht *et al.*, 2007). Therefore we assessed vision in these mice behaviorally with the virtual-reality optomotor system (Prusky *et al.*, 2004) and the visual water task (Prusky *et al.*, 2000). In addition, we performed *in vivo* optical imaging of intrinsic signals (Kalatsky and Stryker, 2003). Our behavioral tests revealed that visual acuity, contrast sensitivity, and temporal resolution were significantly reduced in mutants compared to littermate controls, whereas the time course of visual development was not altered in Bsn^{-/-} mice compared to their littermates. Optical imaging of visual cortical activity revealed no differences between Bsn^{-/-} and Bsn^{+/+} mice, both magnitude of visual responses and quality of retinotopic maps were similar, which we interpret as evidence for the presence of homeostatic mechanisms (Turrigiano and Nelson, 2004). In short, these results show that decent visual performance can be achieved in spite of impaired signal transfer at photoreceptor ribbon synapses.

Since Bsn^{-/-} mice have a modified excitation-inhibition-balance and inhibition plays a major role in ocular dominance (OD) plasticity (Hensch *et al.*, 1998), we studied whether Bsn^{-/-} mice display modified OD plasticity and/or interocular plasticity, in which monocular deprivation (MD) leads to enhanced optokinetic responses selectively through the open eye (Prusky *et al.*, 2006). In order to achieve this we i) visualized cortical activity maps in the visual cortex (V1) of both Bsn^{+/+} and Bsn^{-/-} juvenile mice after four days and in adult mice after seven days of MD using optical imaging of intrinsic signals, and ii) measured visual acuity and contrast sensitivity of the open eye in the virtual-reality optomotor system for both groups. While there was a significant change in the OD after MD in juvenile Bsn^{-/-} mice, OD plasticity was absent in adults in contrast to their wild-type littermates. In juvenile and adult Bsn^{-/-} mice sensory improvement was significantly reduced compared to Bsn^{+/+} littermates.

It was previously shown that adult Bsn^{-/-} mice display an increased number of parvalbumin positive interneurons in the striatum (Ghiglieri *et al.*, 2009) and increased inhibition could be one explanation for the absent OD plasticity of our adult Bsn^{-/-} mice, therefore we performed immunohistochemistry for parvalbumin in the visual cortex. We observed that

the number of parvalbumin positive interneurons was increased in the visual cortex of Bsn^{-/-} mice. The reduced plasticity is most likely due to morphological changes like the increased number of inhibitory parvalbumin positive neurons based on the mutation of Bassoon as well as to alterations due to the increasing frequency of epileptiform seizures (Altrock *et al.*, 2003; Ghiglieri *et al.*, 2009). Taken together, our data indicate that there is loss of OD plasticity after MD in adult Bsn^{-/-} mice and impairment in interocular plasticity after MD in juvenile as well as adult Bsn^{-/-} mice.

To test the role of the postsynaptic density protein 95 (PSD-95) in V1 of mice, we visualized activity of V1 using intrinsic signal optical imaging in PSD-95 knockout (KO) mice (Yao *et al.*, 2004), in wild-type (WT) as well as in heterozygous littermates (HZ) and also measured their visual performance behaviorally. Both visual acuity and contrast sensitivity were only slightly but significantly reduced in PSD-95 KO mice compared to WT/HZ mice. Additionally, we found that optical imaging of V1 activity revealed that the magnitude of optical responses of elevation maps was significantly higher in PSD-95 KO mice, whereas the magnitude of the optical responses of azimuth maps as well as map scatter of both elevation and azimuth maps were indistinguishable from WT/HZ mice.

PSD-95 KO animals show altered hippocampal synaptic plasticity (enhanced long-term potentiation, diminished long-term depression), most likely due to an increased number of AMPA silent synapses, which was also observed in V1 by our cooperating group (Schlüter, Huang from the ENI, Germany) (Huang *et al.*, 2012). Therefore we tested OD plasticity and interocular plasticity of PSD-95 KO mice and their WT/HZ littermates. During MD the improvement of visual acuity and contrast sensitivity through the open eye was similar in PSD-95 KO and WT/HZ mice showing preserved interocular plasticity. In PSD-95 KO mice, juvenile OD plasticity was found in animals of all ages (until postnatal day 507) at which the OD shift was mediated by a significant decrease of deprived-eye responses in V1. To test if the prolonged phase of plasticity of PSD-95 KO mice was due to reduced intracortical inhibition (Hensch *et al.*, 1998) we treated mice during seven days of MD with a dosage of diazepam that reliably blocked OD plasticity in adult WT/HZ mice. Interestingly, diazepam treatment did neither reduce OD plasticity nor interocular plasticity in PSD-95 KO mice compared to WT/HZ mice. Taken together, these results clearly suggest that the preserved OD plasticity in older mice is not caused by changes in the inhibitory tone but rather by a higher number of AMPA silent synapses.

1. Introduction

1.1 Visual pathway

Vision is one of the most important senses that allow many animals, including mammals, to experience their environment. The visual impressions are processed by a highly complex network, which ranges from the retina *via* the thalamus to the visual cortex of the brain (Figure 1).

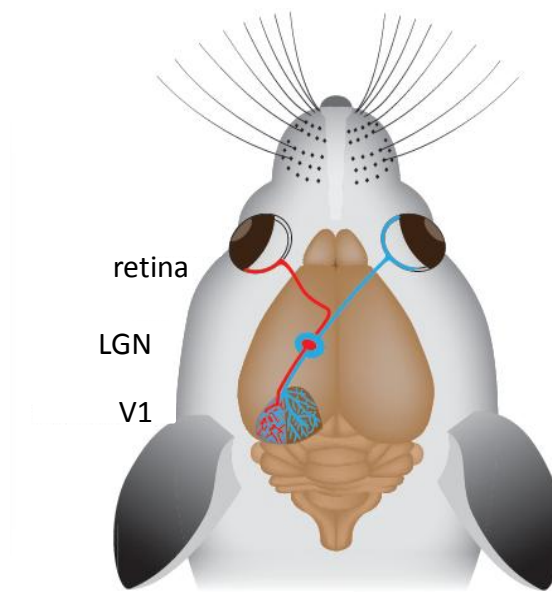


Figure 1: Visual system of mice (Figure modified from Levelt and Hübener, 2012). The majority of retinal ganglion cell axons (blue) (~ 80 %) cross the midline and terminate in the lateral geniculate nucleus (LGN) of the contralateral hemisphere. Only a small number of axons from the temporal retina (red) (~ 20 %) do not cross at the optic chiasm, they terminate in the ipsilateral LGN. The LGN receives inputs from both eyes. The major (medial) part of the primary visual cortex (V1) receives only input from the contralateral retina (blue), whereas the smaller (lateral) third of V1 also receives ipsilateral input (red).

The retina of vertebrates, a light-sensitive tissue, is a part of the central nervous system (CNS) involved in processing and transmission of visual information. The retina contains special types of photoreceptor cells, rods and cones (Figure 2 A), which are able to absorb photons and convert light energy into electrochemical signals.

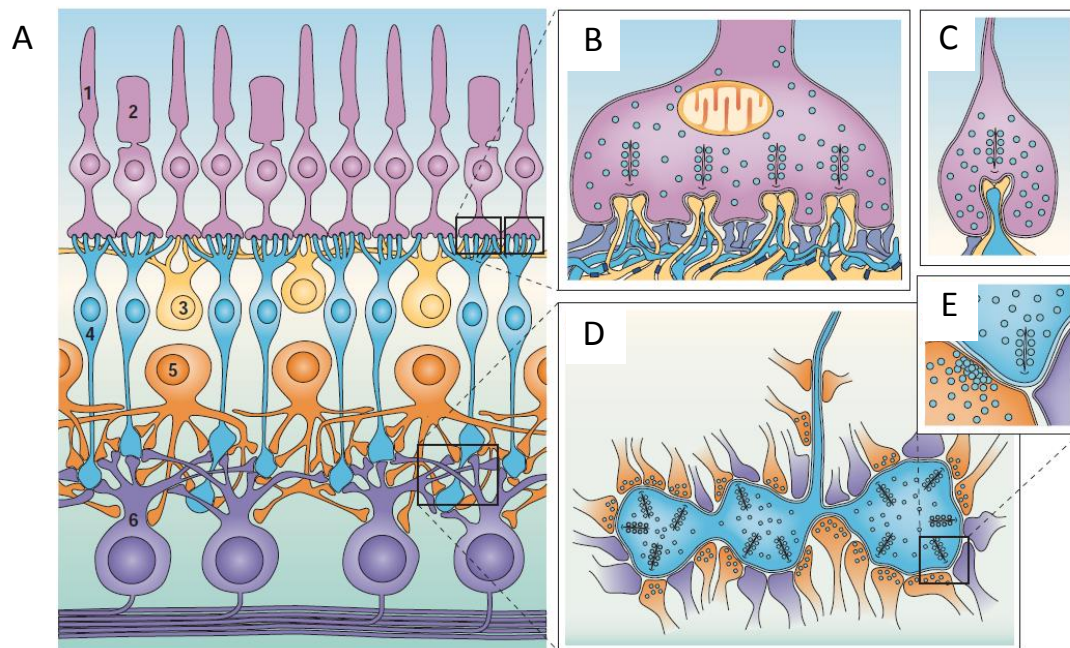


Figure 2: Scheme of the mammalian retina (Figure from Wässle, 2004). (A) Shown are six classes of neurons in the retina: rods (1), cones (2), horizontal cells (3), bipolar cells (4), amacrine cells (5) and retinal ganglion cells (6). (B) A synaptic terminal of a cone. Four presynaptic ribbons are apposed to the invaginating dendrites of bipolar cells (blue) and horizontal cells (yellow). (C) A synaptic terminal of a rod. Only one presynaptic ribbon is apposed to the invaginating axons of bipolar cells (blue) and horizontal cells (yellow). (D) The axon terminal of one bipolar cell (blue) contains up to 50 presynaptic ribbons, and connects to postsynaptic amacrine cell processes (orange) and retinal ganglion cell dendrites (purple). (E) Enlarged view of a bipolar cell ribbon synapse (blue) with an amacrine cell process (orange) and a retinal ganglion cell dendrite (purple). The amacrine cell provides in this connection a feedback synapse onto the bipolar cell.

The transmission of signals to the adjacent bipolar and horizontal cells (Figure 2 A) is achieved by chemical synapses that release the neurotransmitter glutamate constantly in the dark. Tonic release of neurotransmitters requires a special type of chemical synapses, the ribbon synapse (Figure 2 B-E). The ribbon synapse is characterized by a unique mechanism of vesicle fusion, which promotes rapid neurotransmitter release and signal transmission. The ribbon is a functionally and structurally specialized type of the presynaptic active zone and is surrounded by hundreds of synaptic vesicles (Rao-Mirotznik *et al.*, 1995). These ribbon synapses are found in the retina in rods, cones, and bipolar cells (Sjöstrand, 1958; Kidd, 1962; Missotten, 1965; Dowling and Boycott, 1966) (Figure 2 B-E). Adjacent neurons are amacrine and retinal ganglion cells (Figure 2 A). The electrochemical signals in the retina are transferred from photoreceptors *via* bipolar cells to the retinal ganglion cells. This vertical signal processing is completed by additional horizontal connections, promoting lateral inhibition through horizontal and amacrine cells (Figure 2 A). These cells play a decisive role in modulation and adjustment of sensitivity in photopic and scotopic vision

(Wässle, 2004). The signal transfer to the central nervous system is mediated by axons of the retinal ganglion cells that form the optic nerve (*nervus opticus*). Nasal retinal fibers of the optic nerve cross to the contralateral hemisphere of the brain in the optic chiasm (*chiasma opticum*) whereas temporal fibers project ipsilaterally (Figure 1).

In wild-type mice (*Mus musculus*; C57BL/6) around 80 % of these afferent fibers project to the contralateral hemisphere (Dräger, 1975; Mangini and Pearlman, 1980; Wagor *et al.*, 1980; Metin *et al.*, 1988). A projection from both eyes into the same part of the cortex is essential for stereoscopic vision. From the optic chiasm retinal axons form the optic tract (*tractus opticus*) and project as to the lateral geniculate nucleus (LGN) (*corpus geniculatum laterale*) (Figure 1), which is a nucleus of the thalamus. The LGN receives input from retinal axons from the contralateral and the ipsilateral eye (Nicholls *et al.*, 2001). Afferent fibers from the LGN form the optic radiation (*radiatio optica*) and project to layer IV of the primary visual cortex (V1) (Figure 1). The visual projection (*e.g.* in mammals) is retinotopic, which means that adjacent neurons in the retina project to adjacent areas in the LGN and in the visual cortex (Dräger, 1978; Dräger and Olsen, 1980).

Additionally there are also afferent connections from the retina to the accessory optic system (AOS) that is formed by three terminal nuclei, which receive direct visual information from the retina *via* the accessory optic tract (Giolli *et al.*, 2006). In addition to the retinal input, there are afferent connections to the nucleus of the optic tract and the LGN (Giolli *et al.*, 2006). The efferent connections of the AOS are targeting brainstem and other regions in support of visual-oculomotor events such as the optokinetic reflex.

1.2 Ocular dominance

Since in mice 80 % of all axons of the optic nerve cross at the optic chiasm to the contralateral hemisphere, the visual cortex is dominated by input from the contralateral eye (ocular dominance) (Figure 3). Therefore, in mice only the central 30° - 40° of the upper part of each visual hemifield is seen by both retinae (Dräger, 1975; Wagor *et al.*, 1980; Gordon and Stryker, 1996).

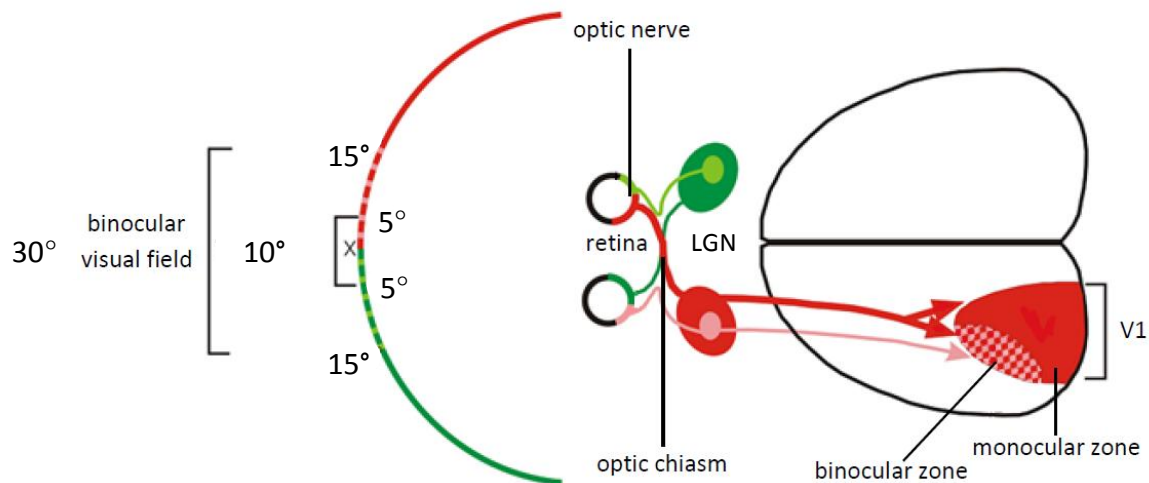


Figure 3: Visual pathway of mice (Figure modified from Gordon and Stryker, 1996). The central 30° - 40° of the upper part of each visual hemifield is seen by both retinae. Most of the axons (80 %) cross in the optic chiasm and project to the contralateral hemisphere and terminate at the lateral geniculate nucleus (LGN) (red). Axons from the LGN project to the primary visual cortex (V1). The remaining axons (20 %), which do not cross in the optic chiasm, project into the visual cortex of the ipsilateral hemisphere (pink). The optic radiation contains information from both eyes and converges in the lateral one third of V1, in the binocular zone.

Inputs from both eyes converge in the primary visual cortex (Hubel and Wiesel, 1963), where competitive interactions determine which eye will dominate both anatomically and functionally (Sugiyama *et al.*, 2008). The relative responsiveness of neurons to the same visual stimulus of either the right or the left eye is called ocular dominance (OD) (Baxter, 1959; Bertuzzi *et al.*, 1999; Tagawa *et al.*, 2005; Hofer *et al.*, 2006b). Ocular dominance was classified by Hubel and Wiesel (Hubel and Wiesel, 1962) based on a 7-point-scale, in which a unit with an ocular dominance rating of 1 is completely dominated by the contralateral eye, 4 is driven equally by both eyes, and 7 is completely dominated by the ipsilateral eye. In the binocular zone of V1, all neurons respond to visual stimuli presented to either eye, but the activation by input from the contralateral eye is two to three times stronger in mice than the activation by input from the ipsilateral eye (Dräger, 1978; Gordon and Stryker, 1996; Sawtell *et al.*, 2003; Frenkel and Bear, 2004). To compute the ocular dominance index (ODI) (Cang *et al.*, 2005a), the binocularly activated region can be pixelwise calculated as $(C-I)/(C+I)$ where C and I representing the raw response magnitude of each pixel to contralateral and ipsilateral eyes, respectively.

1.3 Neuronal plasticity

The mammalian visual system is not fully mature at birth and undergoes through anatomical and physiological changes and further develops after eye-opening and during the first weeks of postnatal life (Hubel, 1963; Hubel and Wiesel, 1963; Blakemore and Van Sluyters, 1975; Dobson and Teller, 1978; Fregnac and Imbert, 1978; Albus and Wolf, 1984; Boothe *et al.*, 1985; Fagiolini *et al.*, 1994). Numerous studies about ocular dominance investigate cortical processing and neuronal plasticity in the brain of mammals for over 50 years (Wiesel and Hubel, 1963a; Dräger, 1978; Yazaki-Sugiyama *et al.*, 2009). OD plasticity in the visual cortex of mammals is a distinguished paradigm to study how visual experience and visual deprivation modifies connections in the brain (Wiesel and Hubel, 1963a; Hubel and Wiesel, 1964; Dräger, 1978; Hofer *et al.*, 2006a, b; Mrsic-Flogel *et al.*, 2007; Blais *et al.*, 2008).

In the visual system, unbalanced sensory experience, like monocular vision, leads to a rapid shift of neuronal responses in favor of the open eye (ocular dominance) accompanied by a rapid increase and decrease of dendritic spines in the visual cortex and later on by thalamocortical axon rearrangement (Wiesel and Hubel, 1963a; Antonini *et al.*, 1999; Hensch, 2005; Sugiyama *et al.*, 2008). Experience-dependent cortical plasticity has intensely been studied by Wiesel and Hubel (Hubel and Wiesel, 1963, 1970), at which monocular deprivation (MD), induces a rapid ocular dominance shift in V1 responses toward the nondeprived eye. They did behavioral experiments and single unit recordings of action potentials of cortical neurons *in vivo* in cats (Wiesel and Hubel, 1963b; Hubel and Wiesel, 1970). Rodents, especially mice, have emerged as a valuable model because of their close genetic and physiological similarities to humans. The genome of mice is easy to manipulate (*e.g.* knockout of a gene and therefore a certain protein) and therefore rendering them eligible for analyzing molecular mechanisms of OD plasticity. Along with single unit recordings in mice (Antonini *et al.*, 1999; Hofer *et al.*, 2006b), additional methods like visual evoked potentials, where electrical potentials are recorded from cortical neurons (Sawtell *et al.*, 2003) and *in vivo* optical imaging of intrinsic signals (Hofer *et al.*, 2006b; Heimel *et al.*, 2007; Kaneko *et al.*, 2008a; Sato and Stryker, 2008) were used to study the plasticity of the visual system in mice.

The selectivity of visual cortical neurons for orientation and direction of visual stimuli in juvenile mice is poor (Wang *et al.*, 2010; Rochefort *et al.*, 2011; Espinosa and Stryker, 2012).

In juvenile as well as in adult mice, neurons selective for different visual stimulus orientations or for different eyes are scattered randomly throughout V1 (Ohki *et al.*, 2005). Binocular vision and ocular dominance are rudimentary in immature animals (Espinosa and Stryker, 2012). The gradual development of these functional properties during subsequent postnatal periods depends on visual experience. During these periods, visual neurons develop their adult functional properties in response to visual stimuli. Hence, an extensive anatomical reorganization of connections in the visual system takes place.

Several days after eye-opening (around postnatal day (P) 14) in mice, neuronal connections in CNS experience a critical period when the visual system is highly plastic (Gordon and Stryker, 1996; Hensch *et al.*, 1998; Hensch, 2005). Both anatomical and functional development depends at least in part on visual experience during this early phase of plasticity. In the visual cortex of mice, this critical period starts at P21 and ends around P35 (Gordon and Stryker, 1996) and is important to match the right and left eye receptive fields of V1 binocular neurons (Wang *et al.*, 2010). In the present study this type of plasticity is termed “juvenile plasticity”.

In the first stage of the critical period OD plasticity in mice, about three days of MD causes a large reduction of the response to the deprived eye measured with visual evoked potential recordings (Sawtell *et al.*, 2003; Hofer *et al.*, 2006b) and imaging of intrinsic signals (Hofer *et al.*, 2006b; Kaneko *et al.*, 2008b; Sato and Stryker, 2008) (Figure 4) and a resulting shift in ocular dominance, with no change in open-eye responses.

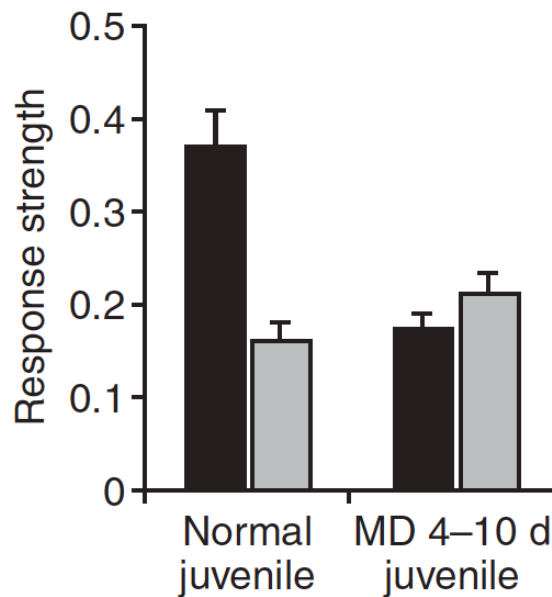


Figure 4: Four days of monocular deprivation (MD) induce an ocular dominance (OD) shift during critical period in the visual cortex of mice (Figure from Hofer *et al.*, 2006b). Response strength values, measured with optical imaging of intrinsic signals, after visual stimulation of the contralateral (black) and the ipsilateral eye (gray). In normal animals without MD there is a strong OD of the contralateral eye whereas after four to ten days of MD there is an OD shift toward the ipsilateral eye. This shift is caused by a decrease of the deprived-eye response strength.

In the second stage, five to six days of MD caused a large increase in the response to the open eye, along with a slight increase in deprived-eye responses measured with imaging of intrinsic signals, completing the shift in ocular dominance (Kaneko *et al.*, 2008b). These second stage findings were not found by others (Hofer *et al.*, 2006b; Sato and Stryker, 2008), who also performed imaging of intrinsic signals in mice, but found no significant increase in the response to the open eye.

The mechanisms underlying the first stage of critical period OD plasticity, the decrease in deprived-eye responses, is hypothesized to be the result of a loss of deprived-eye connections (pruning) or of a depression in their synaptic efficacy (Espinosa and Stryker, 2012). Concordant with this idea, genetically deleting (Roberts *et al.*, 1998) or blocking N-methyl-D-aspartate receptors (NMDARs) (Bear *et al.*, 1990), manipulations that block long-term depression (LTD), prevented a shift in ocular dominance. An alternative mechanism is spike-timing-dependent plasticity that shares a dependence on NMDARs and calcium signaling and might be a potential explanation of changes during MD (Yao and Dan, 2005) to either decrease or increase the strength of connections. Calcium influx through

NMDARs triggers downstream effectors like protein kinases and phosphatases, which are hypothesized to regulate OD plasticity by controlling phosphorylation of substrates which are important for neuronal excitability, synaptic transmission, and morphological stabilization: cAMP-dependent protein kinase A (PKA) (Fischer *et al.*, 2004; Rao *et al.*, 2004) and extracellular-signal-regulated kinase (ERK) (Di Cristo *et al.*, 2001), and the α -calcium/calmodulin-dependent protein kinase II (α CaMKII) (Taha *et al.*, 2002). In all cases, promoting the activation of the phosphatase or preventing the activation of the kinases also prevented reduction of deprived-eye responses (Espinosa and Stryker, 2012). Since in Arc-knockout mice, three days of MD failed to reduce deprived-eye responses (McCurry *et al.*, 2010), the activity-dependent immediate early gene Arc is also a potential mediator of protein-synthesis-dependent plasticity. Arc gene expression and efficient Arc translation are dependent on NMDAR activation (Steward and Worley, 2001). Another activity-dependent immediate early gene, serine protease tissue plasminogen activator (tPA), increases during monocular deprivation in the visual cortex and targets many downstream effectors including growth factors, extracellular-matrix proteins, and membrane receptors. Critical period OD plasticity was impaired in tPA-knockout mice but could be rescued by exogenous tPA (Mataga *et al.*, 2002).

It is not completely clear yet to what extent the changes in visual responses during OD plasticity are the product of anatomical changes in the circuits, such as loss of synapses of the deprived eye, or changes in synaptic efficacy, such as LTD, within a stable anatomical circuit (Espinosa and Stryker, 2012). It may be likely that there are parallel and independent processes regulating anatomical change and synaptic efficacy.

The later increase in open-eye responses involves both homeostatic and long-term potentiation (LTP)-like mechanisms.

The mechanisms underlying the second stage of critical period OD plasticity, the increase of open-eye responses, indicate that homeostatic as well as LTP-like mechanisms are important for the second stage of OD plasticity (Espinosa and Stryker, 2012). Mice deficient for tumor necrosis factor- α (TNF α), a protein necessary for homeostatic scaling of excitatory and inhibitory synapses (Stellwagen and Malenka, 2006) showed no subsequent increase of responses of the open eye measured by intrinsic signal imaging and similar results were found in wild-type mice after blockade TNF receptors in the cortex (Kaneko *et al.*, 2008b).

After this critical period during development, the capacity for experience-dependent changes in the brain is substantially reduced through several mechanisms, there is evidence for several involved mechanisms: neuromodulatory desensitization, persistently potent inhibition, and an increase in structural factors that inhibit neurite remodeling (Bear and Singer, 1986; Celio *et al.*, 1998; Fagiolini and Hensch, 2000; Pizzorusso *et al.*, 2002; Sawtell *et al.*, 2003; McGee *et al.*, 2005; Hofer *et al.*, 2006b; Atwal *et al.*, 2008; Lehmann and Löwel, 2008; Maya Vetencourt *et al.*, 2008; Hofer *et al.*, 2009; Harauzov *et al.*, 2010; Morishita *et al.*, 2010; Espinosa and Stryker, 2012; Lehmann *et al.*, 2012). However, it has been shown that plasticity mechanisms in the brain are different in juvenile and adult mice (Sato and Stryker, 2008). Several studies showed that ocular dominance plasticity can be observed in adult mice until P110 (Lehmann and Löwel, 2008), although a longer monocular deprivation period of seven days was needed to induce an OD shift (Sawtell *et al.*, 2003; Tagawa *et al.*, 2005; Hofer *et al.*, 2006b; Lehmann and Löwel, 2008; Sato and Stryker, 2008) (Figure 5). In the present study this type of plasticity is termed “adult plasticity”.

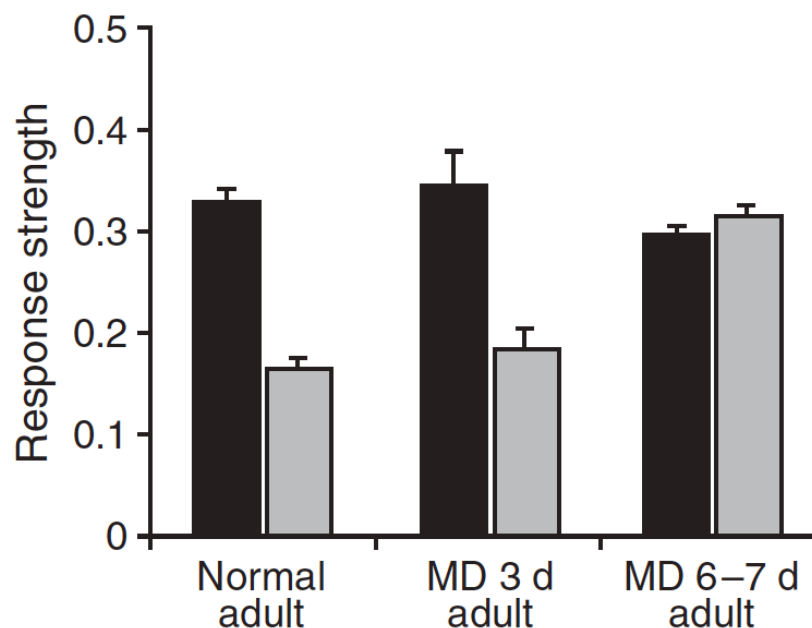


Figure 5: Seven, but not three, days of monocular deprivation (MD) induce an ocular dominance (OD) shift during adulthood in the visual cortex of mice (Figure from Hofer *et al.*, 2006b). Response strength values, measured with optical imaging of intrinsic signals, after visual stimulation of the contralateral (black) and the ipsilateral eye (gray). In normal animals without MD there is a strong OD of the contralateral eye, even after three days of MD. But there is an OD shift toward the ipsilateral eye after seven days of MD. This shift is caused by an increase of the nondeprived-eye response strength.

The OD shift in adult mice induced by contralateral MD is mediated by an increase in open-eye responses (Sawtell *et al.*, 2003; Hofer *et al.*, 2006b; Sato and Stryker, 2008) (Figure 5).

Little is known about the mechanisms of adult OD plasticity in mouse and the extent to which they are similar to those that operate in the critical period. Some mechanisms are shared, *e.g.* the dependence on calcium signaling through NMDARs (Espinosa and Stryker, 2012). Adult mice treated with competitive NMDAR antagonists, or mice lacking NR1 (NMDAR subunit) within the cortex, exhibited no adult OD plasticity (Sawtell *et al.*, 2003; Sato and Stryker, 2008). Adult α CaMKII;T286A mice, which have a point mutation that prevents autophosphorylation of α CaMKII, showed a lack in strengthening of responses of the open eye after MD (Ranson *et al.*, 2012).

In mice younger than 110 days, monocular deprivation of seven days induced a significant ocular dominance shift measured by optical imaging of intrinsic signals, but this shift was absent in animals of 110 - 230 days, even after a longer period of deprivation with 14 days (Lehmann and Löwel, 2008; Greifzu *et al.*, 2012), which discloses that there is an age-dependent OD plasticity in the visual cortex of mice. They concluded that ocular dominance plasticity in mice displays an extended phase after the critical period with reduced susceptibility for monocular deprivation that is absent in animals older than 110 days, which fits to the idea that plasticity does not terminate abruptly but rather declines gradually with age (Banks *et al.*, 1975; Olson and Freeman, 1980; Lehmann and Löwel, 2008).

There are also several studies about interocular plasticity of vision in mice in which eyelid suture termed monocular deprivation (MD) leads to an enhancement of the optokinetic response through the nondeprived eye (Prusky *et al.*, 2006; Lehmann and Löwel, 2008; Goetze *et al.*, 2010b; Greifzu *et al.*, 2011; Tschetter *et al.*, 2011; Lehmann *et al.*, 2012). Measurements with the virtual-reality optomotor system invented by Prusky and his colleagues (2004) (chapter 2.4.1), at which mice were shown moving sine-wave gratings of different spatial frequencies, contrasts, and drift speeds, revealed that juvenile mice show lower values of visual acuity and contrast sensitivity than adult mice, nevertheless they achieve adult-like values (0.4 cycles/degree) at around P28 (Prusky *et al.*, 2004). The researchers characterized the effects of three, five and ten days of monocular deprivation in

adult animals (>P60) on spatial frequency and contrast sensitivity thresholds of the optokinetic response through nondeprived and deprived eyes. During the first three days of MD visual acuity of the nondeprived increased substantially about approximately 36 % above baseline (Prusky *et al.*, 2006). Five and ten days of MD revealed the same enhancement of spatial frequency selectivity to a maximum observed after two to three days of MD. When the deprived eye was opened after five days of MD, the threshold gradually declined, but remained above baseline for five to six days. Contrast sensitivity enhancement revealed similar results; there was a general increase in contrast sensitivity at all spatial frequencies during MD.

Prusky and his colleagues also investigated the specific role of activity in the visual cortex on the enhancement of the optokinetic response sensitivity by inactivating the visual cortex with muscimol-releasing Elvax (muscimol is a selective agonist for GABA_A receptors) before a MD of five days. The enhancement that characteristically follows MD was absent in animals with Elvax located ipsilateral to the monocular deprivation but placing Elvax contralateral to the MD showed that enhanced responses did not persist after the deprived eye was opened (Prusky *et al.*, 2006). This means that the visual cortex ipsilateral to the MD is important for the enhancement itself and the VC contralateral to the MD is important for its persistence. Prusky *et al.* (2006) observed that the enhanced spatial frequency selectivity was restricted to the monocular field of the visual cortex, in spite of the dependence of the plasticity on binocular interactions.

1.4 Synapses

1.4.1 Chemical synapses

Neurons communicate *via* synapses. These synapses can be divided into two general classes: electrical synapses and chemical synapses. Electrical synapses permit direct electrical currents through gap junctions from one neuron to another. In contrast, chemical synapses enable cell-to-cell communication by secretion of neurotransmitters. The key features of all chemical synapses are small, membrane-bounded organelles called synaptic vesicles (SV) within the presynaptic terminal (Figure 6).

These organelles are filled with neurotransmitters, chemical substances secreted from the presynapse at the active zone, the protein complex that mediates the docking and fusion of presynaptic vesicles (Figure 6).

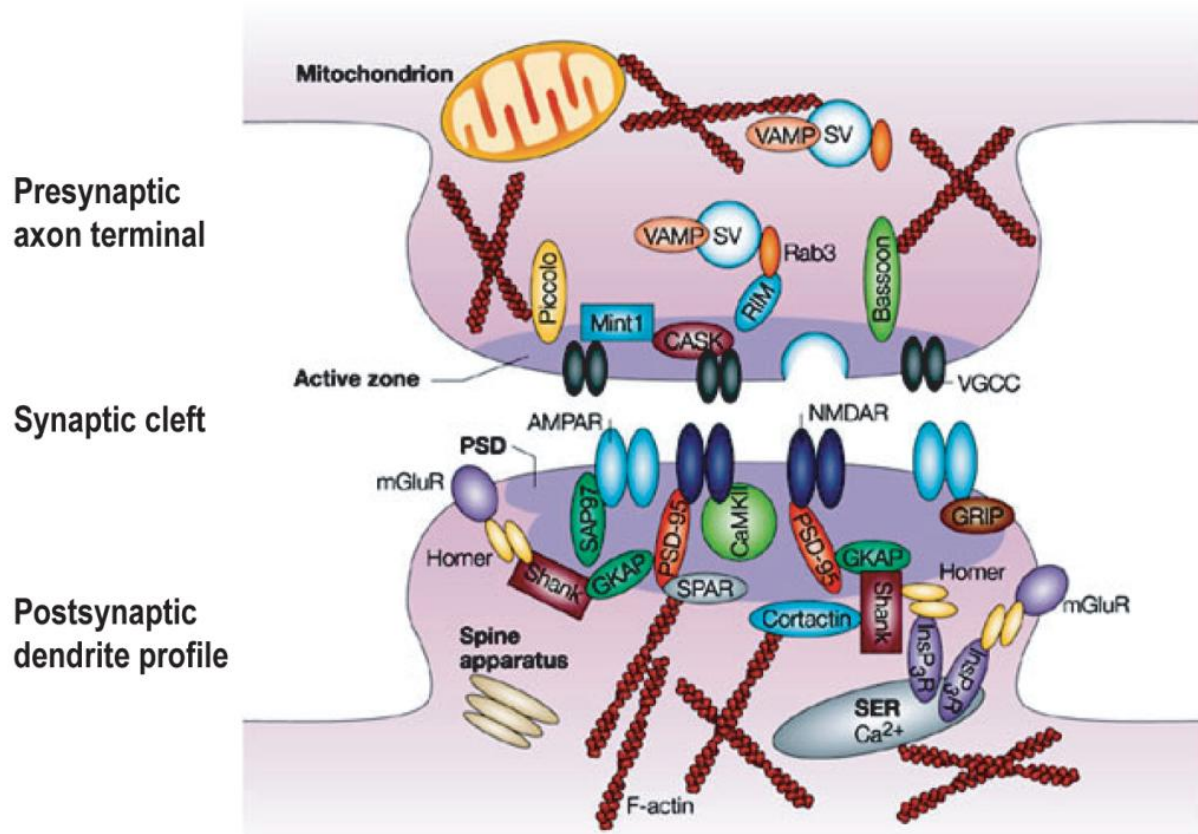


Figure 6: Scheme of an excitatory synapse (Figure from Chiu and Cline, 2010). Synapses are specialized connections between neurons composed of complex membranes and proteins. A synapse consists of three structural parts: a presynaptic axon terminal with the active zone, synaptic vesicles (SV), and release mechanism, a synaptic cleft, and a postsynaptic dendritic counterpart containing the postsynaptic density (PSD) that contains neurotransmitter receptors, scaffold proteins, and signaling mechanisms.

There are many kinds of neurotransmitters. The most frequent excitatory neurotransmitter in the brain is glutamate. In contrast, the most frequent inhibitory neurotransmitter is γ -aminobutyric acid (GABA). Synaptic vesicles fuse with the presynaptic membrane and release neurotransmitters into the synaptic cleft (Figure 6). Neurotransmitters bind to the special receptor proteins in the postsynaptic membrane. There are two major types of receptors (based on their molecular structure and biophysical properties): metabotropic receptors (G protein-coupled receptors), e.g. metabotropic glutamate receptors (mGluRs) and ionotropic receptors (ligand-gated receptors), e.g. α -amino-3-hydroxy-5-methyl-4-

isoxazolepropionic acid receptors (AMPA_Rs), and NMDARs, which are receptors for the ligand glutamate, or the GABA_A receptor (GABA_AR), whose ligand is GABA.

NMDA together with AMPA receptors are mediators of synaptic plasticity (Harris *et al.*, 1984; Dingledine *et al.*, 1999). AMPARs mediate the majority of rapid excitatory synaptic transmission by ensuring fast responses to the presynaptically released neurotransmitter glutamate. NMDARs are normally blocked by magnesium (Mg^{2+}), but open when a sufficient number of AMPARs is activated, which relieves the magnesium blockade (Mayer *et al.*, 1984; Nowak *et al.*, 1984). Once opened, NMDARs allow calcium to flux into the neuron (Malenka, 1991; Malenka and Nicoll, 1993). Intracellular calcium in turn triggers diverse signaling cascades that regulate the trafficking of AMPARs (Carroll *et al.*, 2001; Malinow and Malenka, 2002; Schnell *et al.*, 2002; Song and Huganir, 2002; Brecht and Nicoll, 2003; Derkach *et al.*, 2007). Depending on the frequency of the synaptic activity, AMPARs are either removed from or inserted into postsynapses, resulting in depression or potentiation of synaptic transmission, respectively. Once induced, these activity-dependent changes in strength of synaptic transmission could be persistent, and have thus been termed LTD and LTP.

1.4.2 The presynaptic protein Bassoon

At chemical synapses, the release of neurotransmitters is restricted to the cytomatrix of the active zone (CAZ) of the presynaptic membrane. Previous studies of central nervous synapses showed that there are two proteins, which may play a major role in assembling and organizing the presynaptic CAZ, Piccolo and Bassoon (tom Dieck *et al.*, 1998; Garner *et al.*, 2000; Dresbach *et al.*, 2001). The scaffolding protein Bassoon is present in excitatory and inhibitory presynapses of the brain and in the retina (tom Dieck *et al.*, 1998; Brandstätter *et al.*, 1999; Richter *et al.*, 1999) (Figure 7 A-D) but most likely only in ribbon synapses of photoreceptor cells and not in bipolar cells. Piccolo is found in both photoreceptor and bipolar cells (Brandstätter *et al.*, 1999; Dick *et al.*, 2001).

To further study the function of the protein Bassoon Altmann and his colleagues (2003) created mice, which are mutant for the protein Bassoon. The functional protein Bassoon of wild-type mice has a molecular mass of 420 kDa, whereas in mutant animals a *lacZ/neomycin* cassette replaced the exons 4 and 5 of the Bassoon gene and the nearly functionless protein only has a molecular mass of 180 kDa (Dick, 2002; Altmann *et al.*, 2003).

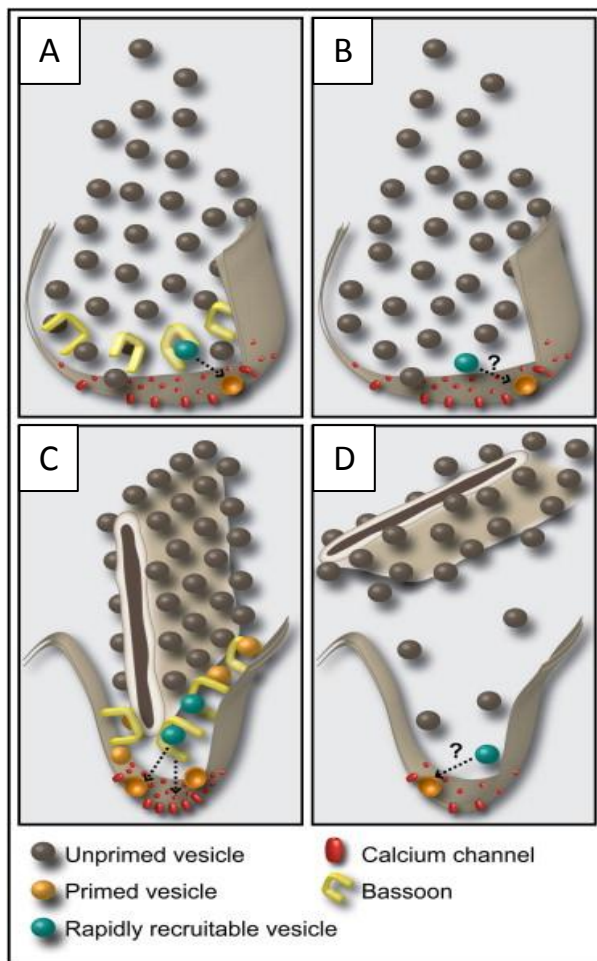


Figure 7: Bassoon at conventional and ribbon synapses (Figure from Joselevitch and Zenisek, 2010). (A) A conventional synapse of wild-type mouse. The presynaptic terminal is filled with unprimed vesicles (brown spheres). Less vesicles are primed and fuse (orange spheres) close to calcium channels (red symbols) clustered at the presynaptic membrane. Bassoon (yellow symbols) interacts with rapidly recruitable vesicles (green spheres) and facilitates the reloading of the active zone with release-ready vesicles (dashed arrow). (B) A conventional synapse of Bassoon mutant mice. Rapid refilling of the active zone with rapidly recruitable vesicles is impaired (dashed arrow) without morphological changes in the presynapse. (C) A ribbon synapse of wild-type mice. Unprimed vesicles tether around a synaptic ribbon that is anchored to the active zone of the presynaptic membrane by direct interactions at its base with the protein Bassoon. Primed vesicles gather at the bottom of the ribbon and are released into the synaptic cleft. (D) A ribbon synapse of Bassoon mutant mice. Bassoon's disruption leads to floating or missing ribbons and a decreased number of unprimed and primed vesicles at the cell membrane. Under these conditions, the reloading of rapidly recruitable vesicles to release sites is impaired.

Altrock and his colleagues revealed that mice mutant for the protein Bassoon (Altrock *et al.*, 2003) showed impairments in structure and function of ribbons in the photoreceptor cells (Figure 7 D), but not in bipolar cells (Brandstätter *et al.*, 1999). Based on these studies, Bassoon plays an essential role in synapse formation, which cannot be compensated by Piccolo. Bassoon is the key protein for anchoring synaptic ribbons to the active zone of photoreceptor cells (tom Dieck *et al.*, 2005) (Figure 7 C,D). In wild-type animals the ribbon is anchored to the active zone (Figure 8 A) whereas in mutant mice the ribbon is free-floating (Figure 8 B) or missing in 99 % of all ribbon synapses of photoreceptor terminals with significantly impaired signal transduction through the retina (Dick *et al.*, 2003) (Figure 7 A-D). It is assumed that the ribbon, a structurally and functionally specialized presynaptic cytomatrix (Figure 2 B-E), is responsible for continuous supply of neurotransmitter vesicles (Figure 7 C). Bassoon also plays a functional and structural role in exocytosis and endocytotic retrieval of synaptic vesicles as well as refilling with neurotransmitters (tom Dieck *et al.*, 1998; Frank *et al.*, 2010; Hallermann *et al.*, 2010). Functionally, this photoreceptor

synaptopathy leads to a disturbed signal transfer from photoreceptor to bipolar cells. This was shown in studies using electroretinographic recordings (ERGs) (Dick *et al.*, 2003). The three major components of ERGs are the a-wave, which mainly originates in photoreceptor cells, the b-wave, which mainly originates in bipolar cells, horizontal cells, and other second-order cells, and the c-wave, which is mainly originated by non-neuronal cells of the retina (Dowling, 1987; Steinberg *et al.*, 1991). In Bassoon mutant mice the b-wave was not only diminished in amplitude but also slowed down compared to their wild-type littermates (Dick *et al.*, 2003) (Figure 8 C,D).

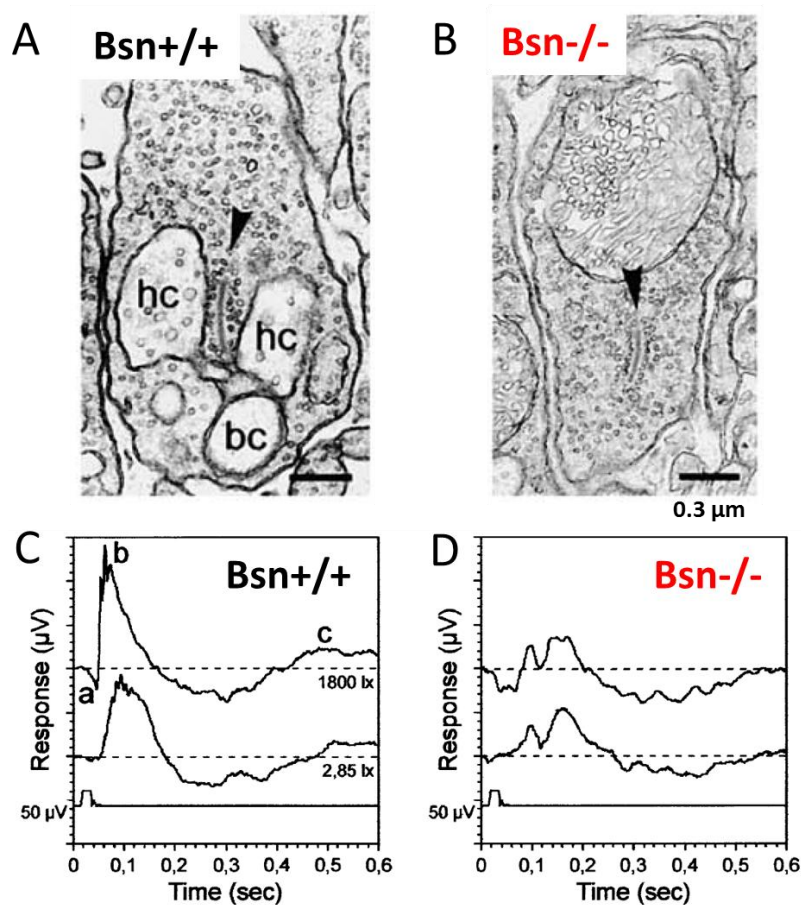


Figure 8: Electron micrographs and electroretinographic recordings (ERG) of Bsn^{+/+} and Bsn^{-/-} mice (Figure modified from Dick *et al.*, 2003). (A) Electron micrograph of a rod terminal in the retina of a Bsn^{+/+} mouse. The presynaptic ribbon (arrowhead) is anchored to the active zone and it faces three postsynaptic elements, a rod bipolar cell dendrite (bc) and two horizontal cell processes (hc). (B) Electron micrograph of a Bsn^{-/-} mouse shows a rod terminal with a free-floating ribbon (arrowhead) and no postsynaptic elements. Electroretinographic recording examples for scotopic responses of a Bassoon wild-type mouse (C) and a Bassoon mutant mouse (D) to 20 ms white flash light of 2.85 and 1800 lux. Bsn^{-/-} animals show a decrease in b-wave and also in c-wave amplitudes and slower b-wave oscillations compared to Bsn^{+/+} mice. The amplitudes of a-waves were similar. The dashed lines represent the dark base level.

Earlier studies showed that in four-week-old Bassoon mutant mice horizontal and bipolar cells dendrites grow into the outer nuclear layer, where the cell bodies of photoreceptor cells are provided, and form new ectopic synapses (Dick *et al.*, 2003; Specht *et al.*, 2007). These ectopic synapses which are absent in the wild-type retina (Specht *et al.*, 2007) could influence visual capabilities of Bassoon mutant mice.

The protein Bassoon is not only present in the retina, but also in the presynapse of hair cells of the inner ear. A study in rodents revealed that Bassoon is highly expressed in the cerebellum, the hippocampus, the olfactory cortex, and the cerebral cortex (tom Dieck *et al.*, 1998). Nevertheless, in the hippocampus synapse density, extension of the active zone, and number and density of attached synapses at the active zone do not differ between Bsn^{+/+} and Bsn^{-/-} mice (Altrock *et al.*, 2003). Hippocampal synapses in mutants are partly inactive (up to 50 % more inactive synapses than in wild-type animals), which means that fewer neurons release neurotransmitters (Altrock *et al.*, 2003) whereas the synaptic release probability of synaptic vesicles is indistinguishable between both genotypes. Bassoon mutant mice show altered hippocampal synaptic transmission between excitatory neurons hence significantly less synaptic depression during stimulation compared to Bassoon wild-type animals, whereas LTD is not altered (Altrock *et al.*, 2003). All these data reveal that Bassoon mutant mice show an excitation-inhibition-imbalance in the cerebral cortex and the hippocampus (Altrock *et al.*, 2003). Bsn^{-/-} mice show a reduction of excitatory drive onto GABAergic interneurons, which may lead to lower excitation of interneurons and therefore to a decrease of GABA release.

It has also been shown that Bassoon mutant mice suffer from epileptiform seizures (Altrock *et al.*, 2003; Ghiglieri *et al.*, 2009; Ghiglieri *et al.*, 2010; Sgobio *et al.*, 2010). In addition, Altrock *et al.* (2003) investigated the cerebral cortex and the hippocampus of these mice using electroencephalographic recording (EEG). EEG is a method to measure summed electrical activity along the scalp by recording voltage fluctuations resulting from ionic currents within neurons. Measurements of Bassoon mutant mice showed that during epileptiform seizures also seizure-like activities occur in the cerebral cortex and the hippocampus, due to the high frequency firing of neurons. In spite of these epileptiform seizures, the basal excitatory synaptic transmission (measured with electrophysiological recordings) is normal within the hippocampus (Ghiglieri *et al.*, 2009). However, intracellular recordings from corticostriatal slices revealed reduced LTP the hippocampus of Bsn^{-/-} mice

but chronic treatment with valproic acid (VPA), an anticonvulsant drug which was already added to the drinking water of the pregnant mother, rescues this form of synaptic plasticity. Ghiglieri and her colleagues (2009) found that striatal neurons are differentially sensitive to frequent seizures triggered in the brain of Bsn^{-/-} mice, and that synaptic plasticity changes develop in response to early-onset epilepsy in these animals. They could also show that the number of paralbumin (PV) positive interneurons in the striatum of Bsn^{-/-} mice was increased. Immunohistochemical analysis of the striatum showed that VPA failed to prevent PV overexpression but VPA was able to reduce the frequency of epileptiform seizures. Ghiglieri and her colleagues suggested that the observed molecular and electrophysiological changes are secondary to the seizure activity rather than being primarily induced by the lack of functional Bassoon protein.

Manganese-enhanced magnetic resonance imaging revealed that Bsn^{-/-} mice have an enlarged brain size, which is mostly caused by an increased volume of the hippocampus (+ 37 %) and of the cortex (+ 15 %) (Angenstein *et al.*, 2007; Heyden *et al.*, 2011). Nevertheless, the observed increase in cortex size is not associated with an obvious change in cortical lamination, whereas cell densities (cells/mm³) did not differ between Bsn^{-/-} and Bsn^{+/+} mice. The increased volume is caused by the reduced number of apoptotic cells, increased cell proliferation, cell survival, and neurogenesis in Bsn^{-/-} mice (Heyden *et al.*, 2011). These findings are due to a highly elevated level of the neurotrophin brain derived neurotropic factor (BDNF) (Heyden *et al.*, 2011) (Figure 9), which is a survival and growth factor for neurons within the CNS. Epileptic seizures are most likely the reason for increased BDNF levels and promoted neurogenesis (Parent *et al.*, 1997; Lee *et al.*, 2002; Altar *et al.*, 2003; Yokoi *et al.*, 2007).

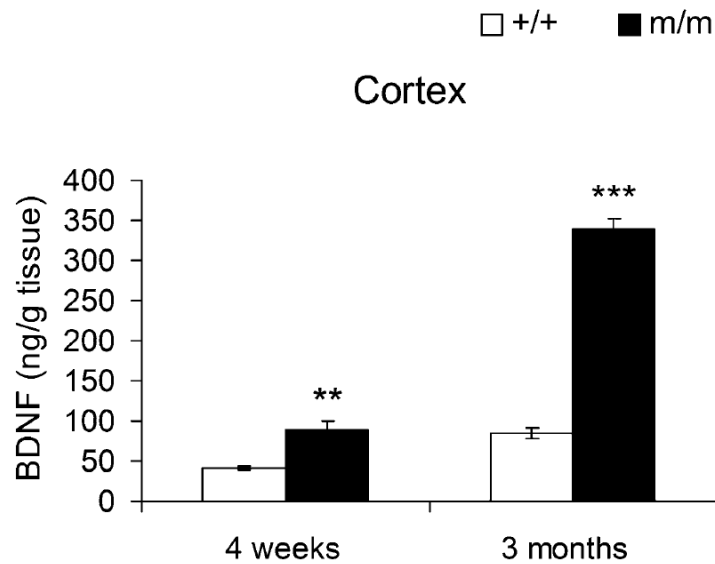


Figure 9: BDNF levels in the cortex of Bsn+/+ and Bsn-/- mice measured with ELISA (Figure from Heyden *et al.*, 2011). At four weeks of age, higher BDNF levels were found in the cortex of Bsn-mutant mice as compared to wild-types and the differences reach statistical significance. At three month, BDNF levels in the cerebral cortex were significantly elevated in Bsn mutants.

The question which we wanted to address in our study is the following: How little neurotransmission in the visual system is sufficient to promote decent visual capabilities and plasticity? Since Bsn-/- mice display a striking loss of synaptic ribbons in photoreceptor terminals, which significantly impairs signal transduction through the retina we tested their vision behaviorally with two different behavioral tasks – a virtual-reality optomotor system and the visual water task – to check visual acuity, contrast sensitivity, and visual temporal resolution. The excitation-inhibition-balance which plays a major role in different forms of neural plasticity is also altered in Bassoon mutant mice, therefore we studied whether juvenile and adult Bsn-/- mice display modified OD plasticity and/or interocular plasticity of vision in which monocular deprivation leads to an enhancement of the optokinetic response through the nondeprived eye. We used MD, as a model of plasticity, which induces a shift in ocular dominance of binocular neurons toward the open eye in the visual cortex of juvenile and adult mice. We also used *in vivo* optical imaging of intrinsic signals to visualize cortical activity maps in V1 and probe vision and plasticity in young and adult Bsn-/- mice and their wild-type littermates with and without MD. Since young adult Bsn-/- mice display an increased number of interneurons which express parvalbumin in the striatum and increased inhibition could be an explanation for an absent OD plasticity of adult Bsn-/- mice, we

performed also immunohistochemistry for parvalbumin in V1. We wanted to know whether reduced plasticity was due to an increasing frequency of epileptiform seizures as previously shown for the striatum or to an increased number of inhibitory parvalbumin expressing neurons. Due to these findings we wanted to address the question whether or not the increased number of interneurons which express parvalbumin was due to an augmented activation of silent/inactive interneurons, which did not express parvalbumin? Therefore we stained PV together with the potassium channel Kv3.1b, which is reputed to be present only in parvalbumin-containing interneurons (Chow *et al.*, 1999). Since four-week-old as well as three-month-old Bsn^{-/-} mice display an elevated level of BDNF in the cortex, we did immunohistochemical stainings of BDNF to check whether there is also an elevated level in the visual cortex.

1.4.3 The postsynaptic protein PSD-95

The postsynaptic membrane contains a variety of scaffold proteins, which in excitatory synapses are organized in a structure termed postsynaptic density (PSD) (Sampedro *et al.*, 1981; Kennedy, 1997) (Figure 10).

One of the most important proteins of the PSD is the postsynaptic density protein of 95 kDa (PSD-95) (Figure 10), which is also called synapse associated protein of 90 kDa (SAP-90) and in humans encoded by the disks large homolog gene 4 (DLG4) (Cho *et al.*, 1992; Stathakis *et al.*, 1997). PSD-95 is a member of the membrane-associated guanylate kinase (MAGUK) family and contains different regions including three PDZ domains (PDZ is an acronym combining the first letters of three proteins: post synaptic density protein, disc large tumor suppressor, and zonula occludens-1 protein), one Src-homology-3 (SH3), and one guanylate kinase (GK) domain (Cho *et al.*, 1992; Craven and Brecht, 1998; Kim and Sheng, 2004) (Figure 10).

PSD-95 is not only present in excitatory synapses in the brain but also in the retina. Measurements with light and electron microscopic immunocytochemistry revealed that there is a strong expression of PSD-95 in both rod and cone photoreceptors terminals, which is likely because of invaginating processes of horizontal cells (Koulen *et al.*, 1998). Thus the PSD-95 protein in photoreceptors would be actually located postsynaptically to horizontal cells. The distribution of PSD-95 showed a clustering of PSD-95 also in terminals postsynaptic to bipolar cell ribbon synapses (Koulen *et al.*, 1998). Koulen and his colleagues (1998)

concluded that both amacrine and ganglion cells express PSD-95 at the synapses they receive from bipolar cells as well.

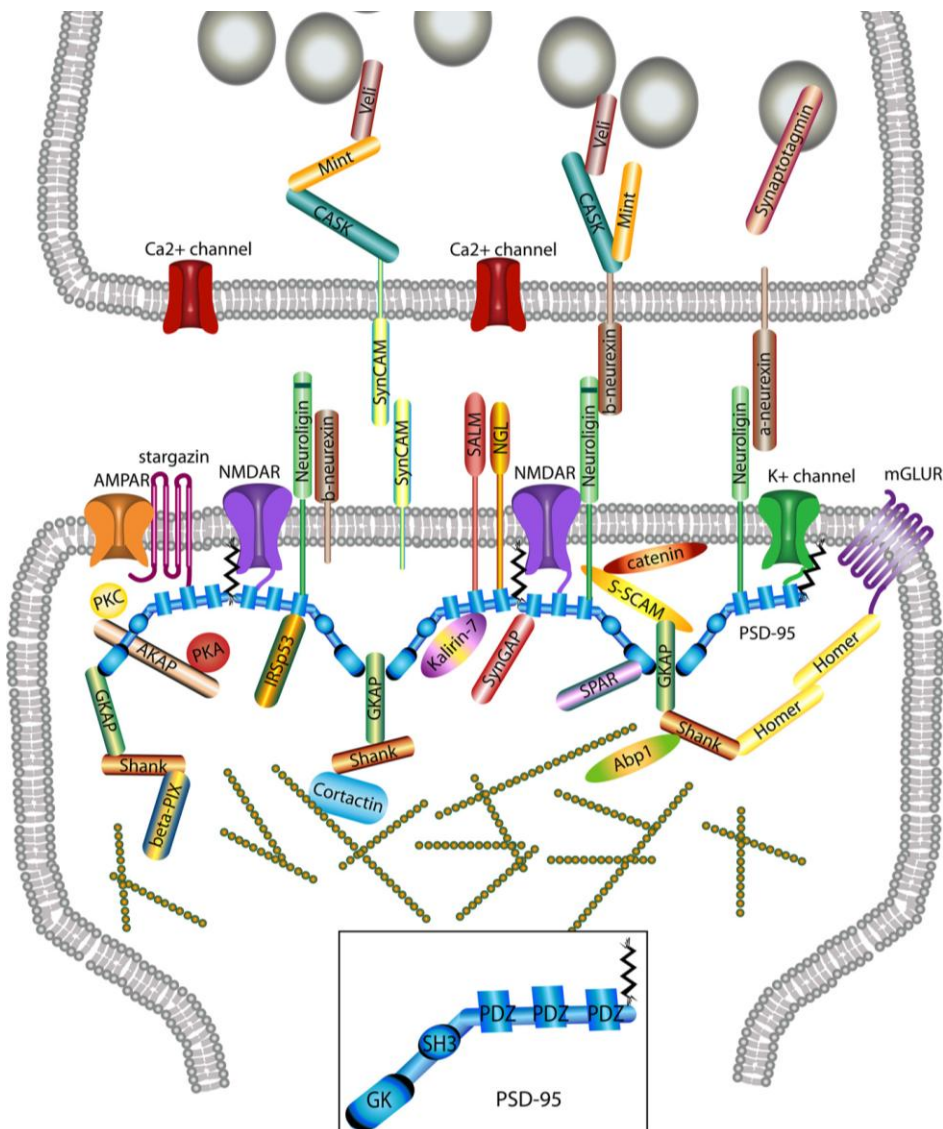


Figure 10: Molecular organization of glutamatergic synapses (Figure from Keith and El-Husseini, 2008). Only major molecules associated with PSD-95 (blue) are shown, *e.g.* NMDARs (purple), neuroligins (green) and indirect with AMPARs (orange) *via* stargazin (pink). These various molecules portrayed regulate synapse function, morphology, trafficking, localization of adhesion molecules, neurotransmitter receptors, and play a role in synaptic plasticity. At the bottom the three domains GK, SH3, and PDZ of the PSD-95 protein are shown in blue.

PSD-95 is not only important for multimeric scaffolding structure but it is also indispensable for direct and indirect anchoring of receptors (*e.g.* AMPARs, NMDARs, mGluRs), ion channels (*e.g.* K⁺ channels), and postsynaptic adhesion molecules (*e.g.* neuroligins) (Sheng and Sala,

2001; Keith and El-Husseini, 2008) (Figure 10). As previously mentioned NMDARs and AMPARs play a major role in synaptic plasticity because trafficking of AMPARs to and from synapses controls the strength of excitatory synaptic transmission. It is known that a change in PSD-95 expression has an effect on the distribution and number of AMPARs in the postsynaptic membrane (Beique *et al.*, 2006; DeGiorgis *et al.*, 2006) by stabilizing AMPARs within the membrane indirect through anchoring over stargazin (Chen *et al.*, 2000; Chetkovich *et al.*, 2002; El-Husseini *et al.*, 2002; Schnell *et al.*, 2002; Dakoji *et al.*, 2003; Tomita *et al.*, 2003; Fukata *et al.*, 2005; Tomita *et al.*, 2005; Bats *et al.*, 2007). In addition, PSD-95 plays a role in mediating AMPAR targeting at mature synapses (Elias *et al.*, 2006). Due to these findings it could be shown that PSD-95 is involved in synaptic plasticity (Migaud *et al.*, 1998; Ehrlich and Malinow, 2004; Yao *et al.*, 2004; Beique *et al.*, 2006; Elias *et al.*, 2006; Keith and El-Husseini, 2008; Sun and Turrigiano, 2011).

In hippocampal neurons, overexpression of PSD-95 drives maturation of excitatory synapses by enhanced synaptic clustering and function of AMPARs (El-Husseini *et al.*, 2000; Tomita *et al.*, 2001) whereas knockdown and knockout of PSD-95 in mice decreases AMPAR-mediated synaptic transmission (Migaud *et al.*, 1998; Carlisle *et al.*, 2008) and leads to a removal of all AMPARs at about half of all excitatory synapses (Migaud *et al.*, 1998; Beique *et al.*, 2006; Elias *et al.*, 2006; Fitzjohn *et al.*, 2006; Ehrlich *et al.*, 2007). Interestingly, in mice targeted disruption of PSD-95 alters synaptic plasticity. In these mice, LTP is enhanced and LTD is eliminated. It seems that these effects can be explained by the role of PSD-95 as a mediator of postsynaptic signaling cascades downstream of NMDARs (Migaud *et al.*, 1998; Tomita *et al.*, 2001; Yao *et al.*, 2004; Carlisle *et al.*, 2008; Xu *et al.*, 2008) toward a specialized role in determining the number of AMPARs at excitatory synapses (Elias and Nicoll, 2007), which play critical roles in LTP and LTD. The enhancement of LTP is not based on changes in NMDAR function. It could be attributed instead to a larger number of AMPA silent synapses that lack AMPARs (Carlisle *et al.*, 2008). AMPA silent synapses possess NMDARs but no functional AMPARs (Malenka and Nicoll, 1997, 1999; Malinow *et al.*, 2000; Tomita *et al.*, 2001; Beique *et al.*, 2006). Interestingly, LTP turns on or “AMPAfies” silent synapses, at which AMPAR subunits move into dendritic spines and are inserted into the synaptic membrane, PDZ proteins (domain of PSD-95) play a basic role in the regulated insertion (Craven and Brecht, 1998; Tomita *et al.*, 2001; Schnell *et al.*, 2002; Dakoji *et al.*, 2003; Ehrlich and Malinow, 2004; Schlüter *et al.*, 2006; Bhattacharyya *et al.*, 2009). Nevertheless, the

adaptive increase of neuronal transmission, described by LTP represents a physiological basis for learning and memory (Yao *et al.*, 2004; Keith and El-Husseini, 2008).

Not much is known to date about PSD-95 in the visual cortex so far. A previous study showed that PSD-95 is involved in synaptic plasticity and measuring fluorescence intensity of PSD-95 puncta during synaptic scaling in the visual cortex of rats revealed that the abundance of PSD-95 is bidirectionally regulated by neuronal activity (Sun and Turrigiano, 2011).

Our cooperating group (Schlüter, Huang from the ENI, Germany) performed slice electrophysiology (voltage clamp) in the visual cortex of PSD-95 knockout (KO) mice and measured AMPAR- and NMDAR-mediated EPSCs (excitatory postsynaptic currents). They observed that PSD-95 KO mice retain a decreased juvenile-like AMPAR/NMDAR ratio into adulthood and a high number of AMPA silent synapses may promote visual cortical plasticity in older mice (Huang *et al.*, 2012). They also measured the inhibitory tone in local cortical circuits in both PSD-95 KO and wild-type (WT) as well as heterozygous (HZ) mice and found a similar GABAR/NMDAR ratio also in adult PSD-95 KO animals which means that the maturation of the inhibitory circuits might not be altered in PSD-95 KO animals.

In addition, *in vivo* single-unit recordings in mature PSD-95 KO mice (>P45) revealed fewer orientation-biased cells (~ 20 % orientation-biased cells) in mouse visual cortex compared to their WT littermates (~ 35 % orientation-biased cells) (Fagiolini *et al.*, 2003). Fagiolini and her colleagues (2003) also observed that adult mice, which lack the NMDAR subunit NR2A failed to exhibit enhancement of the optokinetic response of the nondeprived eye during MD and suggested that adult plasticity might be mediated by the NR2A subunit (Miyamoto *et al.*, 2006). Since PSD-95 is important for anchoring NMDARs to the postsynaptic membrane, disruption of PSD-95 might lead to the same phenotype.

With respect to these findings, we wanted to examine the visual capabilities of PSD-95 KO mice. Therefore we checked visual acuity and contrast sensitivity behaviorally with two different behavioral tasks: a virtual-reality optomotor system and the visual water task. Since PSD-95 KO animals show altered synaptic plasticity, most likely due to an increased number of AMPA silent synapses, we tested interocular plasticity of vision after monocular deprivation, and we studied whether we could induce a shift in ocular dominance of binocular neurons toward the open eye in the visual cortex by MD as a model of plasticity in juvenile and adult mice. We used *in vivo* optical imaging of intrinsic signals to visualize

cortical activity maps in V1 and tested vision and plasticity in adult and old PSD-95 KO mice and their WT and HZ littermates with and without MD.

1.5 Aims

Bassoon mutant mice (Bsn^{-/-}) display a striking loss of synaptic ribbons in photoreceptor terminals, which impairs signal transduction through the retina (Altrock *et al.*, 2003; Specht *et al.*, 2007). Our question was: how little neurotransmission in the visual system is sufficient to promote decent visual capabilities? Therefore, we assessed vision in these mice behaviorally with the virtual-reality optomotor system (Prusky *et al.*, 2004) and the visual water task (Prusky *et al.*, 2000) and performed *in vivo* optical imaging of intrinsic signals (Kalatsky and Stryker, 2003).

Since Bsn^{-/-} mice have a modified excitation-inhibition-balance and inhibition plays a major role in OD plasticity (Hensch *et al.*, 1998), we also studied whether Bsn^{-/-} mice display modified OD plasticity and/or interocular plasticity (Prusky *et al.*, 2006).

Since it was shown that adult Bsn^{-/-} mice display an increased number of parvalbumin positive interneurons in the striatum (Ghiglieri *et al.*, 2009) and inhibition plays a major role in OD plasticity (Hensch *et al.*, 1998) we wanted to know whether this is also the case in the visual cortex and therefore performed immunohistochemistry.

PSD-95 is present in the retina (Koulen *et al.*, 1998) as well as in the brain (Sampedro *et al.*, 1981; Kennedy, 1997). PSD-95 KO mice have fewer orientation-biased cells in the mouse visual cortex compared to their WT littermates (Fagiolini *et al.*, 2003). Therefore we assessed vision in these mice behaviorally with the virtual-reality optomotor system and the visual water task and performed *in vivo* optical imaging of intrinsic signals.

PSD-95 KO animals show altered hippocampal synaptic plasticity. Therefore we tested OD plasticity and interocular plasticity of PSD-95 KO mice and their littermates. To test if the prolonged period of plasticity of PSD 95 KO mice was due to reduced intracortical inhibition (Hensch *et al.*, 1998) we treated mice with diazepam during seven days of MD.

2. Materials and methods

2.1 Animals

2.1.1 Bassoon

Mice mutant for the presynaptic protein Bassoon (Bsn) lacking the central part of the protein encoded by exons 4 and 5 of the Bassoon gene ($Bsn^{\Delta Ex4/5}$, here referred to as Bsn^{-/-}) and their wild-type and heterozygous littermates (Bsn^{+/+} and Bsn^{+/-}) were raised from heterozygous animals in our cooperating lab of Prof. Dr. Eckart D. Gundelfinger at the Leibniz Institute for Neurobiology in Magdeburg, Germany (Altrock *et al.*, 2003). Mice were housed at standard conditions (12 h light/dark cycle) with food and water provided *ad libitum*. The mice exhibit a mixed genetic background of C57BL/6J and 129/SvEmsJ strains, which is controlled by using sustained C57BL-backcrossed and 129 inbred mice to breed the heterozygous parents. We used female and male mice between 13 and 148 days old at the time of the experiments. To analyze the development of visual acuity and contrast sensitivity individual mice were tested from the day of eye opening (between postnatal days 13 and 15) until postnatal day 42. All experiments were done at the Friedrich-Schiller-Universität Jena, Germany.

2.1.2 PSD-95

Wild-type (WT), heterozygous (HZ) and PSD-95 knockout (PSD-95 KO) mice (Yao *et al.*, 2004) were raised from heterozygous animals in our cooperating lab of Dr. Oliver Schlüter at the European Neuroscience Institute (ENI) in Göttingen, Germany. Mice were housed at standard conditions (12 h light/dark cycles) with food and water provided *ad libitum*. The mice exhibit a genetic background of C57BL/6J strain. We used female and male mice between 63 and 507 days old at the time of the experiments. All experiments were done at the Georg-August-Universität Göttingen, Germany.

Experimenters were always blind to the animal's genotype. All animal experiments were performed according to the German Law on the Protection of Animals and the corresponding European Communities Council Directive of November 24, 1986 (86/609/EEC).

2.2 Monocular deprivation

To test the visual cortical plasticity of mice (Lehmann and Löwel, 2008) we (Prof. Dr. Karl-Friedrich Schmidt and I) carried out a monocular deprivation (MD) by suturing the right eyes of mice accordingly to already published protocols (Gordon and Stryker, 1996; Cang *et al.*, 2005; Lehmann and Löwel, 2008). To this end we anaesthetized mice in a box with 3 % halothane in a 3:2 mixture of nitrous oxide (N₂O) and oxygen (O₂). After achievement of surgical anesthesia (toe-pinch test) we reduced the halothane concentration to 1.5 % and applied the analgesic Rimadyl (5 µg/g mouse, intraperitoneally). The mouse was placed on a heating pad and its temperature was automatically adjusted *via* a temperature sensor to maintain a body temperature of 37 °C. The surrounding area of the right eye was cleaned with 70 % ethanol. We trimmed the eyelid margins and then flushed the eye with 0.9 % saline. To avoid inflammation we applied the antibiotic Refobacin directly on top of the right eye. To close the eye we placed two mattress sutures using 7 - 0 silk (Johnson&Johnson Intl). Afterwards, mice were returned to their standard home cages. All mice were checked daily to assure that the deprived eye remained closed and uninfected. Animals got excluded from the experiments as soon as the sutures of the monocularly deprived eyes were open.

2.3 Treatment with diazepam

Since PSD-95 KO animals show a prolonged period of cortical plasticity (chapter 3.11.2) we assumed that might be because of reduced cortical inhibition so we applied the drug diazepam. Diazepam which is a benzodiazepine drug enhances the effect of the neurotransmitter γ-aminobutyric acid (GABA) by binding to the benzodiazepine site on the GABA_A receptor (*via* the constituent chlorine atom) which leads to an increase in GABA_A-mediated inhibition. Diazepam was diluted with 0.9 % saline and injected intraperitoneally (1 µg/g mouse) daily for seven days. In this study, we used a dose of 1 µg drug per mouse gram. In our hands, a dose of 30 µg drug per mouse gram that was used by other groups was lethal (Hensch *et al.*, 1998; Huopaniemi *et al.*, 2004; Kanold *et al.*, 2009).

2.4 Quantification of visual capabilities

2.4.1 Virtual-reality optomotor system

We assessed visual acuity using the virtual-reality optomotor system (Prusky *et al.*, 2004) (Figure 11 A,B). This test does not require any training of the mice because it is based on the optomotor reflex in response to a moving stimulus.

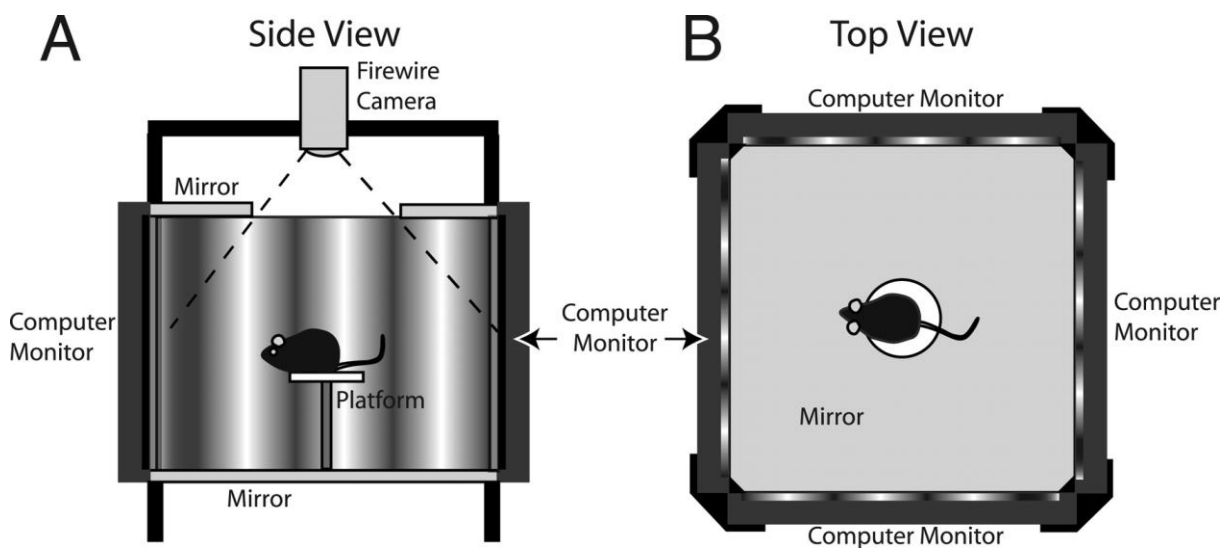


Figure 11: Scheme of the optomotor testing apparatus (Figure from Prusky *et al.*, 2004). (A) Side view. The mouse can freely move on a platform positioned in the middle of an arena created by four quadratically arranged computer screens. Sine wave gratings on the screens are extended vertically with mirrors on ceiling and floor. To display the animal's behavior a video camera from above is used. (B) Top view. The mouse is surrounded by 360° of gratings.

In the optomotor setup, the mouse is surrounded by four monitors showing 360° moving sine wave gratings of different spatial frequencies, contrasts and drifting speeds generated by the software OptoMotry 1.4.0 (CerebralMechanics®, Lethbridge, Alberta, Canada) like previously reported (Prusky *et al.*, 2004; Lehmann and Löwel, 2008; Goetze *et al.*, 2010b). In the testing arena (39 x 39 x 32.5 cm [L x W x H]), the mouse can move freely on a platform which is placed 13 cm over the floor in the middle of the apparatus (Figure 11 A,B). Additionally mirrors are placed on the floor and the ceiling while a video camera in the lid of the apparatus records the animals' behavior. The x-y coordinates of the crosslines were used to center the rotation of the cylinder on the mouse's eyes (Figure 12 A,C). This guarantees a constant distance of the virtual cylinder from the animal.

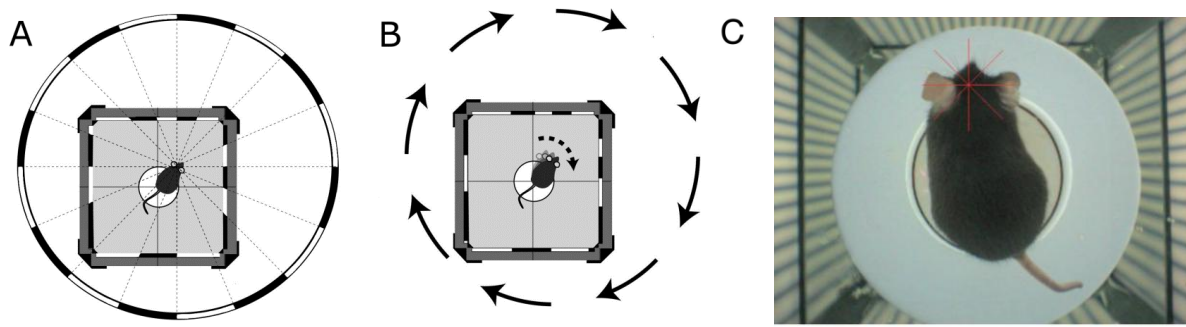


Figure 12: Virtual cylinder and optomotor response (Figures modified from Prusky *et al.*, 2004). (A) In a 3-D coordinate space a virtual cylinder is projected on all four screens. The center of the rotating cylinder is determined by the head of the mouse. (B) When the cylinder is rotating, the mouse tracks the drifting sine wave grating with neck and head movements. (C) A video camera image of a mouse tracking the moving sine wave grating. The red crosslines are positioned between the eyes of the mouse, and the coordinates are used to center the rotation of the virtual cylinder.

Mice will reflexively track the moving vertical sine wave gratings by head movements as long as they can see the gratings (Figure 12 B). In mice only movement in the temporal-to-nasal direction induces tracking therefore it is possible to measure both eyes separately by reversing the direction of the moving sine wave grating (Douglas *et al.*, 2005). Spatial frequency at 100 % contrast, contrast at six different spatial frequencies (0.031 cycles/degree (cyc/deg), 0.064 cyc/deg, 0.092 cyc/deg, 0.103 cyc/deg, 0.192 cyc/deg, 0.272 cyc/deg), and in addition for temporal resolution at 100 % contrast at seven different spatial frequencies (0.064 cyc/deg, 0.103 cyc/deg, 0.150 cyc/deg, 0.192 cyc/deg, 0.200 cyc/deg, 0.272 cyc/deg, and 0.400 cyc/deg) were measured. Contrast sensitivity was calculated for each spatial frequency as a Michelson contrast from the screen luminance $\frac{(\max - \min)}{(\max + \min)}$ and the reciprocal of the threshold (black mean, 0.22 cd/m²; white mean, 152.13 cd/m²).

Drift speed was usually fixed at 12 degrees/second (°/sec). To investigate whether the loss of the presynaptic protein Bassoon had an effect on temporal resolution we tested different drift speeds (Bsn+/+ and Bsn -/- mice were tested at: 0.064 cyc/deg, 0.103 cyc/deg, 0.150 cyc/deg, and 0.192 cyc/deg, in addition, Bsn+/+ mice at 0.272 cyc/deg and 0.400 cyc/deg and Bsn-/- mice at 0.200 cyc/deg). Because of technical reasons we were not able to measure drift speeds higher than 50 °/sec. Experimenters were blind to the animal's

genotype and thresholds were regularly validated independently by more than one observer (Prof. Dr. Karl-Friedrich Schmidt and I).

Additionally, we studied the development of visual acuity and contrast sensitivity of individual young mice. Animals were tested from the day of eye opening throughout development and the genotype was determined after visualizing cortical activity maps.

In mice with a monocular deprivation of the right eyes, visual acuity of the open left eyes was tested daily in the virtual-reality optomotor system.

2.4.2 Visual water task

As a second method to assess visual acuity in mice, we used the visual water task, a visual discrimination task that is based on reinforcement learning (Prusky *et al.*, 2000; Prusky *et al.*, 2004; Prusky and Douglas, 2004) (Figure 13 A-C).

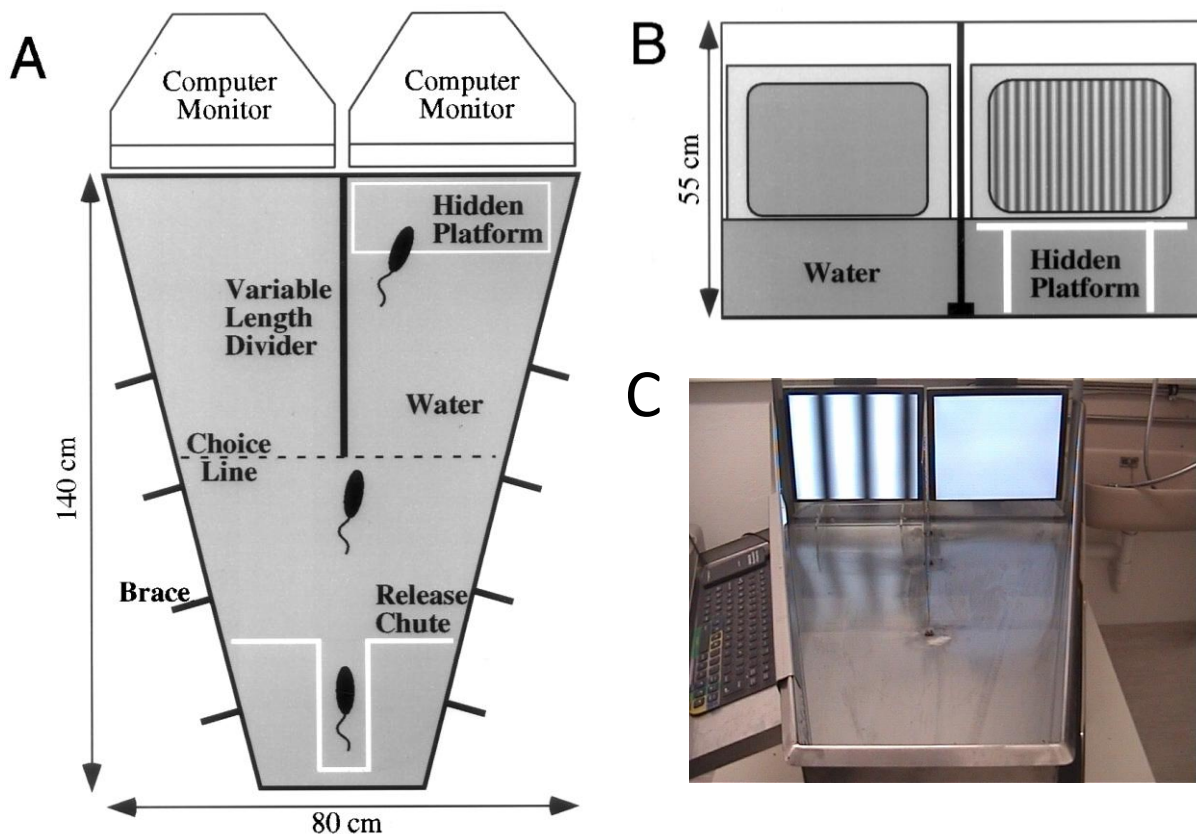


Figure 13: Scheme of the visual water box (Figure from Prusky *et al.*, 2000). (A) View from above illustrating the important components including pool, platform, midline divider, and both monitors. The pool is filled with water (shown in gray). From the release chute, animals learn to swim on the side of the pool on which monitor the grating is projected to find the hidden platform to escape from the water. (B) Front view of both screens, hidden platform and midline divider. (C) Picture of the apparatus from above.

For this task, animals were initially trained to distinguish a low spatial frequency vertical sine-wave grating (0.086 cyc/deg) from an isoluminant grey generated by the software Vista X 3.5.004 (CerebralMechanics®, Lethbridge, Alberta, Canada). Then their ability to recognize higher spatial frequencies was tested. The apparatus consists of a trapezoidal-shaped pool (140 cm long x 80 cm wide x 55 cm high walls, but the pool is wider at one end (80 cm) than the other (25 cm)) with two monitors placed side by side at the wide end (Figure 13 A-C). A midline divider is extended from the wide end into the pool, creating a maze with a stem and two arms. The length of the divider sets the choice point and effective spatial frequency. An escape platform, which is invisible to the animals, is placed below the monitor on which the sine-wave grating is projected. The position of the grating and the platform is alternated in a pseudorandom sequence over the training and test trials. Once mice achieved 90 % accuracy, the discrimination threshold is determined by increasing the spatial frequency of the grating until performance falls below 70 % accuracy. The highest spatial frequency where mice achieved 70 % accuracy is taken as the maximum visual acuity.

2.5 Surgical preparations for optical imaging

After initial anesthesia in a box with 2 % halothane in 1:1 N₂O/O₂ mixture, the animals received injections of the neuroleptic chlorprothixene (0.2 mg/mouse, intramuscularly), atropine (0.3 mg/mouse, subcutaneously) to dilate both pupils equally and to avoid mucous obstructions, and dexamethasone (0.2 mg/mouse, subcutaneously) to prevent brain edema. The animals were placed in a stereotaxic apparatus containing two ear bars and one incisor bar. Anesthesia was maintained with ~ 0.6 % halothane in a mixture of 1:1 N₂O/O₂ applied through a tube over the nose (depth of anesthesia was always tested by toe-pinch test). Body temperature was maintained at 37 °C using a temperature sensor that regulates the temperature of the heating pad. Electrocardiographic leads were fixed to the mouse to monitor the heart rate continuously throughout the experiment. The skin above the skull was shaved, cleaned with 70 % ethanol and we applied locally lidocaine (2 % xylocain jelly) as local anesthetics. We incised the skin to expose the visual cortex of the left hemisphere; imaging was routinely performed through the skull. Low-melting point agarose (2.5 % agarose in 0.9 % saline) and a glass coverslip was placed over the visual cortex. To avoid dehydration of the mouse during the experiment we injected 0.2 ml saline (0.9 %,

subcutaneously). At the end sutured eyelids of mice were opened. To keep the cornea of the eyes moist we applied silicon oil and eye drops.

2.6 Optical imaging of intrinsic signals

Mouse visual cortical responses were recorded using *in vivo* optical imaging of intrinsic signals (Blasdel and Salama, 1986; Grinvald *et al.*, 1986; Bonhoeffer and Grinvald, 1993) which has been further optimized to analyze OD plasticity (Kalatsky and Stryker, 2003). Thereby small changes of reflectance of active neuronal tissue due to the transition of oxy-hemoglobin to deoxy-hemoglobin can be detected. The biggest difference of reflectance is visible at 610 nm (red light) where deoxy-hemoglobin absorbs more light than oxy-hemoglobin.

With this method, a temporally periodic stimulus is continuously presented to the mouse and Fourier analysis extracts the cortical response at the stimulus frequency. We obtained optical images of cortical intrinsic signals using a Dalsa® DS-1A-01M30-12E charge-coupled device (CCD) camera, which converts light into electrical signals (Dalsa®, Waterloo, Canada), controlled by a custom software. The experimental setup is shown in Figure 14.

We imaged a cortical area of $4.6 \times 4.6 \text{ mm}^2$ by using a $135 \times 50 \text{ mm}$ tandem lens configuration (Nikon®, Inc., Melville, NY). The surface vascular pattern of the left visual cortex was visualized with illumination wavelengths set by a green ($550 \pm 2 \text{ nm}$) and intrinsic signal images set by a red ($610 \pm 2 \text{ nm}$) interference filter from a cold-light source (Zeiss KL2500 LCD). After acquisition of a surface image of blood vessels, the camera was focused $600 \mu\text{m}$ below the pial surface to make sure to record at least from cortical layer I-IV. We interposed an additional red filter between the mouse and the CCD camera. Frames were acquired at a rate of 30 Hertz temporally and then binned to 7.5 Hertz and stored as 512×512 pixel images after spatial binning of the camera image.

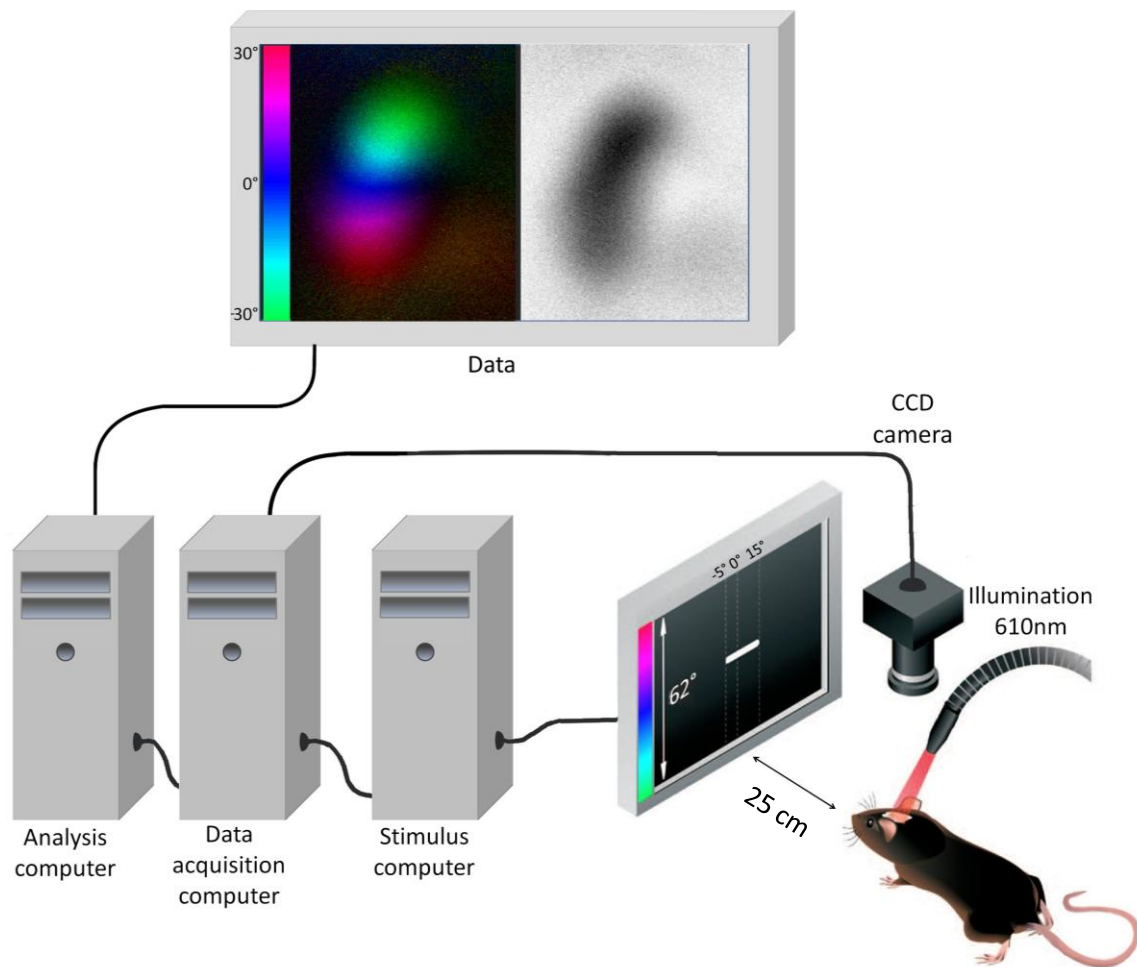


Figure 14: Experimental setup of optical imaging of intrinsic signals (Figure modified from Lehmann and Löwel, 2008, Greifzu *et al.*, 2012, and Sophia Stodieck). The imaging system consists of a flat-screen monitor showing a moving bar as a stimulus generated by the stimulus computer, a CCD camera, which acquires cortical responses after illumination of the visual cortex of 610 nm. The data were sent from the Data acquisition computer to the Analysis computer where they are extracted by Fourier analysis.

2.7 Visual stimuli

To display visual stimuli a high refresh rate monitor (Benq® BL240 (LED), 1920 x 1080, 60 Hertz) was placed in the right visual field of the animal at a distance of 25 cm to optimally stimulate the right eye (contralateral to the recorded hemisphere) (Figure 15 B).

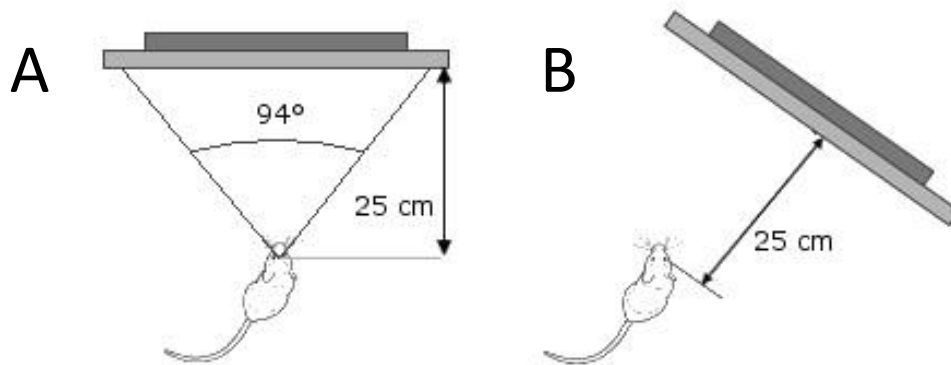


Figure 15: Position of the stimulus monitor (Figure modified from Kalatsky and Stryker, 2003). (A) For an optimal visual stimulation of both eyes (Cang *et al.*, 2005b) the monitor was placed 25 cm in front of the mouse. The width of the monitor constituted a visual angle of 94° . (B) To stimulate as much as possible of the visual cortex of the left hemisphere the monitor was placed 25 cm in front of the mouse's right eye with an angle of 45° .

Vertical ($90^\circ \uparrow$ and $270^\circ \downarrow$; referred to as elevation orientation) or horizontal drifting ($0^\circ \rightarrow$ and $180^\circ \leftarrow$; referred to as azimuth orientation) bars were generated by an ASUS EAH5450, controlled by custom software. The bars were 2° wide, corresponding to a spatial frequency of 0.25 cyc/deg. The bar had a speed of $10^\circ/\text{second}$ and appeared at a distance of 80° at a rate of 0.125 Hertz. One run consists of one direction ($90^\circ \uparrow$, $270^\circ \downarrow$, $0^\circ \rightarrow$ or $180^\circ \leftarrow$) and lasts for five minutes.

To test maximum response and map quality the drifting bars were shown across the full screen (94° azimuth and 62° elevation, respectively) (Figure 16 A,B).

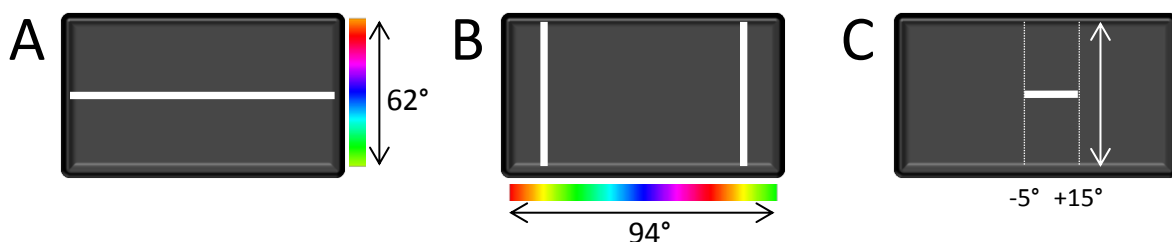


Figure 16: Visual stimuli. Visual stimuli to measure maximum response and map quality of elevation (A) and azimuth maps (B). The stimulus was a white moving bar of 2° . The monitor had a visual angle of 62° height (A) and 94° width (B). The position of the stimulus within the visual field was color-coded to check retinotopy. (C) To compare the cortical activity after the separate visual stimulation of the two eyes the vertical moving bar was restricted to 20° so just the binocular zone of the visual cortex was stimulated.

In respect of the hemodynamic delay (of about one to two seconds) the resulting map of one direction (for example $90^\circ \uparrow$) was only a map of relative retinotopy (Cang *et al.*, 2005b). Therefore we computed maps of absolute retinotopy by reversing the stimulus ($270^\circ \downarrow$), which leads to the reversal of the response sequence in which the delay is the same. The software subtracted the response time to the reversed stimulus ($270^\circ \downarrow$) from the response time to the direct one ($90^\circ \uparrow$) and computed an absolute response map without the hemodynamic delay (Cang *et al.*, 2005b). The same computation was done for maps resulting from the azimuth orientation ($0^\circ \rightarrow$ and $180^\circ \leftarrow$).

Next the monitor was placed 25 cm in front of the mouse (Figure 15 A) and vertical moving bars ($90^\circ \uparrow$ and $270^\circ \downarrow$) were restricted to stimulate only the binocular field of the left hemisphere (-5° to $+15^\circ$ azimuth) (Figure 16 C) and animals were stimulated through either the left or the right eye alternately to assess the ocular dominance of the recorded hemisphere.

Additionally, we assessed visual acuity of Bassoon mutant mice. Therefore we compared the response to the usually used 2° wide bar (~ 0.25 cyc/deg) with the response to a 1° wide bar (~ 0.5 cyc/deg). We quantified maximum response and map quality. We also measured the contrast sensitivity of Bassoon mutant mice and their littermates, dependent on the visual cortex using optical imaging of intrinsic signals. We used twelve different contrasts (100 %, 70 %, 60 %, 50 %, 40 %, 30 %, 25 %, 20 %, 15 %, 10 %, 5 % and 0 %). We also quantified maximum response and map quality.

2.8 Data Analysis

2.8.1 Maximum response and map quality

Maps were calculated from the acquired frames using Fourier analysis to extract the signal at the stimulation frequency using the custom software *iman* (image analysis; VK Imaging, Houston, Texas) (Kalatsky and Stryker, 2003) and the area of the visual cortex was cropped to 300×300 pixel with *mapans* (map analysis single; VK Imaging, Houston, Texas) and the signal of the activated region was normalized with respect to its surrounding background. Maps acquired with the stimulus bar moving up and down (elevation orientation) as well as left and right (azimuth orientation) were combined by *mapanm* (map analysis multiple; VK

Imaging, Houston, Texas) to an average map to correct the hemodynamic delay. The color-coded retinotopic phase map encodes the activated region in the visual cortex, by referring to a position of the stimulus bar on the stimulus monitor. The phase component of the signal is used for the calculation of retinotopy (retinotopic phase map, Figure 17 A). The amplitude component represents the intensity of neuronal activation expressed as fractional change in reflectance $\times 10^{-4}$ (raw magnitude respond map, Figure 17 B). The strongest pixel within the selected area of the visual cortex is set as the value of maximum response ($\times 10^{-4}$). Information of both the retinotopic phase map and the raw magnitude map are combined in the polar map (Figure 17 C).

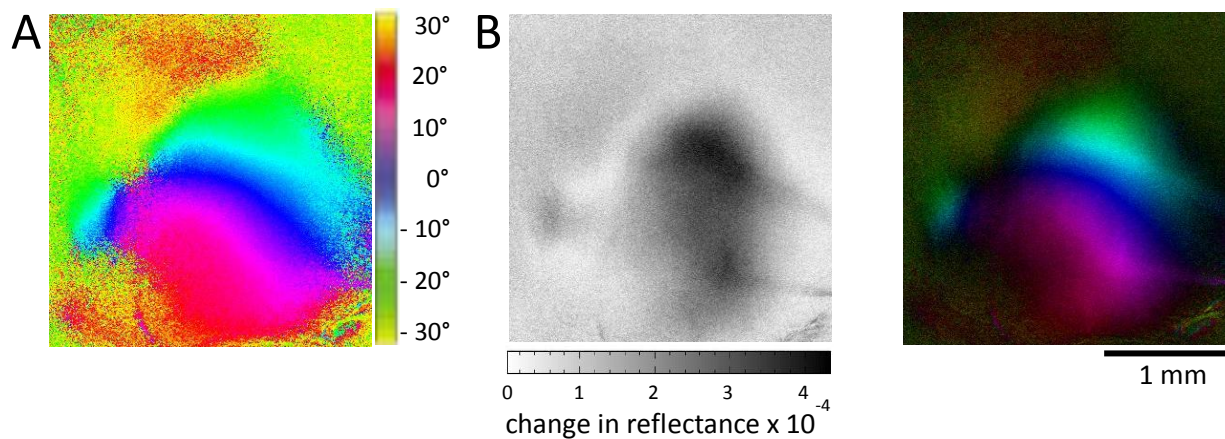


Figure 17: Maps of the left visual cortex after visual stimulation with a horizontal bar, acquired by optical imaging of intrinsic signals. (A) Retinotopic phase map with the color-code, which represents the position (in degree) of the bar on the monitor. **(B)** The raw magnitude respond map which indicates the activity of the visual cortex. The active area is visualized by dark colored pixel, the darker the pixel the higher the maximum response. The maximum response is specified as a change in reflectance $\times 10^{-4}$. **(C)** The polar maps combine the information of both the color-coded phase map **(A)** and the maximum response map **(B)**.

To assess the quality of retinotopic maps, we used the calculation introduced by Cang (Cang *et al.*, 2005a). Both the elevation and azimuth maps were used to select the most responsive 20,000 pixels in the visual cortex. For every pixel, the difference between its position and the mean position of its 25 surrounding pixels was calculated. For maps of high quality, the position differences are very small based on smooth progression. The standard deviation of the position difference was then used as an index of the quality of retinotopic maps with small values indicating high map quality and high values indicating low map quality (Cang *et al.*, 2005b). To calculate map area, magnitude maps were thresholded at 30 % of peak

amplitude, and the area of all selected pixels (1 pixel = $7.9 \times 10^{-5} \text{ mm}^2$) was summed up. The maximum cortical responses to visual stimuli of different contrasts were fitted by a 2nd order polynomial curve.

2.8.2 Ocular dominance index

To quantify ocular dominance (OD) plasticity, an OD score of each pixel in the binocularly activated region was calculated as $\frac{C-I}{C+I}$, with C and I representing the raw response magnitudes of each pixel to visual stimulation of the contralateral (C) and ipsilateral (I) eye, respectively (Figure 18 A). Then an OD index (ODI) as the average of the OD scores of all responsive pixels was computed. Consequently, the ODI ranged from - 1 to + 1, with negative values representing ipsilateral and positive values representing contralateral eye dominance.

We calculated ODIs from blocks of four runs in which the averaged maps for each eye had at least a response magnitude of 1.0×10^{-4} . Typically, we obtained three to five ODIs per animal; experiments with fewer than three ODIs were discarded from further analyses. All ODIs of one animal were averaged for further quantification and data display. The ODIs were color-coded in a 2-D map of the OD scores (OD map): cold blue colors represent negative values (ipsilateral eye dominance) and warm red colors represent positive values (contralateral eye dominance) (Figure 18 C).

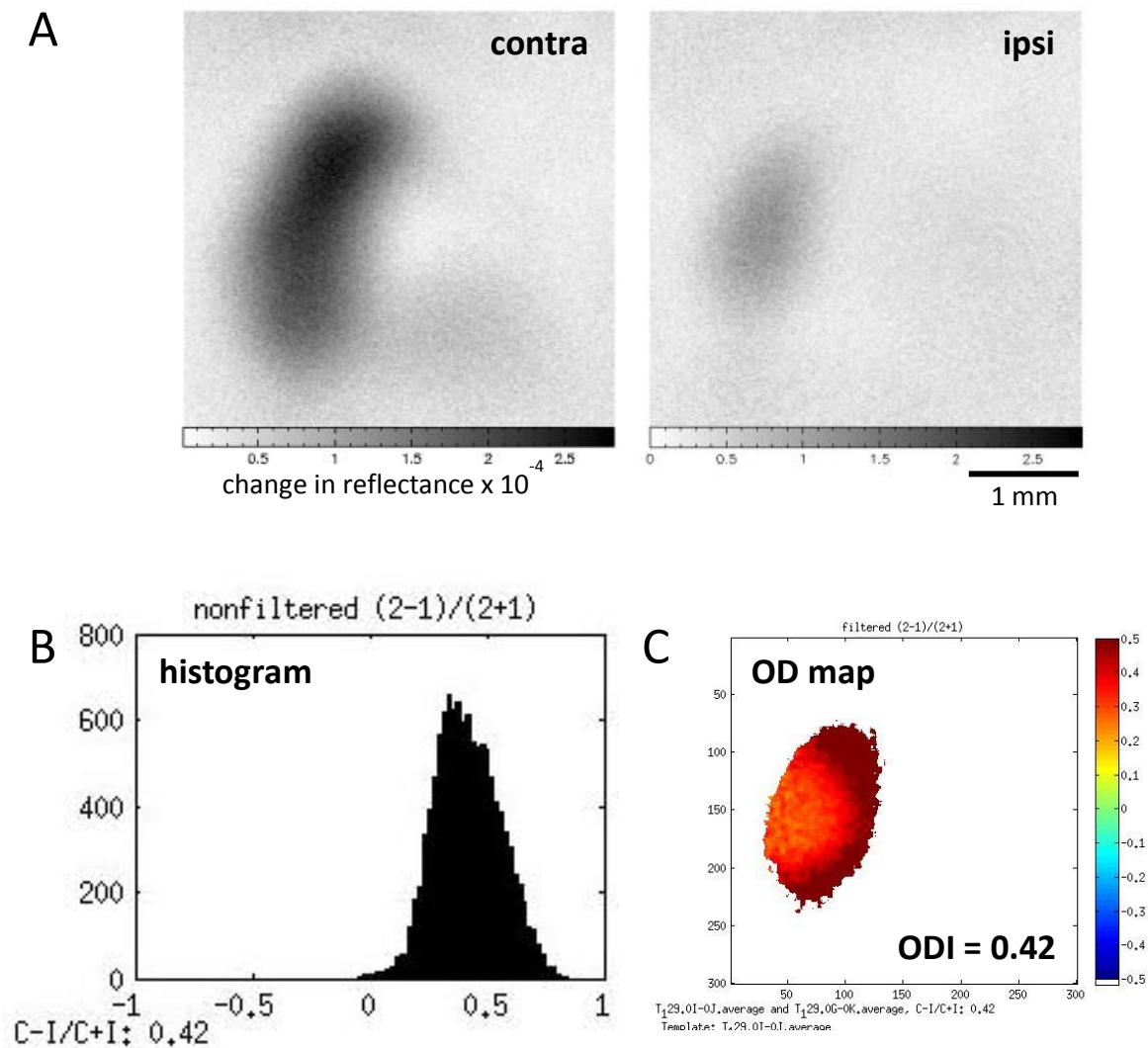


Figure 18: Quantification of the ocular dominance index. (A) The maximum response maps of the left visual cortex after visual stimulation (with a 20° horizontal bar) of the contralateral (left) and the ipsilateral eye (right), respectively. The response is restricted to the binocular zone. (B) Histogram of the single OD scores and their distribution in number of pixel. The ocular dominance index, the average of all single OD scores calculated from the maximum response maps (A) of contra (C) and ipsi (I), are shown in the left corner of the histogram. (D) The calculation of OD scores for every pixel. The pixel are color-coded while cold colored pixel (e.g. blue, green) represent a ocular dominance in the binocular zone of the visual cortex of the ipsilateral eye whereas warm colored pixel (e.g. yellow, red) represent a ocular dominance of the contralateral eye. (Abbreviations: OD = ocular dominance, contra/C = contralateral eye, ipsi/I = ipsilateral eye)

2.9 Immunohistochemistry

2.9.1 Parvalbumin (PV), the potassium voltage-gated channel Kv3.1b and brain derived neurotropic factor (BDNF)

After optical imaging of intrinsic signals, Bsn^{-/-} and Bsn^{+/+} animals were deeply anaesthetized with an injection in the abdominal cavity (intraperitoneally) of 0.3 ml 30 %

chloral hydrate. After checking the depth of the anesthesia with the toe-pinch test, the thoracic cavity was opened to expose the heart. A cannula was inserted into the left ventricle and then the right atrium was cut open. The following perfusion of the animal was done with 50 ml 0.9 % saline including 0.05 ml heparin for two minutes (pump output of 25 ml/min) to flush the blood out of the tissue. Then the mouse was fixed with 75 ml 4 % paraformaldehyde (PFA) in 0.9 % saline for three minutes using a perfusion pump (MC-MS CA8/6, Ismatec, Glattbrugg-Zürich, Switzerland) (pump output of 25 ml/min). Afterwards the brain was removed quickly and placed in 4 % PFA at 4 °C overnight to postfix the brain tissue. Brains were then stored in 1 % PFA including 0.05 % of the biocide sodium azide (to avoid growth of microorganisms) at 4 °C. For cryoprotection, the brains were stored in in 0.1 molar phosphate buffer (PB) containing 10 % sucrose, 20 % glycerol, and 0.02 % sodium azide at 4 °C for 48 hours. Afterwards the brains were cut in frozen state using dry ice in sections of 40 µm with a sliding microtome (©Leica SM 2010R). Coronal brain sections from the visual cortex (2.5 mm - 3.5 mm; bregma; approximately every 160 µm) were used. Four brain slices (free floating) were placed in one well containing 2 ml of 0.1 molar PB. For preincubation PB was extracted with a Pasteur pipette and replaced with 500 µl normal serum (10 % normal donkey serum in 0.1 molar PB including 0.3 % Triton X-100 and 0.02 % sodium azide) for 30 minutes at room temperature on a shaking device. Afterwards, the brain sections were washed three times for five minutes respectively with 0.2 ml PB (0.1 molar) per well on the shaking device at room temperature. Subsequently the slices were incubated for 72 hours at 4 °C with primary antibodies. First we stained the calcium-binding albumin protein parvalbumin (PV) which is present in GABAergic interneurons and the neurotrophin brain-derived neurotrophic factor (BDNF) and second we stained PV and the potassium channel Kv3.1b, which might be present only in parvalbumin-containing interneurons (Chow *et al.*, 1999). We used mouse anti-PV (dilution 1:500) and rabbit anti-BDNF (dilution 1:200) or rabbit anti-Kv3.1b (dilution 1:50) in 0.1 molar PB including 0.3 % Triton X-100 and 0.02 % sodium azide and applied 400 µl in total per well. After washing the primary antibodies off (three times for five minutes with 2 ml 0.1 molar PB per well), the slices were incubated with the secondary antibodies covered with lightproof aluminum foil for two hours at room temperature on a shaking device. The antibodies were donkey anti-mouse (Cy2) (dilution 1:100) and donkey anti-rabbit (Cy3) (dilution 1:100) in 0.1 molar PB including 0.3 % Triton X-100 and 0.02 % sodium azide (in total 400 µl per well). The secondary antibodies

were washed off with PB three times with 2 ml PB for five minutes (lightproof). During the last washing step the sections were additionally stained with 2 μ l of 4',6-Diamidin-2-phenylindole (DAPI) (dilution 1:1,000,000) in PB (0.1 molar) per well for five minutes on a shaking device to visualize all cell nuclei. Afterwards, all brain sections were transferred to microscope slide and dried for 30 minutes (lightproof). Finally, the dried sections were mounted with fluoromount and a glass cover slip has been applied. After drying overnight stored in a lightproof box at 4 °C, the slides were cleaned with 70 % ethanol to remove any residue.

The sensitivity and specificity of our immunohistochemical stainings are shown in Figure 19.

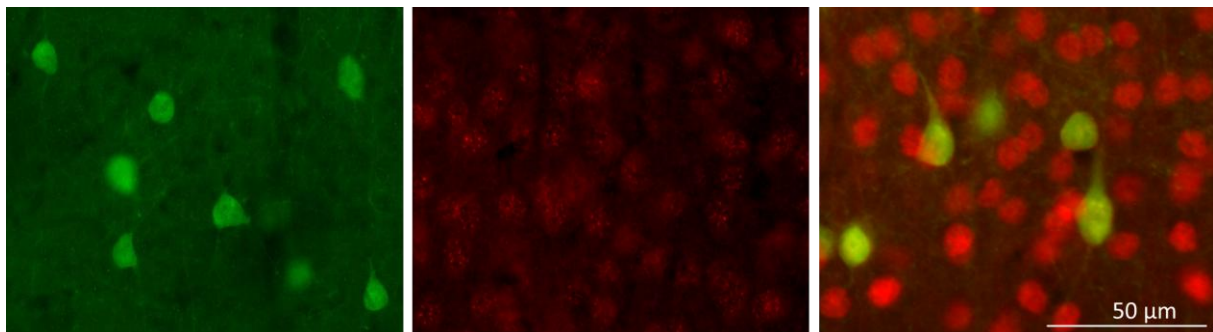


Figure 19: Sensitivity of used antibodies of parvalbumin/Cy3 in green (left), BDNF/Cy2 in red (middle) and parvalbumin/Cy3 in green (right) as well as Kv3.1b/Cy2 in red (right). Parvalbumin was stained to detect parvalbumin positive fast-spiking interneurons in the visual cortex of mice and the potassium channel Kv3.1b might only be present in these interneurons (Chow *et al.*, 1999) and therefore also show silent/inactive interneurons. BDNF in the VC was stained using immunohistochemistry to verify the data from Heyden (2011) of a highly elevated cortical level of BDNF in Bsn^{-/-} mice (measured with ELISA).

2.9.2 Microscopy and analyses

The stained brain sections were examined with a fluorescence microscope (Zeiss Axioskop 50). To quantify the number of parvalbumin positive and Kv3.1b positive cells, and to quantify the intensity of BDNF, the area of interest (visual cortex) was determined by visualizing the cell nuclei with DAPI fluorescence staining to define layers I, II/III and IV in the visual cortex. We focused the area of interest to cortical layers II-IV, which were then recorded using AxioVision 4.8. (Zeiss) with a 20x objective (magnification 200 fold).

Several studies showed that ocular dominance plasticity beyond the critical period in mice (Lehmann and Löwel, 2008) and other animals mostly occurs in superficial cortical layers

(Daw *et al.*, 1992; Pham *et al.*, 2004; Tagawa *et al.*, 2005). In this study we captured images of the visual cortex of layers II-IV like recently published by Beurdeley and colleagues who performed immunohistochemical stainings of parvalbumin in the visual cortex of mice (Beurdeley *et al.*, 2012). Numerous studies could also show that adult somatosensory cortical plasticity involves horizontal connections of neurons in cortical layers II/III, and developmental plasticity involves thalamic inputs to cortical layer IV (Fox, 1992; Diamond *et al.*, 1994; Skibinska *et al.*, 2000; Pham *et al.*, 2004).

For each section we took three images of the visual cortex of each hemisphere, which display cortical layers II-IV defined by DAPI staining. For every region (01 - 06, indicated with red squares in (Figure 20) we took images of DAPI staining (exposure 50 milliseconds), PV staining (exposure two seconds) and BDNF (exposure 450 milliseconds) or Kv3.1b staining (exposure 60 milliseconds), respectively.

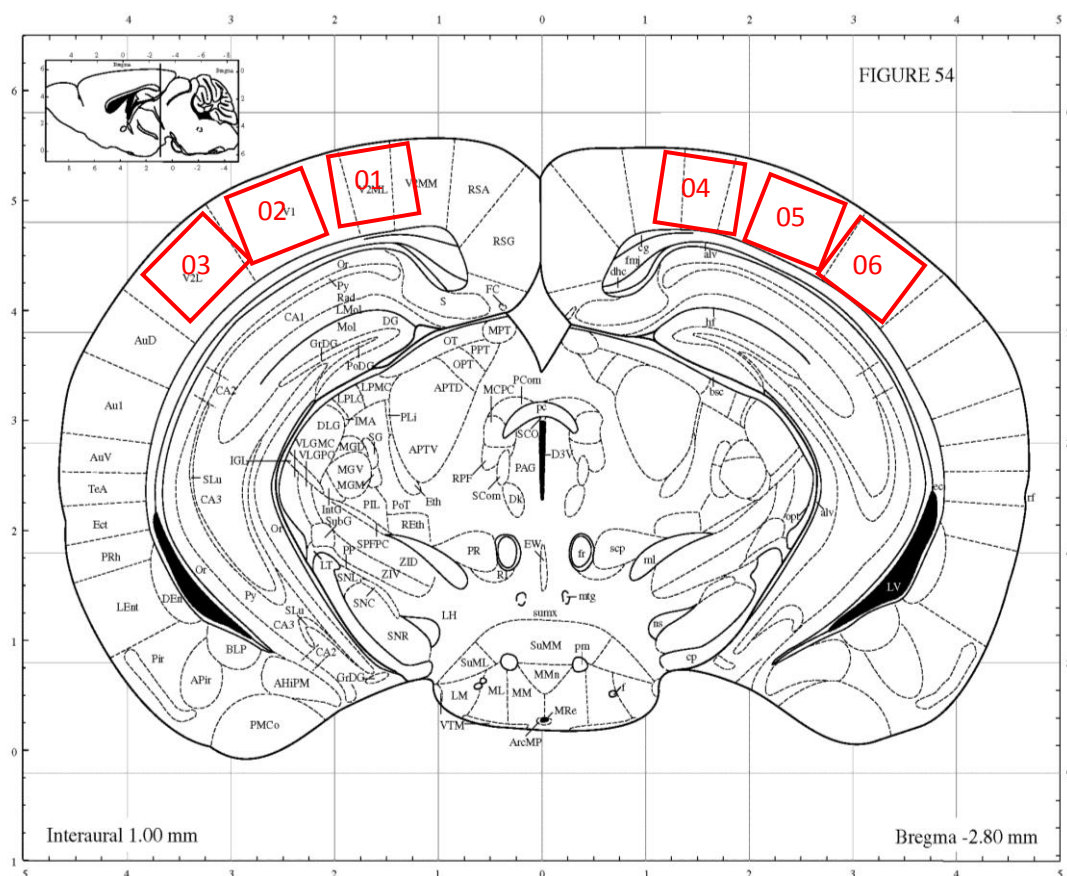


Figure 20: Regions of interest in the visual cortex of a coronal mouse brain section (Figure modified from Paxinos and Franklin, 2003). The six different regions of interest within the visual cortex are marked with red squares (01 - 06), indicating the images used for counting cells. Three pictures from cortical layers II-IV of each hemisphere were taken.

The recorded images with a size of 335.64 μm x 448.38 μm and spanning cortical layers II/III and IV were analyzed using ImageJ (Wayne Rasband, NIH).

The background brightness, taken from a non-stained region of the cortex (*e.g.* the inside of a blood vessel) was subtracted from the brightness measurement to reduce noise. The counting area was kept constant throughout the experiment. We quantified the total amount (not just in the focal plane) of specifically stained cells for PV and Kv3.1b per mm^2 in the visual cortex using the particle analysis cell counter function. To quantify the intensity of BDNF we selected 50 random cells and the fluorescence was measured by ImageJ 1.41d. To compare these relative values of wild-type animals with their Bassoon mutant littermates we set the average of all values of wild-type mice of one group to 100 % and calculated the difference between the two genotypes in percent.

2.10 Chemicals

Table 1: Chemicals

chemicals	company (order number)
1 st antibody mouse anti-PV	Immunological Sciences (MAB-10233)
1 st antibody rabbit anti-BDNF	Immunological Sciences (MAB-10502)
1 st antibody rabbit anti-Kv3.1b	Immunological Sciences (MAB-10722)
2 nd antibody donkey anti-mouse (Cy2)	Jackson ImmunoResearch (715-225-150)
2 nd antibody donkey anti-rabbit (Cy3)	Jackson ImmunoResearch (711-165-152)
4',6-Diamidin-2-phenylindole dihydrochloride (DAPI)	Sigma (D9542)
Agarose	Biomol (1280)
Atropinsulfat (atropine sulfate)	Dr. Franz Köhler Chemie (PZN: 1821288)
Chloral hydrate	Sigma (15307)
Chlorprothixene hydrochloride	Sigma (C1671)
Corneregel® Fluid (eye drops)	Bausch & Lomb
Dexa-ratiopharm® (dexamethasone)	ratiopharm GmbH (PZN: 7720996)
Diazepam 10MG-Rotexmedica (diazepam)	Rotexmedica GmbH (PZN: 3731425)
di-Sodium hydrogen phosphate (Na ₂ HPO ₄)	Roth (P030.2)
Ethanol 70 % denatured	Roth (T913.3)
Fluoromount™	Sigma (F4680-25ML)
glycerol	Roth (3783.1)
halothane	Sigma (B4388)
Heparin (25.000 I.E.)	Rotexmedica GmbH (PZN: 3862340)
normal donkey serum	Jackson ImmunoResearch (017-000-121)
Paraformaldehyde (PFA)	Roth (0335.3)

Refobacin (gentamicin sulfate)	Merck KGaA
Rimadyl® (carprofen)	Pfizer (approval number: 400684.00.00)
saline (NaCl, 0.9 % solution for injection)	B. Braun Melsungen AG
Silicone oil M 20.000	Roth (4060.1)
Sodium azide (NaN ₃)	Roth (K305.1)
Sodium chloride (NaCl)	Roth (3957.1)
Sodium dihydrogen phosphate dihydrate (NaH ₂ PO ₄ x 2H ₂ O)	Roth (T879.2)
sodium hydroxide (NaOH)	VWR (28.244.262)
D(+)-Saccharose (sucrose, C ₁₂ H ₂₂ O ₁₁)	Roth (4621.1)
Triton X-100	Sigma (X100)
Xylocain® Gel 2 % (lidocaine hydrochloride)	AstraZeneca GmbH

2.11 Solutions

Table 2: Solutions

solutions	recipe
agarose (2.5 %)	5 g Agarose add 200 ml 0.9 % saline (NaCl) heat up until boiling and suspension is clear
chloral hydrate	30 g Chloral hydrate add 100 ml aqua bidest.
chlorprothixene	4 mg Chlorprothixene add 1 ml aqua bidest.
cryoprotection	10 g D(+)-Saccharose 20 ml glycerol 0.02 g Sodium azide add 0.1 molar PB to a total volume of 100 ml
diazepam	2 ml Diazepam 10MG-Rotexmedica add 0.9 % saline (NaCl) to a total volume of 40 ml
phosphat buffer (PB) (0.1 molar, ph 7.4)	3.75 g $\text{NaH}_2\text{PO}_4 \times 2\text{H}_2\text{O}$ 9.75 g Na_2HPO_4 add aqua bidest. to a total volume of 1 liter
paraformaldehyde (PFA) (4%, pH 7.4)	40 g paraformaldehyde add 300 ml aqua bidest. heat to ~ 60 °C until suspension is clear (if not, add six to eight drops of 10 molar NaOH) filter solution, adjust to pH 7.4 and cool it down add aqua bidest. to a total volume of 1 liter
paraformaldehyde (PFA) (1%, pH 7.4) with sodium azide	40 g Paraformaldehyde add 300 ml aqua bidest. heat to ~ 60 °C until suspension is clear (if not, add six to eight drops of 10 molar NaOH) filter solution, adjust to pH 7.4 and cool it down 0.50 g Sodium azide add aqua bidest. to a total volume of 1 liter
saline (NaCl) (0.9 %, pH 7.0)	0.9 g NaCl add 1 liter aqua bidest.
heparin in saline (NaCl) (1%)	53.33 ml Heparin (25.000 I.E.) 0.9 g NaCl add aqua bidest. to a total volume of 1 liter

2.12 Statistical analyses

All inter-group comparisons were done by Student's t-test using Microsoft Excel 2010 and SPSS (20.0.0). Data were for normal distribution with the Anderson–Darling test. In analyses in which a within-subject factor was present (*i.e.*, age or spatial frequency), a two-way analysis of variance (ANOVA) with repeated measurements was performed. The levels of significance were set as *: $p < 0.05$; **: $p < 0.01$; ***: $p < 0.001$. Data are represented as means \pm standard error of mean (s.e.m.).

3.A Results of Bassoon mutant mice

3.1 Visual acuity

3.1.1 Virtual-reality optomotor system

A large part of these data were already published in Goetze *et al.*, 2010b.

We tested 25 Bsn^{+/+} and 27 Bsn^{-/-} mice with the virtual-reality optomotor system (Prusky *et al.*, 2004) to determine their visual acuity. We measured both eyes independently.

The visual acuity of wild-type Bsn^{+/+} animals (age 40 to 148 days) was 0.391 ± 0.003 cyc/deg for the left and 0.391 ± 0.003 cyc/deg for the right eye. In contrast, visual acuity of Bassoon mutant mice (age 32 to 121 days) was only 0.215 ± 0.002 cyc/deg for the left eye and 0.215 ± 0.002 cyc/deg for the right eye. Since there were no differences between values of left and right eyes for both Bsn^{+/+} and Bsn^{-/-} mice (t-test, $p > 0.05$ for both comparisons) we averaged values across eyes for both genotypes. Average visual acuity of wild-type Bsn^{+/+} mice was 0.391 ± 0.003 cyc/deg compared to 0.215 ± 0.002 cyc/deg in mutant Bsn^{-/-} animals (Figure 21 A).

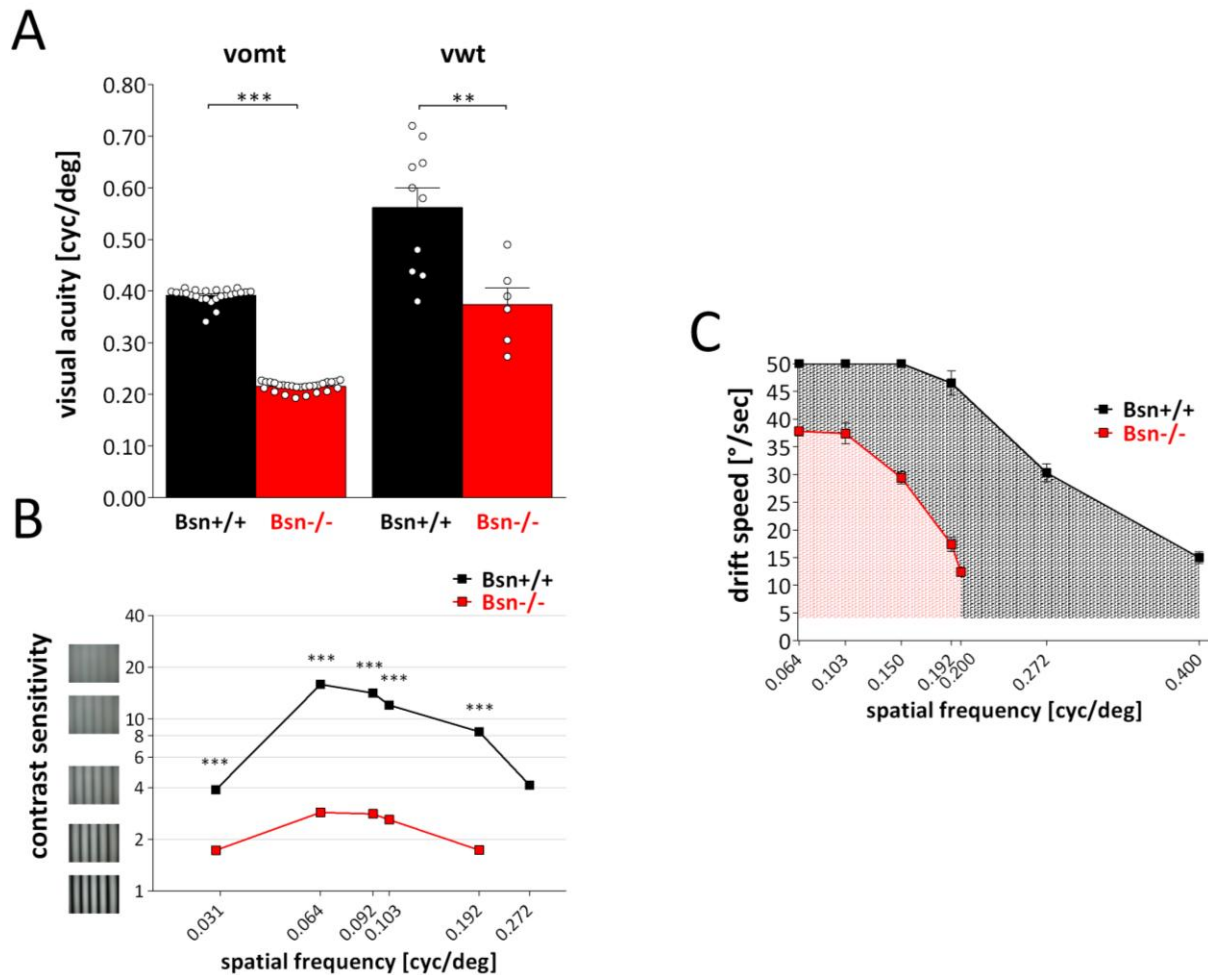


Figure 21: Visual acuity, contrast sensitivity, and temporal resolution of Bsn+/+ and Bsn-/- mice measured with both the virtual-reality optomotor system (vomt) and the visual water task (vwt) (Figure modified from Goetze *et al.*, 2010b). (A) Spatial frequency selectivity plotted in cycles per degree (cyc/deg). Left: Visual acuity of Bsn+/+ mice (black) (n = 25) was 0.391 ± 0.003 cyc/deg compared to 0.215 ± 0.002 cyc/deg in Bsn-/- mice (red) (n = 27). The difference in visual acuity was statistically significant (t-test, $p < 0.001$). Right: Visual acuity of Bsn+/+ mice (black) (n = 10) was 0.562 ± 0.038 cyc/deg compared to 0.374 ± 0.032 cyc/deg in Bsn-/- mice (red) (n = 6). The difference in visual acuity was statistically significant (t-test, $p < 0.01$). The difference in visual acuity between Bsn-/- and Bsn+/+ mice was similar in both behavioral tasks: 0.18 cyc/deg in the virtual-reality optomotor system and 0.19 cyc/deg in the visual water task. (B) Contrast sensitivity plotted as a function of spatial frequency in cycles per degree (cyc/deg). Contrast sensitivity of Bsn-/- mice animals (red) (n = 27) was reduced by a factor of 2 to 6 compared to their Bsn+/+ littermates (black) (n = 25). Maximal contrast sensitivity was 2.9 ± 0.04 (corresponding to 35 % contrast) in Bsn-/- compared to 15.9 ± 0.73 (corresponding to 7 % contrast) in Bsn+/+ mice at the spatial frequency of 0.064 cyc/deg. At all spatial frequencies, contrast sensitivity was significantly different between the two genotypes (t-test, $p < 0.001$ for all comparisons). (C) Temporal resolution plotted drift speed in degree/second (°/sec) as a function of spatial frequency in cycles per degree (cyc/deg). Bassoon wild-type (black) (n = 4) and mutant animals (red) (n = 5) started to respond at drift speeds of about 3.4-3.5 °/sec. At the spatial frequencies of 0.064, 0.103 and 0.150 cyc/deg, all Bsn+/+ mice showed tracking up to a drift speed of 50 °/sec. For technical reasons we were not able to measure vision at drift velocities higher than 50 °/sec, so that our plot is, therefore, truncated. With increasing spatial frequency the highest stimulus velocity at which tracking could be observed decreased down to 15.0 ± 1.08 °/sec at 0.400 cyc/deg. In contrast, Bsn-/- mice had lower temporal resolution: at a spatial frequency of 0.064 cyc/deg, all Bsn-/- mice tracked the moving grating up to a speed of 37.8 ± 0.80 °/sec. With increasing spatial frequency the highest stimulus velocity at which we observed tracking decreased to 12.4 ± 0.81 °/sec at 0.200 cyc/deg. Temporal resolution was significantly different between Bsn+/+ and Bsn-/- mice (ANOVA, $p < 0.001$).

The difference in visual acuity between Bsn^{+/+} and Bsn^{-/-} mice was significant (Figure 21 A) (t-test, $p < 0.001$). Hence Bsn^{-/-} animals showed a decrease in visual acuity about 0.18 cyc/deg compared to their wild-type littermates. Visual acuity of Bsn^{+/+} mice was thus similar as previously described for C57Bl/6J wild-type mice (Prusky *et al.*, 2004).

3.1.2 Visual water task

A large part of these data were already published in Goetze *et al.*, 2010b.

We trained ten Bsn^{+/+} and six Bsn^{-/-} mice in the visual water task (Prusky *et al.*, 2000), a cortex-dependent paradigm of visual discrimination learning, to assess visual acuity (age 60 to 220 days). In this test visual acuity was measured for both eyes together. Visual acuity of Bsn^{+/+} mice was 0.562 ± 0.038 cyc/deg compared to littermate Bsn^{-/-} mice with 0.374 ± 0.032 cyc/deg (Figure 21 A).

Thus Bsn^{-/-} mice reached only $\frac{2}{3}$ of the visual acuity values of their wild-type littermates in this visual discrimination task. The difference in visual acuity between Bsn^{+/+} and Bsn^{-/-} animals was significant (Figure 21 A) (t-test, $p < 0.01$). While the absolute values of visual acuity in the visual water task were thus significantly higher than those measured in the virtual-reality optomotor system for both genotypes (t-test, $p < 0.001$ for both comparisons), the difference between Bsn^{+/+} and Bsn^{-/-} mice was similar in both behavioral tasks: 0.19 cyc/deg in the visual water task and 0.18 cyc/deg in the virtual-reality optomotor system. It was recently described for C57Bl/6J mice that visual acuity measured in the visual water task is consistently higher than in the optomotor task (visual water task: 0.5 - 0.6 cyc/deg (Prusky *et al.*, 2000), virtual-reality optomotor system: 0.4 cyc/deg (Prusky *et al.*, 2004).

3.2 Contrast sensitivity

A large part of these data were already published in Goetze *et al.*, 2010b.

Contrast sensitivity values of 25 Bsn^{+/+} and 27 Bsn^{-/-} mice were measured in the optomotor setup and plotted as a function of spatial frequency. Contrast was measured at six different spatial frequencies: 0.031 cyc/deg, 0.064 cyc/deg, 0.092 cyc/deg, 0.103 cyc/deg, 0.192 cyc/deg, and 0.272 cyc/deg independently for both eyes but since there were no

differences between values of left and right eyes for both Bsn^{+/+} and Bsn^{-/-} mice (t-test, $p > 0.05$ for both comparisons) we averaged values across eyes for both genotypes.

At a spatial frequency of 0.031 cyc/deg Bsn^{+/+} mice had a contrast sensitivity of 3.9 ± 0.08 , at 0.064 cyc/deg 15.9 ± 0.73 , at 0.092 cyc/deg 14.2 ± 0.63 , at 0.103 cyc/deg 12.0 ± 0.54 , at 0.192 cyc/deg 8.5 ± 0.35 , and at 0.272 cyc/deg 4.1 ± 0.14 . The semilog plot (Figure 21 B) revealed a sickle shaped curve. Contrast sensitivity of Bsn^{+/+} mice was thus similar as previously described for C57Bl/6J wild-type mice (Prusky *et al.*, 2004).

In contrast, at a spatial frequency of 0.031 cyc/deg Bsn^{-/-} mice had a contrast sensitivity of 1.7 ± 0.04 , at 0.064 cyc/deg 2.9 ± 0.04 , at 0.092 cyc/deg 2.8 ± 0.06 , at 0.103 cyc/deg 2.6 ± 0.06 , and at 0.192 cyc/deg 1.7 ± 0.04 . Since their visual acuity did not reach values of 0.272 cyc/deg it was not possible to measure contrast sensitivity at this value. The semilog plot (Figure 21 B) revealed a diminished sickle shaped curve compared to Bsn^{+/+} animals.

Hence, contrast sensitivity of Bsn^{+/+} animals was clearly superior to the performance of Bassoon mutant mice. Statistical analyses confirmed that genotype had an impact on contrast sensitivity that was significant (ANOVA, $F_{1,49} = 396.59$, $p < 0.001$). Between both genotypes contrast sensitivity was different at all spatial frequencies (t-test, $p < 0.001$ for all comparisons). The difference of contrast sensitivity in wild-type animals was significant between all spatial frequencies (t-test, $p < 0.001$ for all comparisons), except between 0.031 cyc/deg and 0.272 cyc/deg. In mutant animals, the difference of contrast sensitivity values were significant between all spatial frequencies (ANOVA, $p < 0.001$ for all comparisons), with the exceptions of 0.031 vs. 0.192 cyc/deg and 0.064 vs. 0.092 cyc/deg.

Curves of contrast sensitivity peaked at a spatial frequency of 0.064 cyc/deg for both Bsn^{+/+} and Bsn^{-/-} mice, as previously described for C57Bl/6J mice (Prusky *et al.*, 2004). The maximum deviation (six fold) was measured at a spatial frequency of 0.064 cyc/deg. Bsn^{-/-} mice had a contrast sensitivity of 2.9 ± 0.04 (corresponding to 35 % contrast), while Bsn^{+/+} littermates had a contrast sensitivity of 15.9 ± 0.73 (or 7 % contrast) (Figure 21 B). Whereas at a spatial frequency of 0.031 cyc/deg, the contrast sensitivity values for Bsn^{-/-} mice were 1.7 ± 0.04 (corresponding to 59 % contrast) and for Bsn^{+/+} littermates 3.9 ± 0.08 (or 26 % contrast) and therefore only two fold higher (Figure 21 B). Thus contrast sensitivity in Bsn^{-/-} mice was reduced by a factor of two to six (at the different spatial frequencies) compared to

Bsn^{+/+} littermates indicating that Bsn^{-/-} mice need two to six fold higher contrasts of visual stimuli to trigger the optomotor reflex.

3.3 Temporal resolution

A large part of these data were already published in Goetze *et al.*, 2010b.

To test whether the visual deficit of the Bsn^{-/-} mice lies more in the spatial or in the temporal domain, we tested – for certain spatial frequencies – the maximum temporal frequency that still evoked a tracking response in the optomotor system. Therefore drift speeds of four Bsn^{+/+} and five Bsn^{-/-} mice were tested in the optomotor setup at different spatial frequencies: 0.064 cyc/deg, 0.103 cyc/deg, 0.150 cyc/deg, and 0.192 cyc/deg. In addition, we measured Bsn^{+/+} mice at 0.272 cyc/deg and 0.400 cyc/deg and Bsn^{-/-} mice at 0.200 cyc/deg. Due to technical reasons we were not able to measure drift speeds higher than 50 °/sec. Since there were no differences between values of left and right eyes for both Bsn^{+/+} and Bsn^{-/-} mice (t-test, $p > 0.05$ for both comparisons) we averaged values across eyes for both genotypes.

Bsn^{+/+} animals started tracking at a drift velocity of 3.5 ± 0.29 °/sec at all spatial frequencies (Figure 21 C). At 0.064 cyc/deg, 0.103 cyc/deg and 0.150 cyc/deg, all Bsn^{+/+} mice showed tracking at 50 °/sec, which is the technical speed limit of our system (Figure 21 C). With increasing spatial frequency, starting at a spatial frequency of 0.192 cyc/deg, the highest stimulus velocity at which we observed tracking decreased constantly (ANOVA, $F = 137.07$, $p < 0.001$). At a spatial frequency of 0.192 cyc/deg Bsn^{+/+} mice showed tracking at 46.5 ± 2.18 °/sec, at 0.272 cyc/deg 30.3 ± 1.65 °/sec, and at 0.400 cyc/deg up to 15.0 ± 1.08 °/sec (Figure 21 C).

Bsn^{-/-} animals started tracking from a drift speed of 3.4 ± 0.25 °/sec at all spatial frequencies (Figure 21 C), which was not significantly different from the value measured in Bsn^{+/+} mice (t-test, $p > 0.5$). The highest drift speed at which Bsn^{-/-} mice could track was dependent on spatial frequency (ANOVA, $F = 83.88$, $p < 0.001$), and peaked at 37.8 ± 0.80 °/sec for a 0.064 cyc/deg grating (Figure 21 C). With increasing spatial frequency, the highest stimulus velocity at which we observed tracking also decreased constantly (ANOVA, $p < 0.001$). At a spatial frequency of 0.103 cyc/deg Bsn^{-/-} mice showed tracking at 37.4 ± 1.89 °/sec, at

0.150 cyc/deg 29.4 ± 1.08 °/sec, and at 0.192 cyc/deg 17.4 ± 1.29 °/sec (Figure 21 C). At the visual acuity limit of 0.200 cyc/deg, the maximum drift speed of Bsn^{-/-} mice was 12.4 ± 0.81 °/sec. Statistical analyses showed that temporal resolution across spatial frequencies was significantly different between Bsn^{+/+} and Bsn^{-/-} mice (ANOVA, $p < 0.001$, $F_{1,7} = 639.535$).

3.4 Development of visual function

3.4.1 Visual acuity

A large part of these data were already published in Goetze *et al.*, 2010b.

We followed visual acuity longitudinally in six juvenile Bsn^{-/-} animals and their littermates (15 Bsn^{+/-} and 16 Bsn^{+/+} mice) from the day of eye opening (P13 to P15) throughout visual development until P42 (Figure 22 A; Table 3) measured by the virtual-reality optomotor system. Since there were no differences between values of left and right eyes for Bsn^{+/+}, Bsn^{+/-}, and Bsn^{-/-} mice (t-test, $p > 0.05$ for all comparisons) we averaged values across eyes for both genotypes.

Visual acuity development of Bsn^{+/+} and Bsn^{+/-} mice was nearly identical and will be described first. At P13, average grating acuity of Bsn^{+/+} and Bsn^{+/-} mice was 0.045 ± 0.011 cyc/deg ($n = 11$) and 0.039 ± 0.011 cyc/deg ($n = 10$), respectively (Figure 22 A; Table 3).

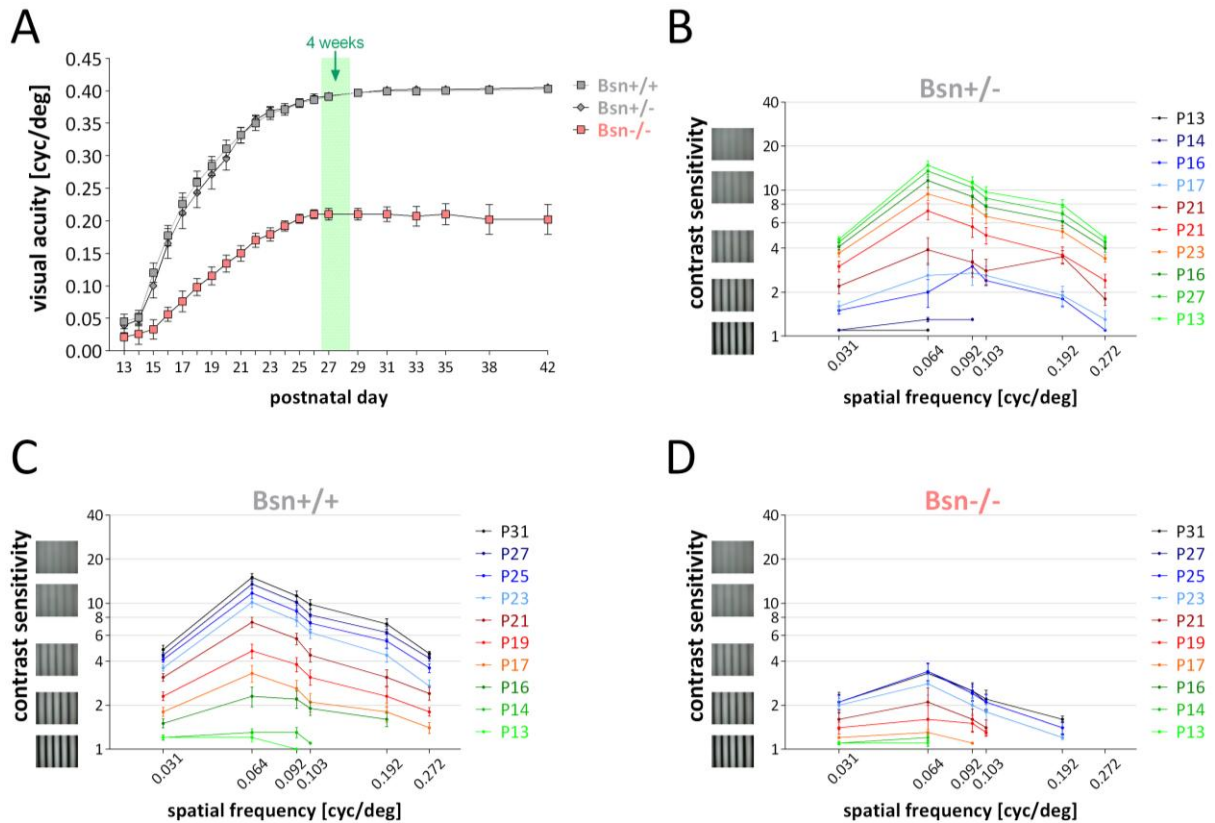


Figure 22: Development of both visual acuity and contrast sensitivity from eye opening throughout visual development in Bassoon mutant mice ($Bsn^{-/-}$, $n = 6$) and their heterozygous ($Bsn^{+/-}$, $n = 15$) and wild-type ($Bsn^{+/+}$, $n = 16$) littermates (Figure modified from Goetze *et al.*, 2010b). (A) Spatial frequency selectivity of the optokinetic response in cycles per degree (cyc/deg) plotted against postnatal days. At P13, average visual acuity of both $Bsn^{+/+}$ (gray square) and $Bsn^{+/-}$ mice (gray diamond) was 0.045 ± 0.011 cyc/deg and 0.039 ± 0.011 cyc/deg. Visual acuity increased rapidly over the following ten days and reached adult values of 0.397 cyc/deg at P29. In contrast, average visual acuity of $Bsn^{-/-}$ mice (pink) was only 0.021 ± 0.021 cyc/deg at P13, but also increased rapidly during the following ten days, and reached adult values of 0.203 ± 0.003 cyc/deg at P25. Development of visual acuity was significantly different between $Bsn^{+/+}$ and $Bsn^{-/-}$ mice (ANOVA, $p < 0.001$) and between $Bsn^{+/-}$ and $Bsn^{-/-}$ mice (ANOVA, $p < 0.001$) but not between $Bsn^{+/+}$ and $Bsn^{+/-}$ mice. (B-D) Contrast sensitivity plotted as a function of spatial frequency in cycles per degree (cyc/deg) at different days of age during development. Between P16 and P17, 0.064 cyc/deg emerged as the spatial frequency with the highest contrast sensitivity and remained at the peak of the curves at all subsequent ages in all three genotypes. Contrast sensitivity increased as the mice aged. (B,C) The development of contrast sensitivity in $Bsn^{+/-}$ and $Bsn^{+/+}$ animals is nearly identical: adult-like values are reached at P31. (D) In $Bsn^{-/-}$ mice, contrast sensitivity also increased during development and reached maximal values of 3.5 ± 0.47 around P26 at 0.064 cyc/deg. Statistical analyzes revealed that there is a significant difference in the development of contrast sensitivity between $Bsn^{-/-}$ mice and their littermates ($Bsn^{+/+}$ and $Bsn^{+/-}$) (ANOVA, $p < 0.001$) but not between $Bsn^{+/+}$ and $Bsn^{+/-}$ mice.

Table 3: Development of visual acuity from eye opening (P13-15) of Bsn+/+ (n = 16), Bsn+/- (n = 15), and Bsn-/- mice (n = 6) until P42

age in days	Bsn+/+		Bsn+/-		Bsn-/-	
	visual acuity [cyc/deg]	±	visual acuity [cyc/deg]	±	visual acuity [cyc/deg]	±
13	0.045	0.011	0.039	0.011	0.021	0.021
14	0.051	0.011	0.048	0.010	0.023	0.016
15	0.120	0.015	0.100	0.019	0.033	0.015
16	0.177	0.016	0.165	0.022	0.056	0.011
17	0.226	0.017	0.212	0.024	0.076	0.016
18	0.259	0.017	0.243	0.023	0.098	0.012
19	0.284	0.015	0.271	0.022	0.115	0.013
20	0.311	0.013	0.296	0.018	0.134	0.013
21	0.332	0.012	0.331	0.012	0.150	0.012
22	0.350	0.011	0.355	0.008	0.170	0.011
23	0.365	0.009	0.369	0.007	0.179	0.010
24	0.371	0.009	0.373	0.007	0.192	0.008
25	0.381	0.007	0.382	0.006	0.203	0.007
26	0.386	0.006	0.389	0.006	0.210	0.007
27	0.391	0.004	0.392	0.005	0.210	0.009
29	0.397	0.003	0.397	0.004	0.210	0.009
31	0.399	0.002	0.401	0.002	0.210	0.011
33	0.399	0.002	0.402	0.002	0.207	0.015
35	0.400	0.001	0.402	0.002	0.210	0.012
38	0.401	0.001	0.403	0.002	0.202	0.024
42	0.403	0.001	0.405	0.001	0.202	0.024

Visual acuity increased rapidly over the following ten days in both genotypes and reached adult values of 0.400 cyc/deg at P29: visual acuity was 0.397 ± 0.003 cyc/deg (n = 16) in Bsn+/+ and 0.397 ± 0.004 cyc/deg in Bsn+/- animals (n = 15). This rapid increase in visual acuity between two and four weeks postnatally is in line with previous experiments in C57Bl/6J mice (Prusky *et al.*, 2004).

In contrast to Bsn+/+ and Bsn+/- mice, average visual acuity of Bsn-/- mice at P13 was 0.021 ± 0.021 cyc/deg (n = 3) and thus about half of the other two genotypes (Figure 22 A; Table 3). Visual acuity increased over the following ten days and reached adult values of 0.201 ± 0.021 cyc/deg (n = 6) at P25. There was little variability in the measures between individual animals on a given day and once visual acuity reached adult values, there was great measurement consistency and stability for each animal. Visual acuity between Bsn+/+ and Bsn-/- mice was significantly different already at P15 (t-test, $p < 0.01$). There was also a significant difference in the development of visual acuity between the two genotypes from P13 to P42 (ANOVA, $p < 0.001$, $F_{2,33} = 30.42$).

Taken together, this longitudinal study indicates that the time course of visual acuity development is not altered in *Bsn*^{-/-} mice compared to their littermates (*Bsn*^{+/+} and *Bsn*^{+/-}): while visual acuity is significantly lower in *Bsn*^{-/-} mice compared to their littermates, all three genotypes reach adult values between P25 and P29.

3.4.2 Contrast sensitivity

A large part of these data were already published in Goetze *et al.*, 2010b.

We also followed contrast sensitivity longitudinally in six juvenile *Bsn*^{-/-} animals and their littermates (15 *Bsn*^{+/-} and 16 *Bsn*^{+/+} mice) from the day of eye opening (P13 to P15) throughout visual development until P42 (Figure 22 B-D; Table 4; Table 5; Table 6) measured by the virtual-reality optomotor system. Since there were no differences between values of left and right eyes for *Bsn*^{+/+}, *Bsn*^{+/-}, and *Bsn*^{-/-} mice (t-test, $p > 0.05$ for all comparisons), we averaged values across eyes for both genotypes.

As previously described for C57Bl/6J mice (Prusky *et al.*, 2004), contrast sensitivity also increased rapidly during the first two weeks after eye opening. Already between P16 and P17, 0.064 cyc/deg emerged as the spatial frequency with the highest contrast sensitivity and remained at the peak at all subsequent ages in all three genotypes. In *Bsn*^{+/+} (Figure 22 C; Table 4) and *Bsn*^{+/-} (Figure 22 B; Table 5) mice, contrast sensitivity at 0.064 cyc/deg increased from 1.2 ± 0.07 (corresponding to 86 % contrast) at P13 to a value of 14.8 ± 0.92 (corresponding to 5 % contrast) and from 1.1 ± 0.02 (corresponding to 90 % contrast) to a value of 14.6 ± 1.04 (corresponding to 6 % contrast) in *Bsn*^{+/-} mice at P31.

In contrast, *Bsn*^{-/-} mice (Figure 22 D; Table 6) did not achieve similarly high values. In *Bsn*^{-/-} mice, contrast sensitivity at 0.064 cyc/deg increased from 1.1 ± 0.00 (corresponding to 90 % contrast) at P13 to a maximum of 3.5 ± 0.47 (corresponding to 29 % contrast) at P26.

Statistical analyzes revealed that there is a significant difference in the development of contrast sensitivity between *Bsn*^{-/-} mice and their littermates (*Bsn*^{+/+} and *Bsn*^{+/-}) (ANOVA, $p < 0.001$). Whereas there is no significant difference between *Bsn*^{+/+} and *Bsn*^{+/-} mice (ANOVA, $p = 1.0$). *Bsn*^{+/+} and *Bsn*^{+/-} animals exhibit the same developmental curve of contrast sensitivity as previously reported for C57Bl/6J mice (Prusky *et al.*, 2004).

Table 4: Development of contrast sensitivity from eye opening (P13-15) of Bsn+/+ (n = 16) until P42

Bsn+/+ contrast sensitivity at:												
age in days	0.031 cyc/deg	±	0.064 cyc/deg	±	0.092 cyc/deg	±	0.103 cyc/deg	±	0.192 cyc/deg	±	0.272 cyc/deg	±
13	1.1	0.04	1.2	0.07	1.0	0.00						
14	1.2	0.05	1.3	0.08	1.2	0.10	1.1	0.00				
15	1.2	0.08	1.5	0.22	1.6	0.17	1.4	0.10	1.1	0.07		
16	1.5	0.11	2.3	0.36	2.2	0.30	1.9	0.20	1.6	0.17		
17	1.7	0.13	3.3	0.43	2.5	0.35	2.0	0.30	1.8	0.27	1.4	0.12
18	2.0	0.15	4.0	0.46	3.2	0.38	2.6	0.31	2.1	0.28	1.5	0.11
19	2.2	0.16	4.6	0.52	3.8	0.42	3.0	0.37	2.3	0.36	1.8	0.12
20	2.7	0.17	6.3	0.52	5.0	0.46	3.9	0.40	2.5	0.38	1.9	0.22
21	3.0	0.18	7.3	0.59	5.6	0.50	4.3	0.45	3.1	0.40	2.4	0.24
22	3.3	0.19	8.4	0.70	6.7	0.63	5.2	0.70	3.6	0.43	2.9	0.21
23	3.6	0.18	10.0	0.70	7.5	0.66	6.2	0.60	4.3	0.47	2.6	0.27
24	3.8	0.19	10.5	0.86	7.9	0.76	6.7	0.67	4.7	0.59	2.9	0.29
25	4.0	0.18	11.6	0.94	8.7	0.81	7.2	0.71	5.5	0.59	3.5	0.25
26	4.3	0.15	12.7	0.93	9.3	0.88	7.8	0.73	6.0	0.58	3.9	0.23
27	4.3	0.16	13.4	0.98	9.9	0.95	8.2	0.82	6.3	0.63	4.2	0.20
29	4.5	0.14	14.7	0.80	10.9	0.83	9.5	0.66	7.2	0.53	4.4	0.16
31	4.8	0.34	14.8	0.92	11.1	0.87	9.6	0.75	7.2	0.60	4.5	0.17
33	4.7	0.13	16.1	0.82	12.3	0.79	10.8	0.67	8.1	0.52	4.6	0.16
35	4.7	0.13	16.8	0.78	12.8	0.75	11.2	0.65	8.5	0.53	4.7	0.15
38	4.8	0.13	17.3	0.73	13.6	0.68	11.8	0.61	8.9	0.52	4.9	0.14
42	4.9	0.13	18.0	0.69	14.2	0.64	12.3	0.57	9.3	0.50	4.9	0.14

Table 5: Development of contrast sensitivity from eye opening (P13-15) of Bsn+/- (n = 15) mice until P42

Bsn+/- contrast sensitivity at:												
age in days	0.031 cyc/deg	±	0.064 cyc/deg	±	0.092 cyc/deg	±	0.103 cyc/deg	±	0.192 cyc/deg	±	0.272 cyc/deg	±
13	1.1	0.02	1.1	0.02								
14	1.1	0.02	1.2	0.04	1.3	0.00						
15	1.3	0.06	1.9	0.29	2.0	0.19	1.6	0.10				
16	1.4	0.09	2.0	0.43	3.0	0.28	2.4	0.19	1.8	0.21	1.1	0.00
17	1.6	0.14	2.6	0.56	2.7	0.48	2.6	0.40	1.9	0.29	1.3	0.19
18	1.9	0.22	3.3	0.73	2.9	0.61	2.8	0.48	3.2	0.27	1.4	0.18
19	2.2	0.25	3.9	0.82	3.2	0.67	2.8	0.55	3.5	0.35	1.8	0.18
20	2.7	0.23	6.0	0.79	4.6	0.67	3.5	0.57	2.9	0.47	2.3	0.17
21	2.9	0.26	7.1	0.94	5.6	0.85	4.8	0.63	3.6	0.47	2.4	0.26
22	3.4	0.23	8.4	0.93	6.7	0.88	5.7	0.82	4.5	0.46	3.0	0.21
23	3.6	0.22	9.3	0.96	7.6	0.89	6.5	0.71	5.2	0.50	3.4	0.20
24	3.9	0.24	10.5	1.10	8.4	0.99	7.0	0.80	5.6	0.57	3.7	0.23
25	4.1	0.23	11.4	1.17	8.9	1.08	7.6	0.83	6.0	0.66	3.9	0.25
26	4.3	0.24	12.8	1.17	10.1	1.15	8.4	0.86	6.6	0.71	4.2	0.25
27	4.4	0.22	13.3	1.18	10.3	1.15	8.7	0.87	6.8	0.71	4.3	0.24
29	4.4	0.21	13.7	1.16	10.6	1.13	9.0	0.86	7.2	0.69	4.4	0.22
31	4.5	0.20	14.6	1.04	11.1	1.09	9.6	0.82	7.8	0.69	4.7	0.18
33	4.6	0.19	15.9	0.91	12.7	0.92	10.6	0.72	8.7	0.61	4.8	0.17
35	4.7	0.19	16.1	0.97	13.1	0.89	11.0	0.74	8.9	0.60	4.9	0.17
38	4.7	0.21	16.4	0.88	13.0	0.91	10.8	0.73	8.7	0.60	4.9	0.18
42	4.7	0.21	17.7	0.89	14.1	0.88	11.9	0.67	9.5	0.59	5.0	0.16

Table 6: Development of contrast sensitivity from eye opening (P13-15) of *Bsn*^{-/-} (n = 6) mice until P42

<i>Bsn</i>^{-/-} contrast sensitivity at:										
age in days	0.031 cyc/deg	±	0.064 cyc/deg	±	0.092 cyc/deg	±	0.103 cyc/deg	±	0.192 cyc/deg	±
13	1.1	0.00	1.1	0.00						
14	1.1	0.03	1.2	0.07						
15	1.1	0.00	1.2	0.06						
16	1.1	0.03	1.1	0.05						
17	1.1	0.02	1.3	0.06	1.1	0.00				
18	1.2	0.10	1.4	0.37	1.3	0.18	1.1	0.06		
19	1.3	0.13	1.6	0.39	1.4	0.20	1.3	0.04		
20	1.5	0.20	1.9	0.47	1.4	0.26	1.3	0.14		
21	1.6	0.24	2.0	0.51	1.5	0.28	1.4	0.18		
22	1.8	0.23	2.4	0.48	1.9	0.23	1.6	0.18	1.1	0.00
23	2.0	0.21	2.7	0.46	2.0	0.25	1.8	0.22	1.1	0.04
24	2.0	0.24	3.0	0.53	2.2	0.28	1.9	0.25	1.2	0.06
25	2.1	0.23	3.3	0.49	2.4	0.28	2.0	0.26	1.4	0.13
26	2.1	0.23	3.5	0.47	2.5	0.27	2.1	0.25	1.4	0.12
27	2.1	0.26	3.4	0.44	2.4	0.26	2.1	0.27	1.4	0.14
29	2.1	0.26	3.4	0.45	2.5	0.27	2.2	0.25	1.5	0.09
31	2.1	0.34	3.2	0.54	2.4	0.35	2.1	0.33	1.6	0.08
33	1.9	0.37	2.9	0.40	2.3	0.30	2.0	0.39	1.6	0.11
35	2.0	0.40	3.0	0.46	2.3	0.34	2.0	0.41	1.7	0.14
38	1.7	0.01	2.6	0.43	2.0	0.02	1.7	0.09	1.5	0.00
42	1.7	0.02	2.6	0.43	2.0	0.03	1.7	0.09	1.5	0.00

3.5 Enhancement of vision after monocular deprivation

3.5.1 Visual acuity

A part of these data were already published in Goetze *et al.*, 2010a.

As previously reported, monocular deprivation (MD) induces an enhancement of the optokinetic response of the nondeprived eye in mice (Prusky *et al.*, 2006). To check if Bassoon mutant mice and their wild-type littermates also show interocular plasticity of vision we performed MD and tested visual acuity of the nondeprived eye daily with the virtual-reality optomotor system. Therefore we used seven days of MD in adult (begin at P76 up to P98) and four days of MD in juvenile animals (begin at P24 up to P29). We tested nine adult and six juvenile *Bsn*^{+/+} mice as well as six adult and 13 juvenile *Bsn*^{-/-} mice.

On each day following a MD, visual acuity increased substantially. In adult *Bsn*^{+/+} animals visual acuity increased from 0.397 ± 0.002 cyc/deg before deprivation to values of

0.502 ± 0.004 cyc/deg on the seventh day after monocular deprivation (Figure 23 A), which represents a gain on baseline of 26.6 ± 1.30 % (Figure 23 B).

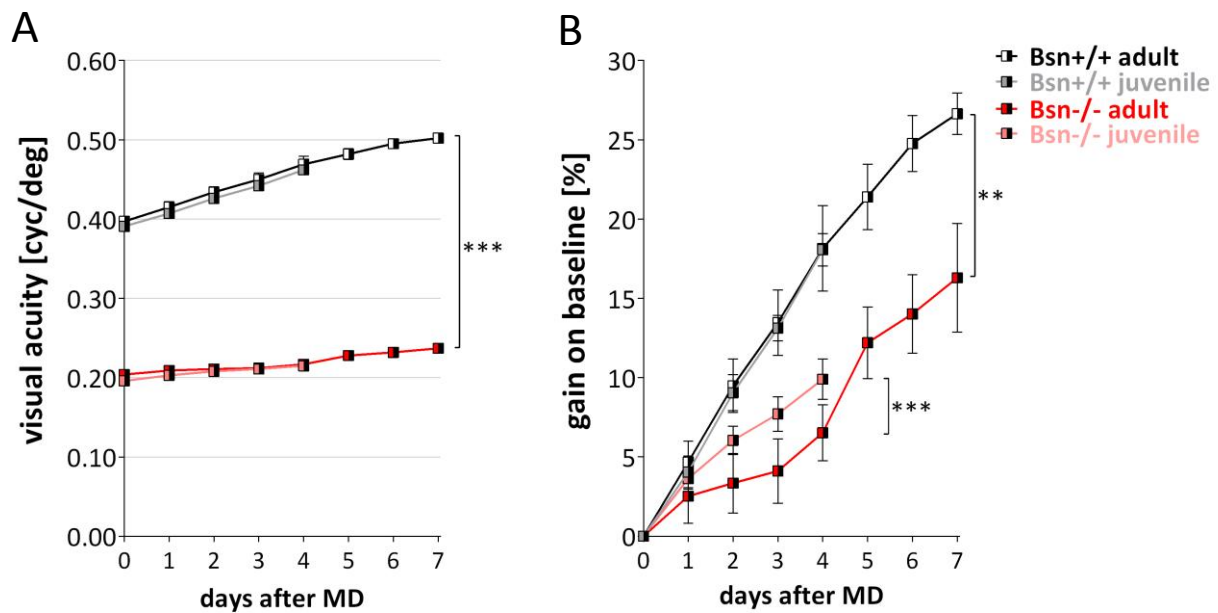


Figure 23: Enhancement of visual acuity after monocular deprivation in adult and juvenile Bsn+/+ (n = 9/n = 6) as well as in adult and juvenile Bsn-/- mice (n = 6/n = 13). **(A)** Spatial frequency selectivity of the optokinetic response in cycles per degree (cyc/deg) plotted against days after MD. During seven days of MD and daily testing, visual acuity of the nondeprived eye increased in adult Bsn+/+ mice (black) from 0.397 ± 0.002 cyc/deg to 0.502 ± 0.004 cyc/deg. During four days of MD juvenile Bsn+/+ animals (pink) visual acuity increased from 0.391 ± 0.004 cyc/deg to 0.462 ± 0.003 cyc/deg. In contrast, adult Bsn-/- animals (red) only increased from 0.204 ± 0.004 cyc/deg to 0.237 ± 0.003 cyc/deg and juvenile Bsn-/- mice (pink) from 0.196 ± 0.003 cyc/deg to 0.215 ± 0.003 cyc/deg. Statistical analyzes revealed that there was a significant difference in the development of visual acuity between adult Bsn-/- and Bsn+/+ mice (ANOVA, p < 0.001) and also between juvenile Bsn-/- and Bsn+/+ mice (ANOVA, p < 0.001) but neither between adult and juvenile Bsn+/+ nor between Bsn-/- mice. **(B)** Gain on baseline of visual acuity in percent (%) plotted against days after MD. During seven days of MD adult Bsn+/+ animals showed a gain on baseline of 26.6 ± 1.30 %. During four days of MD juvenile Bsn+/+ animals showed a gain on baseline of 18.1 ± 1.02 %. In contrast, adult Bsn-/- animals only displayed a gain on baseline of 16.3 ± 3.43 % and juvenile Bsn-/- mice a gain on baseline of 9.1 ± 1.27 %. Statistical analyzes revealed that there was a significant difference of gain on baseline between adult Bsn-/- and Bsn+/+ mice (t-test, p < 0.001) and also between juvenile Bsn-/- and Bsn+/+ mice (t-test, p < 0.001) but neither between adult and juvenile Bsn+/+ nor between Bsn-/- mice.

In contrast, in adult Bsn-/- mice visual acuity only increased from 0.204 ± 0.004 cyc/deg before deprivation to values of 0.237 ± 0.003 cyc/deg on the seventh day after monocular deprivation (Figure 23 A), which represents a gain on baseline of 16.3 ± 3.43 % (Figure 23 B).

In juvenile Bsn+/+ animals visual acuity increased from 0.391 ± 0.004 cyc/deg before deprivation to values of 0.462 ± 0.003 cyc/deg on the fourth day after monocular deprivation (Figure 23 A), which represents a gain on baseline of 18.1 ± 1.02 % (Figure 23 B).

In juvenile Bsn^{-/-} mice visual acuity enhancement was impaired as well and increased from 0.196 ± 0.003 cyc/deg before deprivation to values of 0.215 ± 0.003 cyc/deg on the fourth day after monocular deprivation (Figure 23 A), which represents a gain on baseline of 9.1 ± 1.27 % (Figure 23 B).

In adult animals there was a significant difference in the improvement of visual acuity over seven days of MD of each genotype (ANOVA, $p < 0.001$, $F_{7,7} = 28.53$) and between both genotypes (ANOVA, $p < 0.001$, $F_{1,13} = 1514.14$). In adult Bsn^{+/+} animals, the increase on baseline of visual acuity after MD was 26.6 % in Bsn^{+/+} mice compared to only 16.3 % in Bsn^{-/-} mice and therefore significantly different (t-test, $p < 0.01$).

Juvenile animals also showed a significant difference in the improvement of visual acuity over four days of MD of each genotype (ANOVA, $p < 0.001$, $F_{4,14} = 108.07$) and between both genotypes (ANOVA, $p < 0.001$, $F_{1,17} = 2452.90$). In juvenile animals the increase on baseline of visual acuity after MD was with 18.1 % in Bsn^{+/+} mice twice as high as in Bsn^{-/-} mice with 9.1 % and therefore significantly different (t-test, $p < 0.001$).

Between adult and juvenile Bsn^{+/+} mice were no significant differences. Whereas juvenile Bsn^{-/-} mice showed a significantly higher increase on baseline of visual acuity after MD compared to adult mice (ANOVA, $p < 0.001$, $F_{1,17} = 2,452.90$).

3.5.2 Contrast sensitivity

To check if Bassoon mutant mice and their wild-type littermates show interocular plasticity of vision, we also tested contrast sensitivity of the nondeprived eye daily with the virtual-reality optomotor system. Therefore we measured the same animals as described before for visual acuity (chapter 3.5.1). Contrast sensitivity was measured at six different spatial frequencies and always peaked at 0.064 cyc/deg during all days of MD and in adult and juvenile animals of both genotypes as described previously (Prusky *et al.*, 2006). On each day following MD, contrast sensitivity of all measured spatial frequencies increased substantially.

At 0.064 cyc/deg in adult Bsn^{+/+} animals contrast sensitivity increased from 15.6 ± 0.97 (corresponding to 6 % contrast) before deprivation (Figure 24 A,D,F) to values of 28.0 ± 3.32 (corresponding to 4 % contrast) on the seventh day after monocular deprivation (Figure 24 B,D,F), which represents a gain on baseline of 83.9 ± 22.63 %.

In contrast, in adult *Bsn*^{-/-} mice contrast sensitivity only increased from 2.7 ± 0.09 (corresponding to 36.9 % contrast) before deprivation (Figure 24 A,C,E) to values of 3.0 ± 0.14 (corresponding to 33 % contrast) on the seventh day after monocular deprivation (Figure 24 B,C,E), which represents a gain on baseline of 13.2 ± 2.65 %.

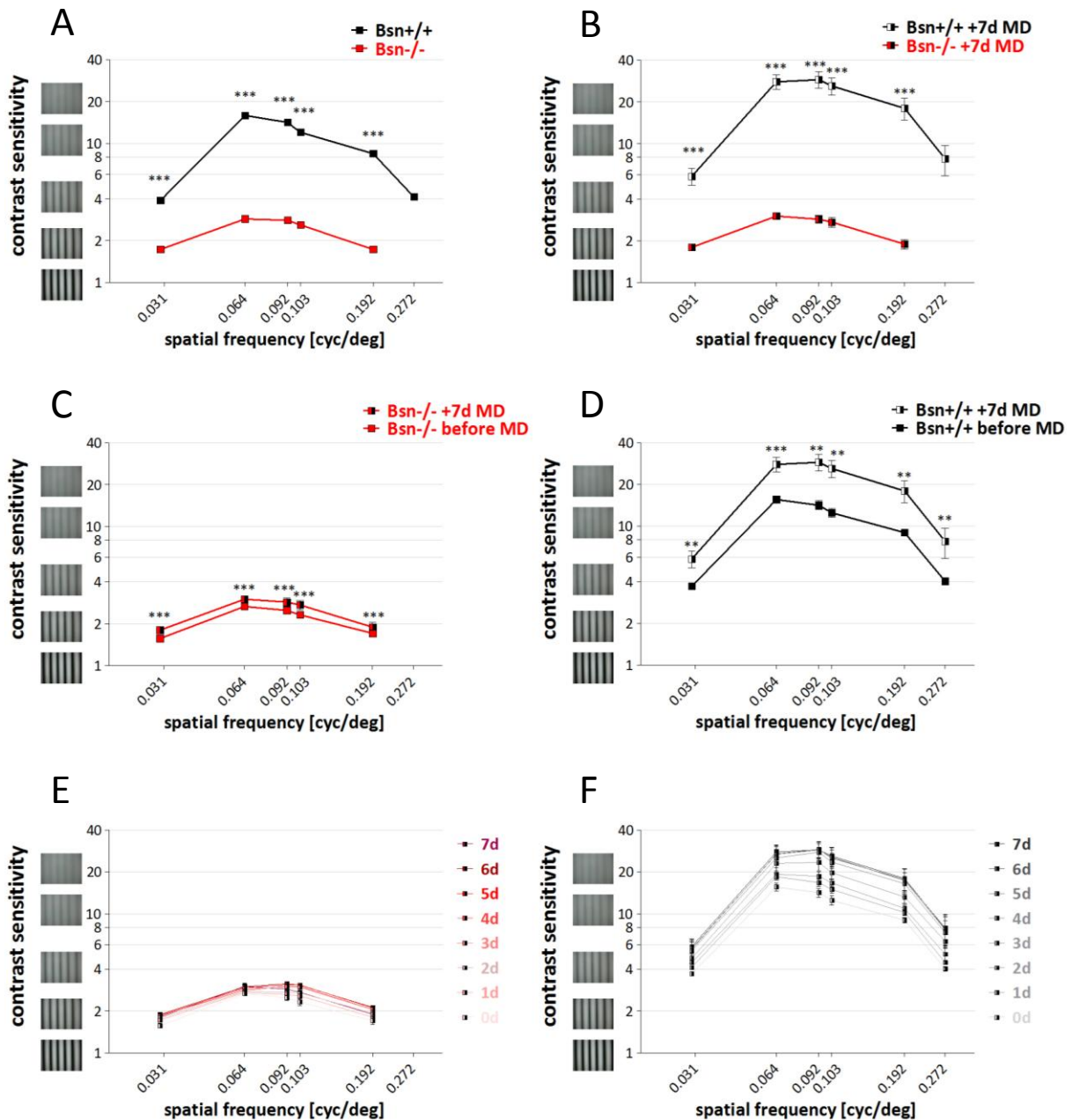


Figure 24: Enhancement of contrast sensitivity after monocular deprivation in adult *Bsn*^{+/+} (n = 9) and *Bsn*^{-/-} mice (n = 6). Contrast sensitivity plotted as a function of spatial frequency in cycles per degree (cyc/deg). Bassoon mutant mice (red) did not achieve approximately similarly high values as *Bsn*^{+/+} animals (black) neither before (A) nor after seven days of MD (B (t-test, $p < 0.001$ for all comparisons)). Nevertheless, *Bsn*^{-/-} (C) as well as *Bsn*^{+/+} mice (D) showed a significant improvement of contrast sensitivity after seven days of MD (t-test, $p < 0.01$ for all comparisons). Daily improvement of contrast sensitivity over seven days of MD of *Bsn*^{-/-} (E) and *Bsn*^{+/+} mice (F) revealed that genotype had a significant influence on the improvement of contrast sensitivity (ANOVA, $p < 0.001$). In adult *Bsn*^{+/+} animals, the increase on baseline of contrast sensitivity after MD was 83.9 % compared to an enormous lower value of 13.2 % in *Bsn*^{-/-} mice and therefore significantly different (t-test, $p < 0.05$).

At 0.064 cyc/deg in juvenile Bsn^{+/+} animals contrast sensitivity increased from 15.9 ± 0.56 (corresponding to 6 % contrast) before deprivation (Figure 25 A,D,F) to values of 22.5 ± 0.86 (corresponding to 4 % contrast) on the fourth day after monocular deprivation (Figure 25 B,D,F), which represents a gain on baseline of 43.1 ± 7.92 %.

In contrast, in juvenile Bsn^{-/-} mice contrast sensitivity only increased from 2.7 ± 0.06 (corresponding to 6 % contrast) before deprivation (Figure 25 A,C,E) to values of 3.1 ± 0.09 (corresponding to 40 % contrast) on the fourth day after monocular deprivation (Figure 25 B,C,E), which represents a gain on baseline of 14.2 ± 1.83 %.

In adult animals there was a significant difference in the improvement of contrast sensitivity over seven days of MD of each genotype (ANOVA, $p < 0.05$, $F_{4,7} = 8.79$) and between both genotypes (ANOVA, $p < 0.001$, $F_{1,10} = 42.47$). Between both genotypes contrast sensitivity was different at all spatial frequencies from each other before and after seven days of MD (t-test, $p < 0.001$, for all comparisons). Nevertheless, adult Bsn^{-/-} as well as Bsn^{+/+} mice showed a significant improvement of contrast sensitivity after seven days of MD (t-test, $p < 0.01$ for all comparisons). In adult Bsn^{+/+} animals, the increase on baseline of contrast sensitivity after MD was 83.9 % in Bsn^{+/+} mice compared to an enormous lower value of 13.2 % in Bsn^{-/-} mice and therefore significantly different (t-test, $p < 0.05$).

Juvenile animals also showed a significant difference in the improvement of contrast sensitivity over four days of MD of each genotype (ANOVA, $p < 0.001$, $F_{4,14} = 41.14$) and between both genotypes (ANOVA, $p < 0.001$, $F_{1,17} = 720.71$). Between both genotypes contrast sensitivity was different at all spatial frequencies from each other before and after four days of MD (t-test, $p < 0.001$ for all comparisons). Nevertheless, juvenile Bsn^{-/-} as well as Bsn^{+/+} mice showed a significant improvement of contrast sensitivity after four days of MD (t-test, $p < 0.01$ for all comparisons). In juvenile animals the increase on baseline of contrast sensitivity after MD was with 43.1 % in Bsn^{+/+} mice thrice as high as in Bsn^{-/-} mice with 14.2 % and therefore significantly different (t-test, $p < 0.001$).

But neither between adult and juvenile Bsn^{+/+} nor between Bsn^{-/-} mice were significant differences observed. Whereas juvenile Bsn^{-/-} mice showed a significantly higher increase on baseline of contrast sensitivity after MD compared to adult mice.

3.A Results of Bassoon mutant mice

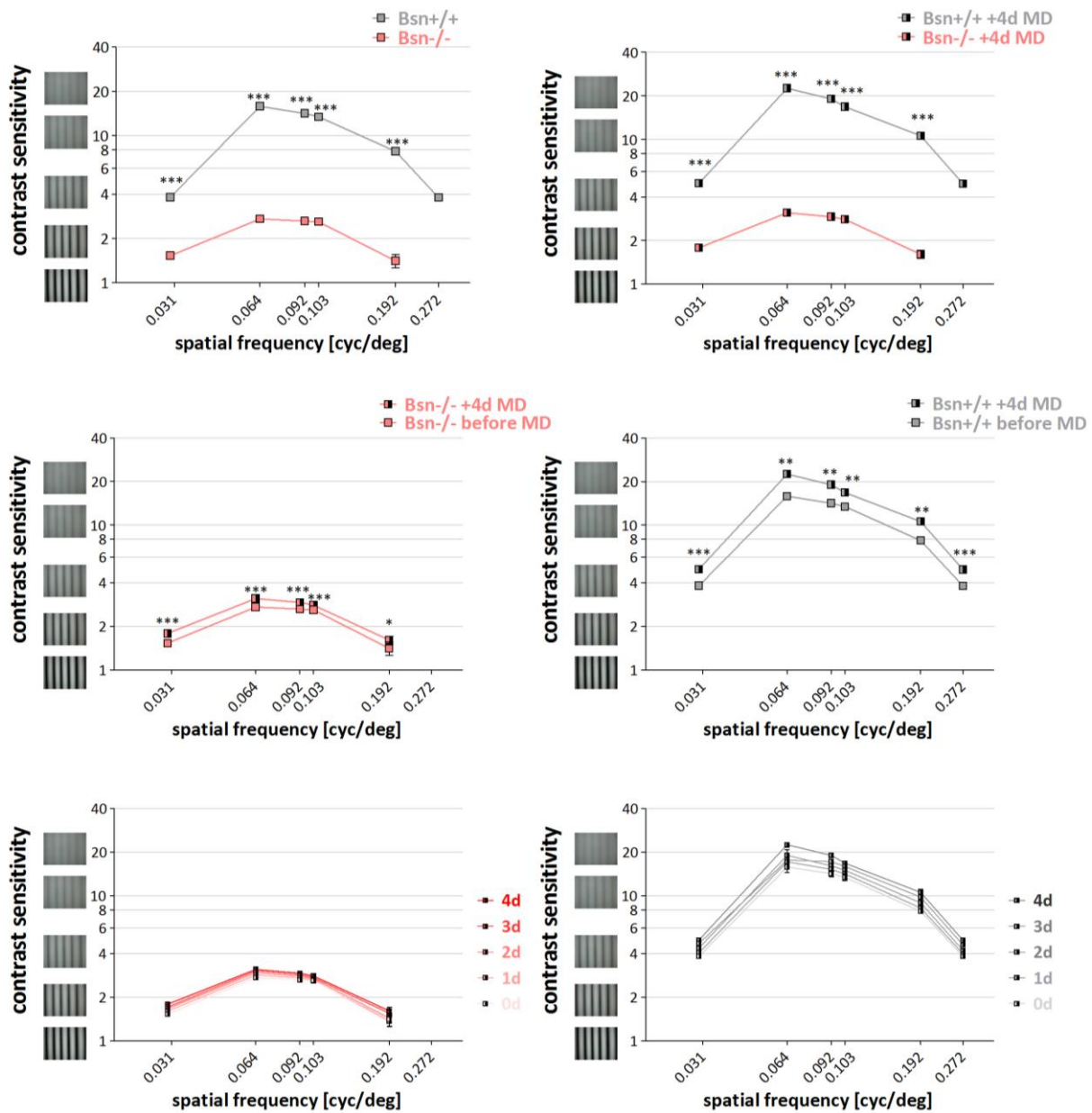


Figure 25: Enhancement of contrast sensitivity after monocular deprivation in juvenile Bsn+/+ (n = 6) and Bsn-/- mice (n = 13). Contrast sensitivity plotted as a function of spatial frequency in cycles per degree (cyc/deg). Bassoon mutant mice (red) did not achieve approximately similarly high values as Bsn+/+ animals (black) neither before (A) nor after four days of MD (B) (t-test, $p < 0.001$ for all comparisons). Nevertheless, Bsn-/- (C) as well as Bsn+/+ mice (D) showed a significant improvement of contrast sensitivity after four days of MD (t-test, $p < 0.01$ for all comparisons). Daily improvement of contrast sensitivity over four days of MD of Bsn-/- (E) and Bsn+/+ mice (F) revealed that genotype had a significant influence on the improvement of contrast sensitivity (ANOVA, $p < 0.001$). In adult Bsn+/+ animals, the increase on baseline of contrast sensitivity after MD was 43.1 % in Bsn+/+ mice compared to an enormous lower value of 14.2 % in Bsn-/- mice and therefore significantly different (t-test, $p < 0.001$).

3.6 Optical imaging of intrinsic signals

3.6.1 Maximum response and map scatter

A large part of these data were already published in Goetze *et al.*, 2010b.

To see if the mutation of the protein Bassoon has any influence on the visual cortex we recorded mouse visual cortical responses *in vivo* using the imaging method developed by Kalatsky and Stryker (2003).

As already mentioned the visual stimuli consisted of full-screen moving horizontal (elevation maps) and vertical bars (azimuth maps) in the right visual field. Therefore we always measured the left hemisphere. Our resulting maps were retinotopic phase maps, raw magnitude response maps, and polar maps, respectively. We calculated maximum response and map quality from 14 adult (P76 to P168) Bsn^{+/+} mice as well as from 16 adult (P75 to P267) Bsn^{-/-} mice according to published protocols (Cang *et al.*, 2005b).

Representative examples of the resulting activity and retinotopic maps of the left visual cortex of adult Bsn^{+/+} and Bsn^{-/-} mice are illustrated in Figure 26, Figure 27, and Figure 28. Most interestingly, Bsn^{+/+} (Figure 28 B,E) and Bsn^{-/-} mice (Figure 28 D,F) had nearly identical maps, indistinguishable in both signal amplitude and quality of retinotopy for both elevation (Figure 28 B,C) and azimuth maps (Figure 28 E,F). This was very surprising given the severely reduced synaptic transmission in the retina of Bsn^{-/-} animals.

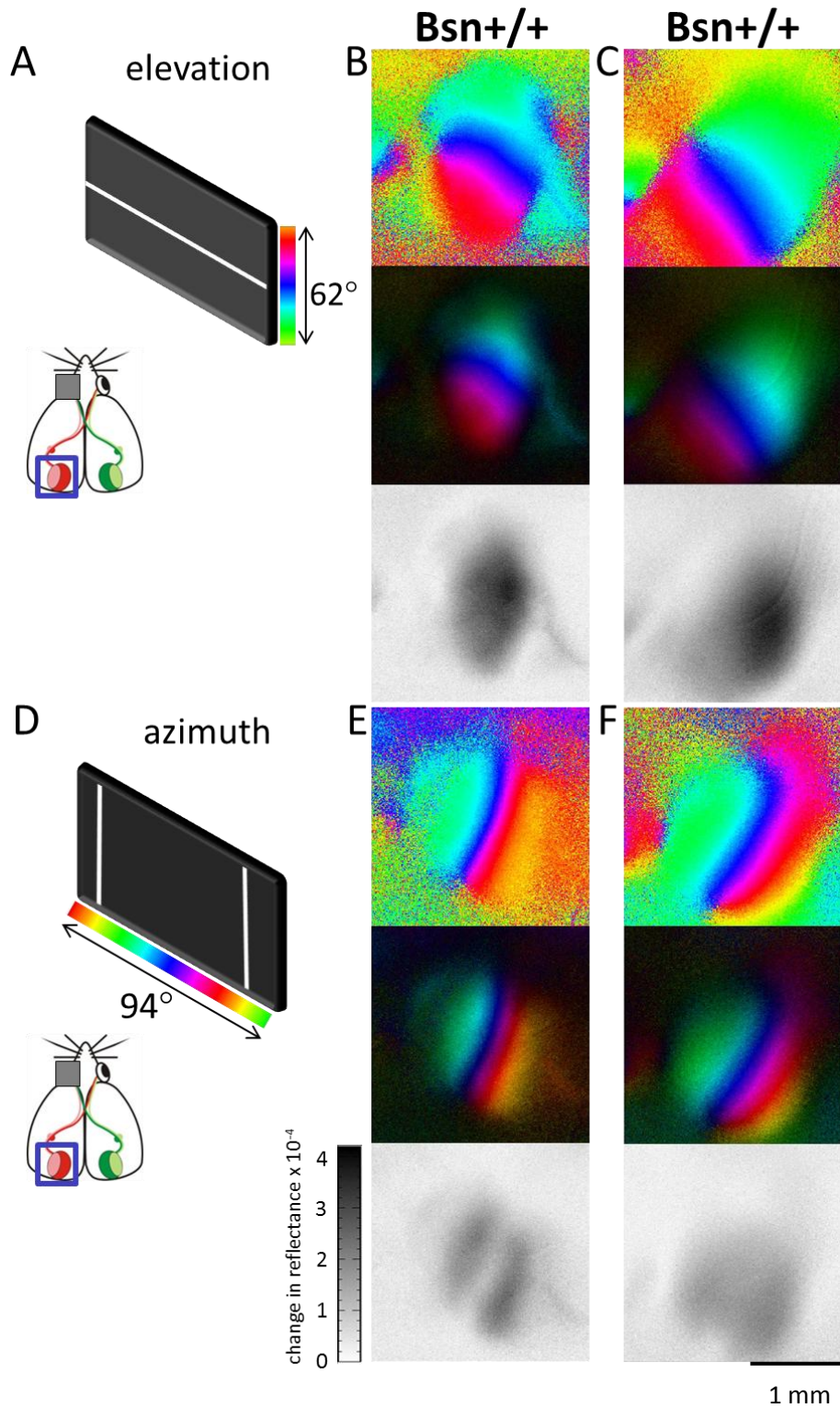


Figure 26: Representative examples of visual cortical maps recorded with intrinsic signal optical imaging of adult *Bsn^{+/+}* mice. Color-coded retinotopic phase map (top), polar maps (middle) and grey-scale coded response magnitude maps (below) of two different *Bsn^{+/+}* mice (**B,C,E,F**) are illustrated. The magnitude of the optical responses is illustrated as fractional change in reflectance $\times 10^{-4}$. Retinotopic maps are color-coded according to the schemes on the left side (**A,D**). Both elevation (**B,C**) and azimuth (**E,F**) maps resulting from visual stimulation of the animals with full-screen moving horizontal (**A**) or vertical bars (**D**) are shown. Visual cortical maps of adult *Bsn^{+/+}* mice have both high response amplitude and excellent retinotopy.

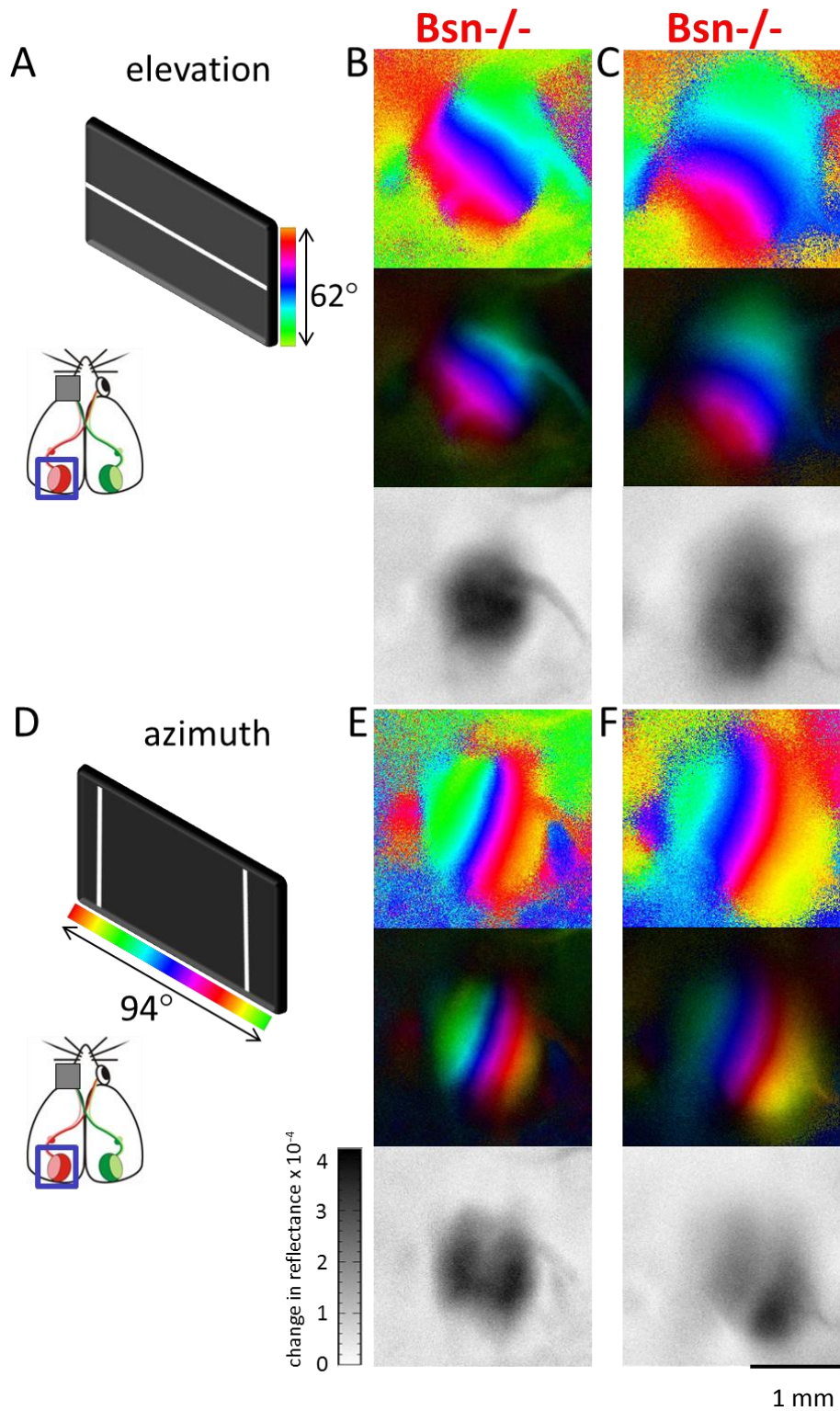
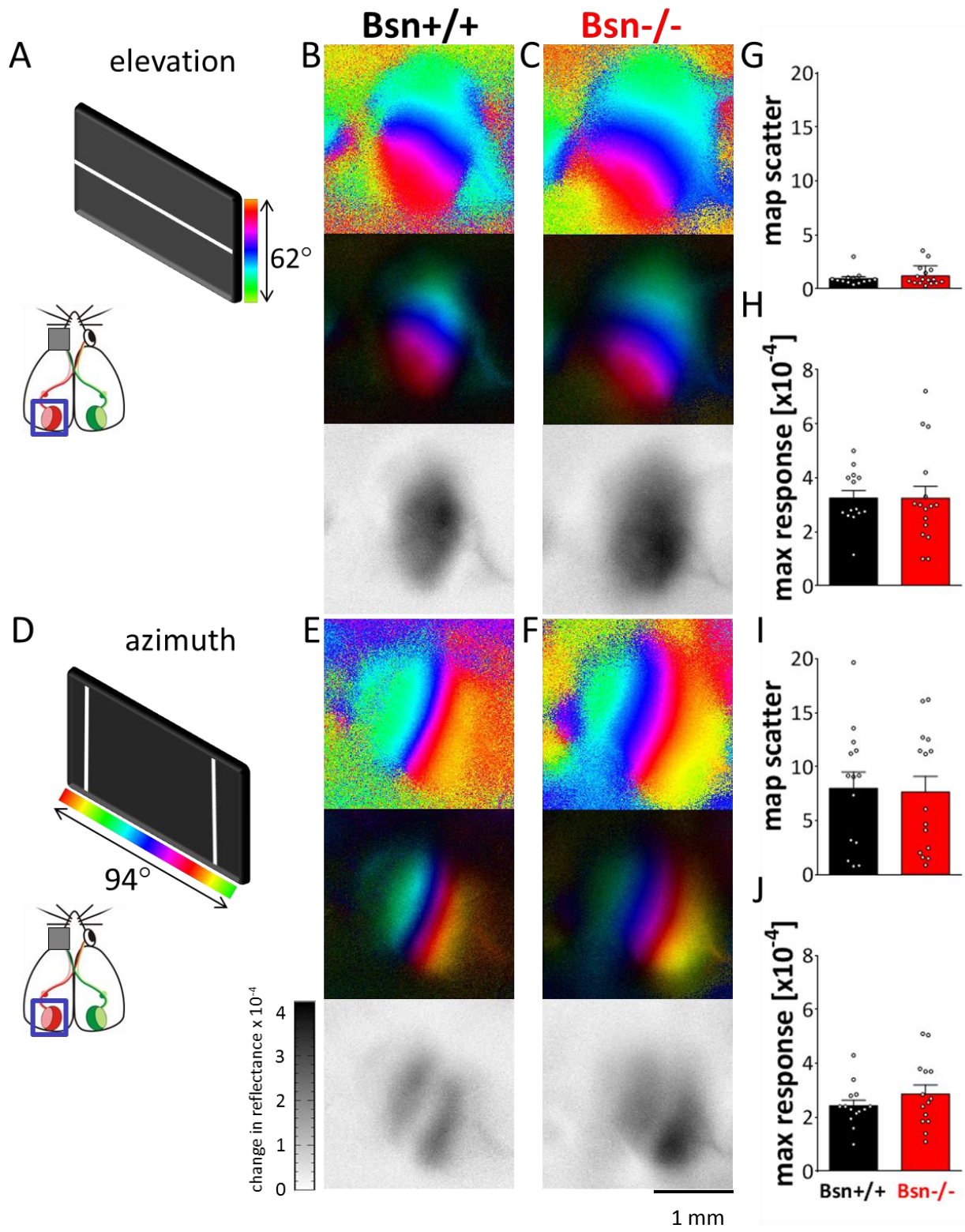


Figure 27: Representative examples of visual cortical maps recorded with intrinsic signal optical imaging of adult *Bsn*^{-/-} mice. Color-coded retinotopic phase map (top), polar maps (middle) and grey-scale coded response magnitude maps (below) of two different *Bsn*^{-/-} mice (**B,C,E,F**) are illustrated. The magnitude of the optical responses is illustrated as fractional change in reflectance $\times 10^{-4}$. Retinotopic maps are color-coded according to the schemes on the left side (**A,D**). Both elevation (**B,C**) and azimuth (**E,F**) maps resulting from visual stimulation of the animals with full-screen moving horizontal (**A**) or vertical bars (**D**) are shown. Visual cortical maps of adult *Bsn*^{-/-} mice have both high response amplitude and excellent retinotopy.



▲
Figure 28: Visual cortical maps recorded with intrinsic signal optical imaging and their quantification of adult Bsn+/+ and Bsn-/- mice (Figure modified from Goetze *et al.*, 2010b). Color-coded retinotopic phase map (top), polar maps (middle) and grey-scale coded response magnitude maps (below) of a Bsn+/+ (**B,E**) and a Bsn-/- mouse (**C,F**) are illustrated. The magnitude of the optical responses is illustrated as fractional change in reflectance $\times 10^{-4}$. Retinotopic maps are color-coded according to the schemes on the left side (**A,D**). Both elevation (**B,C**) and azimuth (**E,F**) maps resulting from visual stimulation of the animals with full-screen moving horizontal (**A**) or vertical bars (**D**) are shown. Visual cortical maps of Bsn-/- mice have both high response amplitude and excellent retinotopy. (**G,I**) Quantification of map quality of adult Bsn+/+ (n = 14) and Bsn-/- mice (n = 16). Map quality plotted as map scatter. Visual cortical maps of Bsn+/+ (black) and Bsn-/- animals (red) are indistinguishable in magnitude of the visual cortical responses for both elevation (**G**) (t-test, $p > 0.05$) and azimuth maps (**I**) (t-test, $p > 0.05$). (**H,J**) Quantification of magnitude maps of adult Bsn+/+ (n = 14) and Bsn-/- mice (n = 16). Maximum cortical response plotted as a change in reflectance $\times 10^{-4}$. Visual cortical maps of Bsn+/+ (black) and Bsn-/- animals (red) are indistinguishable in magnitude of the visual cortical responses for both elevation (**H**) (t-test, $p > 0.05$) and azimuth maps (**J**) (t-test, $p > 0.05$).

To compare the cortical maps of Bsn+/+ and Bsn-/- mice, we quantified both the maximum response of the visual cortex and the quality of the retinotopic maps. After visual stimulation with a full-screen moving horizontal bar, the magnitude of the optical responses in the visual cortex of Bsn+/+ and Bsn-/- mice was nearly identical: 3.25 ± 0.27 and 3.24 ± 0.44 , respectively (elevation maps, Figure 28 H). The values were statistically not different (t-test, $p > 0.05$). Similarly, after visual stimulation with a moving vertical bar, the magnitude of the cortical responses of Bsn+/+ and Bsn-/- mice was also not significantly different: 2.43 ± 0.21 in Bsn+/+ and 2.87 ± 0.33 in Bsn-/- mice (azimuth maps, Figure 28 J). The values are also statistically not different (t-test, $p > 0.05$).

The quality of the retinotopic maps was also similar in both genotypes. Mean scatter of elevation maps of Bsn+/+ mice was 0.96 ± 0.18 and 1.08 ± 0.21 in Bsn-/- mice (Figure 28 G). For azimuth maps, map scatter was 8.01 ± 1.50 in Bsn+/+ mice and 7.67 ± 1.45 in Bsn-/- mice (Figure 28 I). There were no significant differences in map scatter neither for elevation (t-test, $p > 0.05$) nor for azimuth maps (t-test, $p > 0.05$).

In addition, we performed optical imaging of intrinsic signals also in juvenile Bsn-/- animals and compared both signal amplitude and quality of retinotopic maps nine juvenile (P30 to P49) and 16 adult (P75 to P267) Bsn-/- animals.

Representative examples of the resulting activity and retinotopic maps of the left visual cortex of juvenile and adult Bsn-/- mice are illustrated in Figure 29, Figure 30, and Figure 31.

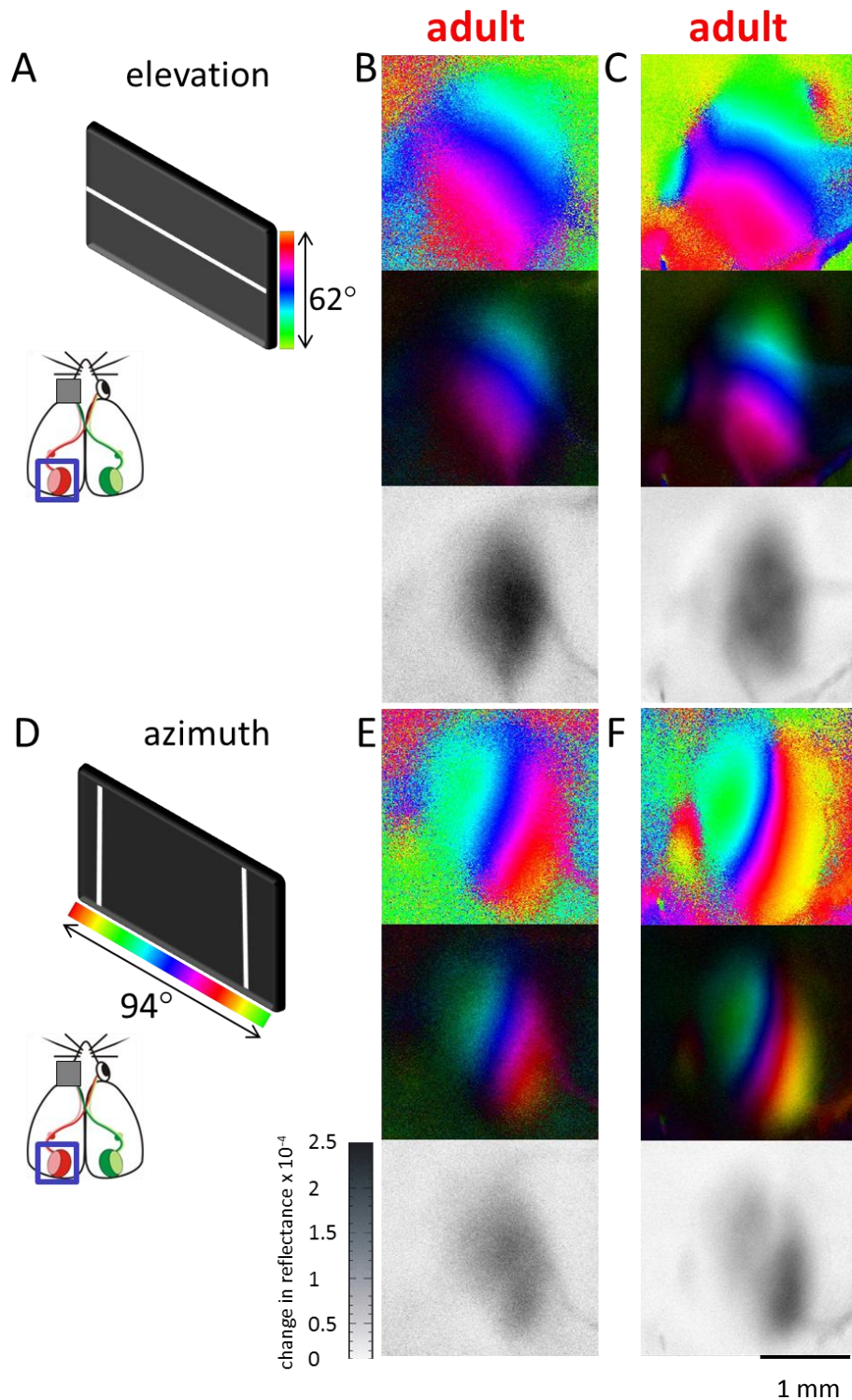


Figure 29: Representatives examples of visual cortical maps recorded with intrinsic signal optical imaging of adult *Bsn*^{-/-} mice. Color-coded retinotopic phase map (top), polar maps (middle) and grey-scale coded response magnitude maps (below) of two adult (100 days old) *Bsn*^{-/-} mice (**B,C,E,F**) are illustrated. The magnitude of the optical responses is illustrated as fractional change in reflectance $\times 10^{-4}$. Retinotopic maps are color-coded according to the schemes on the left side (**A,D**). Both elevation (**B,C**) and azimuth (**E,F**) maps resulting from visual stimulation of the animals with full-screen moving horizontal (**A**) or vertical bars (**D**) are shown. Visual cortical maps of adult *Bsn*^{-/-} mice have both high response amplitude and excellent retinotopy.

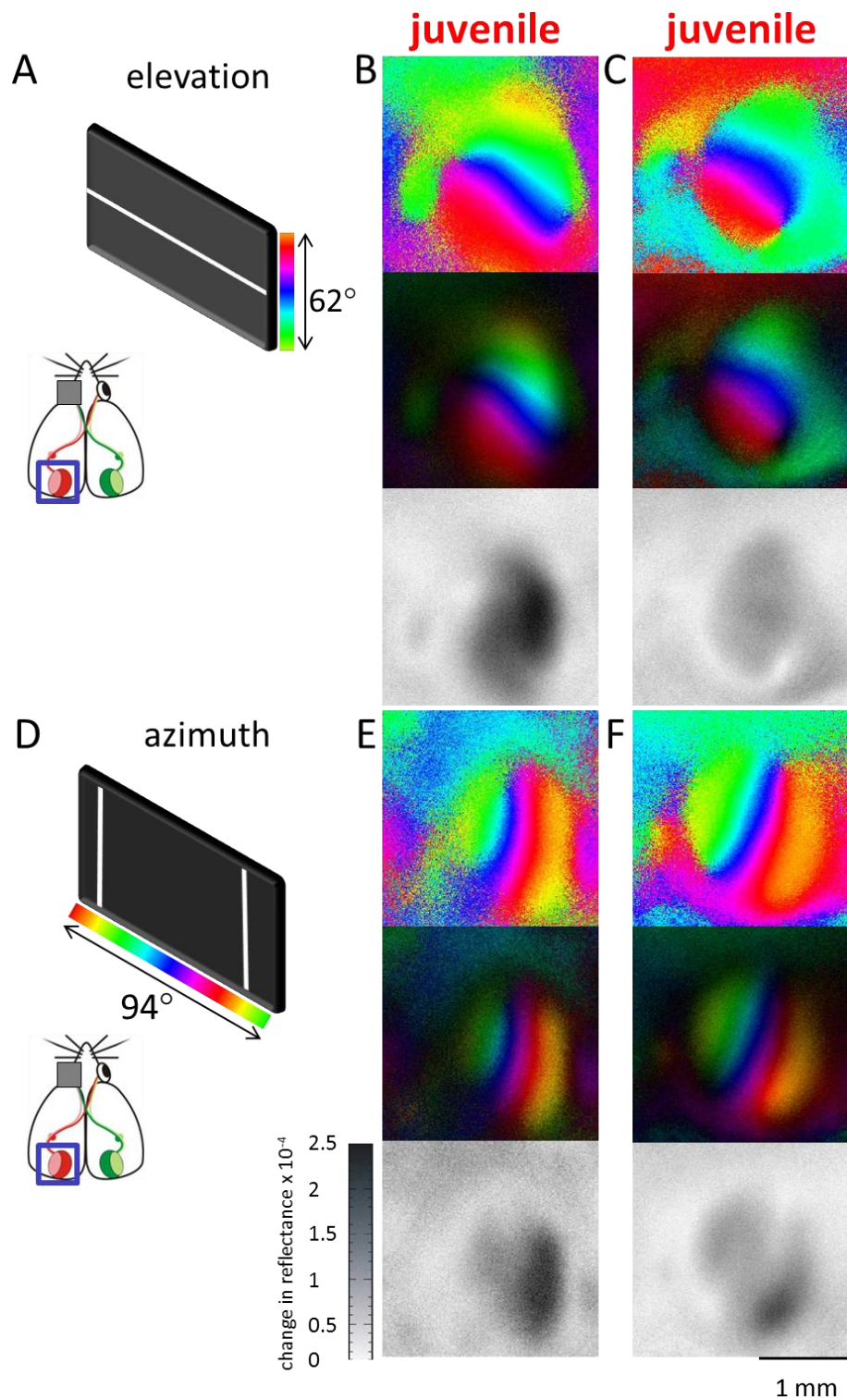


Figure 30: Representatives examples of visual cortical maps recorded with intrinsic signal optical imaging of juvenile *Bsn*^{-/-} mice. Color-coded retinotopic phase map (top), polar maps (middle) and grey-scale coded response magnitude maps (below) of two adult (100 days old) *Bsn*^{-/-} mice (**B,C,E,F**) are illustrated. The magnitude of the optical responses is illustrated as fractional change in reflectance $\times 10^{-4}$. Retinotopic maps are color-coded according to the schemes on the left side (**A,D**). Both elevation (**B,C**) and azimuth (**E,F**) maps resulting from visual stimulation of the animals with full-screen moving horizontal (**A**) or vertical bars (**D**) are shown. Visual cortical maps of juvenile *Bsn*^{-/-} mice have both high response amplitude and excellent retinotopy.

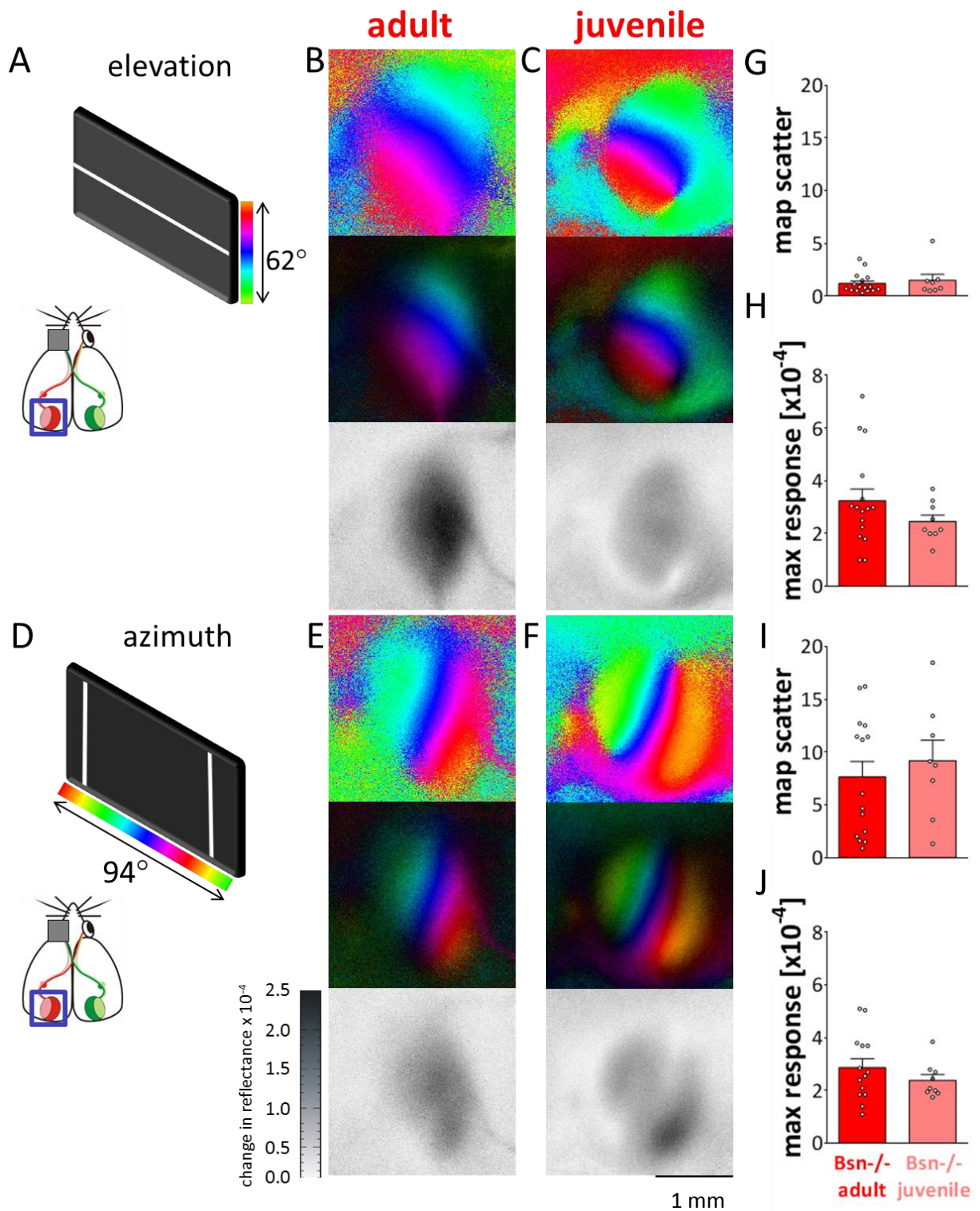




Figure 31: Visual cortical maps recorded with intrinsic signal optical imaging and their quantification of adult and juvenile Bsn^{-/-} mice. Color-coded retinotopic phase map (top), polar maps (middle) and grey-scale coded response magnitude maps (below) of an adult (100 days old) (**B**) and a juvenile Bsn^{-/-} mouse (30 days old) (**C**) are illustrated. The magnitude of the optical responses is illustrated as fractional change in reflectance $\times 10^{-4}$. Retinotopic maps are color-coded according to the schemes on the left side (**A,D**). Both elevation (**B,C**) and azimuth (**E,F**) maps resulting from visual stimulation of the animals with full-screen moving horizontal (**A**) or vertical bars (**D**) are shown. (**G,I**) Quantification of map quality of adult ($n = 15$) and juvenile Bsn^{-/-} mice ($n = 9$). Map quality plotted as map scatter. Visual cortical maps of adult (red) and juvenile Bsn^{-/-} animals (pink) are indistinguishable in magnitude of the visual cortical responses for both elevation (**G**) (t-test, $p > 0.05$) and azimuth maps (**I**) (t-test, $p > 0.05$). (**H,J**) Quantification of magnitude maps of adult ($n = 15$) and juvenile Bsn^{-/-} mice ($n = 9$). Maximum cortical response plotted as a change in reflectance $\times 10^{-4}$. Visual cortical maps of adult (red) and juvenile Bsn^{-/-} animals (pink) are indistinguishable in magnitude of the visual cortical responses for both elevation (**H**) (t-test, $p > 0.05$) and azimuth maps (**J**) (t-test, $p > 0.05$).

Examples of 30-days-old Bsn^{-/-} mice show that visual cortical maps were adult-like already at this age. Adult (Figure 31 B,E) and juvenile Bsn^{-/-} mice (Figure 31 D,F) had similar cortical maps.

Quantitative analyses confirmed this observation and showed that magnitude of the cortical responses for both elevation (Figure 31 B,C) and azimuth maps (Figure 31 E,F) was not significantly different between adult and juvenile Bsn^{-/-} animals (t-test, $p > 0.05$ for all comparisons). The magnitude of the cortical responses for elevation maps was 2.46 ± 0.25 in juvenile and slightly higher with 3.3 ± 0.5 in adult Bsn^{-/-} mice (Figure 31 H). Similarly, the cortical responses for azimuth maps of juvenile and adult Bsn^{-/-} mice were also not significantly different: 2.39 ± 0.22 in juvenile and 2.98 ± 0.34 in adult Bsn^{-/-} mice (Figure 31 J).

Mean scatter of elevation maps of juvenile Bsn^{-/-} mice was 1.51 ± 0.55 and 1.08 ± 0.21 in adult Bsn^{-/-} mice (Figure 31 G). Map quality of azimuth maps of juvenile Bsn^{-/-} mice was 9.20 ± 1.92 and 8.07 ± 1.49 in adult Bsn^{-/-} mice (Figure 31 I). The quality of the retinotopic maps was also similar in both Bsn^{-/-} groups. There were no significant differences in map scatter neither for elevation (t-test, $p > 0.05$) nor for azimuth maps (t-test, $p > 0.05$).

3.6.2 Visual acuity and contrast sensitivity

A large part of these data were already published in Goetze *et al.*, 2010b.

To examine cortical signals also at a higher spatial frequency, near the visual acuity limit of Bassoon mutant mice, we compared the response to the usually used 2° wide bar

(~ 0.25 cyc/deg) with the response to a 1° wide bar (~ 0.5 cyc/deg) in additional experiments for three adult *Bsn*^{-/-} mice. We quantified maximum response and map quality of elevation maps.

Both visual cortical activity level and map quality were similar within the two types of stimuli. For the 1° stimulus, the magnitude of the optical responses was 3.21 ± 0.25 (Figure 32 A) and map quality was 0.89 ± 0.12 (Figure 32 B) and thus not significantly different from the values obtained after visual stimulation with a 2° stimulus in the same animals where the magnitude of the optical responses was 2.69 ± 0.13 (Figure 32 A) and map quality was 0.97 ± 0.08 (Figure 32 B) (t-test, $p > 0.05$ for both comparisons).

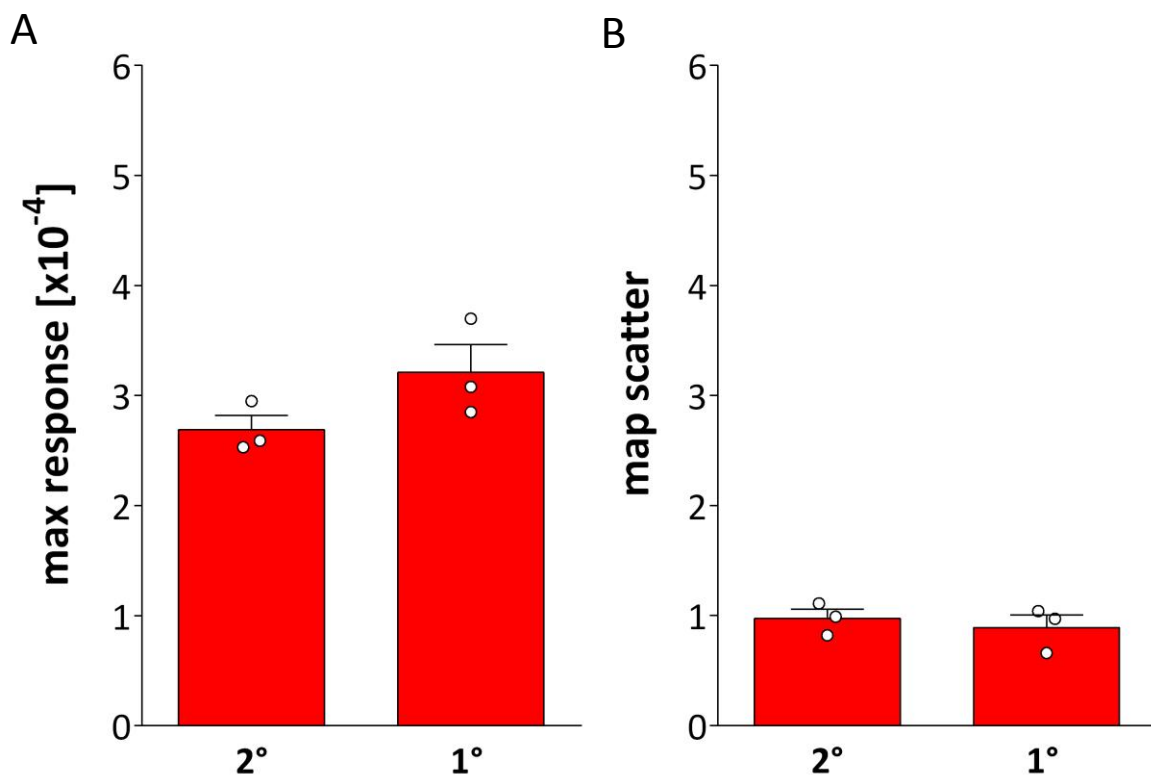


Figure 32: Quantification of magnitude maps and map quality of adult *Bsn*^{-/-} mice (n = 3) at different spatial frequencies. Maximum cortical response plotted as a change in reflectance $\times 10^{-4}$ and map quality plotted as map scatter. Visual cortical maps of adult *Bsn*^{-/-} animals are indistinguishable between a visual stimulus bar of 2° and 1° in magnitude of the visual cortical responses (**A**) as well as map quality (**B**) (t-test, $p > 0.05$).

To have an assessment of contrast sensitivity which is dependent on the visual cortex, we performed additional imaging experiments using visual stimuli of varying contrasts. Figure 33 illustrates some examples of optical recordings in the visual cortex of a wild-type and a mutant animal at 100 %, 70 %, 60 %, 40 %, and 30 % stimulus contrast.

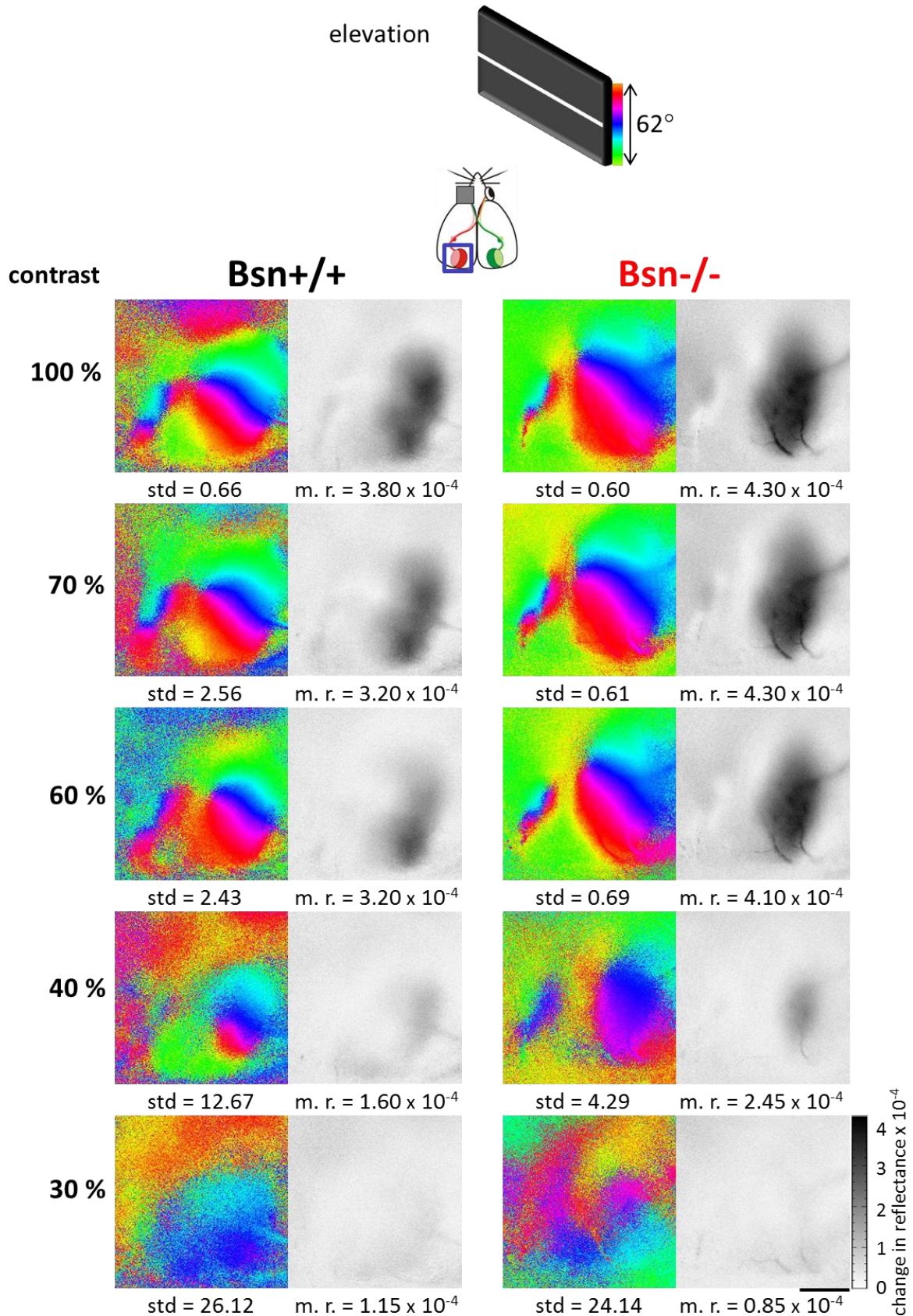


Figure 33: Contrast sensitivity measurements using optical imaging in the visual cortex of adult Bsn+/+ and Bsn-/- mice. Color-coded retinotopic phase maps and gray-scale coded response magnitude maps of visual cortical activation of a Bsn+/+ (left column) and a Bsn-/- (right column) mouse induced by moving horizontal bars (elevation) of decreasing contrast (100 %, 70 %, 60 %, 40 %, and 30 %). Maximum responses (m. r.) and standard deviation (std) of map quality are shown for each cortical map. (Scale bar = 1 mm; Abbreviations: std = standard deviation of map quality, m. r. = maximum response)

The maximum response magnitude of the maps generally decreased while map quality increased gradually with decreasing contrast until there were neither retinotopic phase maps nor cortical activity of at least 0.7×10^{-4} (basal background activity of the cortex) visible.

The comparison of cortical maps revealed that Bsn+/+ mice had an average contrast of 21.52 ± 3.73 % and Bsn-/- mice an average contrast of 26.06 ± 8.85 % (Figure 34). The final contrast values were fitted by a 2nd order polynomial curve with the software MATLAB. Quantifications showed no significant difference between wild-type and Bsn-/- mice (t-test, $p > 0.05$).

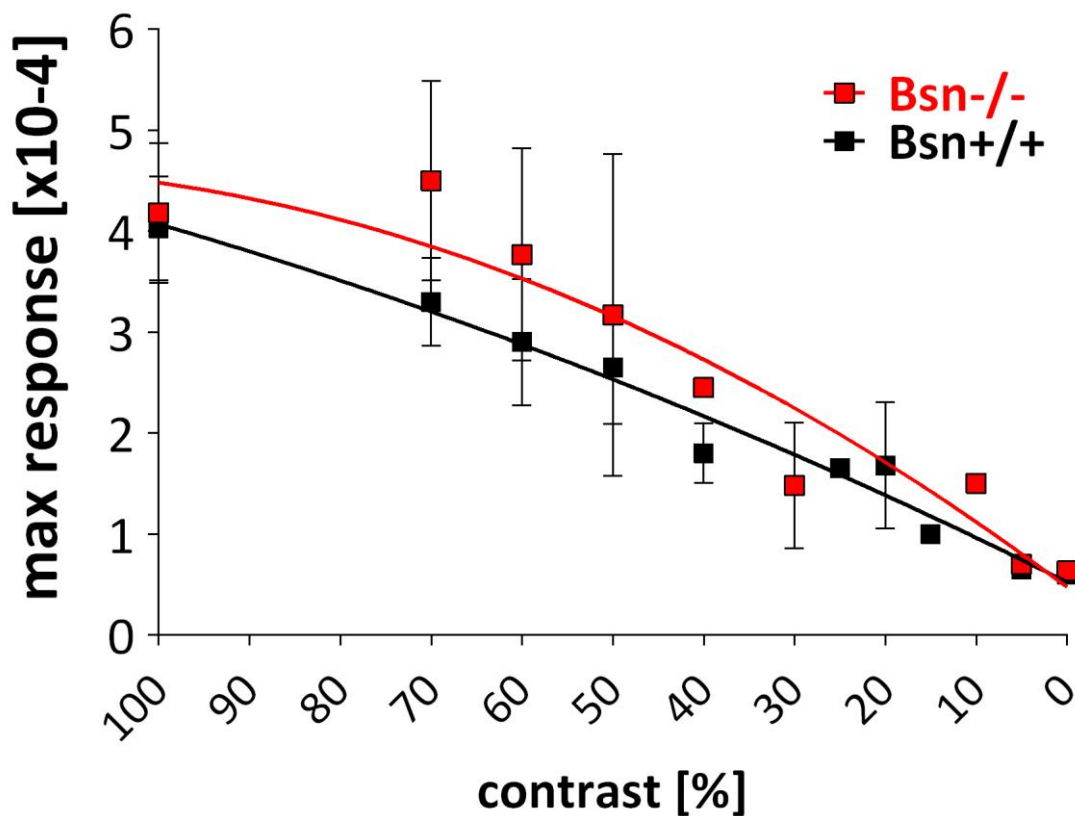


Figure 34: Contrast sensitivity measurements using optical imaging in the visual cortex of adult Bsn+/+ (n = 5) and Bsn-/- mice (n = 4). Maximal cortical responses of Bsn+/+ (black) and Bsn-/- mice (red) plotted as a function of stimulus contrast (100 %, 70 %, 60 %, 50 %, 40 %, 30 %, 25 %, 20 %, 15 %, 10 %, 5 %, and 0 %). Maximum responses decreased gradually with decreasing contrast equally in both genotypes. The data were fitted by a 2nd order polynomial curve. Genotypes were not significantly different (t-test, $p > 0.05$).

3.6.3 Ocular dominance index

A part of these data were already published in Goetze *et al.*, 2010a.

One of the most important questions was if Bassoon mutant mice show cortical plasticity in spite of their excitation-inhibition-imbalance. Using optical imaging of intrinsic signals (Cang *et al.*, 2005a), we compared the response amplitudes in the binocular region of visual cortex after stimulation of the ipsi- and contralateral eye in Bsn^{+/+} and Bsn^{-/-} mice without and with monocular deprivation. Therefore we used seven days of MD in adult (begin at P76 up to P98) mice and tested eight Bsn^{+/+} as well as six Bsn^{-/-} mice and compared them to eleven Bsn^{+/+} and 12 Bsn^{-/-} mice without MD.

In all animals without MD, visual stimulation of the contralateral eye induced stronger cortical activation (activity patches were always darker) than visual stimulation of the ipsilateral eye, which demonstrates the dominance of the contralateral eye in the binocular region of mouse visual cortex (Figure 35 B,C; Figure 36 B,C; Figure 37 B,C). Representative 2-D ocular dominance maps in the binocular region of the left visual cortex of adult Bsn^{+/+} (Figure 35; Figure 37 B,D) and adult Bsn^{-/-} animals (Figure 36; Figure 37 C,E) without and with seven days of MD are displayed in Figure 35, Figure 36, and Figure 37. Additionally, ocular dominance index (ODI) histograms are shown.

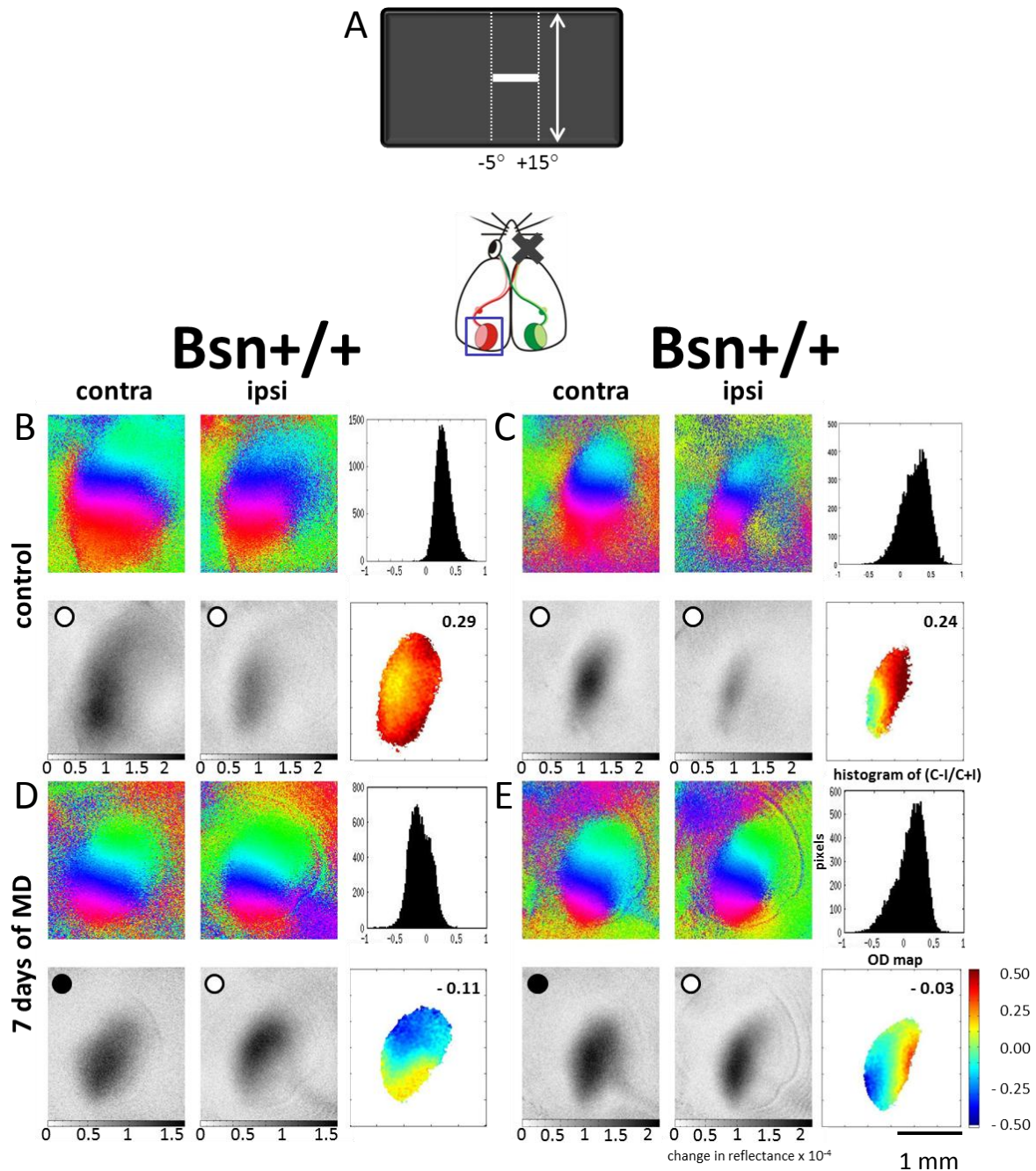


Figure 35: Representative examples of ocular dominance plasticity in adult *Bsn*^{+/+} mice. Optical imaging maps of ipsi- and contralateral responses to the visual stimulation with a horizontal moving bar (elevation) of 20° (**A**) of two control *Bsn*^{+/+} mice (**B,C**) as well as for two *Bsn*^{+/+} mice after seven days of MD (**D,E**) are displayed. Color-coded retinotopic phase maps (top) and gray-scale coded response magnitude maps (bottom) are shown. For each animal the histogram of OD scores, the average ODI and the corresponding 2-D OD maps are included. ODI values are color-coded according to the scheme shown in the lower right corner of the figure: red represents positive values, blue negative values). In control *Bsn*^{+/+} animals, activity patches evoked by the stimulation of the contralateral eye were consistently darker than those after stimulation of the ipsilateral eye (**B,C**) and 2-D OD maps are yellow and red indicating a contralateral dominance. In *Bsn*^{+/+} mice seven days of MD (**D,E**) induced a significant OD shift so that the response magnitude maps of both ipsi- (nondeprived) and contralateral (deprived) eye are now equally dark, the histograms of OD scores shift to the left and colder colors prevail in the 2-D OD maps. (Abbreviations: MD = monocular deprivation, OD = ocular dominance, ODI = ocular dominance index, contra/C = contralateral eye, ipsi/I = ipsilateral eye)

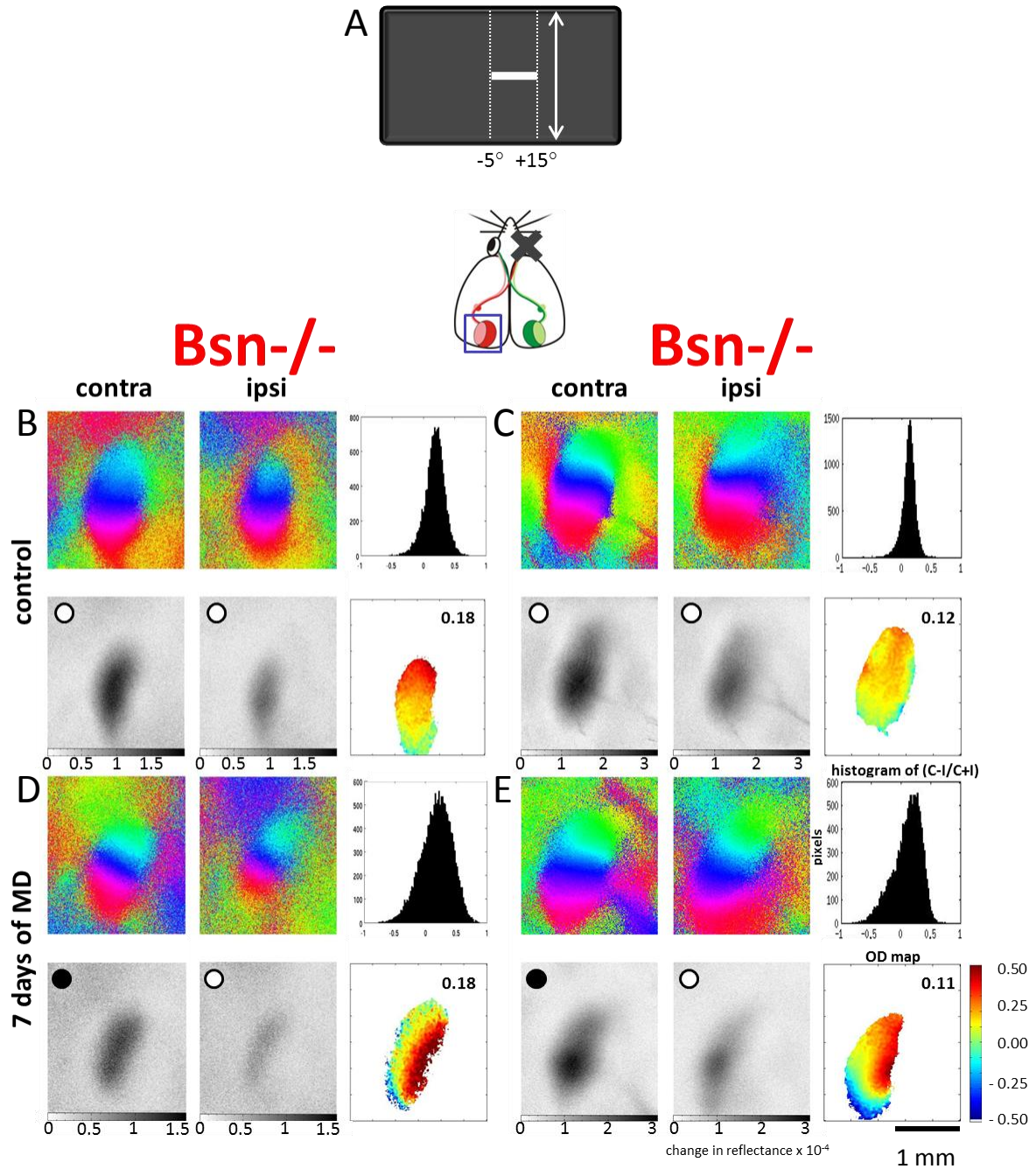


Figure 36: Representative examples of ocular dominance plasticity in adult *Bsn*^{-/-} mice. Optical imaging maps of ipsi- and contralateral responses to the visual stimulation with a horizontal moving bar (elevation) of 20° (**A**) of two control *Bsn*^{-/-} mice (**B,C**) as well as for two *Bsn*^{-/-} mice after seven days of MD (**D,E**) are displayed. Color-coded retinotopic phase maps (top) and gray-scale coded response magnitude maps (bottom) are shown. For each animal the histogram of OD scores, the average ODI and the corresponding 2-D OD maps are included. ODI values are color-coded according to the scheme shown in the lower right corner of the figure: red represents positive values, blue negative values). In control *Bsn*^{-/-} animals, activity patches evoked by the stimulation of the contralateral eye were consistently darker than those after stimulation of the ipsilateral eye (**B,C**) and 2-D OD maps are yellow and red indicating a contralateral dominance. In *Bsn*^{-/-} mice seven days of MD (**D,E**) failed to induce an OD shift (activity patches evoked by the stimulation of the contralateral eye remained equally dark than those after stimulation of the ipsilateral eye) and both histograms of OD scores and 2-D OD maps are similar to control animals. (Abbreviations: MD = monocular deprivation, OD = ocular dominance, ODI = ocular dominance index, contra/C = contralateral eye, ipsi/I = ipsilateral eye)

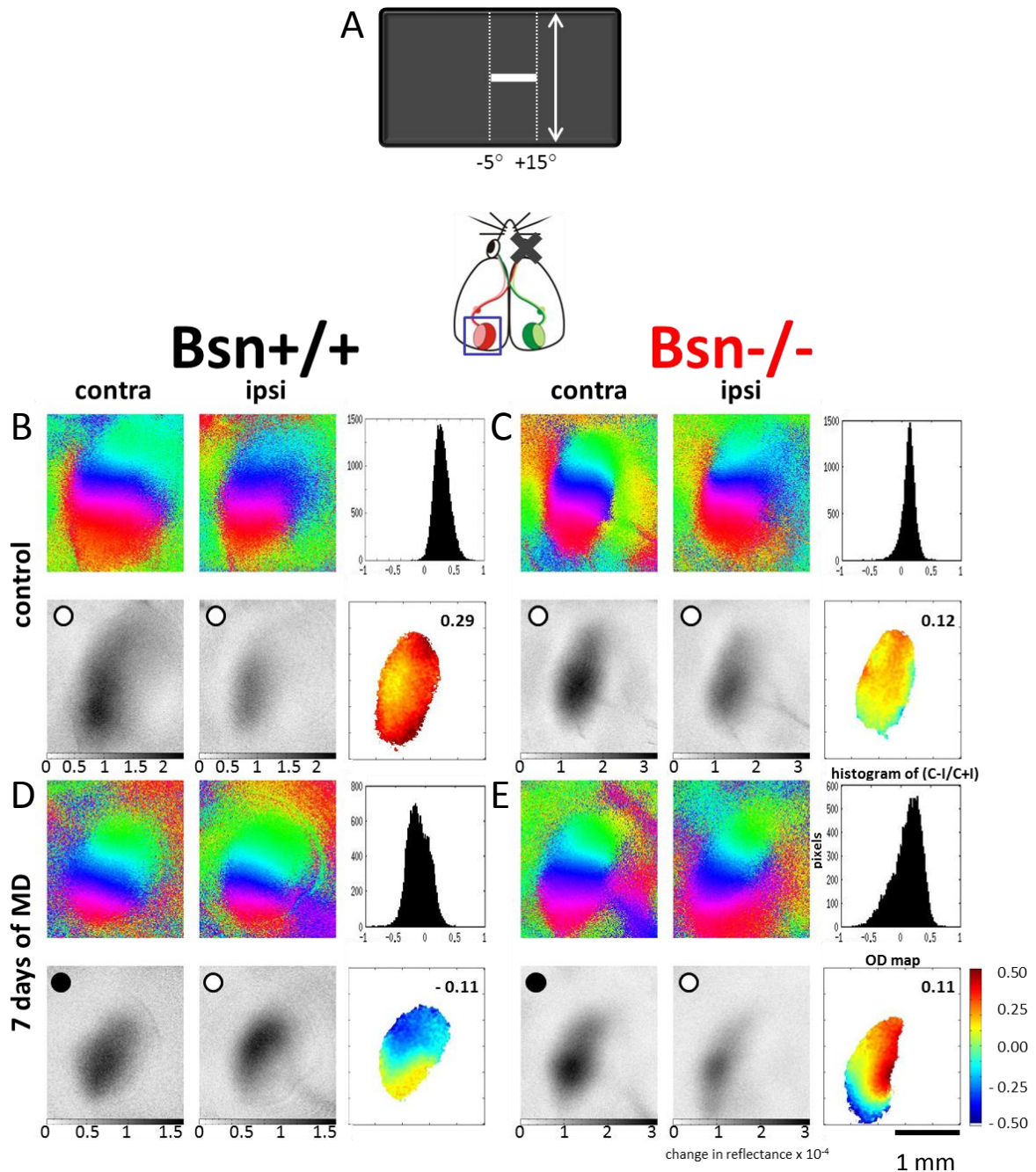


Figure 37: Ocular dominance plasticity in adult *Bsn*^{+/+} and *Bsn*^{-/-} mice. Optical imaging maps of ipsi- and contralateral responses to the visual stimulation with a horizontal moving bar (elevation) of 20° (**A**) of a control *Bsn*^{+/+} (**B**) and a *Bsn*^{-/-} mouse (**C**) as well as for a *Bsn*^{+/+} (**D**) and a *Bsn*^{-/-} mouse (**E**) after seven days of MD are displayed. Color-coded retinotopic phase maps (top) and gray-scale coded response magnitude maps (bottom) are shown. For each animal the histogram of OD scores, the average ODI and the corresponding 2-D OD maps are included. ODI values are color-coded according to the scheme shown in the lower right corner of the figure: red represents positive values, blue negative values). In control *Bsn*^{+/+} and *Bsn*^{-/-} animals, activity patches evoked by the stimulation of the contralateral eye were consistently darker than those after stimulation of the ipsilateral eye (**B,C**) and 2-D OD maps are yellow and red indicating a contralateral dominance. In *Bsn*^{+/+} mice seven days of MD (**D**) induced a significant OD shift so that the response magnitude maps of both ipsi- (nondeprived) and contralateral (deprived) eye are now equally dark, the histograms of OD scores shift to the left and colder colors prevail in the 2-D OD maps. (**E**) In contrast, in *Bsn*^{-/-} mice seven days of MD failed to induce an OD shift (activity patches evoked by the stimulation of the contralateral eye remained equally dark than those after stimulation of the ipsilateral eye) and both histograms of OD scores and 2-D OD maps are similar to control animals. (Abbreviations: MD = monocular deprivation, OD = ocular dominance, ODI = ocular dominance index, contra/C = contralateral eye, ipsi/I = ipsilateral eye)

Adult Bsn^{+/+} animals had average ODIs of 0.23 ± 0.03 (Figure 38) whereas Bsn^{-/-} mice displayed lower average ODIs of 0.13 ± 0.02 (Figure 38). All ocular dominance maps showed warm colors indicating a contralateral dominance (Figure 37 B,C). The comparison of the ODIs in both genotypes showed a significant difference (t-test, $p < 0.01$). To investigate the influence of monocular deprivation on ocular dominance of adult mice, we performed MD for seven days. In Bsn^{+/+} animals seven days of MD had a significant effect on ocular dominance just as in wild-type mice (Lehmann and Löwel, 2008). Visual stimulation of the contralateral eye induced no longer a stronger cortical activation than visual stimulation of the ipsilateral eye (activity patches were equally dark) (Figure 37 B). Bsn^{+/+} mice showed a significant OD shift by showing average ODIs of -0.03 ± 0.04 (t-test, $p < 0.001$) (Figure 38 A). In contrast, after seven days of MD Bassoon mutant mice, visual stimulation of the contralateral eye induced stronger cortical activation (activity patches were darker) than visual stimulation of the ipsilateral eye (Figure 37 E), which demonstrates the dominance of the contralateral eye in the binocular region of mouse visual cortex. Therefore, Bassoon mutant mice showed no significant OD shift by showing average ODIs of 0.14 ± 0.03 (Figure 38 A) (t-test, $p > 0.05$). Compared to their wild-type littermates after seven days of MD, there is a significant difference (t-test, $p < 0.01$).

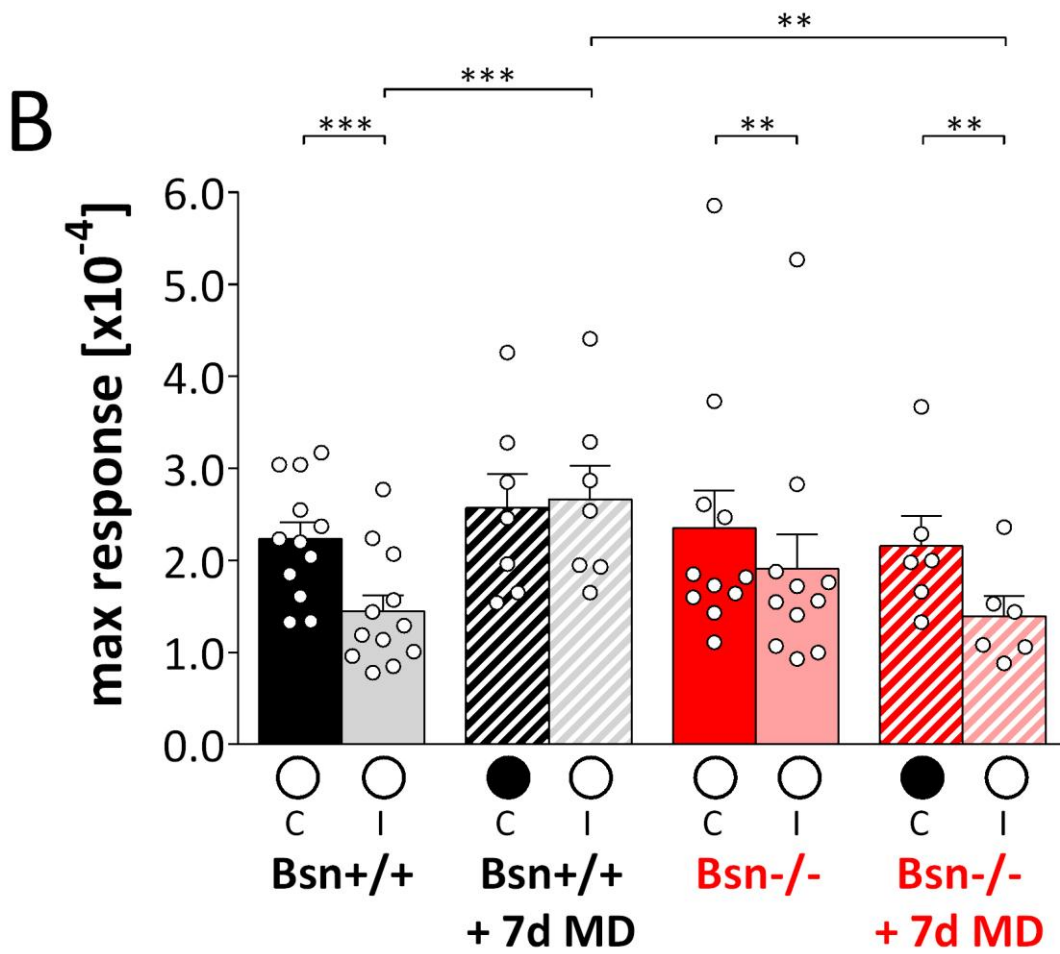
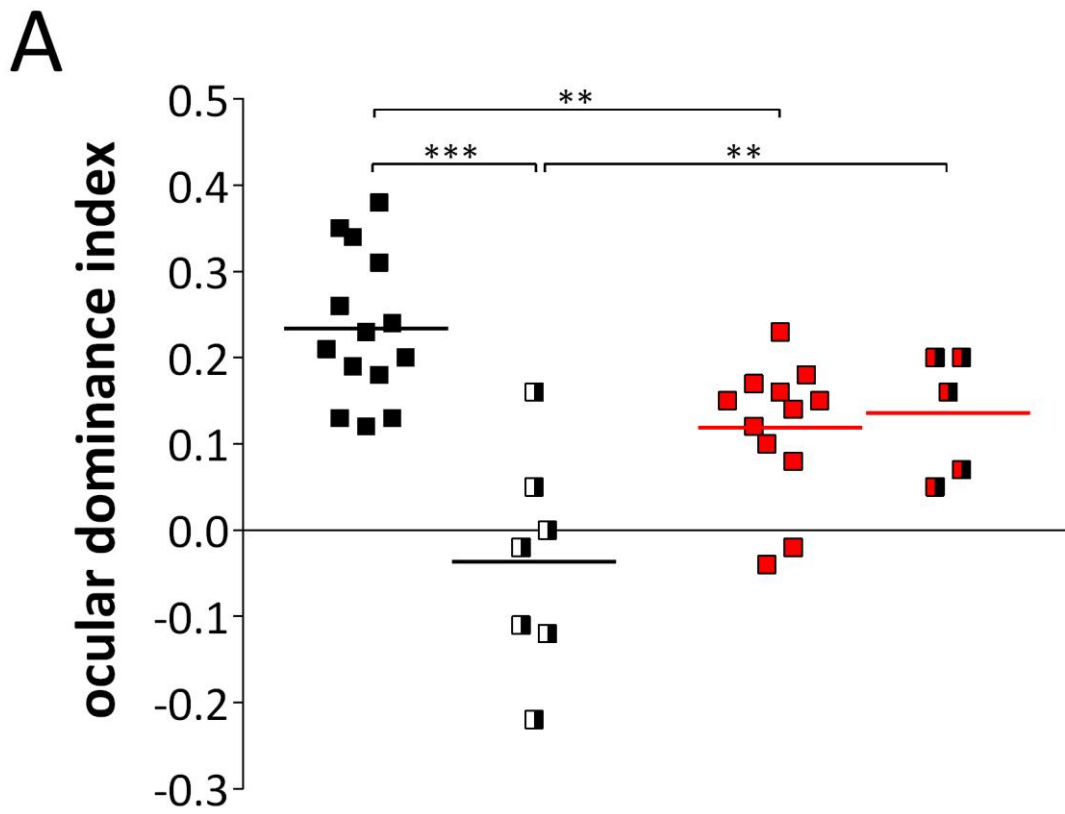




Figure 38: Ocular dominance indices and maximum response magnitude of adult Bsn+/+ (n = 11/n = 8) and Bsn-/- mice (n = 12/n = 6) without and with seven days of MD. (A) A positive ODI indicates dominance of the contralateral eye, a negative ODI ipsilateral dominance. Squares represent ODI values of individual animals; means are marked by thick horizontal lines. Note that Bsn+/+ (black) and Bsn-/- mice (red) without MD showed OD of the contralateral eye but Bsn-/- animals revealed significant lower ODs (t-test, $p < 0.01$). Seven days of monocular deprivation in Bsn+/+ mice induced a significant OD shift toward the open eye (t-test, $p < 0.001$). In contrast, in Bsn-/- mice MD had no such effect (t-test, $p > 0.05$). Thus ODs of Bsn+/+ and Bsn-/- animals after seven days of MD were significantly different from (t-test, $p < 0.01$). **(B)** Maximum cortical response expressed as a change in reflectance $\times 10^{-4}$ by stimulation of the contralateral (C) or ipsilateral (I) eye in Bsn+/+ (black) and Bsn-/- mice (red) without and with seven days of MD. In all control animals, cortical activation after visual stimulation of the contralateral eye was significantly higher than after ipsilateral eye stimulation (t-test, $p < 0.01$), reflecting the dominance of the contralateral eye. In Bsn+/+ mice after seven days of MD, response strengths of the two eyes were no longer significantly different because the nondeprived-eye responses were significantly increased compared with controls (t-test, $p < 0.001$). In contrast, after seven days of MD in Bsn-/- mice, the response strengths of both eyes remained significantly different (t-test, $p < 0.01$).

Without MD control mice of both genotypes displayed significantly higher maximum cortical response after visual stimulation of the contralateral eye (Figure 38 B) (t-test, $p < 0.01$ for both comparisons). The change of ocular dominance in Bsn+/+ mice is mediated by a significantly strengthening of cortical responses after visual stimulation of the nondeprived ipsilateral eye (Figure 38 B) (t-test, $p < 0.001$). This result is consistent with already published data for adult wild-type mice (Hofer *et al.*, 2006b). In contrast, Bsn-/- mice didn't show any change in maximum cortical response after MD (Figure 38 B) given that maximum responses of both eyes were still significantly different (t-test, $p < 0.01$). Thus after MD the maximum response of Bsn+/+ and Bsn-/- animals were significantly different (t-test, $p < 0.01$).

Since adult Bassoon mutant mice lack adult OD plasticity we wanted know if the juvenile type of plasticity is still present in Bsn-/- mice. In addition we used four days of MD in juvenile animals (begin at P24 up to P29) mice and tested three Bsn+/+ as well as five Bsn-/- mice and compared them to five Bsn+/+ and eight Bsn-/- mice without MD.

In all animals without MD, visual stimulation of the contralateral eye induced stronger cortical activation (activity patches were always darker) than visual stimulation of the ipsilateral eye, which demonstrates the dominance of the contralateral eye in the binocular region of mouse visual cortex (Figure 39 B,C; Figure 40 B,C; Figure 41 B,C). Representative two-dimensional ocular dominance maps in the binocular region of the left visual cortex of juvenile Bsn+/+ (Figure 39; Figure 41 B,D) and juvenile Bsn-/- animals (Figure 40; Figure 41 C,E) without and with seven days of MD are displayed in Figure 39, Figure 40, and Figure 41. Additionally, ocular dominance index (ODI) histograms are shown.

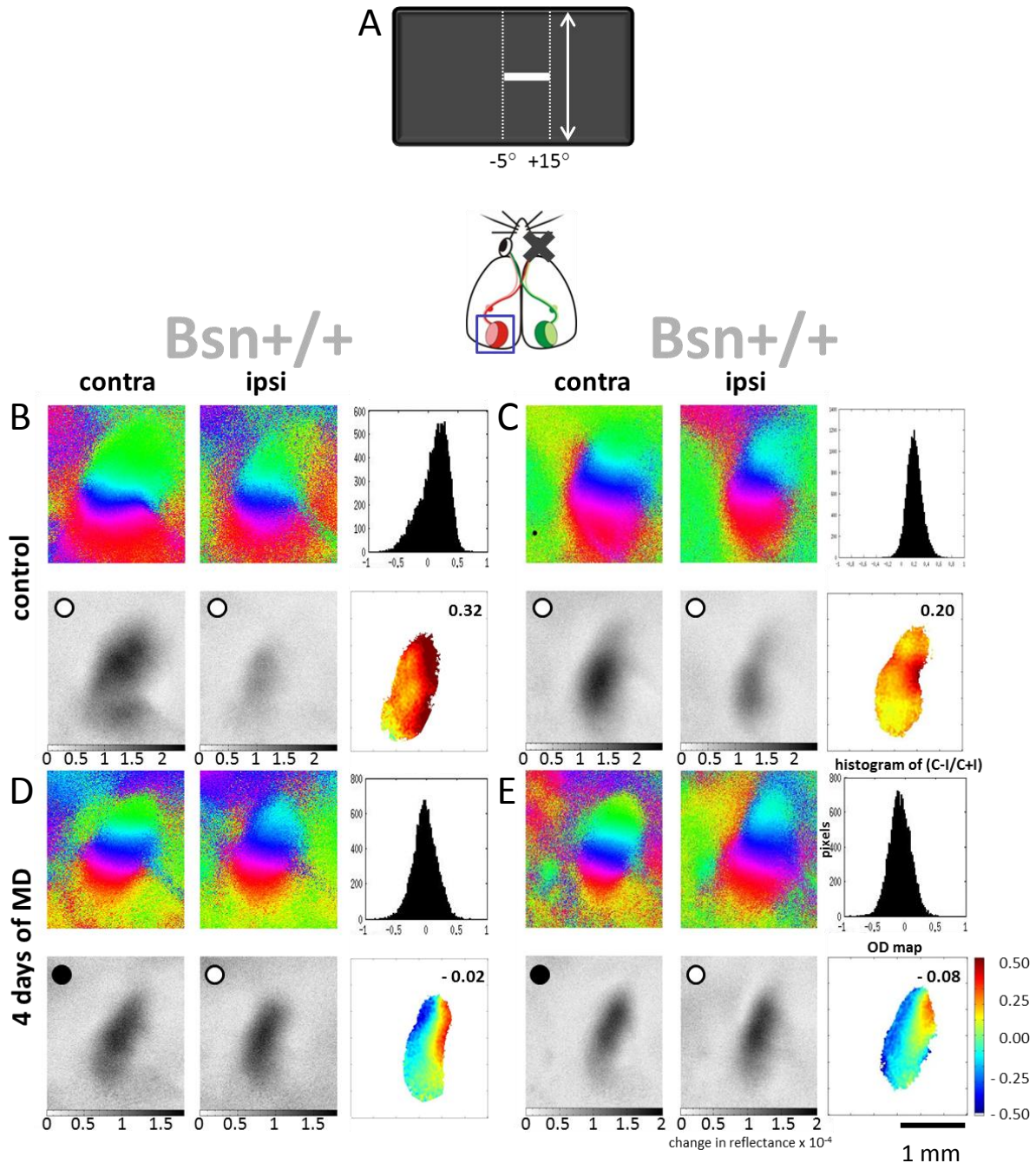


Figure 39: Representative examples of ocular dominance plasticity in juvenile Bsn+/+ mice. Optical imaging maps of ipsi- and contralateral responses to the visual stimulation with a horizontal moving bar (elevation) of 20° (**A**) of two control Bsn+/+ mice (**B,C**) as well as for two Bsn+/+ mice after four days of MD (**D,E**) are displayed. Color-coded retinotopic phase maps (top) and gray-scale coded response magnitude maps (bottom) are shown. For each animal the histogram of OD scores, the average ODI and the corresponding 2-D OD maps are included. ODI values are color-coded according to the scheme shown in the lower right corner of the figure: red represents positive values, blue negative values). In control Bsn+/+ animals, activity patches evoked by the stimulation of the contralateral eye were consistently darker than those after stimulation of the ipsilateral eye (**B,C**) and 2-D OD maps are yellow and red indicating a contralateral dominance. In Bsn+/+ (**D,E**) four days of MD induced a significant OD shift so that the response magnitude maps of both ipsi- (nondeprived) and contralateral (deprived) eye are now equally dark, the histograms of OD scores shift to the left and colder colors prevail in the 2-D OD maps. (Abbreviations: MD = monocular deprivation, OD = ocular dominance, ODI = ocular dominance index, contra/C = contralateral eye, ipsi/I = ipsilateral eye)

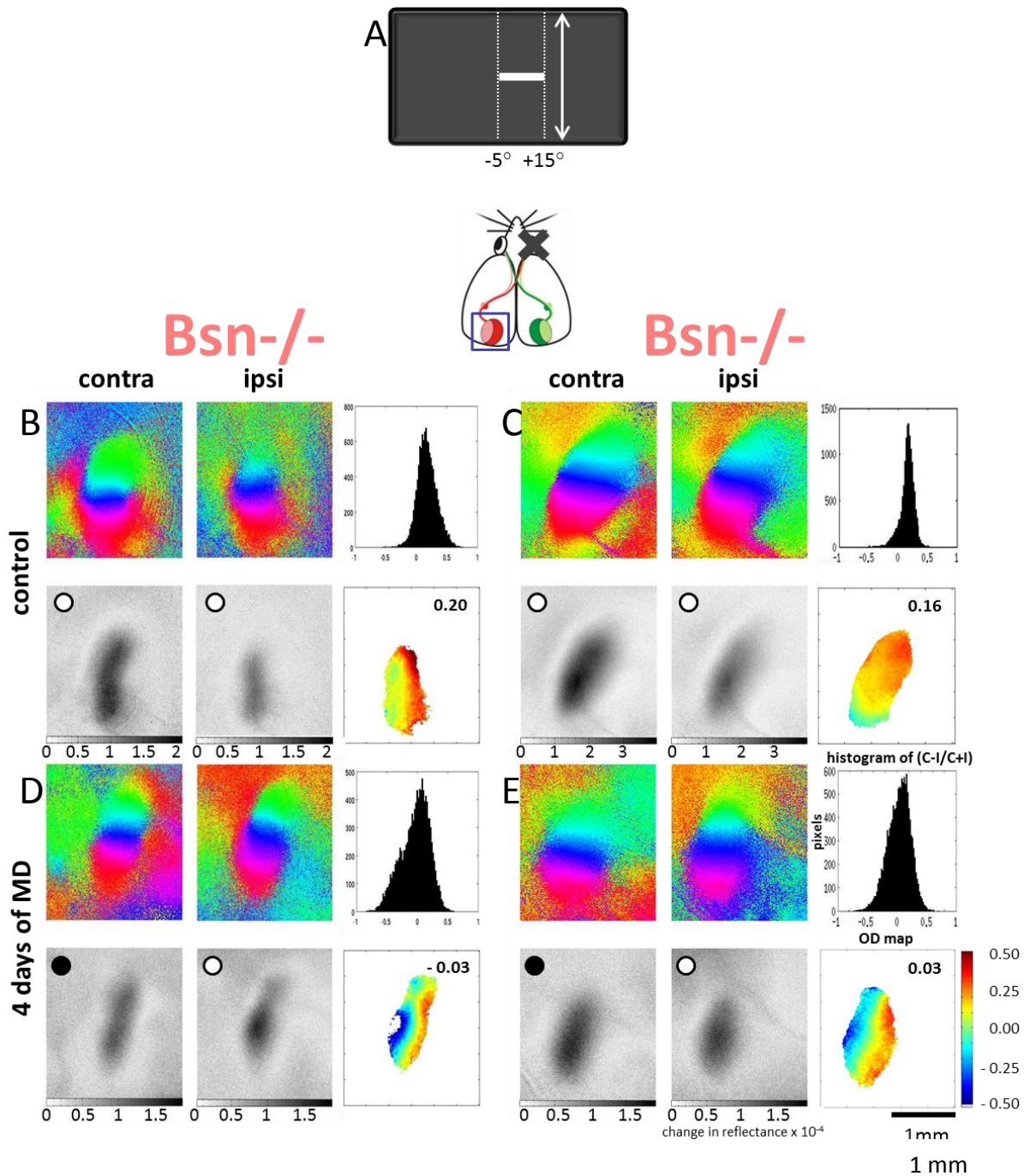


Figure 40: Representative examples of ocular dominance plasticity in juvenile *Bsn*^{-/-} mice. Optical imaging maps of ipsi- and contralateral responses to the visual stimulation with a horizontal moving bar (elevation) of 20° (**A**) of two control *Bsn*^{-/-} mice (**B,C**) as well as for two *Bsn*^{-/-} mice after four days of MD (**D,E**) are displayed. Color-coded retinotopic phase maps (top) and gray-scale coded response magnitude maps (bottom) are shown. For each animal the histogram of OD scores, the average ODI and the corresponding 2-D OD maps are included. ODI values are color-coded according to the scheme shown in the lower right corner of the figure: red represents positive values, blue negative values). In control *Bsn*^{-/-} animals, activity patches evoked by the stimulation of the contralateral eye were consistently darker than those after stimulation of the ipsilateral eye (**B,C**) and 2-D OD maps are yellow and red indicating a contralateral dominance. In *Bsn*^{-/-} mice (**D,E**) four days of MD induced a significant OD shift so that the response magnitude maps of both ipsi- (nondeprived) and contralateral (deprived) eye are now equally dark, the histograms of OD scores shift to the left and colder colors prevail in the 2-D OD maps. (Abbreviations: MD = monocular deprivation, OD = ocular dominance, ODI = ocular dominance index, contra/C = contralateral eye, ipsi/I = ipsilateral eye)

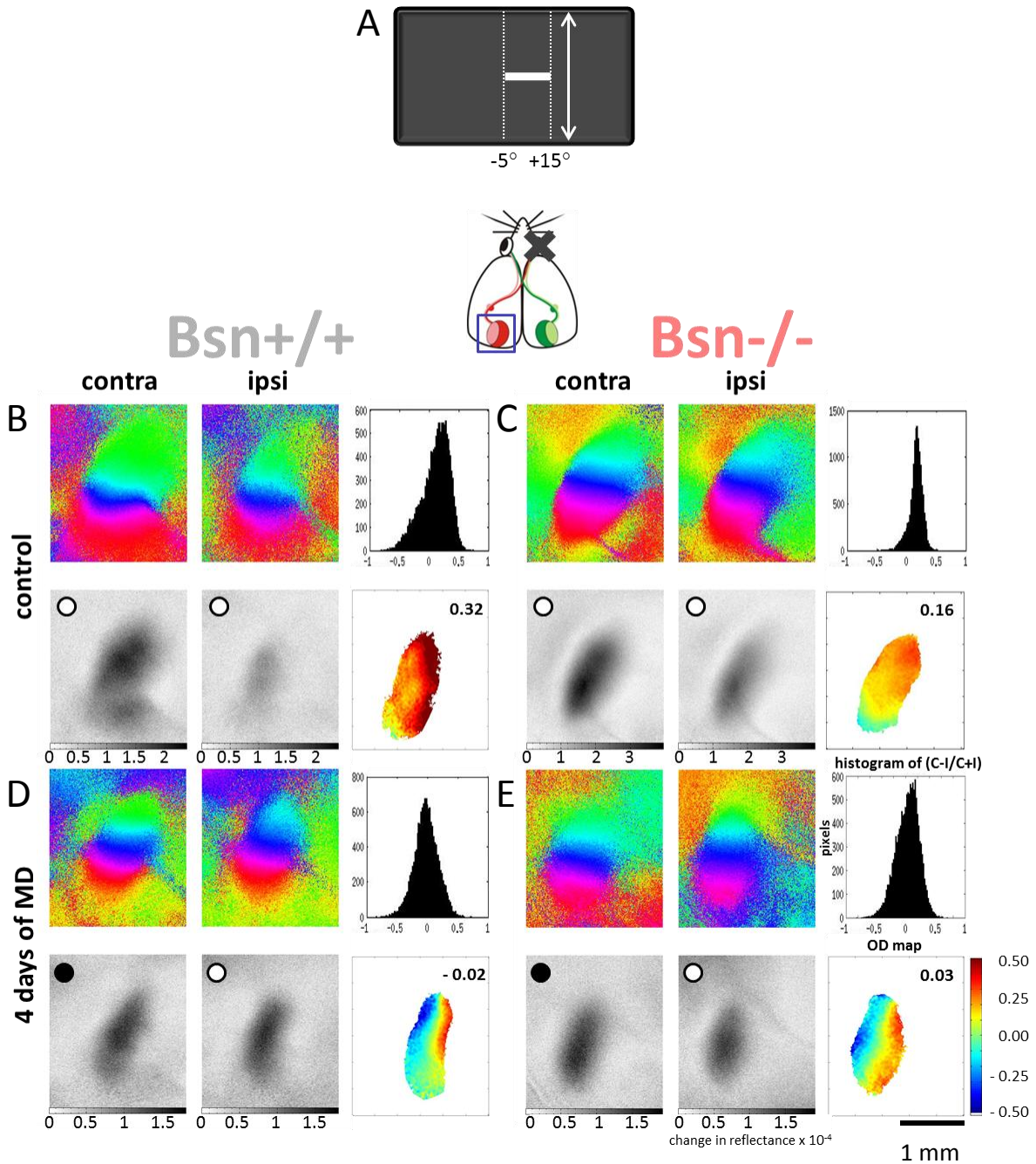


Figure 41: Ocular dominance plasticity in juvenile Bsn+/+ and Bsn-/- mice. Optical imaging maps of ipsi- and contralateral responses to the visual stimulation with a horizontal moving bar (elevation) of 20° (A) of a control Bsn+/+ (B) and a Bsn-/- mouse (C) as well as for a Bsn+/+ (D) and a Bsn-/- mouse (E) after four days of MD are displayed. Color-coded retinotopic phase maps (top) and gray-scale coded response magnitude maps (bottom) are shown. For each animal the histogram of OD scores, the average ODI and the corresponding 2-D OD maps are included. ODI values are color-coded according to the scheme shown in the lower right corner of the figure: red represents positive values, blue negative values). In control Bsn+/+ and Bsn-/- animals, activity patches evoked by the stimulation of the contralateral eye were consistently darker than those after stimulation of the ipsilateral eye (B,C) and 2-D OD maps are yellow and red indicating a contralateral dominance. In Bsn+/+ (D) as well as in Bsn-/- mice (E) four days of MD induced a significant OD shift so that the response magnitude maps of both ipsi- (nondeprived) and contralateral (deprived) eye are now equally dark, the histograms of OD scores shift to the left and colder colors prevail in the 2-D OD maps. (Abbreviations: MD = monocular deprivation, OD = ocular dominance, ODI = ocular dominance index, contra/C = contralateral eye, ipsi/I = ipsilateral eye)

Juvenile Bsn^{+/+} animals had average ODIs of 0.25 ± 0.03 (Figure 42) whereas Bsn^{-/-} mice displayed lower average ODIs of 0.15 ± 0.02 (Figure 42). All ocular dominance maps showed warm colors indicating a contralateral dominance (Figure 41 B,C). The comparison of the ODIs both genotypes showed significant difference (t-test, $p < 0.05$). To investigate the influence of monocular deprivation on ocular dominance of juvenile mice, we now performed MD for four days. In Bsn^{+/+} animals four days of MD had significant effect on ocular dominance just as in wild-type mice (Lehmann and Löwel, 2008). Visual stimulation of the contralateral eye induced no longer a stronger cortical activation than visual stimulation of the ipsilateral eye (activity patches were equally dark) (Figure 41 D). Bsn^{+/+} mice showed a significant OD shift by showing average ODIs of -0.05 ± 0.03 (t-test, $p < 0.001$) (Figure 42 A). Interestingly, after four days of MD also Bassoon mutant mice showed a significant OD shift by showing average ODIs of 0.02 ± 0.03 (Figure 42 A) (t-test, $p < 0.01$). Visual stimulation of the contralateral eye induced no longer a stronger cortical activation than visual stimulation of the ipsilateral eye (activity patches were equally dark) (Figure 41 E). Compared to Bassoon wild-type littermates after four days of MD, there is no significant difference anymore (t-test, $p > 0.05$). But there is a significant difference between ODI values of adult and juvenile Bsn^{-/-} animals after MD (t-test, $p < 0.05$).

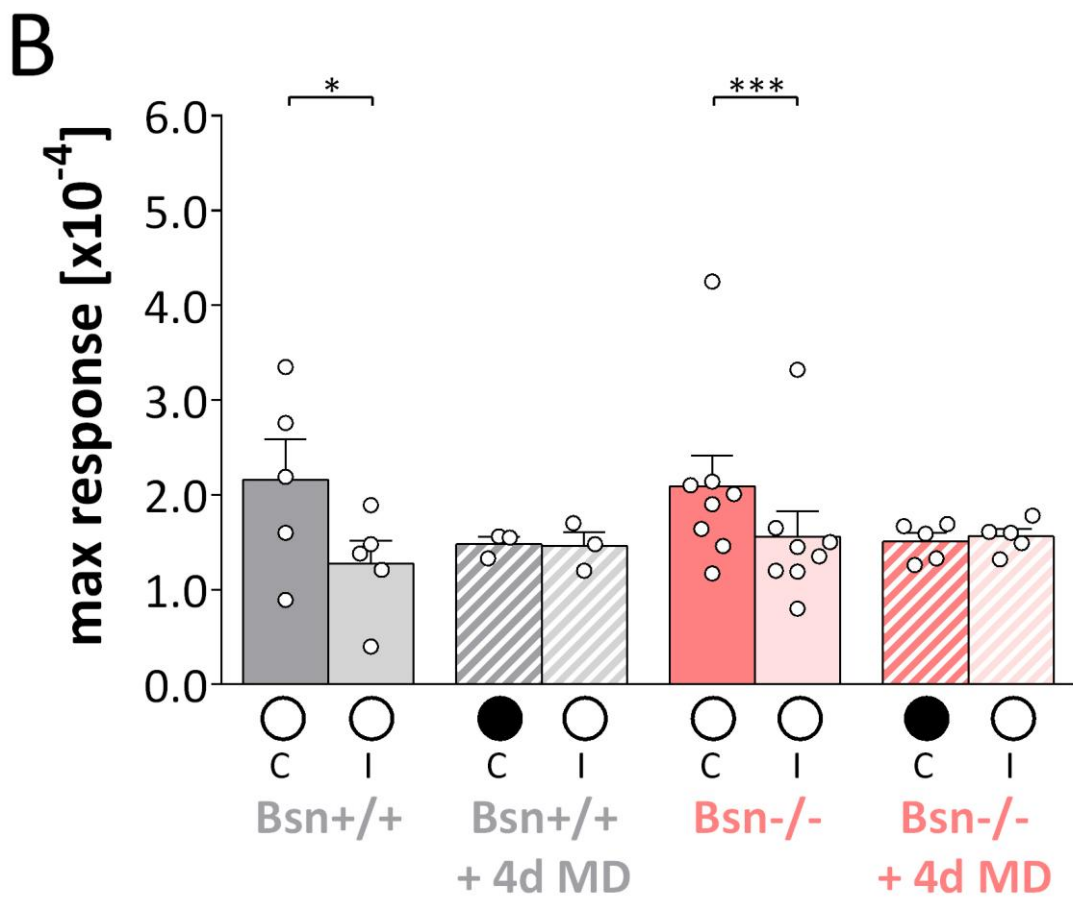
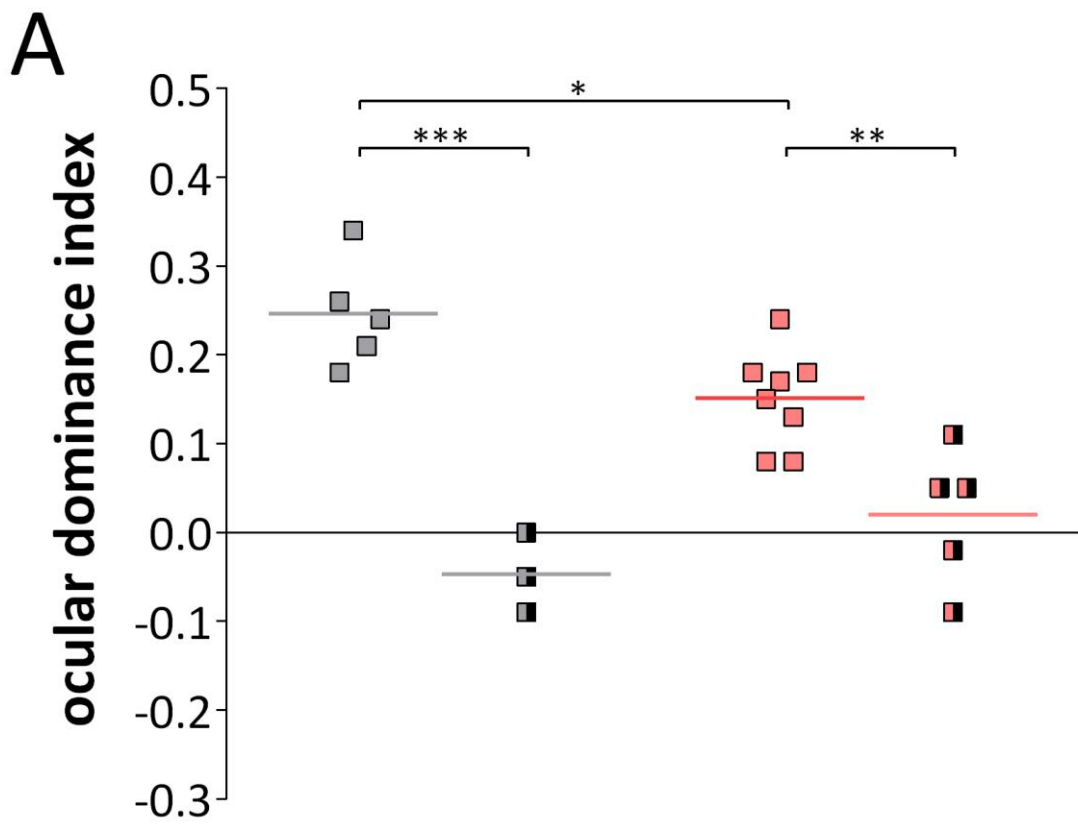




Figure 42: Ocular dominance indices and maximum response magnitude of juvenile Bsn^{+/+} (n = 5/n = 3) and Bsn^{-/-} mice (n = 8/n = 5) without and with seven days of MD. (A) A positive ODI indicates dominance of the contralateral eye, a negative ODI ipsilateral dominance. Squares represent ODI values of individual animals; means are marked by thick horizontal lines. Note that Bsn^{+/+} (gray) and Bsn^{-/-} mice (pink) without MD showed OD of the contralateral eye but Bsn^{-/-} animals revealed significant lower ODIs (t-test, $p < 0.05$). Four days of monocular deprivation in Bsn^{+/+} as well as in Bsn^{-/-} mice induced a significant OD shift toward the open eye (t-test, $p < 0.01$). **(B)** Maximum cortical response expressed as a change in reflectance $\times 10^{-4}$ by stimulation of the contralateral (C) or ipsilateral (I) eye in Bsn^{+/+} (gray) and Bsn^{-/-} mice (pink) without and with four days of MD. In all control animals, cortical activation after visual stimulation of the contralateral eye was significantly higher than after ipsilateral eye stimulation (t-test, $p < 0.05$), reflecting the dominance of the contralateral eye. In Bsn^{+/+} as well as in Bsn^{-/-} mice after four days of MD, response strengths of the two eyes were no longer significantly different because the deprived-eye responses were reduced (t-test, $p > 0.05$ for both comparisons).

Without MD control mice of both genotypes displayed significantly higher maximum cortical response after visual stimulation of the contralateral eye (Figure 42 B) (t-test, $p < 0.05$ for both comparisons) but not after four days of MD (t-test, $p > 0.05$ for both comparisons). The change of ocular dominance in Bsn^{+/+} and Bsn^{-/-} mice is mediated by a weakening of cortical responses after visual stimulation of the deprived contralateral eye (Figure 42 B), which is trending but not significant, perhaps due to low number of animals. This trend is consistent with already published data for juvenile WT mice (Hofer *et al.*, 2006b).

3.7 Immunohistochemistry

3.7.1 Parvalbumin (PV)

Due to the excitation-inhibition-imbalance of Bassoon mutant mice and because inhibition plays a major role in synaptic plasticity we stained parvalbumin in the visual cortex using immunohistochemistry. Given that the expression of parvalbumin in visual cortical interneurons depends on neuronal activity (Patz *et al.*, 2004) there might be a visible increase in parvalbumin expression in parvalbumin negative interneurons. An increased number of PV expressing interneurons might be an explanation for the absence of OD plasticity in adult Bsn^{-/-} animals. Ghiglieri and her colleagues (2009) have already shown that the number of parvalbumin expressing interneurons in the striatum of Bsn^{-/-} mice is increased and this might be the reason for the abnormal striatal plasticity in these animals.

Therefore we stained parvalbumin (Cy2) in three Bsn^{+/+} mice at P22, three at P30, and six at P100 as well as three Bsn^{-/-} mice at P22, three at P30 and five at P100. We counted the number of parvalbumin expressing interneurons per 1 mm² visual cortex. Representative staining examples of the visual cortex of P22, P30, and P100 Bsn^{+/+} and Bsn^{-/-} animals are displayed in Figure 43.

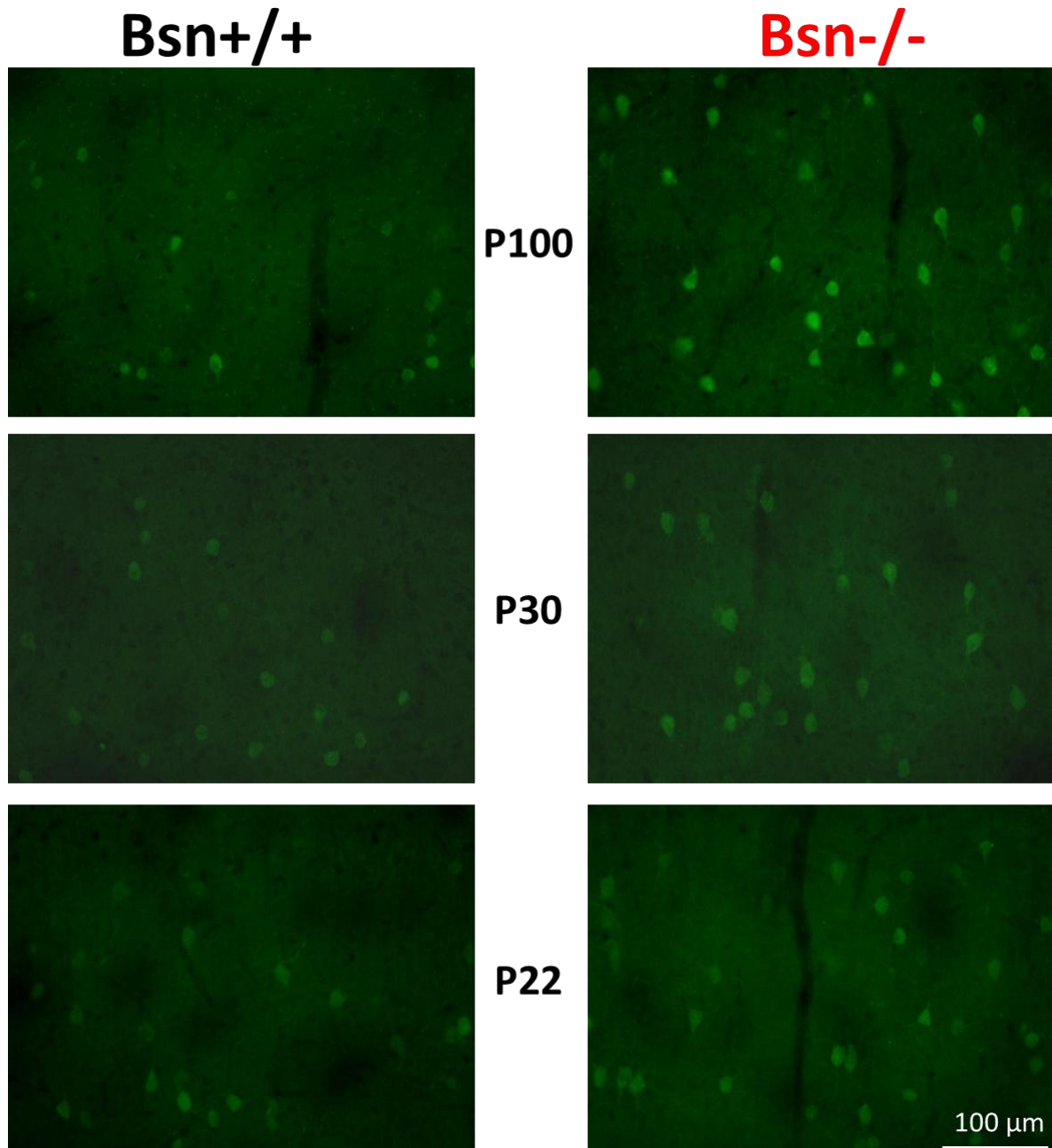


Figure 43: Coronal brain sections of the visual cortex layers II-IV of Bsn^{+/+} and Bsn^{-/-} mice stained against parvalbumin. Illustrated are six coronal sections stained against PV (Cy2, green) from P22 (bottom), P30 (middle), and P100 (top). One can clearly see that Bassoon mutant mice (right column) displayed more PV expressing interneurons per 1 mm² visual cortex in layers II-IV than their Bsn^{+/+} littermates (left column). And additionally this number of PV expressing interneurons increased over time from P22 over P30 up to P100 in Bsn^{-/-} mice.

Bsn^{+/+} mice showed at the age of P22 an average number of parvalbumin positive (PV⁺) interneurons per 1 mm² visual cortex in layers II-IV of 59.7 ± 2.00 , at P30 of 60.4 ± 2.53 , and at P100 of 59.7 ± 3.53 (Figure 44). These values of different ages were not significantly different among each other (t-test, $p > 0.05$ for all comparisons). In contrast, Bsn^{-/-} showed at the age of P22 an average number of PV⁺ interneurons per 1 mm² visual cortex in layers II-IV of 68.0 ± 2.00 , at P30 of 74.7 ± 2.41 , and at P100 of 98.8 ± 3.47 (Figure 44). Surprisingly the number of PV⁺ interneurons increased significantly from P20 to P30 (t-test, $p < 0.05$) and from P30 again to P100 actually significant (t-test, $p < 0.001$). Also P20 and P100 were significantly different in Bsn^{-/-} animals (t-test, $p < 0.001$). The number of PV⁺ interneurons of all different age groups (P20, P30, and P100) were significantly different between Bsn^{+/+} and Bsn^{-/-} mice (Figure 44) (t-test, $p < 0.01$ for all comparisons).

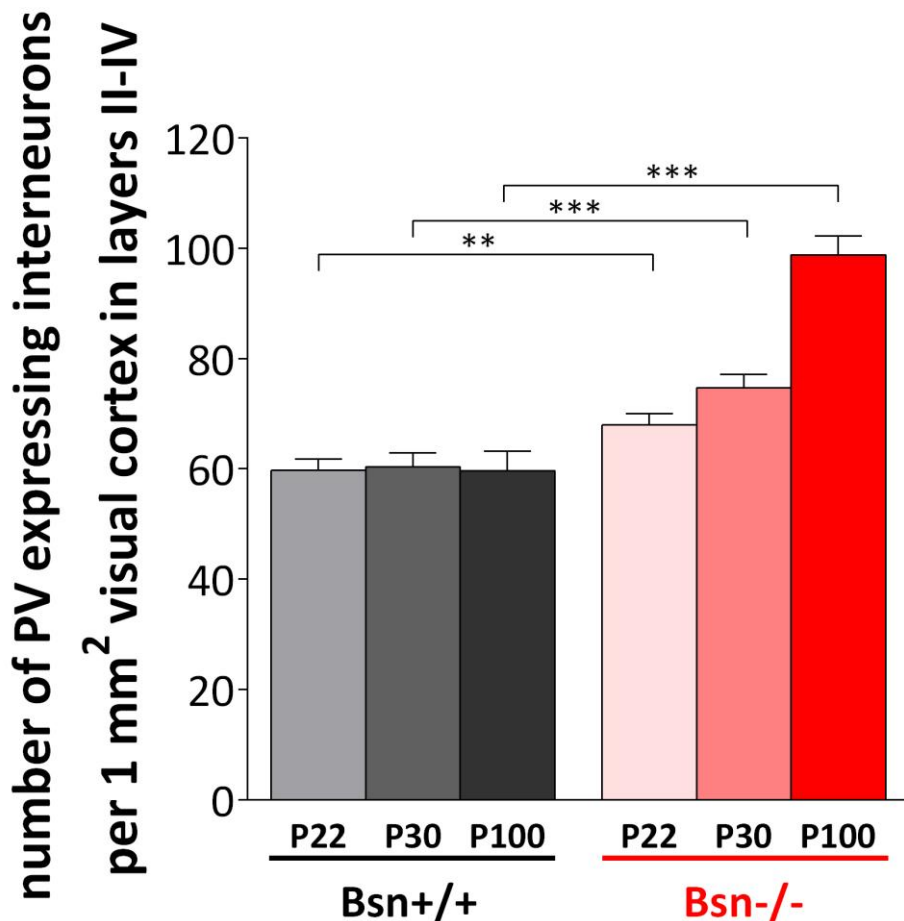


Figure 44: Number of parvalbumin positive interneurons per 1 mm² visual cortex in layers II-IV of Bsn^{+/+} (n = 3/ n = 3/ n = 6) and Bsn^{-/-} mice (n = 3/ n = 3/ n = 6) at the age of P20, P30 and P100. The number of PV expressing interneurons did not differ significantly in Bsn^{+/+} (gray to black) over time (t-test, $p > 0.05$ for all comparisons). Whereas in Bsn^{-/-} mice (pink to red) the number of PV⁺ interneurons increased significant from P20 to P30 up to P100 (t-test, $p < 0.01$ for all comparisons). The number of PV expressing interneurons of all different age groups (P20, P30, and P100) were significantly different between Bsn^{+/+} and Bsn^{-/-} mice (t-test, $p < 0.01$ for all comparisons). (Abbreviation: PV⁺ = parvalbumin positive)

3.7.2 Kv3.1b

Since *Bsn*^{-/-} mice showed an increased number of parvalbumin expressing interneurons we wanted to address the question if this was due to an augmented activation of silent/inactive interneurons, which did not express the calcium-binding protein parvalbumin. Therefore we stained PV together with the potassium channel Kv3.1b, which is reputed to be present only in parvalbumin-containing interneurons (Chow *et al.*, 1999). In mouse somatosensory cortex using double-labeling immunofluorescence, Chow *et al.* (1999) found that the majority of cells (99 %) expressing Kv3.1b proteins are PV positive and most cells expressing PV are positive for Kv3.1b (> 99 %).

Therefore parvalbumin (Cy2) and Kv3.1b (Cy3) was stained in three *Bsn*^{+/+} as well as in the visual cortex of three *Bsn*^{-/-} mice at an age of P100. Representative staining examples of the visual cortex of *Bsn*^{+/+} and *Bsn*^{-/-} animals are displayed in Figure 45.

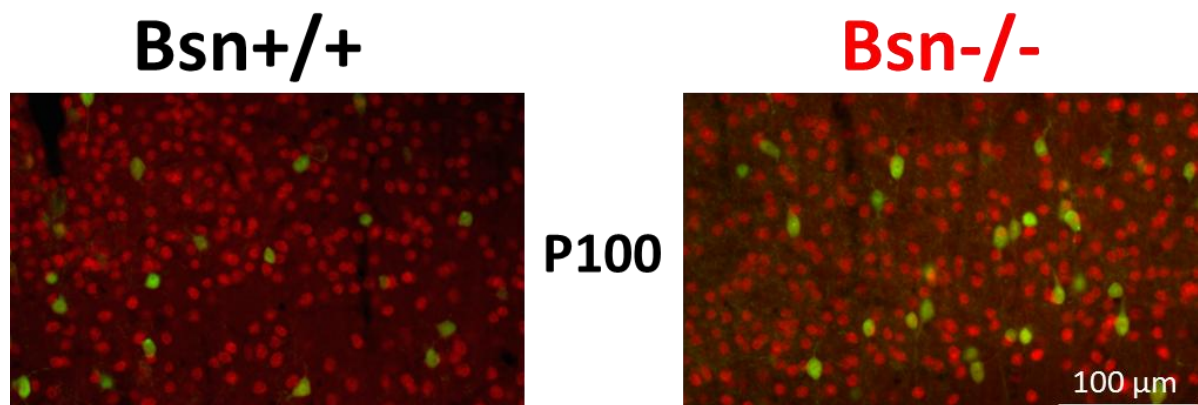


Figure 45: Coronal brain sections of the visual cortex of *Bsn*^{+/+} and *Bsn*^{-/-} mice at P100 stained against PV and Kv3.1b. Illustrated are coronal sections stained against PV (Cy2, green) and Kv3.1b (Cy3, red). There were eight times more Kv3.1b positive cells stained than PV positive cells and they do not co-localize (no yellow). One can clearly see that in our experiments we could not confirm that Kv3.1b is a specific potassium channel in parvalbumin expressing interneurons neither in *Bsn*^{+/+} (left) nor in Bassoon mutant mice (right).

We observed that there were eight times more Kv3.1b positive cells labeled than PV positive cells and they do not co-localize (no yellow color) and hence are not coexpressed (Figure 45). One can clearly see that in our experiments we could not confirm that Kv3.1b is a specific potassium channel only in parvalbumin-containing interneurons neither in *Bsn*^{+/+} nor in Bassoon mutant mice (Figure 45). Therefore, it was not possible to compare the number of active *versus* silent/inactive parvalbumin expressing interneurons in both genotypes using

Kv3.1b as a marker, since Kv3.1b was not coexpressed with parvalbumin-containing interneurons.

3.7.3 Brain-derived neurotropic factor (BDNF)

Due to the findings that four-weeks as well as three-month-old Bsn^{-/-} mice displayed a highly elevated level of the neurotrophin brain derived neurotropic factor (BDNF) (Heyden *et al.*, 2011), which is a survival and growth factor for neurons within the CNS. Since Heyden and her colleagues did BDNF extraction from diverse brain tissues and quantification by means of a sandwich enzyme-linked immunosorbent assay (ELISA) we wanted to test if Bassoon mutant mice also show higher BDNF levels when BDNF is stained by immunohistochemistry.

Therefore we stained BDNF (Cy3) in three Bsn^{+/+} mice in each case at P22, P30, and P100 as well as three Bsn^{-/-} mice in each case at P22, P30, and P100. We measured the intensity of BDNF in cells and defined values of Bsn^{+/+} mice as 100 % to calculate the values of Bsn^{-/-} mice as percent of controls. Representative staining examples of the visual cortex of P22, P30, and P100 Bsn^{+/+} and Bsn^{-/-} animals are displayed in Figure 46.

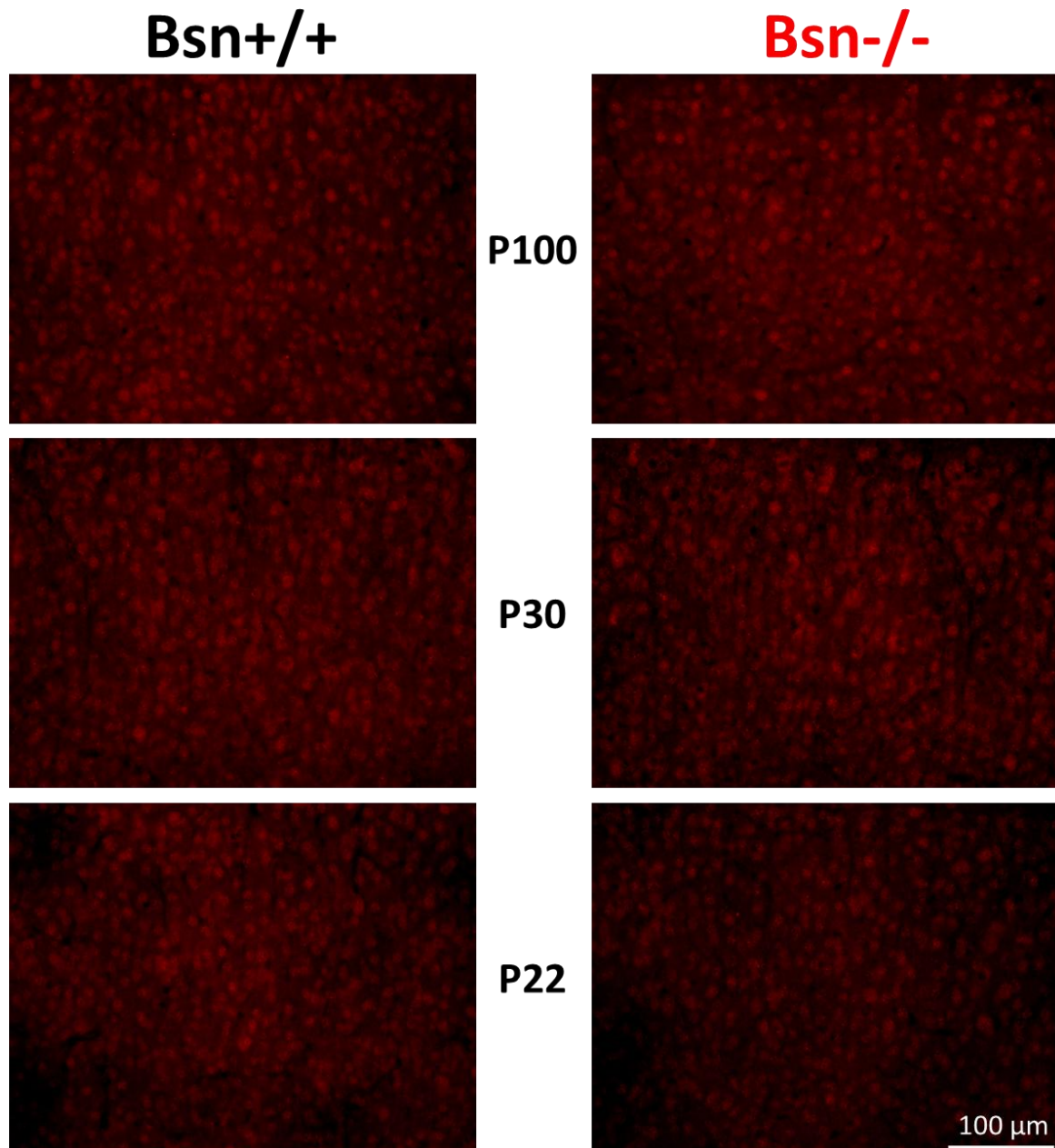


Figure 46: Coronal brain sections of the visual cortex layers II-IV of Bsn+/+ and Bsn-/- mice stained against BDNF. Illustrated are six coronal sections stained against BDNF (Cy3, red) from P22 (bottom), P30 (middle), and P100 (top). One can see that at P22 Bassoon mutant mice (right column) displayed less BDNF in the visual cortex in cortical layers II-IV than their Bsn+/+ littermates (left column). Nevertheless at P30 as well as P100 there were no differences in BDNF levels between Bsn+/+ and Bsn-/- mice.

Bsn-/- mice at the age of P22 showed a significantly decreased level of BDNF of about - 18.6 % within the visual cortex in layers II-IV (Figure 47) (t-test, $p < 0.001$). In contrast, at P30 and P100 Bsn-/- showed that the amount of BDNF did not differ anymore since Bsn-/- reached control levels with 99.4 % and 100.1 %, respectively (Figure 47) (t-test, $p > 0.05$ for both comparisons). Thus we could not see highly elevated BDNF levels in adult

Bsn^{-/-} animals like already published for diverse brain tissues and quantified by ELISA (Heyden *et al.*, 2011).

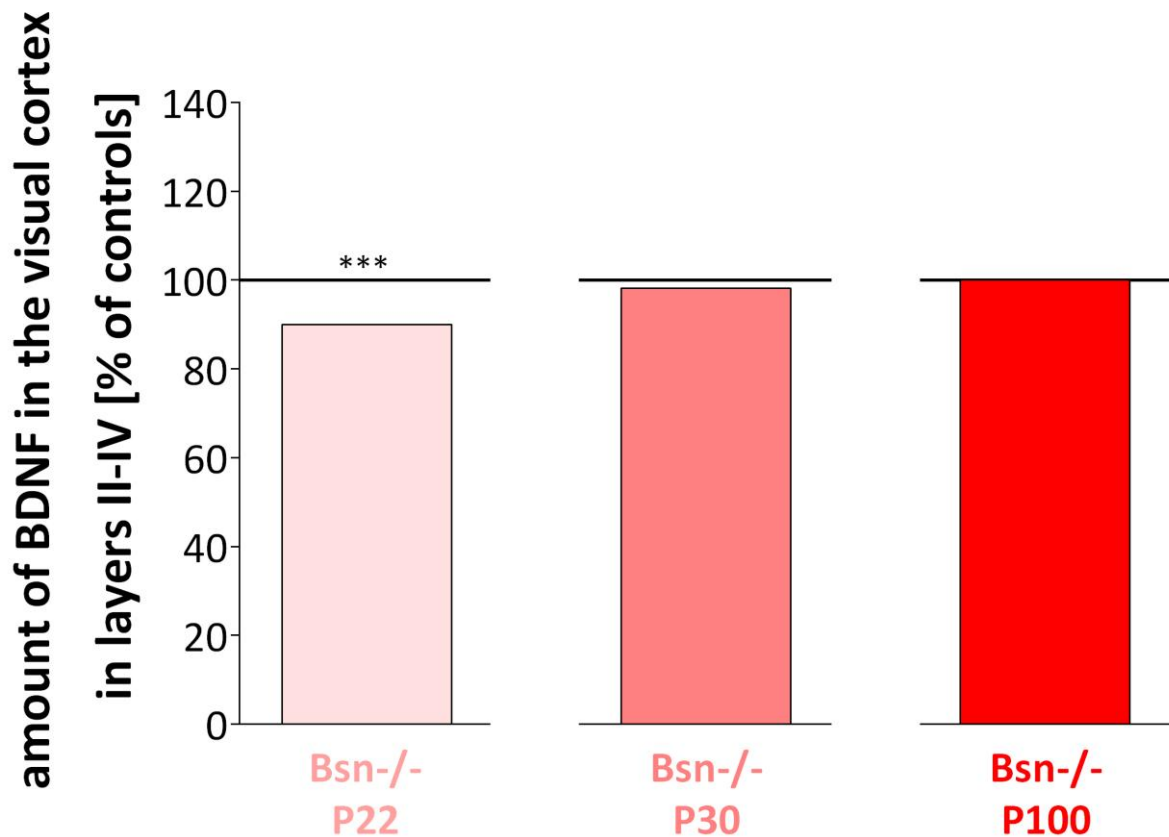


Figure 47: Amount of BDNF within the visual cortex in layers II-IV of Bsn^{+/+} (n = 3/ n = 3/ n = 3) and Bsn^{-/-} mice (n = 3/n = 3/n = 3) at the age of P20, P30 and P100. The amount of BDNF in Bsn^{-/-} animals (pink to red) is plotted as percent (%) of control Bsn^{+/+} animals. At P22 the amount of BDNF in Bsn^{-/-} mice was significant reduced about - 18.6 % (t-test, p < 0.001). Whereas the amount of BDNF at P30 and P100 did not differ since Bsn^{-/-} mice reached control levels (t-test, p > 0.05 for both comparisons).

3.B Results of PSD-95 KO mice

3.8 Visual acuity

3.8.1 Virtual-reality optomotor system

A part of the data are already published in Goetze *et al.*, 2012.

We tested 17 wild-type (WT) and heterozygous (HZ) mice as well as 20 PSD-95 KO mice with the virtual-reality optomotor system (Prusky *et al.*, 2004) to determine their visual acuity. Since there were always no differences between WT and HZ animals (t-test, $p > 0.05$) we pooled these groups to one WT/HZ group. We measured both eyes independently.

The visual acuity of WT/HZ animals (age 63 to 304 days) was 0.373 ± 0.002 cyc/deg for the left and 0.373 ± 0.002 cyc/deg for the right eye. In contrast, visual acuity of PSD-95 KO mice (age 63 to 289 days) was only slightly reduced with 0.357 ± 0.003 cyc/deg for the left eye and 0.357 ± 0.003 for the right eye. Since there were no differences between values of left and right eyes for both WT/HZ and PSD-95 KO mice (t-test, $p > 0.05$ for both comparisons) we averaged values across eyes for both genotypes. Average visual acuity of WT/HZ mice was 0.373 ± 0.002 cyc/deg compared to 0.357 ± 0.003 cyc/deg in PSD-95 KO animals (Figure 48 A).

The difference in visual acuity between WT/HZ and PSD-95 KO mice was only slightly reduced but significant (Figure 48 A) (t-test, $p < 0.001$). Visual acuity of WT/HZ mice was thus similar as previously described for C57Bl/6J wild-type mice (Prusky *et al.*, 2004).

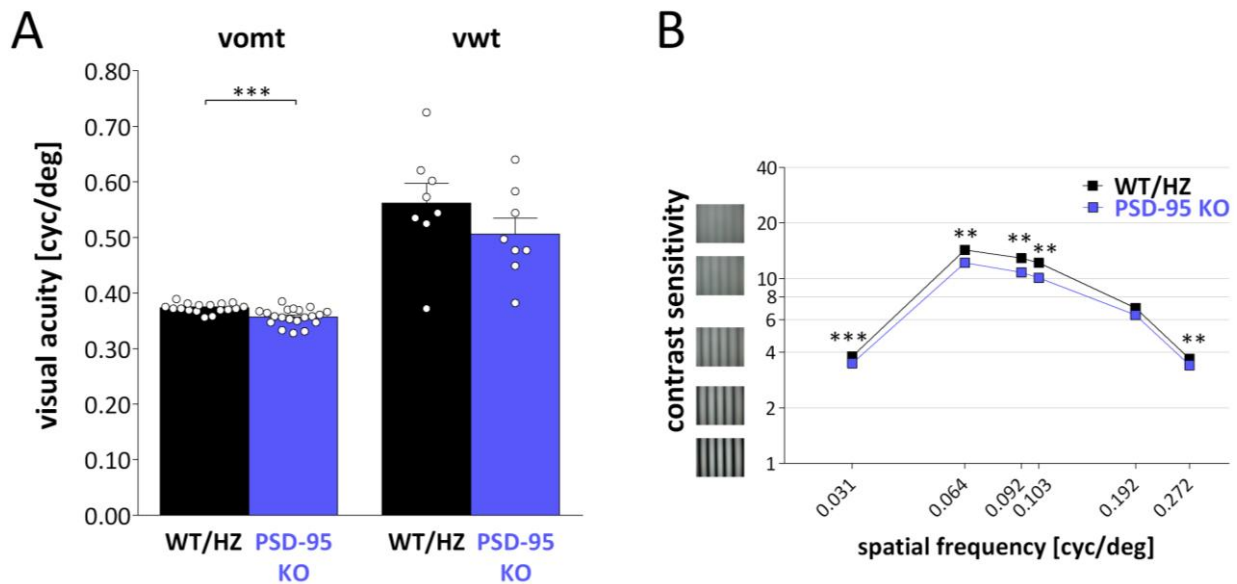


Figure 48: Visual acuity and contrast sensitivity of WT/HZ and PSD-95 KO mice measured with both the virtual-reality optomotor system (vomt) and the visual water task (vwt). (A) Left: Spatial frequency selectivity plotted in cycles per degree (cyc/deg). Visual acuity of WT/HZ (black) ($n = 17$) was 0.373 ± 0.002 cyc/deg compared to 0.357 ± 0.003 cyc/deg in PSD-95 KO mice (blue) ($n = 20$). The difference in visual acuity was only slightly reduced but statistically significant (t-test, $p < 0.001$). Right: Visual acuity of WT/HZ mice (black) ($n = 8$) was 0.562 ± 0.035 cyc/deg compared to 0.506 ± 0.029 cyc/deg in PSD-95 KO mice (blue) ($n = 8$). The difference in visual acuity was statistically not significant (t-test, $p > 0.05$). (C) Contrast sensitivity plotted as a function of spatial frequency in cycles per degree (cyc/deg). Contrast sensitivity of PSD-95 KO animals (blue) ($n = 20$) was only slightly reduced compared to their WT/HZ littermates (black) ($n = 17$). Maximal contrast sensitivity was 12.2 ± 0.56 (corresponding to 9 % contrast) in Bsn^{-/-} compared to 14.3 ± 0.44 (corresponding to 7 % contrast) in WT/HZ mice at the spatial frequency of 0.064 cyc/deg. At all spatial frequencies, contrast sensitivity was significantly different between the two genotypes, except for 0.192 cyc/deg (t-test, $p < 0.01$ for all comparisons, except for 0.192 cyc/deg).

3.8.2 Visual water task

We trained eight WT/HZ and eight PSD-95 KO mice in the visual water task (Prusky *et al.*, 2000), a cortex-dependent paradigm of visual discrimination learning, to assess visual acuity (age 97 to 477 days). In this test visual acuity was always measured for both eyes together. Visual acuity of WT/HZ mice was 0.562 ± 0.035 cyc/deg compared to littermate PSD-95 KO mice with 0.506 ± 0.029 cyc/deg (Figure 48 A).

Thus PSD-95 KO mice reached the same values of visual acuity values of their wild-type littermates in this visual discrimination task. The difference in visual acuity between WT/HZ and PSD-95 KO animals was not significant (Figure 48 A) (t-test, $p > 0.05$). The absolute values of visual acuity in the visual water task were thus significant higher than those measured in the virtual-reality optomotor system for both genotypes (t-test, $p < 0.001$ for both comparisons). It was recently described for C57Bl/6J mice that visual acuity measured

in the visual water task is consistently higher than in the optomotor task (visual water task: 0.5 - 0.6 cyc/deg (Prusky *et al.*, 2000), virtual-reality optomotor system: 0.4 cyc/deg (Prusky *et al.*, 2004).

3.9 Contrast sensitivity

A part of the data were already published in Goetze *et al.*, 2012.

Contrast sensitivity values of 17 WT/HZ and 20 PSD-95 KO mice were measured in the optomotor setup and plotted as a function of spatial frequency. Contrast was measured at six different spatial frequencies: 0.031 cyc/deg, 0.064 cyc/deg, 0.092 cyc/deg, 0.103 cyc/deg, 0.192 cyc/deg, and 0.272 cyc/deg independently for both eyes but since there were no differences between values of left and right eyes for both WT/HZ and PSD-95 KO mice (t-test, $p > 0.05$ for both comparisons) we averaged values across eyes for both genotypes.

At a spatial frequency of 0.031 cyc/deg WT/HZ mice had a contrast sensitivity of 3.8 ± 0.04 , at 0.064 cyc/deg 14.3 ± 0.44 , at 0.092 cyc/deg 12.92 ± 0.46 , at 0.103 cyc/deg 12.2 ± 0.46 , at 0.192 cyc/deg 6.9 ± 0.25 , and at 0.272 cyc/deg 3.7 ± 0.05 . The semilog plot (Figure 48 B) revealed a sickle shaped curve. Contrast sensitivity of WT/HZ mice was thus similar as previously described for C57Bl/6J wild-type mice (Prusky *et al.*, 2004).

At a spatial frequency of 0.031 cyc/deg PSD-95 KO mice had a contrast sensitivity of 3.5 ± 0.04 , at 0.064 cyc/deg 12.2 ± 0.56 , at 0.092 cyc/deg 10.8 ± 0.50 , at 0.103 cyc/deg 10.1 ± 0.47 , at 0.192 cyc/deg 6.4 ± 0.22 , and at 0.272 cyc/deg 3.4 ± 0.08 . The semilog plot (Figure 48 B) revealed a sickle shaped curve similar to WT/HZ animals.

Hence, contrast sensitivity of PSD-95 KO mice was slightly reduced compared to WT/HZ animals. Statistical analyses confirmed that genotype had an impact on contrast sensitivity that was significant (ANOVA, $F_{1,35} = 9.33$, $p < 0.01$). Contrast sensitivity of WT/HZ mice was significantly different from PSD-95 KO mice at all spatial frequencies, except for 0.192 cyc/deg (Figure 48 B) (t-test, $p < 0.01$ for all comparisons, except for 0.192 cyc/deg). Contrast sensitivity in WT/HZ animals was significantly different between all spatial frequencies (t-test, $p < 0.01$ for all comparisons), except between 0.031 cyc/deg and 0.272 cyc/deg, 0.092 cyc/deg and 0.103 cyc/deg as well as 0.064 cyc/deg and 0.092 cyc/deg.

In PSD-95 KO animals, contrast sensitivity values was significantly different between all spatial frequencies (t-test, $p < 0.01$ for all comparisons), except between 0.031 cyc/deg and 0.272 cyc/deg, 0.092 cyc/deg and 0.103 cyc/deg, as well as 0.064 cyc/deg and 0.092 cyc/deg.

Curves of contrast sensitivity peaked at a spatial frequency of 0.064 cyc/deg for both genotypes, as previously described for C57Bl/6J mice (Prusky *et al.*, 2004).

3.10 Enhancement of vision after monocular deprivation

3.10.1 Visual acuity

A part of the data were already published in Goetze *et al.*, 2012.

As already mentioned, MD induces an enhancement of the optokinetic response of the nondeprived eye in mice (Prusky *et al.*, 2006). To check if PSD-95 KO mice and their wild-type littermates also show an enhancement of visual acuity we performed MD and tested visual acuity of the nondeprived eye daily with the virtual-reality optomotor system. We used seven days of MD in adult and in older mice (begin at P63 up to P304). We tested four WT/HZ and eight PSD-95 KO mice.

On each day following a MD, visual acuity increased substantially. In WT/HZ animals visual acuity increased from 0.377 ± 0.004 cyc/deg before deprivation to values of 0.461 ± 0.006 cyc/deg on the seventh day after monocular deprivation (Figure 49 A), corresponding to a gain on baseline of 22.1 ± 1.24 % (Figure 49 B).

In PSD-95 KO animals visual acuity increased from 0.361 ± 0.005 cyc/deg before deprivation to values of 0.441 ± 0.006 cyc/deg on the seventh day after monocular deprivation (Figure 49 A), which represents a gain on baseline of 22.4 ± 0.99 % (Figure 49 B).

There was a significant difference in the improvement over seven days of visual acuity of each genotype (ANOVA, $p < 0.001$, $F_{7,4} = 93.78$) and between the genotypes (ANOVA, $p < 0.05$, $F_{1,10} = 8.81$) only because of lower visual acuity values of PSD-95 KO mice before MD compared to their WT/HZ littermates. But in all genotypes, the increase on baseline of visual acuity after MD was around 22 % thus there was no significant difference between

WT/HZ and PSD-95 KO mice (t-test, $p > 0.05$) (Figure 49 B). PSD-95 KO mice show similar enhancement of visual acuity as their WT/HZ littermates.

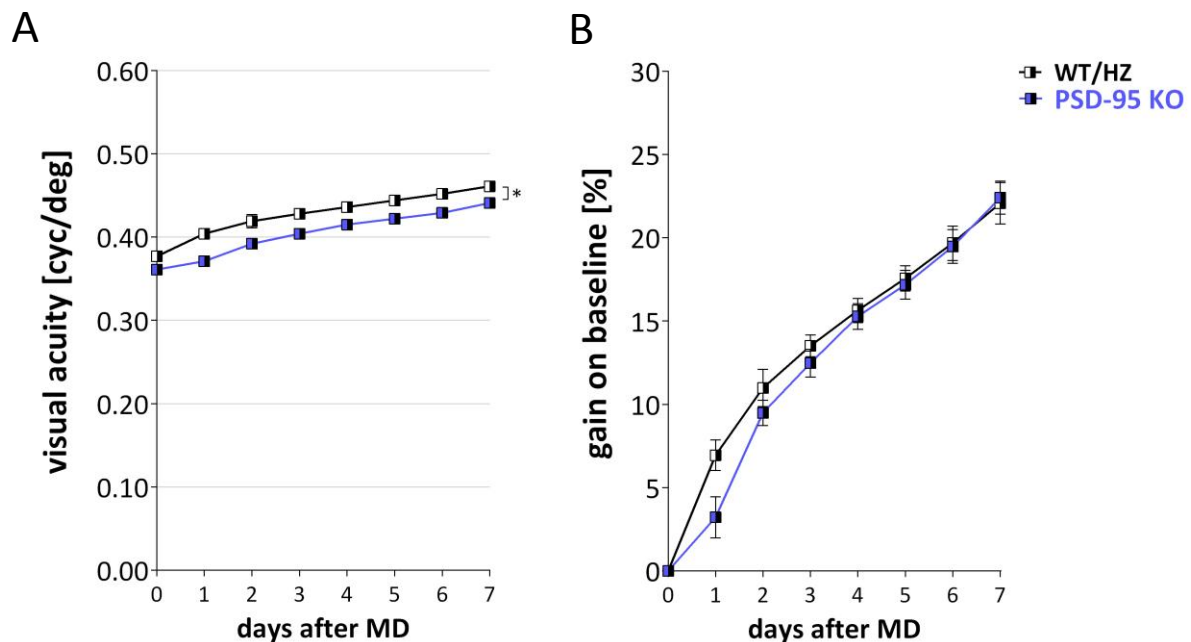


Figure 49: Enhancement of visual acuity after monocular deprivation in WT/HZ (n = 4) as well as in PSD-95 KO mice (n = 8). (A) Spatial frequency selectivity of the optokinetic response in cycles per degree (cyc/deg) plotted against days after MD. During seven days of MD and daily testing, visual acuity of the nondeprived eye increased in WT/HZ mice (black) from 0.377 ± 0.004 cyc/deg to 0.461 ± 0.006 cyc/deg. In contrast, PSD-95 KO animals (blue) increased slightly less from 0.361 ± 0.005 cyc/deg to 0.441 ± 0.006 cyc/deg. Statistical analyzes revealed that there was a significant difference in the development of visual acuity between WT/HZ and PSD-95 KO mice (ANOVA, $p < 0.05$). (B) Gain on baseline of visual acuity in percent (%) plotted against days after MD. During seven days of MD WT/HZ animals showed a gain on baseline of 22.1 ± 1.24 %, PSD-95 KO mice displayed an equal gain on baseline of 22.4 ± 0.99 %. Statistical analyzes revealed that there were no significant differences of gain on baseline between both genotypes (t-test, $p > 0.05$).

Since PSD-95 KO animals displayed a prolonged period of cortical plasticity (chapter 3.11.2) we assumed this might be due to reduced cortical inhibition so we applied the drug diazepam to investigate whether it prevents this prolonged period of plasticity and tested visual acuity and contrast sensitivity (chapter 3.10.2) daily during diazepam treatment. We measured WT/HZ and PSD-95 KO animals and their wild-type littermates after performing MD and tested visual acuity of the nondeprived eye daily with the virtual-reality optomotor system during daily treatment with diazepam, which increases the efficiency of GABAergic inhibition.

We used seven days of MD in adult mice (begin at P76 up to P103). We tested five WT/HZ and five PSD-95 KO mice.

On each of the following seven days of MD with diazepam treatment (1 $\mu\text{g/g}$ daily), visual acuity increased substantially as well. In WT/HZ animals visual acuity increased from 0.375 ± 0.008 cyc/deg before deprivation to values of 0.452 ± 0.004 cyc/deg on the seventh day after monocular deprivation (Figure 50 A), which represents a gain on baseline of 20.3 ± 1.04 % (Figure 50 B).

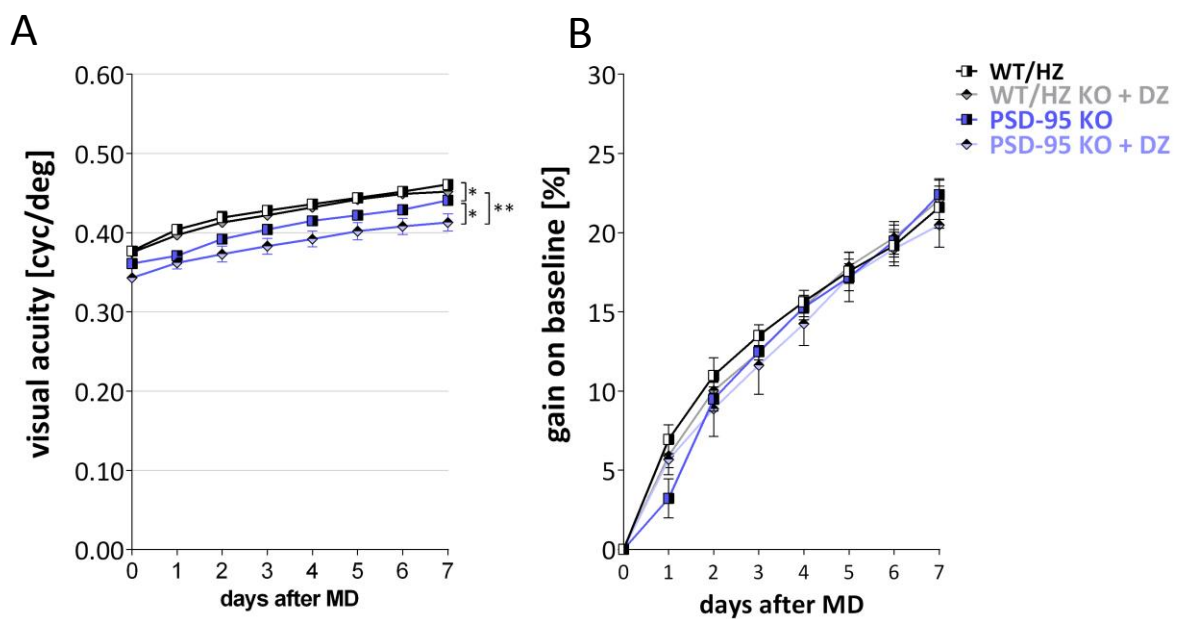


Figure 50: Enhancement of visual acuity after monocular deprivation in WT/HZ (n = 5) as well as in PSD-95 KO mice (n = 5) with and without diazepam treatment. (A) Spatial frequency selectivity of the optokinetic response in cycles per degree (cyc/deg) plotted against days after MD. During seven days of MD and daily testing, visual acuity of the nondeprived eye increased in WT/HZ mice (gray) treated with DZ from 0.375 ± 0.008 cyc/deg to 0.452 ± 0.004 cyc/deg similar values as in WT/HZ mice (black) without treatment where values increased from 0.377 ± 0.004 cyc/deg to 0.461 ± 0.006 cyc/deg. PSD-95 KO animals (blue) increased significantly slightly less without treatment from 0.361 ± 0.005 cyc/deg to 0.441 ± 0.006 cyc/deg compared to WT/HZ without treatment (t-test, $p < 0.05$). In contrast, PSD-95 KO animals with DZ treatment (light blue) increased less because of lower visual acuity values from the start. Visual acuity increased from 0.343 ± 0.004 cyc/deg to 0.413 ± 0.009 cyc/deg. Statistical analyzes revealed that there were significant differences in the development of visual acuity between WT/HZ and PSD-95 KO mice with DZ (ANOVA, $p < 0.01$) and without treatment (ANOVA, $p < 0.05$) but not between WT/HZ and WT/HZ after DZ treatment (ANOVA, $p > 0.05$). **(B)** Gain on baseline of visual acuity in percent (%) plotted against days after MD. During seven days of MD WT/HZ animals showed a gain on baseline of 22.1 ± 1.24 %, similar as WT/HZ treated with DZ with a gain on baseline of 20.3 ± 1.04 %. PSD-95 KO mice displayed an equal gain on baseline of 22.4 ± 0.99 %, even after DZ treatment with values of 20.5 ± 1.39 %. Statistical analyzes revealed that there are no significant differences of gain on baseline between both genotypes with and without DZ treatment, respectively (t-test, $p > 0.05$ for both comparisons). There were also no significant differences between WT/HZ and WT/HZ after DZ treatment as well as no differences between PSD-95 KO and PSD-95 KO after DZ treatment (t-test, $p > 0.05$ for both comparisons). (Abbreviation: DZ = diazepam)

In PSD-95 KO animals visual acuity increased from 0.343 ± 0.004 cyc/deg before deprivation to values of 0.413 ± 0.009 cyc/deg on the seventh day after monocular deprivation (ANOVA, $p < 0.05$, $F_{7,2} = 38.10$) (Figure 50 A), which represents a gain on baseline of 20.5 ± 1.39 % (Figure 50 B).

Treatment with diazepam reduced the visual acuity improvement during seven days of MD significantly in PSD-95 KO mice, but not in WT/HZ mice (ANOVA, $p < 0.01$, $F_{1,8} = 15.85$), which was due to significant lower initial visual acuity values of PSD-95 KO (t-test, $p < 0.05$) but not of WT/HZ mice (t-test, $p > 0.05$).

Statistical analyzes revealed that there were significant differences in the improvement of visual acuity between PSD-95 KO mice without and with diazepam treatment (ANOVA, $p < 0.05$, $F_{1,11} = 5.52$) because of lower visual acuity values before MD of the diazepam treated group of PSD-95 KO mice. There were no significant differences in the improvement of visual acuity between WT/HZ and WT/HZ after diazepam treatment (ANOVA, $p > 0.05$).

Gain on baseline of visual acuity after MD was 20 % in both genotypes and therefore not significantly different (Figure 50 B) (t-test, $p > 0.05$). There were also no significant differences between WT/HZ and WT/HZ mice after diazepam treatment as well as no differences between PSD-95 KO and PSD-95 KO mice after diazepam treatment (t-test, $p > 0.05$ for both comparisons).

Taken together these data revealed that the enhancement of visual acuity (gain on baseline) of PSD-95 KO mice is similar to their WT/HZ littermates, also after diazepam treatment.

3.10.2 Contrast sensitivity

To check if PSD-95 KO mice and their wild-type littermates show interocular plasticity of vision, we also tested contrast sensitivity of the nondeprived eye daily with the virtual-reality optomotor system. Therefore we measured the same animals as described before for visual acuity (chapter 3.10.1). Contrast sensitivity was measured at six different spatial frequencies and always peaked at 0.064 cyc/deg during all days of MD and in animals of both genotypes as described previously (Prusky *et al.*, 2006). On each day following MD, contrast sensitivity of all measured spatial frequencies increased substantially.

At 0.064 cyc/deg in WT/HZ animals contrast sensitivity increased from 14.8 ± 0.38 (corresponding to 6 % contrast) before deprivation (Figure 51 A,D,F) to values of 21.6 ± 0.30 (corresponding to 4 % contrast) on the seventh day after monocular deprivation (Figure 51 B,D,F), which represents a gain on baseline of 45.6 ± 2.18 %.

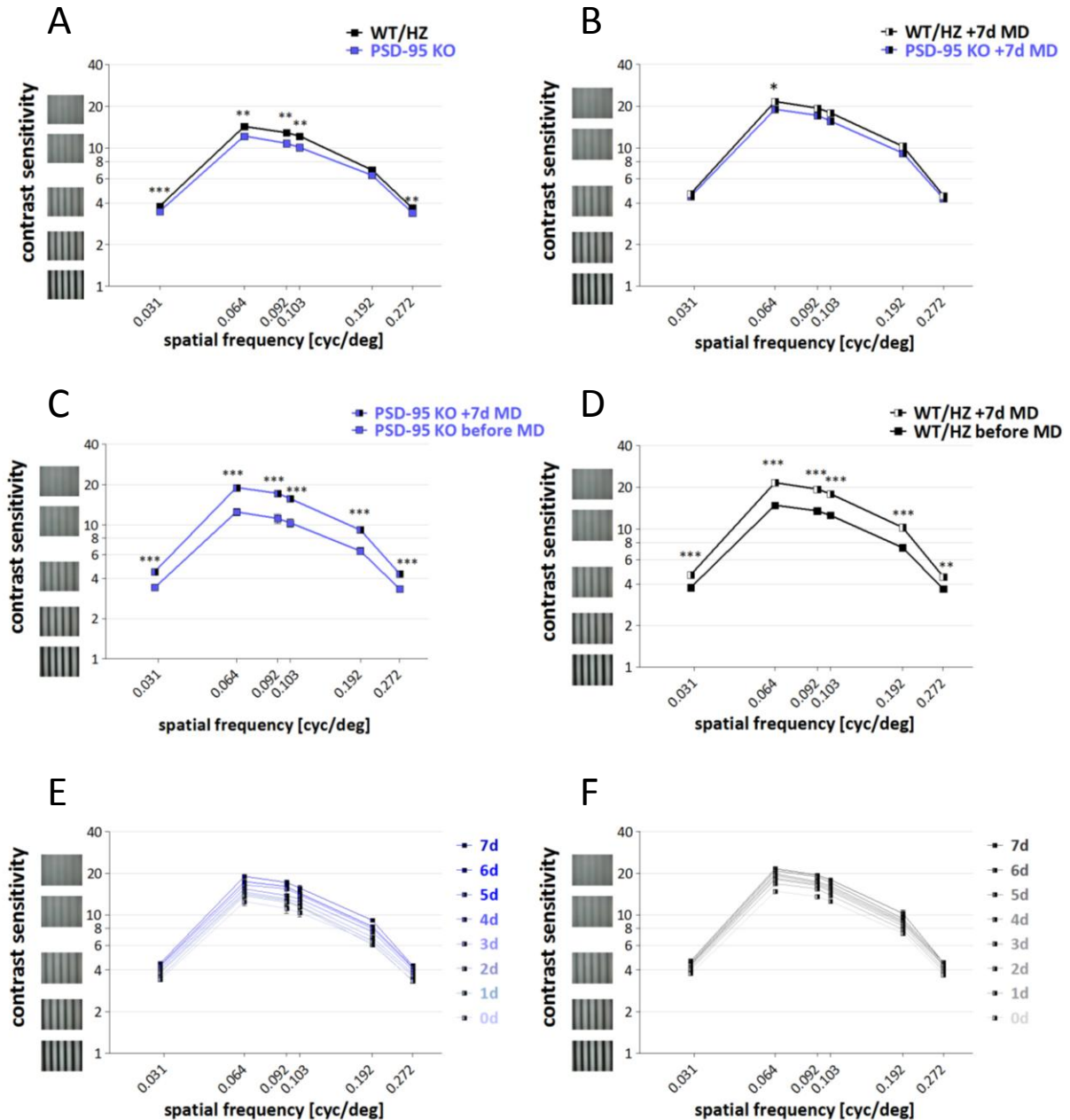


Figure 51: Enhancement of contrast sensitivity after monocular deprivation in WT/HZ (n = 17) and PSD-95KO mice (n = 20). Contrast sensitivity plotted as a function of spatial frequency in cycles per degree (cyc/deg). PSD-95 KO mice (blue) did achieve slightly lower values (except for 0.192 cyc/deg) as WT/HZ animals (black) before MD (A) (t-test, $p < 0.01$ for all comparisons, except for 0.192 cyc/deg). After seven days of MD (B) PSD-95 KO mice were only significantly different to WT/HZ animals at 0.064 cyc/deg (t-test, $p < 0.05$). Nevertheless, PSD-95 KO (C) as well as WT/HZ mice (D) showed a significant improvement of contrast sensitivity after seven days of MD (t-test, $p < 0.01$ for all comparisons). Daily improvement of contrast sensitivity over seven days of MD of PSD-95 KO (E) and WT/HZ mice (F) revealed that genotype had no significant influence on the improvement of contrast sensitivity (ANOVA, $p > 0.05$). In WT/HZ animals, the increase on baseline of contrast sensitivity after MD was 45.6 % compared to a similar value of 55.2 % in PSD-95 KO mice and therefore not significantly different (t-test, $p < 0.05$).

In contrast, in PSD-95 KO mice contrast sensitivity increased from 12.5 ± 0.82 (corresponding to 8 % contrast) before deprivation (Figure 51 A,C,E) to values of 19.0 ± 0.70 (corresponding to 5 % contrast) on the seventh day after monocular deprivation (Figure 51 B,C,E), which represents a gain on baseline of 55.2 ± 8.12 %.

There was a significant difference in the improvement of contrast sensitivity over seven days of MD of each genotype (ANOVA, $p < 0.001$, $F_{4,7} = 252.59$) but no difference between both genotypes (ANOVA, $p > 0.05$). Between both genotypes contrast sensitivity was significantly different at all spatial frequencies (except at 0.192 cyc/deg) before MD (t-test, $p < 0.01$, for all comparisons, except for 0.192 cyc/deg) and surprisingly after seven days of MD contrast sensitivity was only significantly different at 0.064 cyc/deg (t-test, $p < 0.05$). Nevertheless, WT/HZ and PSD-95 KO mice showed a significant improvement of contrast sensitivity after seven days of MD (t-test, $p < 0.01$ for all comparisons). The increase on baseline of contrast sensitivity after MD was 45.6 % in WT/HZ mice compared to a slightly higher value of 55.2 % in PSD-95 KO mice but there was no significant difference (t-test, $p > 0.05$).

In addition, we measured WT/HZ and PSD-95 KO animals and their wild-type littermates performing MD and tested contrast sensitivity of the nondeprived eye daily with the virtual-reality optomotor system under daily treatment with diazepam.

Therefore we measured the same animals as described before for visual acuity (chapter 3.10.1). Contrast sensitivity was measured at six different spatial frequencies and always peaked at 0.064 cyc/deg during all days of MD and in animals of both genotypes as described previously (Prusky *et al.*, 2006). On each day following MD, contrast sensitivity of all measured spatial frequencies increased substantially.

At 0.064 cyc/deg in WT/HZ animals with diazepam treatment contrast sensitivity increased from 14.4 ± 0.36 (corresponding to 7 % contrast) before deprivation (Figure 52 A,D,F) to values of 21.2 ± 0.24 (corresponding to 5 % contrast) on the seventh day after monocular deprivation (Figure 52Figure 51 B,D,F), which represents a gain on baseline of 45.9 ± 4.83 %.

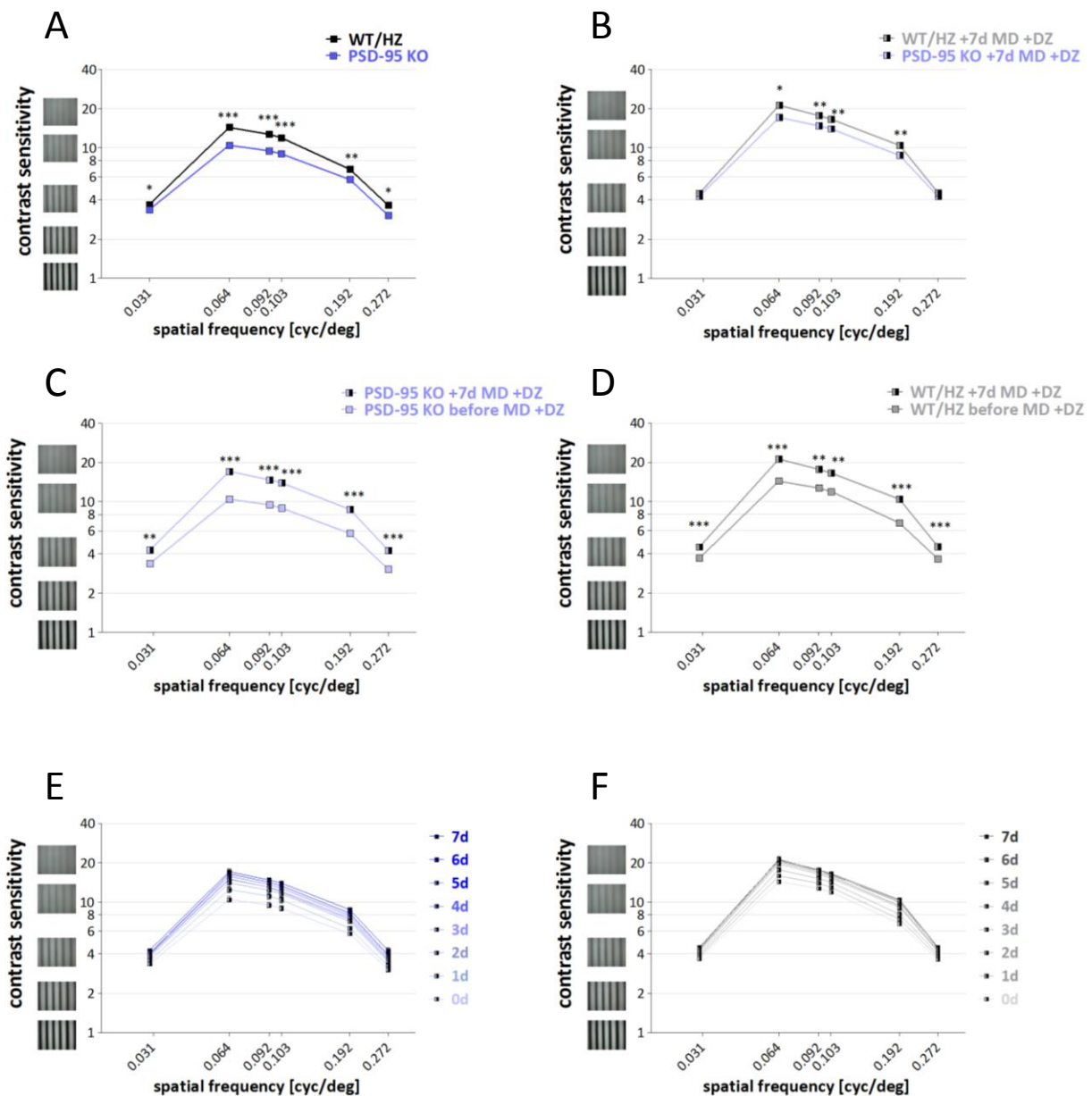


Figure 52: Enhancement of contrast sensitivity after monocular deprivation in WT/HZ ($n = 5$) and PSD-95 KO mice ($n = 5$) with diazepam treatment. Contrast sensitivity plotted as a function of spatial frequency in cycles per degree (cyc/deg). PSD-95 KO mice (blue) did achieve slightly lower values as WT/HZ animals (black) before MD and without treatment (**A**) (t-test, $p < 0.05$ for all comparisons). After seven days of MD and DZ treatment (**B**) PSD-95 KO mice significantly different to WT/HZ animals at 0.064 cyc/deg, 0.092 cyc/deg, 0.103 cyc/deg and 0.192 cyc/deg (t-test, $p < 0.05$). Nevertheless, PSD-95 KO (**C**) as well as WT/HZ mice (**D**) showed a significant improvement of contrast sensitivity after seven days of MD and DZ treatment (t-test, $p < 0.01$ for all comparisons). Daily improvement of contrast sensitivity over seven days of MD and DZ treatment of PSD-95 KO (**E**) and WT/HZ mice (**F**) revealed that genotype had a significant influence on the improvement of contrast sensitivity (ANOVA, $p < 0.05$). In WT/HZ animals, the increase on baseline of contrast sensitivity after MD was 45.9 % compared to a value of 57.3 % in PSD-95 KO mice and therefore significantly different (t-test, $p < 0.05$). (Abbreviation: DZ = diazepam)

In contrast, in PSD-95 KO mice contrast sensitivity increased from 10.5 ± 0.51 (corresponding to 9 % contrast) before deprivation (Figure 52 A,C,E) to values of 17.1 ± 0.89 (corresponding to 6 % contrast) on the seventh day after monocular deprivation (Figure 52 B,C,E), which represents a gain on baseline of 57.3 ± 2.91 %.

There was a significant difference in the improvement of contrast sensitivity over seven days of MD of each genotype (ANOVA, $p < 0.01$, $F_{2,7} = 98.71$) and between both genotypes (ANOVA, $p < 0.01$, $F_{1,8} = 13.80$) because of lower visual acuity values before MD of the diazepam treated group of PSD-95 KO mice. Between both genotypes contrast sensitivity was significantly different at all spatial frequencies from each other before MD (t-test, $p < 0.05$, for all comparisons) and after seven days of MD contrast sensitivity was only significantly different at 0.064 cyc/deg, 0.092 cyc/deg, 0.103 cyc/deg, and at 0.192 cyc/deg (t-test, $p < 0.05$ for all comparisons). Nevertheless, WT/HZ and PSD-95 KO mice showed a significant improvement of contrast sensitivity after seven days of MD (t-test, $p < 0.01$ for all comparisons). The increase on baseline of contrast sensitivity after MD was 45.9 % in WT/HZ mice after diazepam treatment compared to a higher value of 57.3 % in PSD-95 KO mice after diazepam treatment and therefore significantly different (t-test, $p < 0.05$).

Statistical analyzes revealed that there were neither significant differences in the improvement of contrast sensitivity between PSD-95 KO mice without and with diazepam treatment nor between WT/HZ and WT/HZ mice after diazepam treatment (ANOVA, $p > 0.05$ for both comparisons).

Gain on baseline of contrast sensitivity after MD was neither significantly different between PSD-95 KO mice with or without diazepam treatment nor between WT/HZ and WT/HZ mice after diazepam treatment (ANOVA, $p > 0.05$ for both comparisons).

Taken together these data revealed that the enhancement of contrast sensitivity (gain on baseline) of PSD-95 KO mice is similar to their WT/HZ littermates, also after diazepam treatment.

3.11 Optical imaging of intrinsic signals

3.11.1 Maximum response and map scatter

To determine if the knockout of the protein PSD-95 had any influence on the visual cortex we recorded mouse visual cortical responses *in vivo* using the imaging method developed by Kalatsky and Stryker (2003).

As previously mentioned the visual stimuli consisted of full-screen moving horizontal (elevation maps) and vertical bars (azimuth maps) in the right visual field therefore we always measured the left hemisphere. Our achieved maps were retinotopic phase maps, raw magnitude response maps, and polar maps, respectively. We calculated maximum response and map quality from six (P97 to P488) WT/HZ mice as well as from seven (P83 to P496) PSD-95 KO mice according to published protocols (Cang *et al.*, 2005b).

Representative examples of the resulting activity and retinotopic maps of the left visual cortex of WT/HZ and PSD-95 KO mice are illustrated in Figure 53, Figure 54, and Figure 55. Most interestingly, WT/HZ (Figure 55 B,E) and PSD-95 KO mice (Figure 55 D,F) had nearly identical maps, indistinguishable in both signal amplitude and quality of retinotopy for both elevation (Figure 55 B,C) and azimuth maps (Figure 55 E,F).

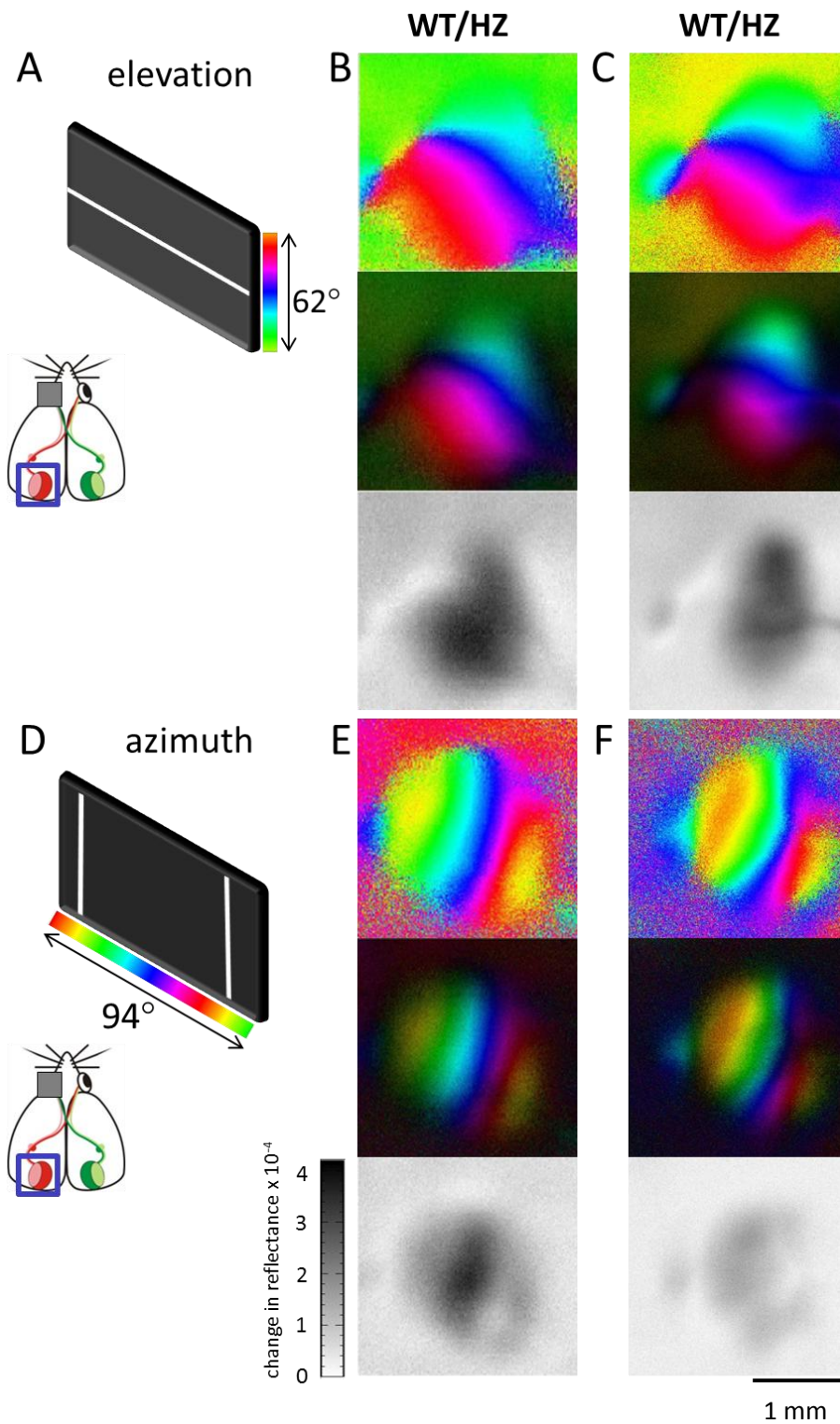


Figure 53: Representative examples of visual cortical maps recorded with intrinsic signal optical imaging of WT/HZ mice. Color-coded retinotopic phase map (top), polar maps (middle) and grey-scale coded response magnitude maps (below) of WT/HZ mice (**B,C**) are illustrated. The magnitude of the optical responses is illustrated as fractional change in reflectance $\times 10^{-4}$. Retinotopic maps are color-coded according to the schemes on the left side (**A,D**). Both elevation (**B,C**) and azimuth (**E,F**) maps resulting from visual stimulation of the animals with full-screen moving horizontal (**A**) or vertical bars (**D**) are shown. Visual cortical maps of WT/HZ mice have both high response amplitude and excellent retinotopy.

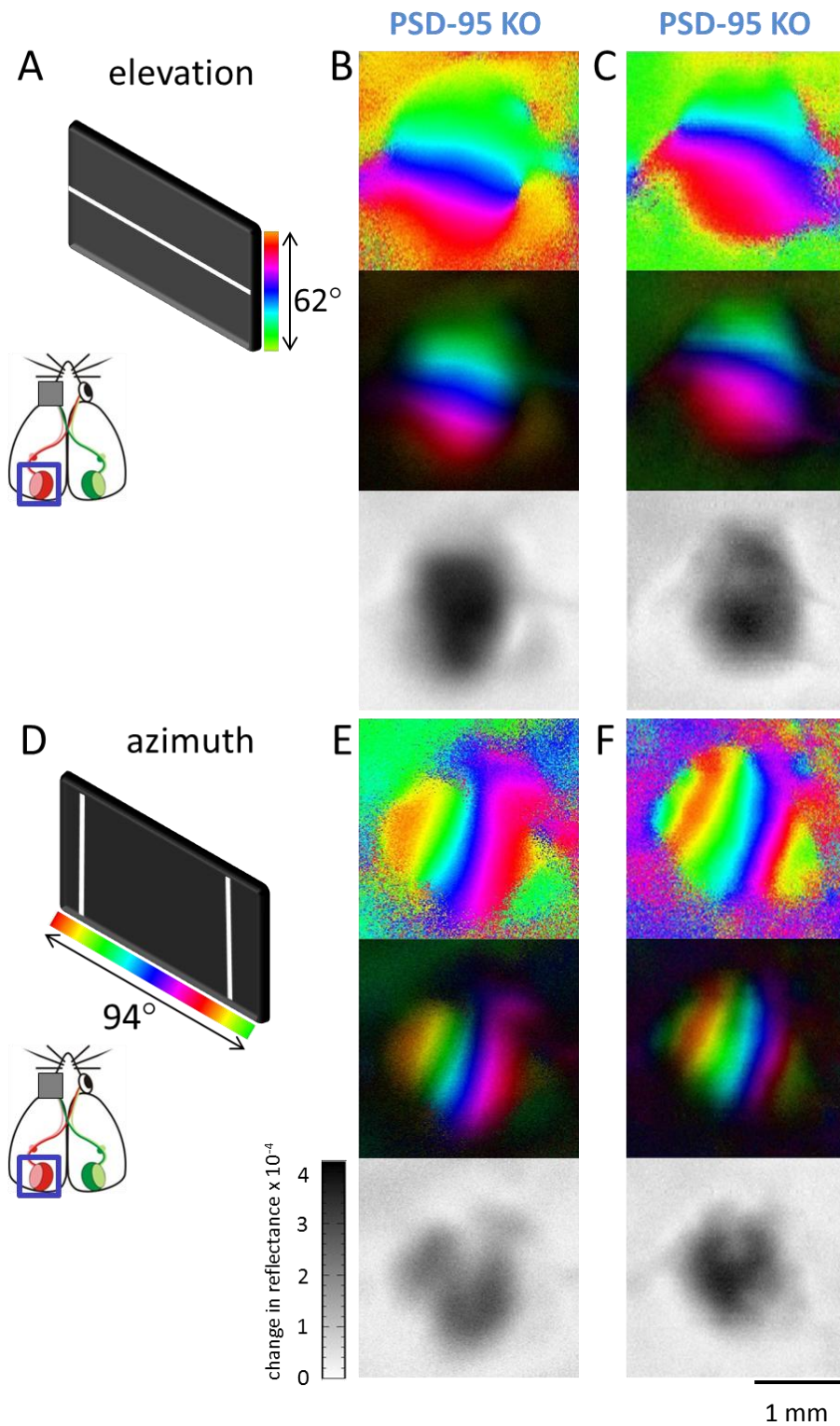


Figure 54: Representative examples of visual cortical maps recorded with intrinsic signal optical imaging of PSD-95 KO mice. Color-coded retinotopic phase map (top), polar maps (middle) and grey-scale coded response magnitude maps (below) of PSD-95 KO mice (**B,C**) are illustrated. The magnitude of the optical responses is illustrated as fractional change in reflectance $\times 10^{-4}$. Retinotopic maps are color-coded according to the schemes on the left side (**A,D**). Both elevation (**B,C**) and azimuth (**E,F**) maps resulting from visual stimulation of the animals with full-screen moving horizontal (**A**) or vertical bars (**D**) are shown. Visual cortical maps of PSD-95 KO mice have both high response amplitude and excellent retinotopy.

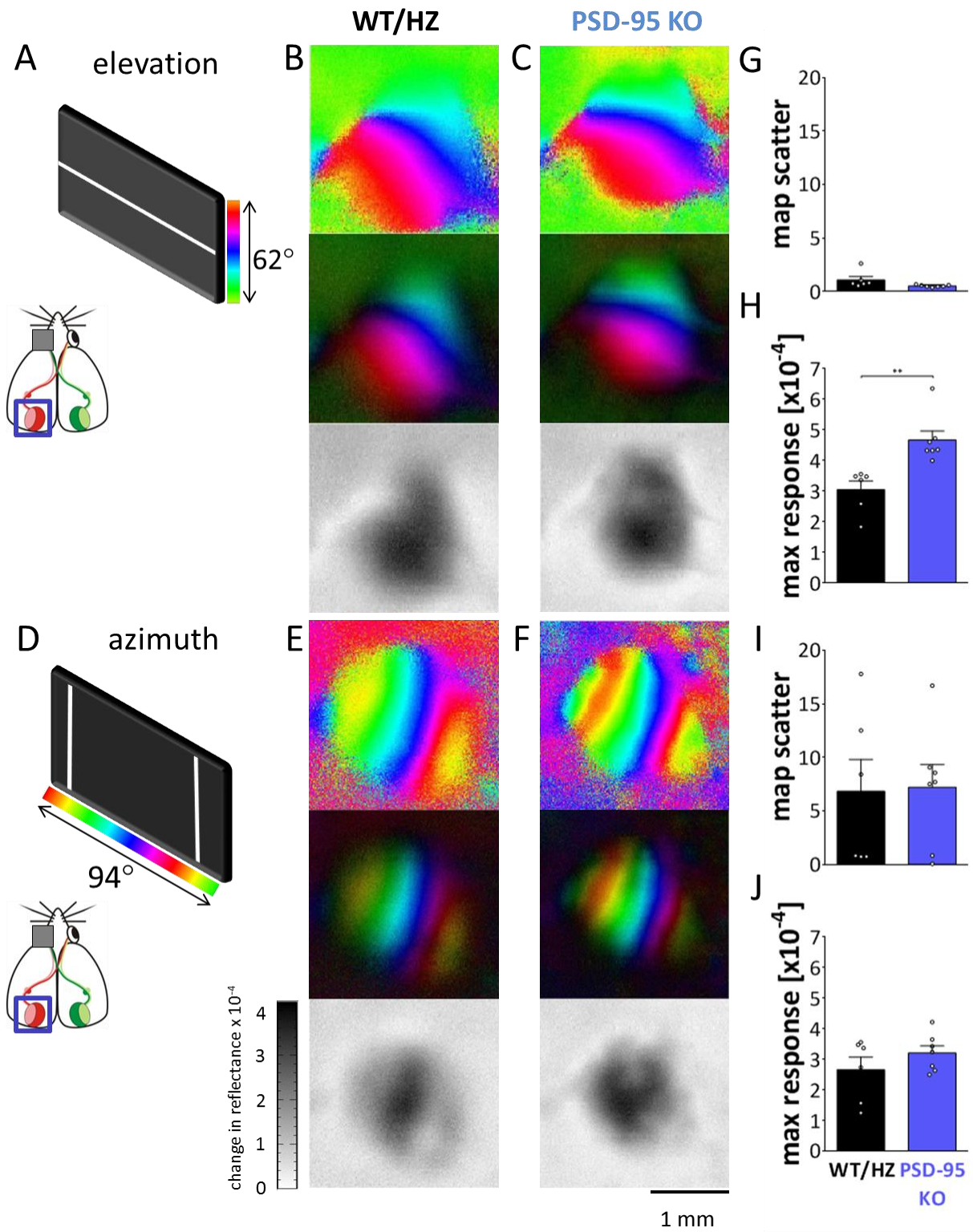




Figure 55: Visual cortical maps recorded with intrinsic signal optical imaging and their quantification of WT/HZ and PSD-95 KO mice. Color-coded retinotopic phase map (top), polar maps (middle) and grey-scale coded response magnitude maps (below) of a WT/HZ (**B**) and a PSD-95 KO mouse (**C**) are illustrated. The magnitude of the optical responses is illustrated as fractional change in reflectance $\times 10^{-4}$. Retinotopic maps are color-coded according to the schemes on the left side (**A,D**). Both elevation (**B,C**) and azimuth (**E,F**) maps resulting from visual stimulation of the animals with full-screen moving horizontal (**A**) or vertical bars (**D**) are shown. (**G,I**) Quantification of map quality of WT/HZ ($n = 6$) and PSD-95 KO mice ($n = 8$). Map quality plotted as map scatter. Visual cortical maps of Bsn+/+ (black) and Bsn-/- animals (red) are indistinguishable in magnitude of the visual cortical responses for both elevation (**G**) (t-test, $p > 0.05$) and azimuth maps (**I**) (t-test, $p > 0.05$). (**H,J**) Quantification of magnitude maps of WT/HZ ($n = 6$) and PSD-95 KO mice ($n = 16$). Maximum cortical response plotted as a change in reflectance $\times 10^{-4}$. Magnitude of the visual cortical of WT/HZ (black) and PSD-95 KO animals (blue) are significantly different for elevation maps (**H**) (t-test, $p < 0.01$) but not for azimuth maps (**J**) (t-test, $p > 0.05$).

To compare the cortical maps of WT/HZ and PSD-95 KO mice, we quantified both the maximum response magnitude of cortical responses and the quality of the retinotopic maps after visual stimulation of the left eye with a full-screen moving horizontal bar. The magnitude of the optical responses of WT/HZ mice was 3.05 ± 0.28 whereas in PSD-95 mice 4.77 ± 0.75 (elevation maps, Figure 55 H). The values had a clear statistical difference (t-test, $p < 0.01$). After visual stimulation with a moving vertical bar, the magnitude of the cortical responses of WT/HZ and PSD-95 KO mice was not significantly different (t-test, $p > 0.05$): 2.66 ± 0.42 in WT/HZ and slightly higher with 3.21 ± 0.23 in PSD-95 KO mice (azimuth maps, Figure 55 J).

The quality of the retinotopic maps was also similar in both genotypes. Mean scatter of elevation maps of WT/HZ mice was 1.09 ± 0.32 and slightly better with 0.53 ± 0.04 in PSD-95 KO mice (Figure 55 G). For azimuth maps, map scatter was 6.84 ± 2.87 in WT/HZ mice and 7.21 ± 2.11 in PSD-95 KO mice (Figure 55 I). There were no significant differences in map scatter neither for elevation (t-test, $p > 0.05$) nor for azimuth maps (t-test, $p > 0.05$).

3.11.2 Ocular dominance

A part of the data were already published in Goetze *et al.*, 2012.

One of the most important questions was if PSD-95 KO mice showed any change in cortical plasticity because the important function of PSD-95 as an anchor protein (for *e.g.* NMDARs) and because LTP is enhanced and LTD is eliminated and both are very important for plasticity. Using optical imaging of intrinsic signals (Cang *et al.*, 2005a) we compared the response amplitudes in the binocular region of visual cortex after stimulation of the ipsi- and

contralateral eye in WT/HZ and PSD-95 KO mice without and with monocular deprivation. We used seven days of MD (begin at P63 up to P93 in adult mice and P116 up to P500 in old mice) and tested three adult and six old WT/HZ as well as three adult and seven old PSD-95 KO mice and compared them to six WT/HZ and seven PSD-95 KO mice control animals without MD.

In all animals without MD, visual stimulation of the contralateral eye induced stronger cortical activation (activity patches were always darker) than visual stimulation of the ipsilateral eye, which demonstrates the dominance of the contralateral eye in the binocular region of mouse visual cortex (Figure 56 B,C; Figure 57 B,C; Figure 58 B,C). Representative 2-D ocular dominance maps in the binocular region of the left visual cortex of an old WT/HZ (Figure 56; Figure 58 B,D) and an old PSD-95 KO animal (Figure 57; Figure 58 C,E) without and with seven days of MD are displayed in Figure 56, Figure 57, and Figure 58. Additionally, ocular dominance index (ODI) histograms are shown.

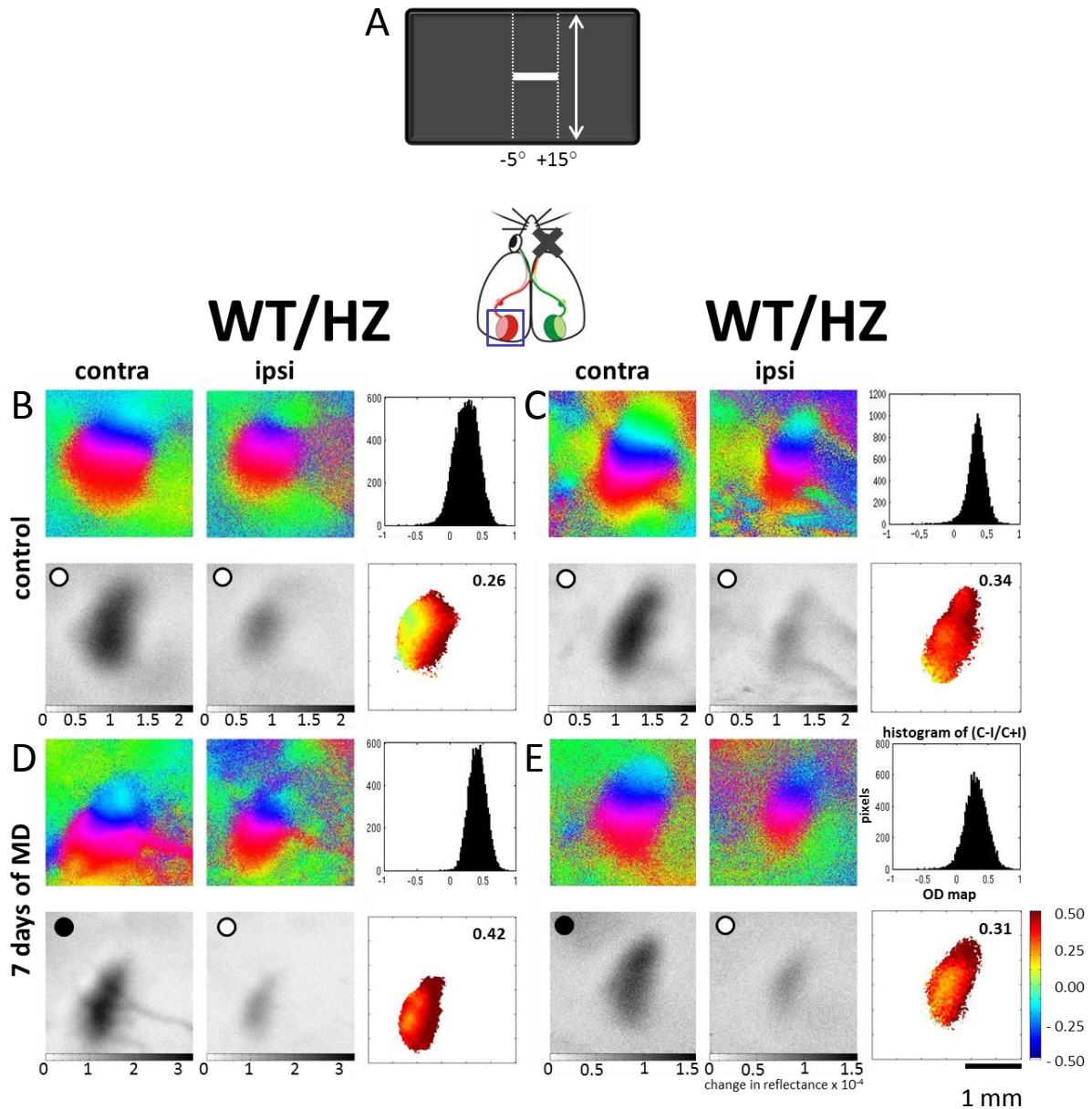


Figure 56: Representative examples of ocular dominance plasticity in old WT/HZ mice. Optical imaging maps of ipsi- and contralateral responses to the visual stimulation with a horizontal moving bar (elevation) of 20° (A) of two control WT/HZ mice (B,C) as well as for two WT/HZ mice after seven days of MD (D,E) are displayed. Color-coded retinotopic phase maps (top) and gray-scale coded response magnitude maps (bottom) are shown. For each animal the histogram of OD scores, the average ODI and the corresponding 2-D OD maps are included. ODI values are color-coded according to the scheme shown in the lower right corner of the figure: red represents positive values, blue negative values). In control WT/HZ animals, activity patches evoked by the stimulation of the contralateral eye were consistently darker than those after stimulation of the ipsilateral eye (B,C) and 2-D OD maps are yellow and red indicating a contralateral dominance. In WT/HZ mice over P110 seven days of MD (D,E) induced no significant OD shift anymore so that the response magnitude maps of the contralateral (deprived) eye remained darker than of the ipsilateral (nondeprived) eye and both histograms of OD scores and 2-D OD maps are similar to control animals. (Abbreviations: MD = monocular deprivation, OD = ocular dominance, ODI = ocular dominance index, contra/C = contralateral eye, ipsi/I = ipsilateral eye)

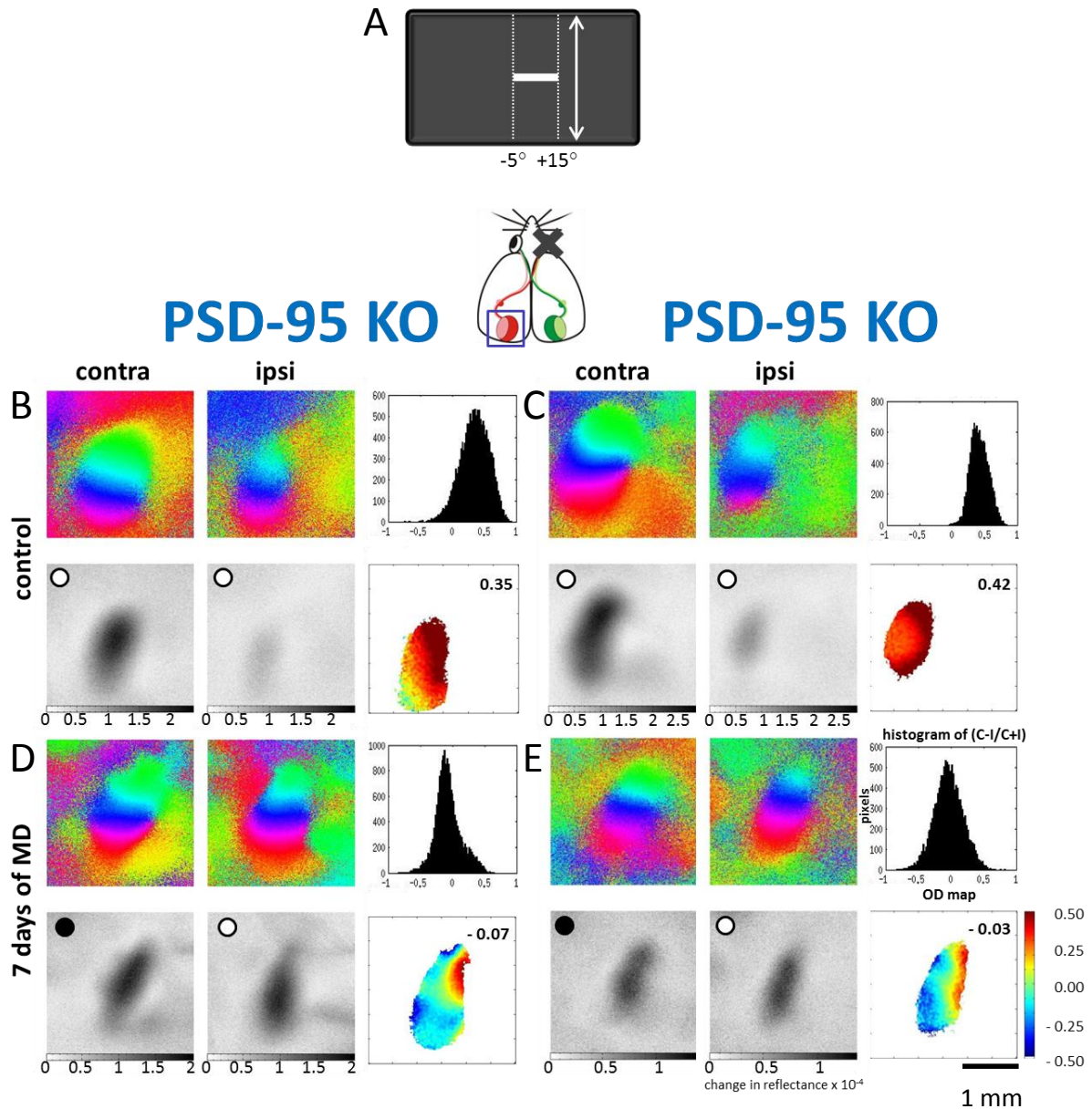


Figure 57: Representative examples of ocular dominance plasticity in old PSD-95 KO mice. Optical imaging maps of ipsi- and contralateral responses to the visual stimulation with a horizontal moving bar (elevation) of 20° (**A**) of two control PSD-95 KO mice (**B,C**) as well as for two PSD-95 KO mice after seven days of MD (**D,E**) are displayed. Color-coded retinotopic phase maps (top) and gray-scale coded response magnitude maps (bottom) are shown. For each animal the histogram of OD scores, the average ODI and the corresponding 2-D OD maps are included. ODI values are color-coded according to the scheme shown in the lower right corner of the figure: red represents positive values, blue negative values). In control PSD-95 KO animals, activity patches evoked by the stimulation of the contralateral eye were consistently darker than those after stimulation of the ipsilateral eye (**B,C**) and 2-D OD maps are yellow and red indicating a contralateral dominance. In PSD-95 KO mice over P110 seven days of MD (**D,E**) induced a significant OD shift so that the response magnitude maps of both eyes were equally dark, the histograms of OD scores shift to the left and colder colors prevail in the 2-D OD maps. (Abbreviations: MD = monocular deprivation, OD = ocular dominance, ODI = ocular dominance index, contra/C = contralateral eye, ipsi/I = ipsilateral eye)

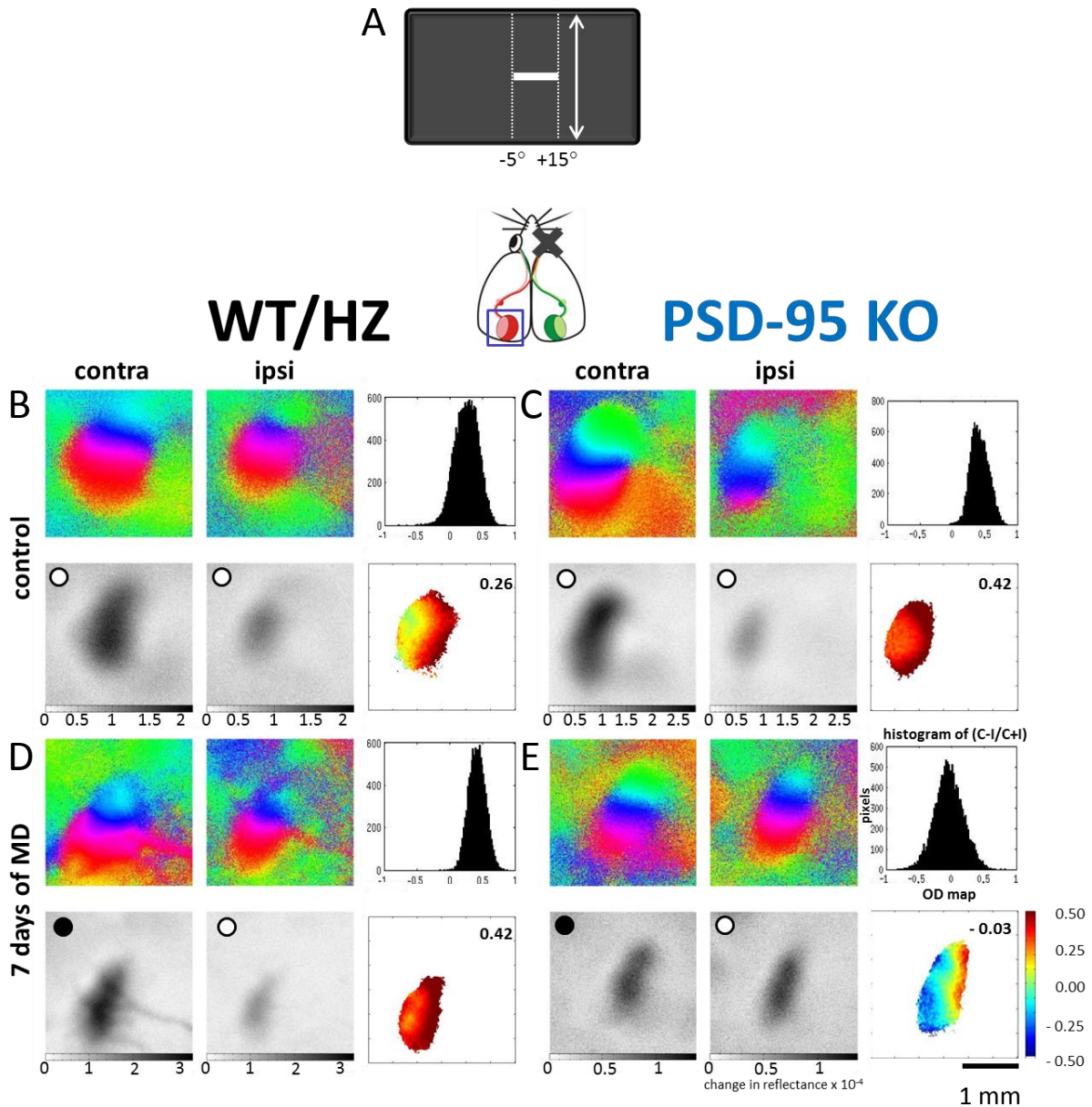


Figure 58: Ocular dominance plasticity in old WT/HZ and PSD-95 KO mice. Optical imaging maps of ipsi- and contralateral responses to the visual stimulation with a horizontal moving bar (elevation) of 20° (A) of a control WT/HZ (B) and a PSD-95 KO mouse (C) as well as for a WT/HZ (D) and a PSD-95 KO mouse (E) after seven days of MD are displayed. Color-coded retinotopic phase maps (top) and gray-scale coded response magnitude maps (bottom) are shown. For each animal the histogram of OD scores, the average ODI and the corresponding 2-D OD maps are included. ODI values are color-coded according to the scheme shown in the lower right corner of the figure: red represents positive values, blue negative values). In control WT/HZ and PSD-95 KO animals, activity patches evoked by the stimulation of the contralateral eye were consistently darker than those after stimulation of the ipsilateral eye (B,C) and 2-D OD maps are yellow and red indicating a contralateral dominance. In WT/HZ mice over P110 seven days of MD (D) induced no significant OD shift anymore so that the response magnitude maps of the contralateral (deprived) eye remained darker than of the ipsilateral (nondeprived) eye and both histograms of OD scores and 2-D OD maps are similar to control animals. (E) In contrast, in PSD-95 KO mice the response magnitude maps of both eyes were equally dark, the histograms of OD scores shift to the left and colder colors prevail in the 2-D OD maps. (Abbreviations: MD = monocular deprivation, OD = ocular dominance, ODI = ocular dominance index, contra/C = contralateral eye, ipsi/I = ipsilateral eye)

WT/HZ animals had average ODIs of 0.29 ± 0.02 (Figure 59 A) and PSD-95 KO mice displayed nearly identical average ODIs of 0.30 ± 0.03 (Figure 59 A). All ocular dominance maps showed warm colors indicating a clear contralateral dominance (Figure 58 B,C). The comparison of the ODIs of the different genotypes showed no significant difference (t-test, $p > 0.05$). To investigate the influence of monocular deprivation on ocular dominance of mice, we performed monocular deprivation for seven days.

In WT/HZ animals until 110 days seven days of MD had a significant effect on the ocular dominance (Lehmann and Löwel, 2008). Thus WT/HZ mice showed a significant effect on the ocular dominance by showing a significant shift of the ODI down to 0.06 ± 0.03 (t-test, $p < 0.001$) (Figure 59 A). Seven days of MD induced a similar significant OD shift in PSD-95 KO mice down to 0.03 ± 0.04 (t-test, $p < 0.001$). After seven days of MD there was no significant difference between both genotypes (t-test, $p > 0.05$).

In contrast, in WT/HZ animals over 110 days seven days of MD had no significant effect on the ocular dominance anymore (Lehmann and Löwel, 2008). Visual stimulation of the contralateral eye induced stronger cortical activation (activity patches were darker) than visual stimulation of the ipsilateral eye (Figure 58 D). Thus WT/HZ mice showed no significant effect on the ocular dominance by showing identical average ODIs of 0.29 ± 0.02 (t-test, $p > 0.05$) (Figure 59 A). Whereas after seven days of MD PSD-95 KO mice still showed a significant shift of the ODI down to 0.01 ± 0.01 (t-test, $p < 0.001$) like juvenile animals around P25 (Lehmann and Löwel, 2008) (Figure 59 A). Visual stimulation of the contralateral eye induced no longer a stronger cortical activation than visual stimulation of the ipsilateral eye (activity patches were equally dark) (Figure 58 E). The oldest PSD-95 KO mouse we tested so far was 507 days old and had an ODI of 0.03 after seven days of MD. Compared to their control littermates after seven days of MD there was a significant difference (t-test, $p < 0.001$).

Statistical analyzes revealed that there were significant differences of ODI values after seven days of MD between adult (<P110) and old (>P110) WT/HZ mice (t-test, $p < 0.001$), whereas no significant differences could be found between adult (<P110) and old (>P110) PSD-95 KO mice (t-test, $p > 0.05$).

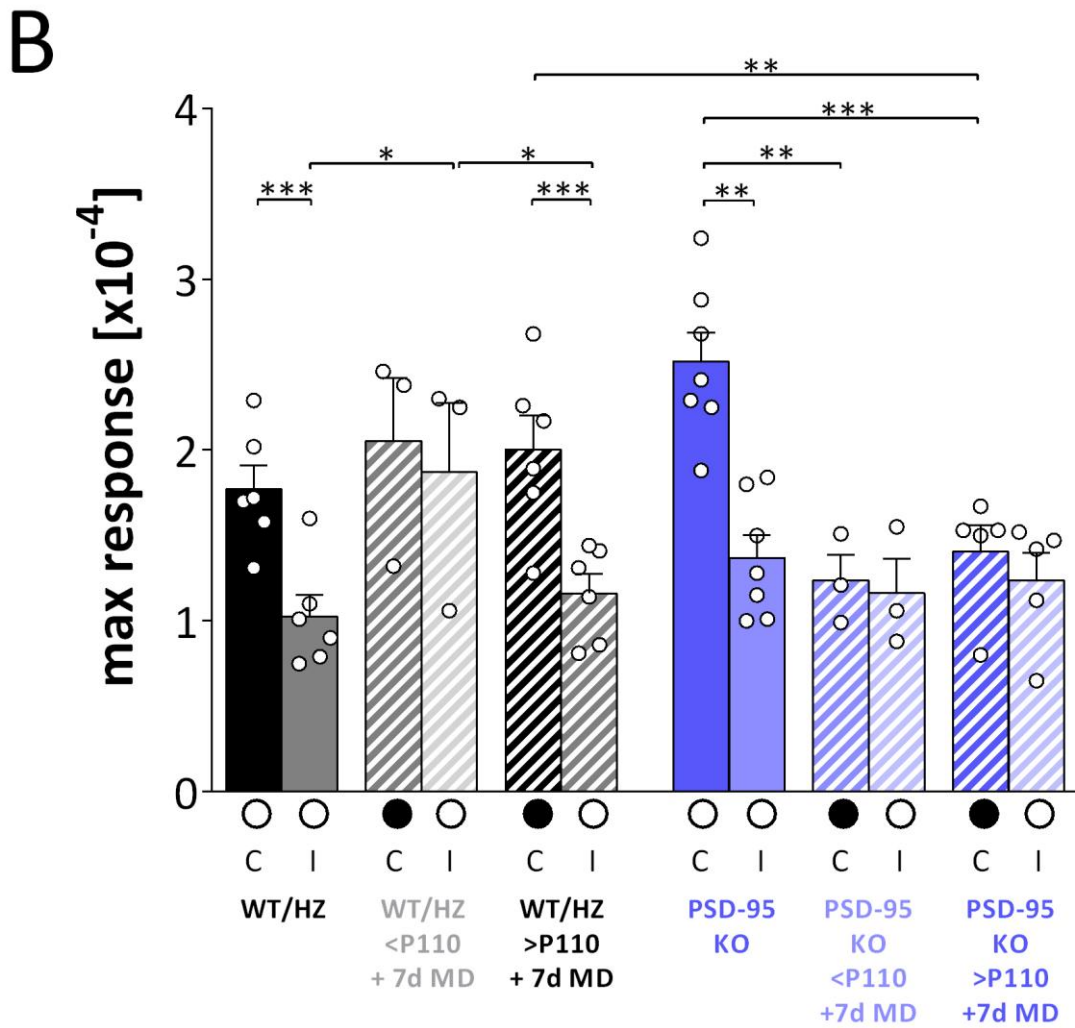
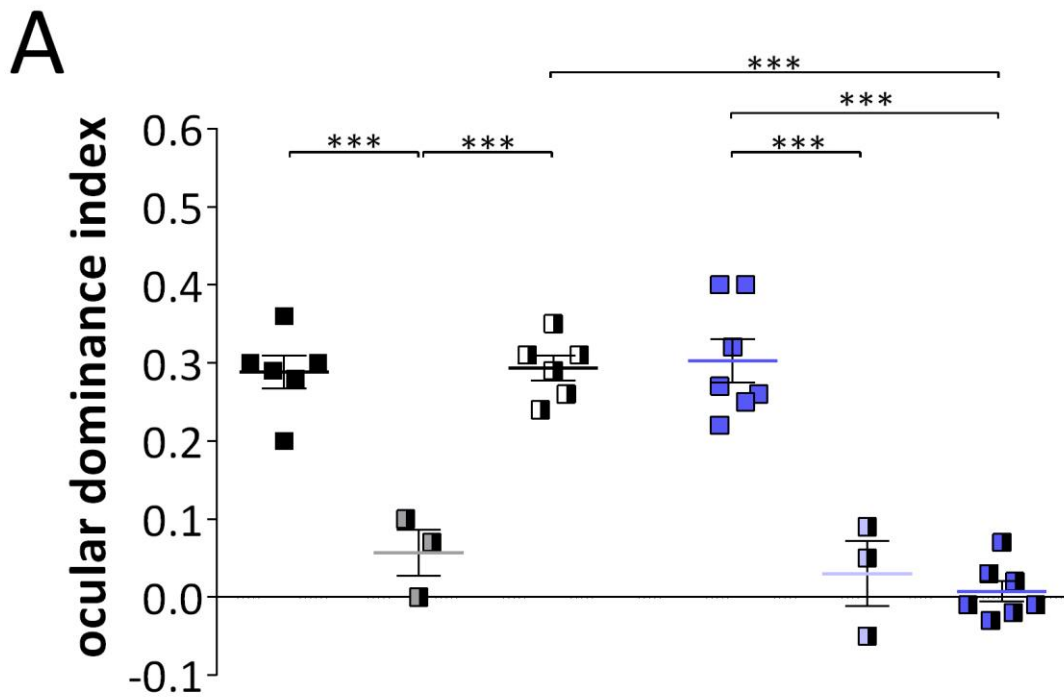




Figure 59: Ocular dominance indices and maximum response magnitude of adult and old WT/HZ (n = 3/n = 6) and PSD-95 KO mice (n = 3/n = 7) without and with seven days of MD. (A) A positive ODI indicates dominance of the contralateral eye, a negative ODI ipsilateral dominance. Squares represent ODI values of individual animals; means are marked by thick horizontal lines. WT/HZ (black) and PSD-95 KO mice (blue) without MD showed OD of the contralateral eye and show similar ODI values ODIs (t-test, $p > 0.05$). Seven days of monocular deprivation in adult WT/HZ and PSD-95 KO mice ($<P110$) induced a significant OD shift toward the open eye (t-test, $p < 0.001$ for both comparisons). After seven days of MD there was no significant difference between both adult genotypes (t-test, $p > 0.05$). In contrast, seven days of monocular deprivation in old WT/HZ mice ($>P110$) induced no significant OD shift toward the open eye anymore (t-test, $p > 0.05$), whereas in old PSD-95 KO mice ($>P110$) seven days of MD still induced a significant OD shift toward the open eye (t-test, $p < 0.001$). After seven days of MD there was a significant difference between both old genotypes (t-test, $p < 0.001$). **(B)** Maximum cortical response expressed as a change in reflectance $\times 10^{-4}$ by stimulation of the contralateral (C) or ipsilateral (I) eye in WT/HZ (black) and PSD-95 KO mice (blue) without and with seven days of MD. In all control animals, cortical activation after visual stimulation of the contralateral eye was significantly higher than after ipsilateral eye stimulation (t-test, $p < 0.01$), reflecting the dominance of the contralateral eye. In adult WT/HZ mice ($<P110$) after seven days of MD, response strengths of the two eyes were no longer significantly different because the nondeprived-eye responses were significantly increased compared with controls (t-test, $p < 0.05$). In contrast, after seven days of MD in adult PSD-95 KO mice response strengths of the two eyes were no longer significantly different because the deprived-eye responses were significantly reduced compared with controls (t-test, $p < 0.001$). In old WT/HZ mice ($>P110$) after seven days of MD, the response strengths of both eyes remained significantly different (t-test, $p < 0.001$). Whereas after seven days of MD in PSD-95 KO mice response strengths of both eyes were also not significantly different because the deprived-eye responses were still significantly reduced compared with controls (t-test, $p > 0.05$).

Without MD control mice of both genotypes displayed significantly higher maximum cortical response after visual stimulation of the contralateral eye (Figure 59 B) (t-test, $p < 0.01$ for both comparisons). The change of the ocular dominance in adult WT/HZ mice ($<P110$) is mediated by a strengthening of cortical responses after visual stimulation of the nondeprived ipsilateral eye (Figure 59 B) (t-test, $p < 0.05$). In contrast, the change of OD in adult PSD-95 KO mice ($<P110$) is mediated by a significant weakening of cortical responses after visual stimulation of the deprived contralateral eye (Figure 59 B) (t-test, $p < 0.01$). This result indicates that there was a juvenile-like type of plasticity as it is observed in WT mice during the critical period ($\sim P28$) (Hofer *et al.*, 2006b).

After seven days of MD in old WT/HZ mice ($>P110$) displayed neither an OD shift nor changes of maximum cortical responses after visual stimulation of the contralateral or the ipsilateral eye (Figure 59 B) and still showed significantly higher maximum cortical response after visual stimulation of the contralateral deprived eye (Figure 59 B) (t-test, $p < 0.001$). In contrast, the change of OD in old PSD-95 KO mice ($>P110$) is mediated by a significant weakening of cortical responses after visual stimulation of the deprived contralateral eye (Figure 59 B) (t-test, $p < 0.001$).

To test whether this juvenile-like plasticity of PSD-95 KO animals is due to reduced cortical inhibition we measured ocular dominance indices and maximum response magnitude in V1 after seven days of MD under daily treatment with diazepam, which increases the efficiency of GABAergic inhibition.

Therefore we used seven days of MD (begin at P73 up to P99 in adult mice) and tested five WT/HZ as well as four PSD-95 KO mice and compared them to six WT/HZ and seven PSD-95 KO mice control animals without MD as well as to the three adult WT/HZ and three adult PSD-95 KO animals (<P110) after seven days of MD without treatment.

In all animals without MD, visual stimulation of the contralateral eye induced stronger cortical activation (activity patches were always darker) than visual stimulation of the ipsilateral eye, which demonstrates the dominance of the contralateral eye in the binocular region of mouse visual cortex (Figure 60 B,C; Figure 61 B,C; Figure 62 B,C). Representative 2-D ocular dominance maps in the binocular region of the left visual cortex of adult WT/HZ (Figure 60; Figure 62 B,D) and adult PSD-95 KO animals (Figure 61; Figure 62 C,E) without and with seven days of MD and diazepam treatment are displayed in Figure 60, Figure 61, and Figure 62. Additionally, ocular dominance index (ODI) histograms are shown.

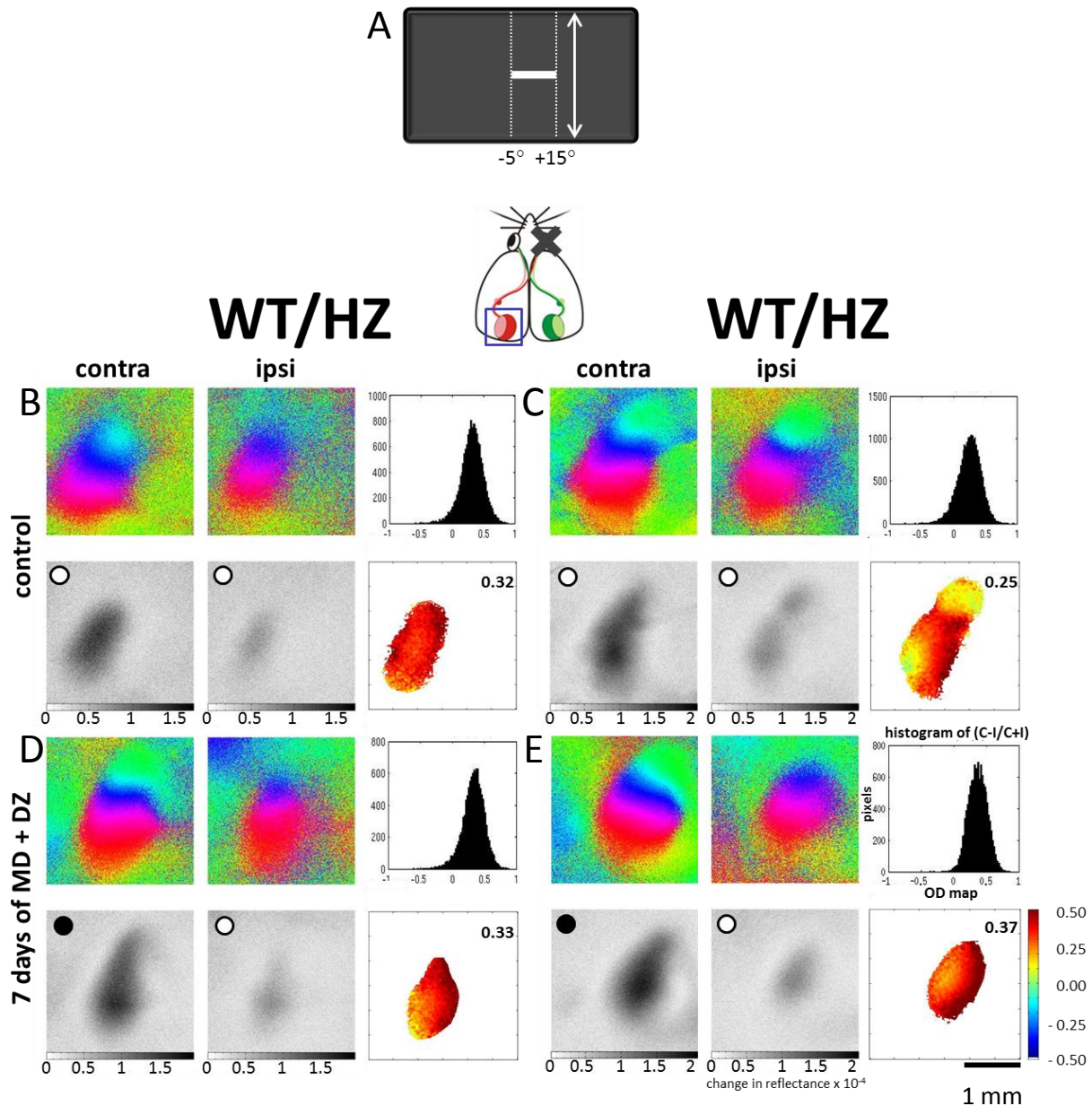


Figure 60: Representative examples of ocular dominance plasticity in adult WT/HZ mice after diazepam treatment. Optical imaging maps of ipsi- and contralateral responses to the visual stimulation with a horizontal moving bar (elevation) of 20° (A) of two control WT/HZ mice (B,C) as well as for two WT/HZ mice after seven days of MD and DZ treatment (D,E) are displayed. Color-coded retinotopic phase maps (top) and gray-scale coded response magnitude maps (bottom) are shown. For each animal the histogram of OD scores, the average ODI and the corresponding 2-D OD maps are included. ODI values are color-coded according to the scheme shown in the lower right corner of the figure: red represents positive values, blue negative values). In control WT/HZ animals, activity patches evoked by the stimulation of the contralateral eye were consistently darker than those after stimulation of the ipsilateral eye (B,C) and 2-D OD maps are yellow and red indicating a contralateral dominance. In WT/HZ mice until P110 seven days of MD and DZ treatment (D,E) induced no significant OD shift anymore so that the response magnitude maps of the contralateral (deprived) eye was still darker than of the ipsilateral (nondeprived) eye (activity patches evoked by the stimulation of the contralateral eye remained consistently darker than those after stimulation of the ipsilateral eye) and both histograms of OD scores and 2-D OD maps are similar to control animals. (Abbreviations: MD = monocular deprivation, OD = ocular dominance, ODI = ocular dominance index, contra/C = contralateral eye, ipsi/I = ipsilateral eye, DZ = diazepam)

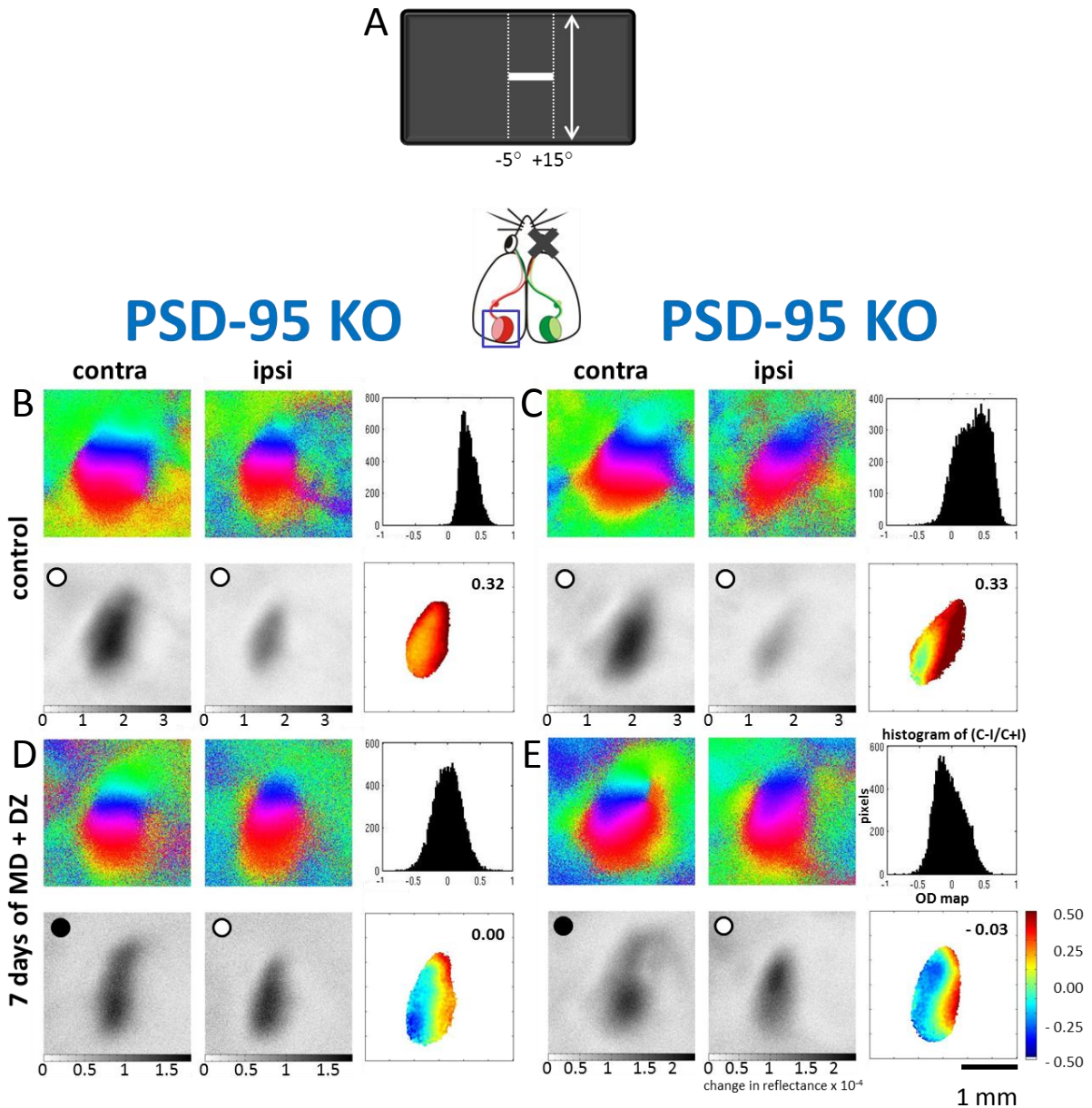


Figure 61: Representative examples of ocular dominance plasticity in adult PSD-95 KO mice after diazepam treatment. Optical imaging maps of ipsi- and contralateral responses to the visual stimulation with a horizontal moving bar (elevation) of 20° (**A**) of two control PSD-95 KO mice (**B,C**) as well as for two PSD-95 KO mice after seven days of MD and DZ treatment (**D,E**) are displayed. Color-coded retinotopic phase maps (top) and gray-scale coded response magnitude maps (bottom) are shown. For each animal the histogram of OD scores, the average ODI and the corresponding 2-D OD maps are included. ODI values are color-coded according to the scheme shown in the lower right corner of the figure: red represents positive values, blue negative values). In control WT/HZ and PSD-95 KO animals, activity patches evoked by the stimulation of the contralateral eye were consistently darker than those after stimulation of the ipsilateral eye (**B,C**) and 2-D OD maps are yellow and red indicating a contralateral dominance. In PSD-95 KO mice until P110 seven days of MD and DZ treatment (**D,E**) induced a significant OD shift so that the response magnitude maps of both eyes were equally dark, the histograms of OD scores shift to the left and colder colors prevail in the 2-D OD maps. (Abbreviations: MD = monocular deprivation, OD = ocular dominance, ODI = ocular dominance index, contra/C = contralateral eye, ipsi/I = ipsilateral eye, DZ = diazepam)

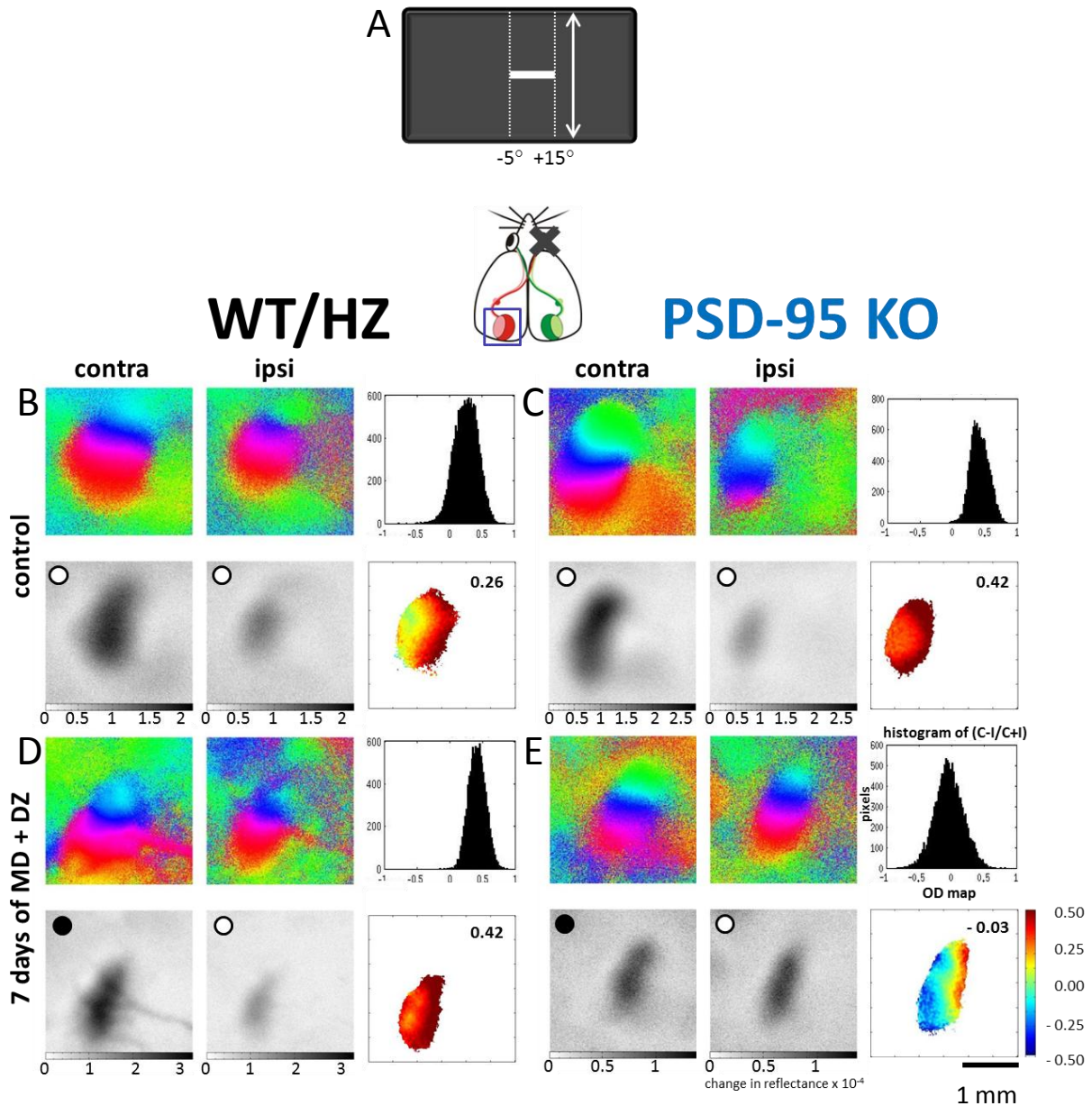
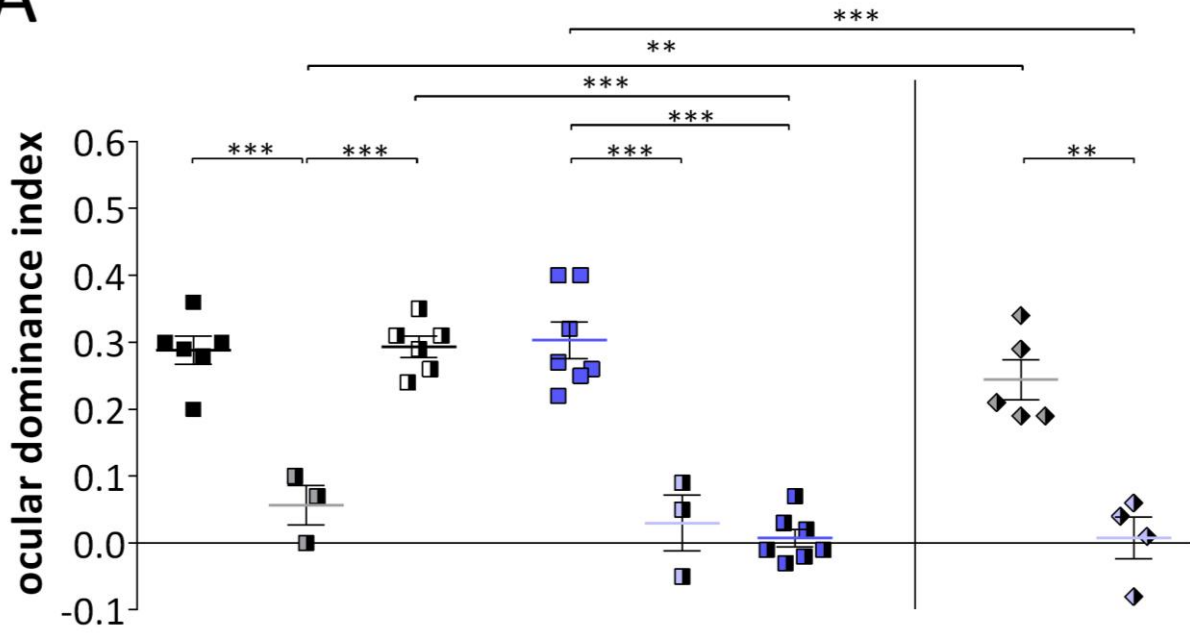


Figure 62: Ocular dominance plasticity in adult WT/HZ and PSD-95 KO mice after diazepam treatment. Optical imaging maps of ipsi- and contralateral responses to the visual stimulation with a horizontal moving bar (elevation) of 20° (**A**) of a control WT/HZ (**B**) and a PSD-95 KO mouse (**C**) as well as for a WT/HZ (**D**) and a PSD-95 KO mouse (**E**) after seven days of MD and DZ treatment are displayed. Color-coded retinotopic phase maps (top) and gray-scale coded response magnitude maps (bottom) are shown. For each animal the histogram of OD scores, the average ODI and the corresponding 2-D OD maps are included. ODI values are color-coded according to the scheme shown in the lower right corner of the figure: red represents positive values, blue negative values). In control WT/HZ and PSD-95 KO animals, activity patches evoked by the stimulation of the contralateral eye were consistently darker than those after stimulation of the ipsilateral eye (**B,C**) and 2-D OD maps are yellow and red indicating a contralateral dominance. In WT/HZ mice until P110 seven days of MD and DZ treatment (**D**) induced no significant OD shift anymore so that the response magnitude maps of the contralateral (deprived) eye was still darker than of the ipsilateral (nondeprived) eye (activity patches evoked by the stimulation of the contralateral eye remained consistently darker than those after stimulation of the ipsilateral eye) and both histograms of OD scores and 2-D OD maps are similar to control animals. (**E**) In contrast, in PSD-95 KO mice the response magnitude maps of both eyes were equally dark, the histograms of OD scores shift to the left and colder colors prevail in the 2-D OD maps. (Abbreviations: MD = monocular deprivation, OD = ocular dominance, ODI = ocular dominance index, contra/C = contralateral eye, ipsi/I = ipsilateral eye, DZ = diazepam)

In WT/HZ animals under 110 days seven days of MD causes a significant shift of the ODI from 0.23 to 0.09 (Lehmann and Löwel, 2008). We also observed a significant shift of the ODI from 0.29 ± 0.02 to 0.06 ± 0.03 in WT/HZ littermate animals under 110 days (Figure 63 A) (t-test, $p < 0.001$). Treatment with diazepam abolished the ODI shift in WT/HZ animals under 110 days. Visual stimulation of the contralateral eye induced stronger cortical activation (activity patches were darker) than visual stimulation of the ipsilateral eye (Figure 62 D). The average ODI of the diazepam treated animals with 0.24 ± 0.03 was not significantly different from the average ODI of WT/HZ animals without MD (Figure 63 A) (t-test, $p > 0.05$).

As already mentioned PSD-95 KO mice displayed nearly identical average ODIs of 0.30 ± 0.03 (Figure 63 A). The comparison of the ODIs of the different genotypes showed no significant difference (t-test, $p > 0.05$). We observed a significant shift of the ODI from 0.30 ± 0.02 to 0.03 ± 0.04 (t-test, $p < 0.001$) in PSD-95 KO animals under 110 days (Figure 63 A). Interestingly, the abolishment of the OD shift by diazepam was not observed in PSD-95 KO mice. Visual stimulation of the contralateral eye induced no longer a stronger cortical activation than visual stimulation of the ipsilateral eye (activity patches were equally dark) (Figure 62 E). Compared to PSD-95 KO mice without MD after seven days of MD these mice still displayed an average ODI of 0.01 ± 0.03 after treatment with diazepam (Figure 63 A) (t-test, $p < 0.001$) which differed significantly from average ODI of WT/HZ mice after diazepam treatment (Figure 63 A) (t-test, $p < 0.01$).

A



B

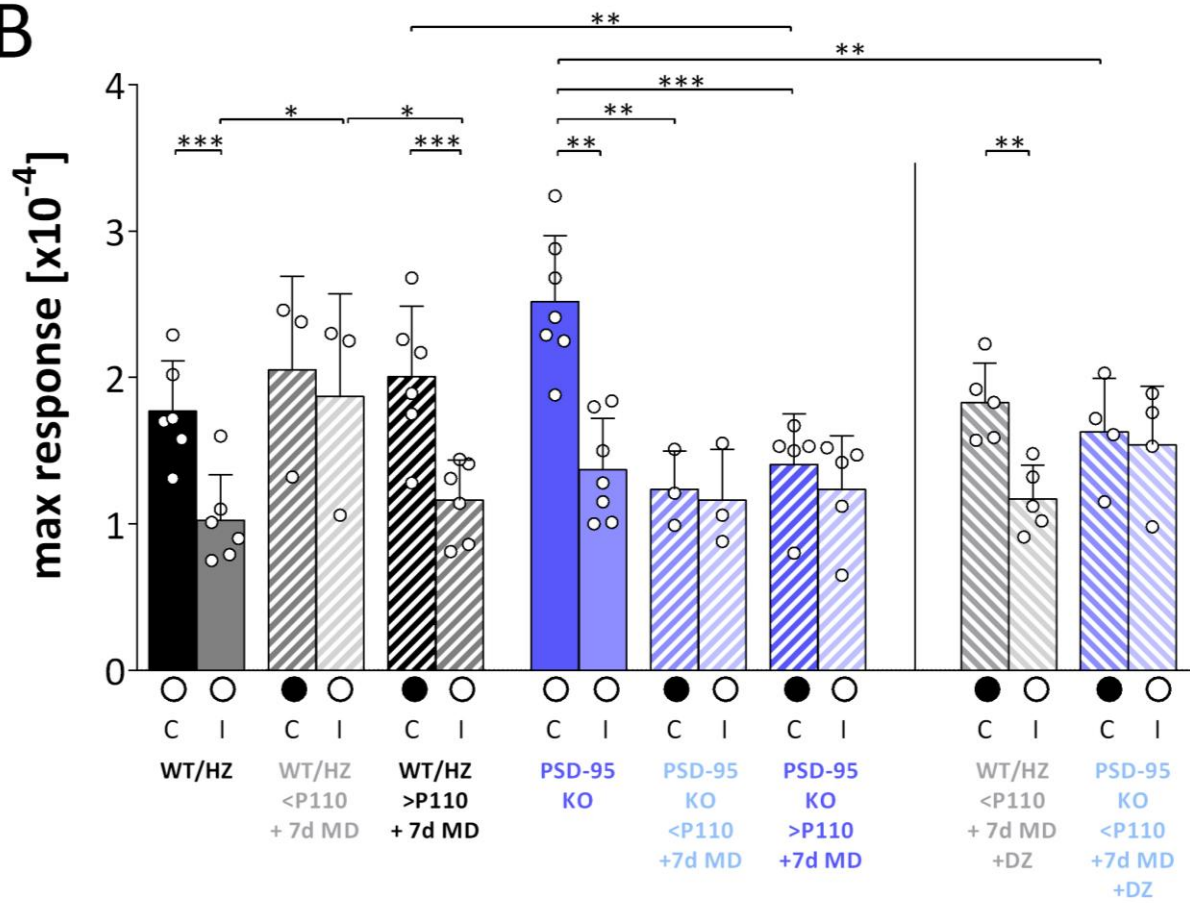




Figure 63: Ocular dominance indices and maximum response magnitude of adult and old WT/HZ (n = 5) and PSD-95 KO mice (n = 4) without and with seven days of MD and after diazepam treatment as well as of adult WT/HZ (n = 5) and PSD-95 KO mice (n = 4) with seven days of MD and diazepam treatment. (A) A positive ODI indicates dominance of the contralateral eye, a negative ODI ipsilateral dominance. Squares represent ODI values of individual animals; means are marked by thick horizontal lines. WT/HZ (black) and PSD-95 KO mice (blue) without MD showed OD of the contralateral eye and show similar ODI values ODIs (t-test, $p > 0.05$). Seven days of monocular deprivation in adult WT/HZ and PSD-95 KO mice ($<P110$) induced a significant OD shift toward the open eye (t-test, $p < 0.001$ for both comparisons). After seven days of MD there was no significant difference between both adult genotypes (t-test, $p > 0.05$). In contrast, seven days of monocular deprivation in old WT/HZ mice ($>P110$) induced no significant OD shift toward the open eye anymore (t-test, $p > 0.05$), whereas in old PSD-95 KO mice ($>P110$) seven days of MD still induced a significant OD shift toward the open eye (t-test, $p < 0.001$). After seven days of MD there was a significant difference between both old genotypes (t-test, $p < 0.001$). **(B)** Maximum cortical response expressed as a change in reflectance $\times 10^{-4}$ by stimulation of the contralateral (C) or ipsilateral (I) eye in WT/HZ (black) and PSD-95 KO mice (blue) without and with seven days of MD. In all control animals, cortical activation after visual stimulation of the contralateral eye was significantly higher than after ipsilateral eye stimulation (t-test, $p < 0.01$), reflecting the dominance of the contralateral eye. In adult WT/HZ mice ($<P110$) after seven days of MD, response strengths of the two eyes were no longer significantly different because the nondeprived-eye responses were significantly increased compared with controls (t-test, $p < 0.05$). In contrast, after seven days of MD in adult PSD-95 KO mice response strengths of the two eyes were no longer significantly different because the deprived-eye responses were significantly reduced compared with controls (t-test, $p < 0.01$). In old WT/HZ mice ($>P110$) after seven days of MD, the response strengths of both eyes remained significantly different (t-test, $p < 0.001$). Whereas after seven days of MD in PSD-95 KO mice response strengths of both eyes were also not significantly different because the deprived-eye responses were still significantly reduced (t-test, $p < 0.001$) compared with controls (t-test, $p > 0.05$). In adult WT/HZ animals ($<P110$) this potentiation was absent after treatment with DZ (t-test, $p > 0.05$) the response strengths of both eyes remained significantly different (t-test, $p < 0.01$). But interestingly, even after diazepam treatment, adult PSD-95 KO animals ($<P110$) showed a significant juvenile-like weakening of the deprived eye compared to PSD-95 KO animals without MD (t test, $p < 0.01$) because the deprived-eye responses were still significantly reduced compared with controls (t-test, $p > 0.05$).

The shift of the ocular dominance in adult WT mice ($<P110$) is normally mediated by the potentiation of cortical responses after visual stimulation of the non-deprived eye inputs (Hofer *et al.*, 2006b; Lehmann and Löwel, 2008). In our experiment adult WT/HZ animals around 80 days also showed this potentiation after seven days of MD (t-test, $p < 0.05$). In adult WT/HZ animals ($<P110$) this potentiation was absent after treatment with diazepam (Figure 63 B) (t-test, $p > 0.05$). But interestingly, even after diazepam treatment, adult PSD-95 KO animals ($<P110$) showed a significant juvenile-like weakening of cortical responses after visual stimulation of the deprived eye compared to PSD-95 KO animals without MD (t-test, $p < 0.01$) (Figure 63 B) (Hofer *et al.*, 2006b).

4. Discussion

4.1 Robust visual performance of Bsn^{-/-} mice

In the present study, we used Bassoon mutant mice, which display reduced signal transfer from photoreceptor to bipolar cells (Dick *et al.*, 2003) to study the central processing and visual capabilities of animals with disturbed retinal signals. In Bsn^{-/-} mice, neuronal transmission from photoreceptor to bipolar cells is impaired. Electroretinographic recordings revealed that the b-wave, which represents activity in 2nd order retinal neurons, was diminished and had a slower time course in Bsn^{-/-} mice (Dick *et al.*, 2003). While these results showed that there is residual synaptic transmission from photoreceptors to bipolar cells in the retina of Bsn^{-/-} mice, they did not show to which extent the remaining neurotransmission is used for the activation of the central vision system and for behavioral tasks.

To address these questions mice were behaviorally tested in two different paradigms: the virtual-reality optomotor system (Prusky *et al.*, 2004) and the visual water task (Prusky *et al.*, 2000). In addition, visual cortical maps were recorded by optical imaging of intrinsic signals (Kalatsky and Stryker, 2003).

Visual acuity measured with the virtual-reality optomotor system was significantly reduced in mutants compared to littermate controls but also reached adult values already at four weeks of age. In the visual water task, both Bsn^{+/+} and Bsn^{-/-} mice had higher visual acuity than in the virtual-reality optomotor system. This difference was previously observed for C57Bl/6J mice (Prusky *et al.*, 2000) and is most likely due to different neuronal subsystems subserving the behavioral responses in optomotor and reinforcement-based tasks: optokinetic movements are driven by subcortical low-frequency visual pathways while grating acuity in the visual water task is driven by cortical circuits (Prusky *et al.*, 2000; Prusky *et al.*, 2004; Douglas *et al.*, 2005).

Interestingly, the difference in visual acuity between mutants and controls was identical in both tasks: Bsn^{-/-} mice had visual thresholds about approximately 0.2 cyc/deg lower than Bsn^{+/+} mice. Our results indicate that mice can achieve a visual acuity of about 0.4 cyc/deg

even in the absence of proper ribbon synapses and that Bassoon-dependent fast exocytosis is necessary “only” for the additional 0.2 cyc/deg observed in wild-type mice.

The contrast sensitivity of the mutants was notably reduced in the optomotor test, while mutants and wild-type mice performed similarly in the optical imaging experiments. This interesting result may be explained by a compensation of lost contrast enhancing mechanisms in the retina by contrast enhancing mechanisms in more central parts of the visual system which are not involved in mediating optomotor reflexes. Conversely, the reason for the reduction of contrast sensitivity in the optomotor task in *Bsn*^{-/-} mice may be that the retinal signals for the optomotor reflexes are processed by subcortical pathways, so that a loss of contrast enhancing mechanisms in the retina cannot be compensated for by central parts of the visual system. A possible explanation for reduced contrast sensitivity mechanisms in the retina of *Bsn*^{-/-} animals may be based on the morphology of the ribbon synapse. In this particular synapse, the postsynaptic dendritic contacts of horizontal cells seem to embrace the anchor site of the ribbons, whereas the contact sites of the bipolar cells are somewhat more distant. This morphology makes it reasonable to assume that a loss of ribbons may affect the synaptic transfer between photoreceptors and horizontal cells more severely than the transfer between photoreceptors and bipolar cells and therefore reduce the efficiency of the inhibitory periphery of the receptive fields. Such a reduction of the inhibitory interactions should result in a reduction of both contrast sensitivity and spatial resolution, as we have indeed observed in our experiments.

Both of our behavioral tests clearly showed that ribbon-dependent fast exocytosis from photoreceptor cells is essential for normal visual capabilities. These data also confirm previous observations that synaptic ribbons are essential for the precise information processing at photoreceptor synapses as well as at inner ear hair cell synapses and that active zones without ribbons still retain sufficient functional performance to mediate sensory signal transduction reaching central systems (Dick *et al.*, 2003; Khimich *et al.*, 2005). The possibility that the reduced visual capabilities of Bassoon mutant mice are at least in part due to the function of the Bassoon protein in synapses of the cerebral cortex cannot be excluded (Altrock *et al.*, 2003; Angenstein *et al.*, 2007; Angenstein *et al.*, 2008).

Furthermore, since the range of the inhibitory system is tuned to the optimal spatial frequency (Sagi and Hochstein, 1985; Shapley and Lennie, 1985), it can be expected that the

reduction of contrast sensitivity is largest at this particular spatial frequency. This was also observed in our experiments in the virtual-reality optomotor system: the reduction of contrast sensitivity was highest at the optimal spatial frequency of 0.064 cyc/deg (six times) and much less (two to five times) at other spatial frequencies. It is therefore possible that contrast enhancing mechanisms in the retina (Kamermans and Spekreijse, 1999) are reduced or switched off while the projection *via* the bipolar cells is still more or less intact. A reduced input to retinal horizontal cells could also explain the alterations in the b-wave of the electroretinogram in Bassoon mutants (Dick *et al.*, 2003). A reduced and prolonged b-wave could result when the inhibitory system of the horizontal cells is switched off. Thus, the absence of activity in horizontal cells could account for the reduced amplitude of the b-wave and the absence of inhibitory interactions could explain its prolonged duration.

Interestingly, our tests in the optomotor system with different stimulus velocities revealed a significant difference in the temporal sensitivity between wild-type and mutant animals: Bsn^{-/-} mice tracked grating stimuli up to 38 °/sec while littermates continued to track the gratings to over 50 °/sec, the technical speed limit of our system. These results are further evidence for decelerated neuronal processing in the visual pathway of Bsn^{-/-} mice, presumably at early stages of synaptic processing in the retina, as it is indicated by the prolonged duration of the ERG b-wave (Dick *et al.*, 2003). While the residual synaptic transmission from photoreceptors to bipolar cells is sufficient to mediate basic visual capabilities for Bsn^{-/-} mice, a deficit becomes obvious when the system is challenged with higher stimulus velocities.

Surprisingly, we found that optical imaging of visual cortical activity (Kalatsky and Stryker, 2003) revealed essentially no differences between Bsn^{-/-} mice and wild-type littermates. Cortical maps were also adult-like at four weeks of age. These results show that i) robust visual performance can be achieved in absence of synaptic ribbons, ii) development and maintenance of visual cortical maps are independent of synaptic ribbons and iii) visual development of Bsn^{-/-} mice is completed at four weeks of age, which indicates that later developing ectopic synapses (Dick *et al.*, 2003; Specht *et al.*, 2007) do not seem to contribute to visual capabilities nor improve central visual processing. Hence, the central visual system can make use of slow and weak retinal signals from a diseased retina to subserve surprisingly robust vision.

Furthermore, optical imaging of intrinsic signals in the visual cortex did not reflect the impairment of the afferent visual signal, but must have been amplified either by some intrinsic cortical processing or at some stage of the afferent visual pathway beyond the defective retinal transmission. Thus, retinal ganglion cells or more central stages of visual information processing are obviously able to compensate a loss of lateral inhibition in the retina.

In the absence of functional Bassoon, ectopic photoreceptor synapses are formed in the outer nuclear layer of the retina starting at about four weeks postnatally (Dick *et al.*, 2003). By examining mutant retinæ over a period of two years long-lasting plastic changes were observed: ectopic photoreceptor synapses were formed *de novo* by sprouting of both bipolar and horizontal cells resulting in a dense synaptic plexus in the outer nuclear layer, which is absent in wild-type retina. To check whether ectopic synapses are responsible for our observations in adult Bsn^{-/-} mice, we followed vision longitudinally in individual animals from eye opening and also imaged visual cortical maps. These experiments revealed that Bsn^{-/-} mice reached adult values of both visual acuity and contrast sensitivity at four weeks of age and thus before ectopic synapse formation modified retinal structure. In addition, visual cortical maps were adult-like at the same age. It is therefore highly unlikely that the formation and remodeling of ectopic synapses, which lasts for at least one year (Specht *et al.*, 2007) is responsible for the visual abilities of Bsn^{-/-} mice or improves vision or central visual processing. It rather indicates that the remaining neuronal transmission of the photoreceptor synapse in mutant mice, that is basic exocytosis at ribbon-deficient synapses and additional fusion outside the active zone (Dick *et al.*, 2003; Khimich *et al.*, 2005), is sufficient to sustain decent visual capabilities and activate central visual processing structures.

Taken together, our analyses showed that while Bassoon-dependent fast exocytosis is essential for normal visual capabilities behaviorally relevant visual discrimination was still possible in Bsn^{-/-} mice.

Our results are consistent with a previous report showing that the development of precise retinotopic maps in the visual cortex of mice does not depend on experience-dependent sensory input but is due to waves of spontaneous retinal activity during the first postnatal week. By using a mutant mouse line that has uncorrelated retinal activity during

development due to the deletion of the $\beta 2$ -subunit of the nicotinic acetylcholine receptor it was demonstrated that the geniculocortical map reaches adult precision by postnatal day eight and is not further refined by later retinal waves or visual experience (Cang *et al.*, 2005b).

Furthermore, our optical imaging results show that the slower and reduced input signals from the Bassoon mutant retina into visual cortex are not only sufficient to sustain retinotopic maps but also to activate the cortex as strongly as in normal mice. We take this observation as a strong indication of homeostatic mechanisms (Turrigiano and Nelson, 2004). While it is generally believed that Hebbian type of network modifications is crucial for shaping cortical circuits after sensory experience, additional homeostatic plasticity might ensure that network compensation can be achieved in spite of a wide range of sensory perturbations (Mrsic-Flogel *et al.*, 2007; Maffei and Turrigiano, 2008). We suggest that in Bsn^{-/-} mice, homeostatic synaptic scaling might have adjusted excitatory synaptic strengths of neurons in the afferent visual pathway or in the visual cortex to compensate for reduced synaptic transmission in the retina.

Overall our results show that the central visual system has an extraordinarily high potential to process altered inputs from the retina and hence to be instrumental in sustaining behaviorally relevant visual capabilities (Goetze *et al.*, 2010b).

4.2 Impaired OD plasticity in adult Bsn^{-/-} mice

The protein Bassoon is not only present in ribbon synapses but also in conventional synapses in the brain and important for assembling the active zone of the presynaptic membrane. Hence, Bassoon mutant mice showed a reduction in normal synaptic transmission, which might be due to the inactivation of a part of glutamatergic synapses (Altrock *et al.*, 2003). Therefore Bassoon plays a role in the regulation of neurotransmitter release from a subset of glutamatergic synapses (Altrock *et al.*, 2003). Since inhibition plays a major role in OD plasticity (Hensch *et al.*, 1998) and Bassoon mutant mice showed an excitation-inhibition-imbalance and impaired striatal plasticity (Ghiglieri *et al.*, 2009), we wanted to investigate whether mutant mice also display impaired neuronal plasticity in the visual cortex.

Intrinsic optical imaging of V1 revealed a significant shift of OD due to decreased deprived-eye responses after four days of MD in juvenile *Bsn*^{-/-} mice similar to their juvenile *Bsn*^{+/+} littermates. Interestingly, OD plasticity was absent in adult *Bsn*^{-/-} animals in contrast to their wild-type littermates, which displayed a significant shift of OD due to increased open-eye responses after seven days of MD.

Juvenile (P20) as well as adult (P60) Bassoon mutant mice suffer from epileptiform seizures, whereas adult mice display up to twice as much and more severe seizures as juvenile mice (Altrock *et al.*, 2003; Ghiglieri *et al.*, 2009). Based on these findings the physiological and morphological impairments due to the seizures might be more severe in adult than in juvenile mutant animals, which would fit to our data.

Bassoon mutant mice showed decreased LTP in corticostriatal synapses (Ghiglieri *et al.*, 2009), which is due to the presence of epileptiform seizures. LTP plays a major role in neuronal plasticity by increasing cortical responses of the open eye after MD (Espinosa and Stryker, 2012). This might also be an explanation for the absent OD plasticity in the visual cortex in adult mutant mice. The impairment of LTP might be the result of altered NMDAR subunit composition in mutants (Ghiglieri *et al.*, 2009). In fact, activation, accurate assembly, and localization of NMDARs in the cytoplasmic surface below the postsynaptic membrane of glutamatergic synapses termed postsynaptic density (PSD), are essential for LTP (Picconi *et al.*, 2004) whereas the PSD is altered in brain areas with occurring seizures (Wyneken *et al.*, 2001; Wyneken *et al.*, 2003; Finardi *et al.*, 2006). Bassoon mutant mice showed altered NMDAR organization in the striatal PSD, NR2A and NR2B levels were modified and revealed an increase in the NR2A/NR2B ratio (Ghiglieri *et al.*, 2009), this might also be the case in V1. The regulation of the NR2A/NR2B ratio plays a crucial role in the control of cortical synaptic plasticity (Yashiro and Philpot, 2008). In the visual cortex of mice a reduction of the NMDAR subunit NR2A enhances the activity-dependent strengthening of synapses during MD (Cho *et al.*, 2009). Chow and her colleagues (2009) hypothesized that a reduction in the NR2A/NR2B ratio during MD is permissive for the compensatory potentiation of open-eye inputs. In contrast, Bassoon mutant mice showed an increase in NR2A/NR2B ratio, which one could conclude that this increase leads to hindered or even absent potentiation of open-eye responses, like we observed in adult Bassoon mutant mice.

Monocular deprivation in adult mice increases presynaptic release of glutamate (Yashiro *et al.*, 2005). Hippocampal glutamatergic synapses in *Bsn*^{-/-} mice are partly inactive (up to 50 % more inactive synapses than in wild-type animals), which leads to a fewer number of neurons that are able to release neurotransmitters (Altrock *et al.*, 2003). It is not clear whether Bassoon mutant mice show this increase in glutamate release during MD and if so this increase of the remaining active synapses might not be sufficient to induce OD plasticity.

Interestingly, immunohistochemistry revealed that juvenile as well as adult Bassoon mutant mice displayed a higher number of parvalbumin positive fast-spiking interneurons in the visual cortex, which was previously only reported for the striatum (Ghiglieri *et al.*, 2009). Additionally, we found that this number increased during age. As previously reported Bassoon mutant mice display an excitation-inhibition-imbalance partly due to a reduction of excitatory drive onto GABAergic interneurons, which may lead to lower excitation of interneurons and therefore to decreased GABA release (Altrock *et al.*, 2003). This finding is most likely the reason for epileptiform seizures and seizures can cause extensive neuronal loss and severe brain damage (Olney *et al.*, 1983; Sloviter, 1983, 1996). To prevent this kind of damage, the brain might adapt by increasing inhibition *via* an increased number of PV positive interneurons. Since in juvenile animals PV increases in visual cortex with eye opening, which correlates with higher activity (Patz *et al.*, 2004; Sugiyama *et al.*, 2008), cortical activity based on visual experience is necessary that a neuron commences PV expression (Patz *et al.*, 2004). Since there is a gain in quantity of epileptiform seizures in Bassoon mutant mice with age, this might explain the increased number of PV positive interneurons possibly by an augmented activation of silent/inactive interneurons, which did not yet express parvalbumin. Enhanced inhibition could be the explanation for the absent adult OD plasticity in Bassoon mutant mice. The conclusion that GABAergic inhibition limits adult plasticity in the visual cortex was drawn after pharmacological reduction of intracortical inhibition (obtained through infusion of an inhibitor of GABA synthesis or a GABA_A antagonist directly into the visual cortex) reactivated OD plasticity in response to MD in adult rats (Harauzov *et al.*, 2010).

Noteworthy, a recent study showed that Bassoon mutant mice displayed a highly elevated level of BDNF measured by ELISA (Heyden *et al.*, 2011). Epileptic seizures are most likely the reason for increased BDNF levels and promoted neurogenesis (Parent *et al.*, 1997; Lee *et al.*, 2002; Altar *et al.*, 2003; Yokoi *et al.*, 2007). Previous studies revealed that BDNF

overexpression in transgenic mice induced premature start as well as termination of the critical period in the visual cortex (Hanover *et al.*, 1999; Huang *et al.*, 1999). BDNF is involved in regulating efficacy and number of inhibitory synapses, hence the amount of inhibition that pyramidal cells receive (Huang *et al.*, 1999). If not only the critical period but also the period of adult plasticity would be terminated precociously, this might be an explanation for the phenotype of absent adult plasticity in adult but not in juvenile mutant mice. Unfortunately we couldn't find this elevated level of BDNF with immunohistochemical staining. This might be because of different reasons: i) ELISA is a much more sensitive method to measure even small amounts of proteins than immunohistochemical staining, ii) Heyden and her colleagues (2011) measured the whole cerebral cortex whereas we only stained the visual cortex and there might not be that highly elevated level of BDNF present, or iii) the amount of BDNF antibody was too low to stain the whole amount of protein and therefore didn't reveal any differences between Bsn^{+/+} and Bsn^{-/-} mice.

The stability of synapses requires complex interactions with an extracellular matrix structure; the perineuronal nets (PNNs). PNNs form a lattice-like configuration around the synapses on the proximal and somata dendrites of certain neurons (Hockfield *et al.*, 1990; Brückner *et al.*, 1993), and therefore influence synaptic integrity and stability (Frischknecht and Gundelfinger, 2012). Chondroitin sulfate proteoglycans, *e.g.* neurocan and brevican, are major components of the PNNs (Yamaguchi, 2000). Numerous studies revealed that chondroitin sulfate proteoglycans play a role in plasticity (Pizzorusso *et al.*, 2002; Dityatev and Schachner, 2003; Pizzorusso *et al.*, 2006; Tropea *et al.*, 2009; Frischknecht and Gundelfinger, 2012). After degradation of chondroitin sulfate proteoglycans with chondroitinase-ABC in adult rats, OD plasticity was reactivated and MD caused an OD shift toward the nondeprived eye (Pizzorusso *et al.*, 2002). Thus, the mature extracellular matrix is inhibitory for experience-dependent plasticity. *Status epilepticus*, a state in which the brain is in persistent seizure, leads to an increased expression of neurocan and brevican (Kurazono *et al.*, 2001; Matsui *et al.*, 2002; Yuan *et al.*, 2002; Galtrey and Fawcett, 2007; McRae *et al.*, 2012; McRae and Porter, 2012) and might therefore prevent neuronal plasticity. This would fit with our observation of the absent OD plasticity in adult Bassoon mutant mice. From our data it is not clear if the absent adult OD plasticity is due to the mutation in the Bassoon gene *per se*, or whether the frequent epileptiform seizures in the mutant mice affect the OD plasticity.

4.3 Impaired interocular plasticity in Bsn^{-/-} mice

Monocular deprivation gradually improves visual acuity and contrast sensitivity of the open eye in mice and depends on the monocular field of the ipsilateral visual cortex (Prusky *et al.*, 2006).

Our experiments revealed that juvenile as well as adult Bsn^{+/+} mice showed similar improvement of visual acuity and contrast sensitivity after MD as previously described for C57Bl/6J mice (Prusky *et al.*, 2006). On the other hand, juvenile and adult Bsn^{-/-} mice showed reduced improvement compared to their wild-type littermates. In fact, adult mutant mice revealed even more affected interocular plasticity than juvenile mutants.

As already mentioned Bassoon mutant mice showed decreased LTP in corticostriatal synapses (Ghiglieri *et al.*, 2009), which is due to the presence of epileptiform seizures, and since LTP plays a major role in neuronal plasticity, this might also be a reason for the reduced interocular plasticity of adult mutant mice.

Since our immunohistochemistry data revealed that adult Bassoon mutant mice displayed a higher number of parvalbumin positive fast-spiking interneurons or a higher expression of PV in the visual cortex than juvenile mutants, enhanced inhibition could be an explanation for stronger reduced adult interocular plasticity in adult Bassoon mutant mice compared to juvenile mutant animals.

The increasing frequency of epileptiform seizures might correlate with an increased expression of the chondroitin sulfate proteoglycans neurocan and brevican (Kurazono *et al.*, 2001; Matsui *et al.*, 2002; Yuan *et al.*, 2002; Galtrey and Fawcett, 2007; McRae *et al.*, 2012; McRae and Porter, 2012). As already mentioned chondroitin sulfate proteoglycans are inhibitory for experience-dependent plasticity (Pizzorusso *et al.*, 2002) and might therefore inhibit interocular plasticity even stronger in adult than in juvenile Bassoon mutant mice.

4.4 Normal visual capabilities of PSD-95 KO mice

PSD-95 is present in the retina in horizontal cells, amacrine and ganglion cells (Koulen *et al.*, 1998) as well as in the brain (Sampedro *et al.*, 1981; Kennedy, 1997). PSD-95 KO mice have fewer orientation-biased cells in the mouse visual cortex compared to their WT littermates

(measured with *in vivo* single-unit recordings) (Fagiolini *et al.*, 2003). Therefore, we wanted to study the central processing and visual capabilities of animals with the deletion of PSD-95.

The virtual-reality optomotor system (Prusky *et al.*, 2004) revealed that visual acuity of PSD-95 KO mice was only slightly but significantly reduced, whereas the visual water task (Prusky *et al.*, 2000), which is based on reinforcement learning, revealed no differences in visual acuity and clearly showed that PSD-95 KO mice show normal visual capabilities. The contrast sensitivity of the PSD-95 KO mice was also slightly but significantly reduced in the optomotor test.

Since the deletion of PSD-95 in the hippocampus of mice had no influence on glutamatergic synaptic transmission (Elias *et al.*, 2006), synaptic transmission through the retina might also be only slightly affected and therefore an explanation for normal visual capabilities of PSD-95 KO mice.

Additionally, we found that optical imaging of visual cortical activity (Kalatsky and Stryker, 2003) revealed that the magnitude of the optical responses of elevation maps was significantly higher in PSD-95 KO mice, whereas the magnitude of the optical responses of azimuth maps as well as map scatter of both elevation and azimuth were indistinguishable from WT/HZ mice.

In the primary visual cortex of mice neurons are sensitive for orientation of visual stimuli and show a bias toward horizontal orientation (elevation). The distribution of the number of neurons selective for stimulus orientations had a marked peak at horizontal orientation, which has been reported in studies using electrophysiology (Dräger, 1975), optical imaging (Cang *et al.*, 2005b; Yoshida *et al.*, 2012), two-photon imaging (Mank *et al.*, 2008; Kreile *et al.*, 2011; Rochefort *et al.*, 2011; Yoshida *et al.*, 2012), and visual evoked potentials (Frenkel *et al.*, 2006). Fagiolini and her colleagues (2003) showed that PSD-95 KO mice have only ~ 20 % orientation-biased cells in the visual cortex compared to ~ 35 % in WT animals. Since there are more unbiased cells, these cells are most likely able to respond to the horizontal orientation stimulus, which might explain the significant higher magnitude of optical responses of elevation maps in PSD-95 KO mice as well as the tendency of the higher magnitude of optical responses of azimuth maps.

4.5 Juvenile-like OD plasticity for life in PSD-95 KO mice

Our cooperating group (Schlüter, Huang from the ENI, Germany) performed slice electrophysiology (voltage clamp) in the visual cortex of PSD-95 KO mice and measured AMPAR- and NMDAR-mediated EPSCs. They observed that PSD-95 KO mice retain a decreased juvenile-like AMPAR/NMDAR ratio into adulthood (P60) as well as an approximately nine times higher number of AMPA silent synapses compared to their WT/HZ littermates (Huang *et al.*, 2012). Since PSD-95 KO animals show altered synaptic plasticity (enhanced LTP, diminished LTD), most likely due to an increased number of AMPA silent synapses, we tested whether there is a shift in OD of binocular neurons toward the open eye in the visual cortex by MD as a model of plasticity in juvenile and adult mice.

Intrinsic optical imaging revealed that juvenile-like OD plasticity is preserved into late adulthood (>P500) and most likely for life in PSD-95 KO mice. We observed OD shifts, which were mediated by a decrease of deprived-eye responses in V1, which were only observed so far in juvenile animals during the critical period. In contrast, WT/HZ mice (<P110) displayed adult plasticity, at which the OD shift is mediated by an increase in open-eye responses (Sawtell *et al.*, 2003; Sato and Stryker, 2008) and which is absent in animals older than 110 days of age (Lehmann and Löwel, 2008).

Previous studies indicated that the development of the inhibitory tone in the cortex determines beginning and termination of the critical period (Sale *et al.*, 2010; Espinosa and Stryker, 2012; Levelt and Hübener, 2012). Therefore, we tested whether the prolonged phase of juvenile-like OD plasticity that is present in PSD-95 KO mice might be mediated by lowered inhibition. We treated adult PSD-95 KO mice with a dosage of diazepam that reliably blocked OD plasticity in adult WT/HZ mice. Interestingly, juvenile-like OD plasticity in PSD-95 KO mice could not be blocked by diazepam. The cooperating lab of Oliver Schlüter also measured the inhibitory tone in local cortical circuits in both PSD-95 KO and WT/HZ mice using *in vitro* electrophysiology and found a similar GABAR/NMDAR ratio also in adult PSD-95 KO animals, which showed that the maturation of inhibitory circuits might not be altered in PSD-95 KO animals. These results clearly suggest that the preserved juvenile-like OD plasticity must be mediated by mechanisms different from a lowered inhibitory tone.

PSD-95 might be an essential molecule for activity-dependent regulation of AMPARs and stabilization of synapses, which are crucial for synaptic development, maturation, synaptic

strengthening, and plasticity (Tomita *et al.*, 2001; Beique *et al.*, 2006; Elias *et al.*, 2006). Knockdown of PSD-95 in brain slice cultures of rats leads to arrested normal development of synaptic function and structure (Ehrlich *et al.*, 2007). In immature synapses and during development LTP can add an AMPAR-mediated component of transmission to solely NMDAR-mediated responses (Isaac *et al.*, 1995; Liao *et al.*, 1995). These electrophysiological studies suggested that during development AMPARs are progressively added, most likely through LTP (Kullmann and Nicoll, 1992; Liao *et al.*, 1992; Lisman and Harris, 1993; Manabe and Nicoll, 1994; Petralia *et al.*, 1999). Disruption of PSD-95 alters synaptic plasticity, LTP is enhanced. It seems that these effects can be explained by the role of PSD-95 as a mediator of postsynaptic signaling cascades downstream of NMDARs (Migaud *et al.*, 1998; Tomita *et al.*, 2001; Yao *et al.*, 2004; Carlisle *et al.*, 2008; Xu *et al.*, 2008) toward a specialized role in determining the number of AMPARs at excitatory synapses (Elias and Nicoll, 2007), which play critical roles in LTP and LTD. During altered visual experience, like MD, enhanced LTP might lead to inserting AMPARs and/or NMDARs into the postsynapse. Since PSD-95 KO mice displayed a huge pool of AMPA silent synapses this could explain the strong OD shift as well as the extended period of neuronal plasticity.

Considerable evidence indicates that calcium influx *via* NMDARs leads to a signaling cascade downstream that activates CaMKII, which probably plays a crucial role during juvenile plasticity and the decrease of deprived-eye responses (Espinosa and Stryker, 2012). Previous studies could demonstrate that the insertion of AMPARs is also dependent on CaMKII (Hayashi *et al.*, 2000; Tomita *et al.*, 2001). In PSD-95 KO mice enhanced LTP during MD might lead to increased exocytosis of AMPARs and/or NMDARs into the postsynaptic membrane and therefore to potential higher calcium influx, thus to higher activation of CaMKII, which plays an important role in reduction of deprived-eye responses during the critical period. This could explain the juvenile-like type of neuronal plasticity in old PSD-95 KO mice.

Of notable interest, signaling through PSD-95 is essential for activity-dependent spine growth (Steiner *et al.*, 2008). Steiner and his colleagues found that knockdown of PSD-95 in hippocampal slices of rats impaired early as well as late phases of spine growth. This might be an explanation for the juvenile-like plasticity in PSD-95. The decrease of deprived-eye responses in these animals is possible due to pruning of the synapses, which are driven by the input of the contralateral eye (Espinosa and Stryker, 2012).

Another possible reason for decreased deprived-eye responses after MD is pruning

facilitated by the PSD-95 binding partner neuroligin 1 in excitatory synapses. The level of PSD-95 can influence the level of neuroligins at excitatory *versus* inhibitory synapses (Craig and Kang, 2007). Neuroligins together with their presynaptic binding partner neuexins induce synapses and protein assembly at excitatory contacts and are used as an attractive model for controlling the number of newly formed synapses (Graf *et al.*, 2004; Chih *et al.*, 2005; Keith and El-Husseini, 2008). If in PSD-95 KO mice the number of neuroligins would be reduced the stability of the synapse might be impaired and pruning facilitated.

Hyperplasticity, like observed in PSD-95 KO mice could have beneficial implications for sensory recovery and brain injury repair, such as stroke. A previous study showed that a photothrombotic lesion in somatosensory cortex prevented OD plasticity after seven days of MD in the mouse visual system (<P110) (Greifzu *et al.*, 2011). On the other hand, PSD-95 KO mice, which obtained a photothrombotic lesion in somatosensory cortex, displayed preserved OD plasticity after seven days of MD (Parthier, 2012).

However there might also be a detriment of the hyperplastic phenotype of PSD-95 KO mice. There must be a biological purpose for the normal reduction in plasticity, which occurs during brain maturation. Otherwise network stabilization would be impossible and environmental experience would have the same dramatic impact on neural circuits that they do during development: brains would probably be in a frequent state of flux, with rearranging the cortical wiring done by previous experiences. Learning and memory would be impaired. Spatial learning in a watermaze (Morris *et al.*, 1986) revealed, that PSD-95 mutant mice showed significantly longer swim paths to find the hidden platform in the pool and thus impaired learning compared to wild-type mice (Migaud *et al.*, 1998). This sort of failure of stabilizing neural circuits may also play a role in neurodevelopmental disorders. In fact, a decreased hippocampal level of PSD-95 has been found in schizophrenia (Toro and Deakin, 2005).

4.6 Similar interocular plasticity in PSD-95 KO mice

Fagiolini and her colleagues (2003) observed that adult mice, which lack the NMDAR subunit NR2A failed to exhibit enhancement of the optokinetic response of the nondeprived eye during MD and suggested that adult plasticity might be mediated by the NR2A subunit

(Miyamoto *et al.*, 2006). Since PSD-95 is important for anchoring NMDARs to the postsynaptic membrane, disruption of PSD-95 might lead to the same phenotype. Therefore we tested visual acuity and contrast sensitivity of PSD-95 KO mice and their wild-type and heterozygous littermates during seven days of MD with the virtual-reality optomotor system. As already mentioned MD improves visual acuity and contrast sensitivity of the open eye and relies on the monocular field of the visual cortex in mice (Prusky *et al.*, 2006).

Interestingly, our experiments revealed that PSD-95 KO mice and WT/HZ littermates showed a similar increase on baseline of visual acuity as well as contrast sensitivity after MD.

Since PSD-95 KO animals showed this unique juvenile-like OD plasticity we wanted to test whether this might be because of reduced cortical inhibition so we applied the drug diazepam to investigate whether it prevents not only OD plasticity but also interocular plasticity and tested visual acuity and contrast sensitivity during diazepam treatment. Interestingly, improvement of both visual acuity and contrast sensitivity compared to their WT/HZ littermates in PSD-95 KO mice could not be blocked by diazepam and revealed a similar increase on baseline of visual acuity as well as contrast sensitivity after MD with and without treatment. Together with *in vitro* electrophysiology data at which Schlüter and his colleagues could show that PSD-95 KO mice displayed similar GABAR/NMDAR ratio these results clearly suggest that neither the preserved juvenile-like OD plasticity nor the interocular plasticity is influenced by changes in the inhibitory tone.

5. References

- Albus, K., and Wolf, W. (1984). Early post-natal development of neuronal function in the kitten's visual cortex: a laminar analysis. *J Physiol* *348*, 153-185.
- Altar, C.A., Whitehead, R.E., Chen, R., Wortwein, G., and Madsen, T.M. (2003). Effects of electroconvulsive seizures and antidepressant drugs on brain-derived neurotrophic factor protein in rat brain. *Biol Psychiatry* *54*, 703-709.
- Altrock, W.D., tom Dieck, S., Sokolov, M., Meyer, A.C., Sigler, A., Brakebusch, C., Fässler, R., Richter, K., Boeckers, T.M., Potschka, H., *et al.* (2003). Functional inactivation of a fraction of excitatory synapses in mice deficient for the active zone protein bassoon. *Neuron* *37*, 787-800.
- Angenstein, F., Hilfert, L., Zuschratter, W., Altrock, W.D., Niessen, H.G., and Gundelfinger, E.D. (2008). Morphological and metabolic changes in the cortex of mice lacking the functional presynaptic active zone protein bassoon: a combined ¹H-NMR spectroscopy and histochemical study. *Cereb Cortex* *18*, 890-897.
- Angenstein, F., Niessen, H.G., Goldschmidt, J., Lison, H., Altrock, W.D., Gundelfinger, E.D., and Scheich, H. (2007). Manganese-enhanced MRI reveals structural and functional changes in the cortex of Bassoon mutant mice. *Cereb Cortex* *17*, 28-36.
- Antonini, A., Fagiolini, M., and Stryker, M.P. (1999). Anatomical correlates of functional plasticity in mouse visual cortex. *J Neurosci* *19*, 4388-4406.
- Atwal, J.K., Pinkston-Gosse, J., Syken, J., Stawicki, S., Wu, Y., Shatz, C., and Tessier-Lavigne, M. (2008). PirB is a functional receptor for myelin inhibitors of axonal regeneration. *Science* *322*, 967-970.
- Banks, M.S., Aslin, R.N., and Letson, R.D. (1975). Sensitive period for the development of human binocular vision. *Science* *190*, 675-677.
- Bats, C., Groc, L., and Choquet, D. (2007). The interaction between Stargazin and PSD-95 regulates AMPA receptor surface trafficking. *Neuron* *53*, 719-734.
- Baxter, B.L. (1959). An Electrophysiological Study of the Effects of Sensory Deprivation. Doctoral Dissertation. University of Chicago, Chicago, USA.
- Bear, M.F., Kleinschmidt, A., Gu, Q.A., and Singer, W. (1990). Disruption of experience-dependent synaptic modifications in striate cortex by infusion of an NMDA receptor antagonist. *J Neurosci* *10*, 909-925.
- Bear, M.F., and Singer, W. (1986). Modulation of visual cortical plasticity by acetylcholine and noradrenaline. *Nature* *320*, 172-176.
- Beique, J.C., Lin, D.T., Kang, M.G., Aizawa, H., Takamiya, K., and Huganir, R.L. (2006). Synapse-specific regulation of AMPA receptor function by PSD-95. *Proc Natl Acad Sci U S A* *103*, 19535-19540.
- Bertuzzi, S., Hindges, R., Mui, S.H., O'Leary, D.D., and Lemke, G. (1999). The homeodomain protein *vax1* is required for axon guidance and major tract formation in the developing forebrain. *Genes Dev* *13*, 3092-3105.
- Beurdeley, M., Spatazza, J., Lee, H.H., Sugiyama, S., Bernard, C., Di Nardo, A.A., Hensch, T.K., and Prochiantz, A. (2012). Otx2 binding to perineuronal nets persistently regulates plasticity in the mature visual cortex. *J Neurosci* *32*, 9429-9437.
- Bhattacharyya, S., Biou, V., Xu, W., Schlüter, O., and Malenka, R.C. (2009). A critical role for PSD-95/AKAP interactions in endocytosis of synaptic AMPA receptors. *Nat Neurosci* *12*, 172-181.

- Blais, B.S., Frenkel, M.Y., Kuindersma, S.R., Muhammad, R., Shouval, H.Z., Cooper, L.N., and Bear, M.F. (2008). Recovery from monocular deprivation using binocular deprivation. *J Neurophysiol* *100*, 2217-2224.
- Blakemore, C., and Van Sluyters, R.C. (1975). Innate and environmental factors in the development of the kitten's visual cortex. *J Physiol* *248*, 663-716.
- Blasdel, G.G., and Salama, G. (1986). Voltage-sensitive dyes reveal a modular organization in monkey striate cortex. *Nature* *321*, 579-585.
- Bonhoeffer, T., and Grinvald, A. (1993). The layout of iso-orientation domains in area 18 of cat visual cortex: optical imaging reveals a pinwheel-like organization. *J Neurosci* *13*, 4157-4180.
- Boothe, R.G., Dobson, V., and Teller, D.Y. (1985). Postnatal development of vision in human and nonhuman primates. *Annu Rev Neurosci* *8*, 495-545.
- Brandstätter, J.H., Fletcher, E.L., Garner, C.C., Gundelfinger, E.D., and Wässle, H. (1999). Differential expression of the presynaptic cytomatrix protein bassoon among ribbon synapses in the mammalian retina. *Eur J Neurosci* *11*, 3683-3693.
- Bredt, D.S., and Nicoll, R.A. (2003). AMPA receptor trafficking at excitatory synapses. *Neuron* *40*, 361-379.
- Brückner, G., Brauer, K., Hartig, W., Wolff, J.R., Rickmann, M.J., Derouiche, A., Delpech, B., Girard, N., Oertel, W.H., and Reichenbach, A. (1993). Perineuronal nets provide a polyanionic, glia-associated form of microenvironment around certain neurons in many parts of the rat brain. *Glia* *8*, 183-200.
- Cang, J., Kalatsky, V.A., Löwel, S., and Stryker, M.P. (2005a). Optical imaging of the intrinsic signal as a measure of cortical plasticity in the mouse. *Vis Neurosci* *22*, 685-691.
- Cang, J., Renteria, R.C., Kaneko, M., Liu, X., Copenhagen, D.R., and Stryker, M.P. (2005b). Development of precise maps in visual cortex requires patterned spontaneous activity in the retina. *Neuron* *48*, 797-809.
- Carlisle, H.J., Fink, A.E., Grant, S.G., and O'Dell, T.J. (2008). Opposing effects of PSD-93 and PSD-95 on long-term potentiation and spike timing-dependent plasticity. *J Physiol* *586*, 5885-5900.
- Carroll, R.C., Beattie, E.C., von Zastrow, M., and Malenka, R.C. (2001). Role of AMPA receptor endocytosis in synaptic plasticity. *Nat Rev Neurosci* *2*, 315-324.
- Celio, M.R., Spreafico, R., De Biasi, S., and Vitellaro-Zuccarello, L. (1998). Perineuronal nets: past and present. *Trends Neurosci* *21*, 510-515.
- Chen, L., Chetkovich, D.M., Petralia, R.S., Sweeney, N.T., Kawasaki, Y., Wenthold, R.J., Bredt, D.S., and Nicoll, R.A. (2000). Stargazin regulates synaptic targeting of AMPA receptors by two distinct mechanisms. *Nature* *408*, 936-943.
- Chetkovich, D.M., Chen, L., Stocker, T.J., Nicoll, R.A., and Bredt, D.S. (2002). Phosphorylation of the postsynaptic density-95 (PSD-95)/discs large/zona occludens-1 binding site of stargazin regulates binding to PSD-95 and synaptic targeting of AMPA receptors. *J Neurosci* *22*, 5791-5796.
- Chih, B., Engelman, H., and Scheiffele, P. (2005). Control of excitatory and inhibitory synapse formation by neuroligins. *Science* *307*, 1324-1328.
- Chiu, S.L., and Cline, H.T. (2010). Insulin receptor signaling in the development of neuronal structure and function. *Neural development* *5*, 7.
- Cho, K.K., Khibnik, L., Philpot, B.D., and Bear, M.F. (2009). The ratio of NR2A/B NMDA receptor subunits determines the qualities of ocular dominance plasticity in visual cortex. *Proc Natl Acad Sci U S A* *106*, 5377-5382.

- Cho, K.O., Hunt, C.A., and Kennedy, M.B. (1992). The rat brain postsynaptic density fraction contains a homolog of the *Drosophila* discs-large tumor suppressor protein. *Neuron* 9, 929-942.
- Chow, A., Erisir, A., Farb, C., Nadal, M.S., Ozaita, A., Lau, D., Welker, E., and Rudy, B. (1999). K(+) channel expression distinguishes subpopulations of parvalbumin- and somatostatin-containing neocortical interneurons. *J Neurosci* 19, 9332-9345.
- Craig, A.M., and Kang, Y. (2007). Neurexin-neuroigin signaling in synapse development. *Curr Opin Neurobiol* 17, 43-52.
- Craven, S.E., and Brecht, D.S. (1998). PDZ proteins organize synaptic signaling pathways. *Cell* 93, 495-498.
- Dakoji, S., Tomita, S., Karimzadegan, S., Nicoll, R.A., and Brecht, D.S. (2003). Interaction of transmembrane AMPA receptor regulatory proteins with multiple membrane associated guanylate kinases. *Neuropharmacology* 45, 849-856.
- Daw, N.W., Fox, K., Sato, H., and Czepita, D. (1992). Critical period for monocular deprivation in the cat visual cortex. *J Neurophysiol* 67, 197-202.
- DeGiorgis, J.A., Galbraith, J.A., Dosemeci, A., Chen, X., and Reese, T.S. (2006). Distribution of the scaffolding proteins PSD-95, PSD-93, and SAP97 in isolated PSDs. *Brain cell biology* 35, 239-250.
- Derkach, V.A., Oh, M.C., Guire, E.S., and Soderling, T.R. (2007). Regulatory mechanisms of AMPA receptors in synaptic plasticity. *Nat Rev Neurosci* 8, 101-113.
- Di Cristo, G., Berardi, N., Cancedda, L., Pizzorusso, T., Putignano, E., Ratto, G.M., and Maffei, L. (2001). Requirement of ERK activation for visual cortical plasticity. *Science* 292, 2337-2340.
- Dick, O. (2002). Funktion von Zytomatrixproteinen an den Synapsen der Netzhaut von Säugetieren. Doctoral Dissertation. Johannes-Gutenberg-Universität, Mainz, Germany.
- Dick, O., Hack, I., Altmann, W.D., Garner, C.C., Gundelfinger, E.D., and Brandstätter, J.H. (2001). Localization of the presynaptic cytomatrix protein Piccolo at ribbon and conventional synapses in the rat retina: comparison with Bassoon. *J Comp Neurol* 439, 224-234.
- Dick, O., tom Dieck, S., Altmann, W.D., Ammermüller, J., Weiler, R., Garner, C.C., Gundelfinger, E.D., and Brandstätter, J.H. (2003). The presynaptic active zone protein bassoon is essential for photoreceptor ribbon synapse formation in the retina. *Neuron* 37, 775-786.
- Dingledine, R., Borges, K., Bowie, D., and Traynelis, S.F. (1999). The glutamate receptor ion channels. *Pharmacol Rev* 51, 7-61.
- Dityatev, A., and Schachner, M. (2003). Extracellular matrix molecules and synaptic plasticity. *Nat Rev Neurosci* 4, 456-468.
- Dobson, V., and Teller, D.Y. (1978). Visual acuity in human infants: a review and comparison of behavioral and electrophysiological studies. *Vision Res* 18, 1469-1483.
- Douglas, R.M., Alam, N.M., Silver, B.D., McGill, T.J., Tschetter, W.W., and Prusky, G.T. (2005). Independent visual threshold measurements in the two eyes of freely moving rats and mice using a virtual-reality optokinetic system. *Vis Neurosci* 22, 677-684.
- Dowling, J.E. (1987). *The Retina: An Approachable Part of the Brain* (Cambridge: Belknap Press of Harvard University Press).
- Dowling, J.E., and Boycott, B.B. (1966). Organization of the primate retina: electron microscopy. *Proc R Soc Lond B Biol Sci* 166, 80-111.

- Dräger, U.C. (1975). Receptive fields of single cells and topography in mouse visual cortex. *J Comp Neurol* *160*, 269-290.
- Dräger, U.C. (1978). Observations on monocular deprivation in mice. *J Neurophysiol* *41*, 28-42.
- Dräger, U.C., and Olsen, J.F. (1980). Origins of crossed and uncrossed retinal projections in pigmented and albino mice. *J Comp Neurol* *191*, 383-412.
- Dresbach, T., Qualmann, B., Kessels, M.M., Garner, C.C., and Gundelfinger, E.D. (2001). The presynaptic cytomatrix of brain synapses. *Cell Mol Life Sci* *58*, 94-116.
- Ehrlich, I., Klein, M., Rumpel, S., and Malinow, R. (2007). PSD-95 is required for activity-driven synapse stabilization. *Proc Natl Acad Sci U S A* *104*, 4176-4181.
- Ehrlich, I., and Malinow, R. (2004). Postsynaptic density 95 controls AMPA receptor incorporation during long-term potentiation and experience-driven synaptic plasticity. *J Neurosci* *24*, 916-927.
- El-Husseini, A.-D., Schnell, E., Dakoji, S., Sweeney, N., Zhou, Q., Prange, O., Gauthier-Campbell, C., Aguilera-Moreno, A., Nicoll, R.A., and Brecht, D.S. (2002). Synaptic strength regulated by palmitate cycling on PSD-95. *Cell* *108*, 849-863.
- El-Husseini, A.E., Schnell, E., Chetkovich, D.M., Nicoll, R.A., and Brecht, D.S. (2000). PSD-95 involvement in maturation of excitatory synapses. *Science* *290*, 1364-1368.
- Elias, G.M., Funke, L., Stein, V., Grant, S.G., Brecht, D.S., and Nicoll, R.A. (2006). Synapse-specific and developmentally regulated targeting of AMPA receptors by a family of MAGUK scaffolding proteins. *Neuron* *52*, 307-320.
- Elias, G.M., and Nicoll, R.A. (2007). Synaptic trafficking of glutamate receptors by MAGUK scaffolding proteins. *Trends in cell biology* *17*, 343-352.
- Espinosa, J.S., and Stryker, M.P. (2012). Development and plasticity of the primary visual cortex. *Neuron* *75*, 230-249.
- Fagiolini, M., and Hensch, T.K. (2000). Inhibitory threshold for critical-period activation in primary visual cortex. *Nature* *404*, 183-186.
- Fagiolini, M., Katagiri, H., Miyamoto, H., Mori, H., Grant, S.G., Mishina, M., and Hensch, T.K. (2003). Separable features of visual cortical plasticity revealed by N-methyl-D-aspartate receptor 2A signaling. *Proc Natl Acad Sci U S A* *100*, 2854-2859.
- Fagiolini, M., Pizzorusso, T., Berardi, N., Domenici, L., and Maffei, L. (1994). Functional postnatal development of the rat primary visual cortex and the role of visual experience: dark rearing and monocular deprivation. *Vision Res* *34*, 709-720.
- Finardi, A., Gardoni, F., Bassanini, S., Lasio, G., Cossu, M., Tassi, L., Caccia, C., Taroni, F., LoRusso, G., Di Luca, M., and Battaglia, G. (2006). NMDA receptor composition differs among anatomically diverse malformations of cortical development. *Journal of neuropathology and experimental neurology* *65*, 883-893.
- Fischer, Q.S., Beaver, C.J., Yang, Y., Rao, Y., Jakobsdottir, K.B., Storm, D.R., McKnight, G.S., and Daw, N.W. (2004). Requirement for the RIIbeta isoform of PKA, but not calcium-stimulated adenylyl cyclase, in visual cortical plasticity. *J Neurosci* *24*, 9049-9058.
- Fitzjohn, S.M., Doherty, A.J., and Collingridge, G.L. (2006). Promiscuous interactions between AMPA-Rs and MAGUKs. *Neuron* *52*, 222-224.
- Frank, T., Rutherford, M.A., Strenzke, N., Neef, A., Pangrsic, T., Khimich, D., Fejtova, A., Gundelfinger, E.D., Liberman, M.C., Harke, B., *et al.* (2010). Bassoon and the synaptic ribbon organize Ca²⁺ channels and vesicles to add release sites and promote refilling. *Neuron* *68*, 724-738.

- Fregnac, Y., and Imbert, M. (1978). Early development of visual cortical cells in normal and dark-reared kittens: relationship between orientation selectivity and ocular dominance. *J Physiol* 278, 27-44.
- Frenkel, M.Y., and Bear, M.F. (2004). How monocular deprivation shifts ocular dominance in visual cortex of young mice. *Neuron* 44, 917-923.
- Frenkel, M.Y., Sawtell, N.B., Diogo, A.C., Yoon, B., Neve, R.L., and Bear, M.F. (2006). Instructive effect of visual experience in mouse visual cortex. *Neuron* 51, 339-349.
- Frischknecht, R., and Gundelfinger, E.D. (2012). The brain's extracellular matrix and its role in synaptic plasticity. *Advances in experimental medicine and biology* 970, 153-171.
- Fukata, Y., Tzingounis, A.V., Trinidad, J.C., Fukata, M., Burlingame, A.L., Nicoll, R.A., and Brecht, D.S. (2005). Molecular constituents of neuronal AMPA receptors. *J Cell Biol* 169, 399-404.
- Galtrey, C.M., and Fawcett, J.W. (2007). The role of chondroitin sulfate proteoglycans in regeneration and plasticity in the central nervous system. *Brain Res Rev* 54, 1-18.
- Garner, C.C., Kindler, S., and Gundelfinger, E.D. (2000). Molecular determinants of presynaptic active zones. *Curr Opin Neurobiol* 10, 321-327.
- Ghiglieri, V., Picconi, B., Sgobio, C., Bagetta, V., Barone, I., Paille, V., Di Filippo, M., Polli, F., Gardoni, F., Altmann, W., *et al.* (2009). Epilepsy-induced abnormal striatal plasticity in Bassoon mutant mice. *Eur J Neurosci* 29, 1979-1993.
- Ghiglieri, V., Sgobio, C., Patassini, S., Bagetta, V., Fejtova, A., Giampa, C., Marinucci, S., Heyden, A., Gundelfinger, E.D., Fusco, F.R., *et al.* (2010). TrkB/BDNF-Dependent Striatal Plasticity and Behavior in a Genetic Model of Epilepsy: Modulation by Valproic Acid. *Neuropsychopharmacology*.
- Giolli, R.A., Blanks, R.H., and Lui, F. (2006). The accessory optic system: basic organization with an update on connectivity, neurochemistry, and function. *Prog Brain Res* 151, 407-440.
- Goetze, B., Schmidt, K.F., Altmann, W.D., Gundelfinger, E.D., and Löwel, S. (2010a). Impaired sensory learning and cortical plasticity in Bassoon mutant mice. *FENS Forum 2010*, Amsterdam, The Netherlands, vol. 5, 081.6.
- Goetze, B., Schmidt, K.F., Huang, X., Schlüter, O.M., and Löwel, S. (2012). PSD-95 KO mice retain juvenile ocular dominance plasticity into adulthood. *FENS Forum 2012*, Barcelona, Spain,
- Goetze, B., Schmidt, K.F., Lehmann, K., Altmann, W.D., Gundelfinger, E.D., and Löwel, S. (2010b). Vision and visual cortical maps in mice with a photoreceptor synaptopathy: Reduced but robust visual capabilities in the absence of synaptic ribbons. *Neuroimage* 49, 1622-1631.
- Gordon, J.A., and Stryker, M.P. (1996). Experience-dependent plasticity of binocular responses in the primary visual cortex of the mouse. *J Neurosci* 16, 3274-3286.
- Graf, E.R., Zhang, X., Jin, S.X., Linhoff, M.W., and Craig, A.M. (2004). Neurexins induce differentiation of GABA and glutamate postsynaptic specializations *via* neuroligins. *Cell* 119, 1013-1026.
- Greifzu, F., Schmidt, S., Schmidt, K.F., Kreikemeier, K., Witte, O.W., and Löwel, S. (2011). Global impairment and therapeutic restoration of visual plasticity mechanisms after a localized cortical stroke. *Proc Natl Acad Sci U S A* 108, 15450-15455.
- Greifzu, F., Wolf, F., and Löwel, S. (2012). Network influences on cortical plasticity. *e-Neuroforum* 3, 41-48.

- Grinvald, A., Lieke, E., Frostig, R.D., Gilbert, C.D., and Wiesel, T.N. (1986). Functional architecture of cortex revealed by optical imaging of intrinsic signals. *Nature* 324, 361-364.
- Hallermann, S., Fejtova, A., Schmidt, H., Weyhersmuller, A., Silver, R.A., Gundelfinger, E.D., and Eilers, J. (2010). Bassoon speeds vesicle reloading at a central excitatory synapse. *Neuron* 68, 710-723.
- Hanover, J.L., Huang, Z.J., Tonegawa, S., and Stryker, M.P. (1999). Brain-derived neurotrophic factor overexpression induces precocious critical period in mouse visual cortex. *J Neurosci* 19, RC40.
- Harauzov, A., Spolidoro, M., DiCristo, G., De Pasquale, R., Cancedda, L., Pizzorusso, T., Viegi, A., Berardi, N., and Maffei, L. (2010). Reducing intracortical inhibition in the adult visual cortex promotes ocular dominance plasticity. *J Neurosci* 30, 361-371.
- Harris, E.W., Ganong, A.H., and Cotman, C.W. (1984). Long-term potentiation in the hippocampus involves activation of N-methyl-D-aspartate receptors. *Brain Res* 323, 132-137.
- Hayashi, Y., Shi, S.H., Esteban, J.A., Piccini, A., Poncer, J.C., and Malinow, R. (2000). Driving AMPA receptors into synapses by LTP and CaMKII: requirement for GluR1 and PDZ domain interaction. *Science* 287, 2262-2267.
- Heimel, J.A., Hartman, R.J., Hermans, J.M., and Levelt, C.N. (2007). Screening mouse vision with intrinsic signal optical imaging. *Eur J Neurosci* 25, 795-804.
- Hensch, T.K. (2005). Critical period plasticity in local cortical circuits. *Nat Rev Neurosci* 6, 877-888.
- Hensch, T.K., Fagiolini, M., Mataga, N., Stryker, M.P., Baekkeskov, S., and Kash, S.F. (1998). Local GABA circuit control of experience-dependent plasticity in developing visual cortex. *Science* 282, 1504-1508.
- Heyden, A., Ionescu, M.C., Romorini, S., Kracht, B., Ghiglieri, V., Calabresi, P., Seidenbecher, C., Angenstein, F., and Gundelfinger, E.D. (2011). Hippocampal enlargement in Bassoon-mutant mice is associated with enhanced neurogenesis, reduced apoptosis, and abnormal BDNF levels. *Cell and tissue research* 346, 11-26.
- Hockfield, S., Kalb, R.G., Zaremba, S., and Fryer, H. (1990). Expression of neural proteoglycans correlates with the acquisition of mature neuronal properties in the mammalian brain. *Cold Spring Harbor symposia on quantitative biology* 55, 505-514.
- Hofer, S.B., Mrsic-Flogel, T.D., Bonhoeffer, T., and Hubener, M. (2006a). Lifelong learning: ocular dominance plasticity in mouse visual cortex. *Curr Opin Neurobiol* 16, 451-459.
- Hofer, S.B., Mrsic-Flogel, T.D., Bonhoeffer, T., and Hubener, M. (2006b). Prior experience enhances plasticity in adult visual cortex. *Nat Neurosci* 9, 127-132.
- Hofer, S.B., Mrsic-Flogel, T.D., Bonhoeffer, T., and Hubener, M. (2009). Experience leaves a lasting structural trace in cortical circuits. *Nature* 457, 313-317.
- Huang, X., Goetze, B., Löwel, S., and Schlüter, O.M. (2012). PSD-95 lacking synapses in the visual cortex retain a high degree of AMPA receptor silence. *FENS Forum* 2012, Barcelona, Spain,
- Huang, Z.J., Kirkwood, A., Pizzorusso, T., Porciatti, V., Morales, B., Bear, M.F., Maffei, L., and Tonegawa, S. (1999). BDNF regulates the maturation of inhibition and the critical period of plasticity in mouse visual cortex. *Cell* 98, 739-755.
- Hubel, D.H. (1963). The Visual Cortex of the Brain. *Sci Am* 209, 54-62.
- Hubel, D.H., and Wiesel, T.N. (1962). Receptive fields, binocular interaction and functional architecture in the cat's visual cortex. *J Physiol* 160, 106-154.

- Hubel, D.H., and Wiesel, T.N. (1963). Receptive Fields of Cells in Striate Cortex of Very Young, Visually Inexperienced Kittens. *J Neurophysiol* 26, 994-1002.
- Hubel, D.H., and Wiesel, T.N. (1964). Effects of Monocular Deprivation in Kittens. *Naunyn Schmiedebergs Arch Exp Pathol Pharmacol* 248, 492-497.
- Hubel, D.H., and Wiesel, T.N. (1970). The period of susceptibility to the physiological effects of unilateral eye closure in kittens. *J Physiol* 206, 419-436.
- Huopaniemi, L., Keist, R., Randolph, A., Certa, U., and Rudolph, U. (2004). Diazepam-induced adaptive plasticity revealed by alpha1 GABAA receptor-specific expression profiling. *J Neurochem* 88, 1059-1067.
- Isaac, J.T., Nicoll, R.A., and Malenka, R.C. (1995). Evidence for silent synapses: implications for the expression of LTP. *Neuron* 15, 427-434.
- Joselevitch, C., and Zenisek, D. (2010). The cytomatrix protein bassoon contributes to fast transmission at conventional and ribbon synapses. *Neuron* 68, 604-606.
- Kalatsky, V.A., and Stryker, M.P. (2003). New paradigm for optical imaging: temporally encoded maps of intrinsic signal. *Neuron* 38, 529-545.
- Kamermans, M., and Spekrijse, H. (1999). The feedback pathway from horizontal cells to cones. A mini review with a look ahead. *Vision Res* 39, 2449-2468.
- Kaneko, M., Hanover, J.L., England, P.M., and Stryker, M.P. (2008a). TrkB kinase is required for recovery, but not loss, of cortical responses following monocular deprivation. *Nat Neurosci* 11, 497-504.
- Kaneko, M., Stellwagen, D., Malenka, R.C., and Stryker, M.P. (2008b). Tumor necrosis factor-alpha mediates one component of competitive, experience-dependent plasticity in developing visual cortex. *Neuron* 58, 673-680.
- Kanold, P.O., Kim, Y.A., GrandPre, T., and Shatz, C.J. (2009). Co-regulation of ocular dominance plasticity and NMDA receptor subunit expression in glutamic acid decarboxylase-65 knock-out mice. *J Physiol* 587, 2857-2867.
- Keith, D., and El-Husseini, A. (2008). Excitation Control: Balancing PSD-95 Function at the Synapse. *Front Mol Neurosci* 1, 4.
- Kennedy, M.B. (1997). The postsynaptic density at glutamatergic synapses. *Trends Neurosci* 20, 264-268.
- Khimich, D., Nouvian, R., Pujol, R., tom Dieck, S., Egner, A., Gundelfinger, E.D., and Moser, T. (2005). Hair cell synaptic ribbons are essential for synchronous auditory signalling. *Nature* 434, 889-894.
- Kidd, M. (1962). Electron microscopy of the inner plexiform layer of the retina in the cat and the pigeon. *J Anat* 96, 179-187.
- Kim, E., and Sheng, M. (2004). PDZ domain proteins of synapses. *Nat Rev Neurosci* 5, 771-781.
- Koulen, P., Fletcher, E.L., Craven, S.E., Brecht, D.S., and Wässle, H. (1998). Immunocytochemical localization of the postsynaptic density protein PSD-95 in the mammalian retina. *J Neurosci* 18, 10136-10149.
- Kreile, A.K., Bonhoeffer, T., and Hubener, M. (2011). Altered visual experience induces instructive changes of orientation preference in mouse visual cortex. *J Neurosci* 31, 13911-13920.
- Kullmann, D.M., and Nicoll, R.A. (1992). Long-term potentiation is associated with increases in quantal content and quantal amplitude. *Nature* 357, 240-244.
- Kurazono, S., Okamoto, M., Sakiyama, J., Mori, S., Nakata, Y., Fukuoka, J., Amano, S., Oohira, A., and Matsui, H. (2001). Expression of brain specific chondroitin sulfate

- proteoglycans, neurocan and phosphacan, in the developing and adult hippocampus of Ihara's epileptic rats. *Brain Res* 898, 36-48.
- Lee, J., Duan, W., and Mattson, M.P. (2002). Evidence that brain-derived neurotrophic factor is required for basal neurogenesis and mediates, in part, the enhancement of neurogenesis by dietary restriction in the hippocampus of adult mice. *J Neurochem* 82, 1367-1375.
- Lehmann, K., and Löwel, S. (2008). Age-dependent ocular dominance plasticity in adult mice. *PLoS One* 3, e3120.
- Lehmann, K., Schmidt, K.F., and Löwel, S. (2012). Vision and visual plasticity in ageing mice. *Restorative neurology and neuroscience* 30, 161-178.
- Levelt, C.N., and Hübener, M. (2012). Critical-Period Plasticity in the Visual Cortex. *Annu Rev Neurosci*.
- Liao, D., Hessler, N.A., and Malinow, R. (1995). Activation of postsynaptically silent synapses during pairing-induced LTP in CA1 region of hippocampal slice. *Nature* 375, 400-404.
- Liao, D., Jones, A., and Malinow, R. (1992). Direct measurement of quantal changes underlying long-term potentiation in CA1 hippocampus. *Neuron* 9, 1089-1097.
- Lisman, J.E., and Harris, K.M. (1993). Quantal analysis and synaptic anatomy--integrating two views of hippocampal plasticity. *Trends Neurosci* 16, 141-147.
- Maffei, A., and Turrigiano, G.G. (2008). Multiple modes of network homeostasis in visual cortical layer 2/3. *J Neurosci* 28, 4377-4384.
- Malenka, R.C. (1991). Postsynaptic factors control the duration of synaptic enhancement in area CA1 of the hippocampus. *Neuron* 6, 53-60.
- Malenka, R.C., and Nicoll, R.A. (1993). NMDA-receptor-dependent synaptic plasticity: multiple forms and mechanisms. *Trends Neurosci* 16, 521-527.
- Malenka, R.C., and Nicoll, R.A. (1997). Silent synapses speak up. *Neuron* 19, 473-476.
- Malenka, R.C., and Nicoll, R.A. (1999). Long-term potentiation--a decade of progress? *Science* 285, 1870-1874.
- Malinow, R., Mainen, Z.F., and Hayashi, Y. (2000). LTP mechanisms: from silence to four-lane traffic. *Curr Opin Neurobiol* 10, 352-357.
- Malinow, R., and Malenka, R.C. (2002). AMPA receptor trafficking and synaptic plasticity. *Annu Rev Neurosci* 25, 103-126.
- Manabe, T., and Nicoll, R.A. (1994). Long-term potentiation: evidence against an increase in transmitter release probability in the CA1 region of the hippocampus. *Science* 265, 1888-1892.
- Mangini, N.J., and Pearlman, A.L. (1980). Laminar distribution of receptive field properties in the primary visual cortex of the mouse. *J Comp Neurol* 193, 203-222.
- Mank, M., Santos, A.F., Drenth, S., Mrcic-Flogel, T.D., Hofer, S.B., Stein, V., Hendel, T., Reiff, D.F., Levelt, C., Borst, A., *et al.* (2008). A genetically encoded calcium indicator for chronic in vivo two-photon imaging. *Nat Methods* 5, 805-811.
- Mataga, N., Nagai, N., and Hensch, T.K. (2002). Permissive proteolytic activity for visual cortical plasticity. *Proc Natl Acad Sci U S A* 99, 7717-7721.
- Matsui, F., Kawashima, S., Shuo, T., Yamauchi, S., Tokita, Y., Aono, S., Keino, H., and Oohira, A. (2002). Transient expression of juvenile-type neurocan by reactive astrocytes in adult rat brains injured by kainate-induced seizures as well as surgical incision. *Neuroscience* 112, 773-781.
- Maya Vetencourt, J.F., Sale, A., Viegi, A., Baroncelli, L., De Pasquale, R., O'Leary, O.F., Castren, E., and Maffei, L. (2008). The antidepressant fluoxetine restores plasticity in the adult visual cortex. *Science* 320, 385-388.

- Mayer, M.L., Westbrook, G.L., and Guthrie, P.B. (1984). Voltage-dependent block by Mg²⁺ of NMDA responses in spinal cord neurones. *Nature* 309, 261-263.
- McCurry, C.L., Shepherd, J.D., Tropea, D., Wang, K.H., Bear, M.F., and Sur, M. (2010). Loss of Arc renders the visual cortex impervious to the effects of sensory experience or deprivation. *Nat Neurosci* 13, 450-457.
- McGee, A.W., Yang, Y., Fischer, Q.S., Daw, N.W., and Strittmatter, S.M. (2005). Experience-driven plasticity of visual cortex limited by myelin and Nogo receptor. *Science* 309, 2222-2226.
- McRae, P.A., Baranov, E., Rogers, S.L., and Porter, B.E. (2012). Persistent decrease in multiple components of the perineuronal net following status epilepticus. *Eur J Neurosci* 36, 3471-3482.
- McRae, P.A., and Porter, B.E. (2012). The perineuronal net component of the extracellular matrix in plasticity and epilepsy. *Neurochem Int* 61, 963-972.
- Metin, C., Godement, P., and Imbert, M. (1988). The primary visual cortex in the mouse: receptive field properties and functional organization. *Exp Brain Res* 69, 594-612.
- Migaud, M., Charlesworth, P., Dempster, M., Webster, L.C., Watabe, A.M., Makhinson, M., He, Y., Ramsay, M.F., Morris, R.G., Morrison, J.H., *et al.* (1998). Enhanced long-term potentiation and impaired learning in mice with mutant postsynaptic density-95 protein. *Nature* 396, 433-439.
- Missotten, L. (1965). The ultrastructure of the human retina. (Brussels: Arscia Uitgaven N.V.).
- Miyamoto, H., Surti, T., and K., H.T. (2006). Distinct mechanisms underlie adult perceptual learning and classical ocular dominance plasticity in mouse visual cortex. FENS Forum 2006, Vienna, Austria, vol. 3, A195.7.
- Morishita, H., Miwa, J.M., Heintz, N., and Hensch, T.K. (2010). Lynx1, a Cholinergic Brake, Limits Plasticity in Adult Visual Cortex. *Science* 330, 1238-1240.
- Morris, R.G., Anderson, E., Lynch, G.S., and Baudry, M. (1986). Selective impairment of learning and blockade of long-term potentiation by an N-methyl-D-aspartate receptor antagonist, AP5. *Nature* 319, 774-776.
- Mrsic-Flogel, T.D., Hofer, S.B., Ohki, K., Reid, R.C., Bonhoeffer, T., and Hübener, M. (2007). Homeostatic regulation of eye-specific responses in visual cortex during ocular dominance plasticity. *Neuron* 54, 961-972.
- Nicholls, J.G., Martin A. R., Wallace, B.G., and Fuchs, P.A. (2001). *From Neuron to Brain: A Cellular and Molecular Approach to the Function of the Nervous System*, fourth edn (Sinauer Associates).
- Nowak, L., Bregestovski, P., Ascher, P., Herbet, A., and Prochiantz, A. (1984). Magnesium gates glutamate-activated channels in mouse central neurones. *Nature* 307, 462-465.
- Ohki, K., Chung, S., Ch'ng, Y.H., Kara, P., and Reid, R.C. (2005). Functional imaging with cellular resolution reveals precise micro-architecture in visual cortex. *Nature* 433, 597-603.
- Olney, J.W., deGubareff, T., and Sloviter, R.S. (1983). "Epileptic" brain damage in rats induced by sustained electrical stimulation of the perforant path. II. Ultrastructural analysis of acute hippocampal pathology. *Brain Res Bull* 10, 699-712.
- Olson, C.R., and Freeman, R.D. (1980). Profile of the sensitive period for monocular deprivation in kittens. *Exp Brain Res* 39, 17-21.
- Parent, J.M., Yu, T.W., Leibowitz, R.T., Geschwind, D.H., Sloviter, R.S., and Lowenstein, D.H. (1997). Dentate granule cell neurogenesis is increased by seizures and contributes to aberrant network reorganization in the adult rat hippocampus. *J Neurosci* 17, 3727-3738.

- Parthier, D. (2012). Role of the postsynaptic density protein 95 for visual plasticity after stroke. Bachelor Thesis. Georg-August-Universität, Göttingen, Germany.
- Patz, S., Grabert, J., Gorba, T., Wirth, M.J., and Wahle, P. (2004). Parvalbumin expression in visual cortical interneurons depends on neuronal activity and TrkB ligands during an Early period of postnatal development. *Cereb Cortex* *14*, 342-351.
- Paxinos, G., and Franklin, K.B.J. (2003). *The Mouse Brain in Stereotaxic Coordinates*, second edn (Academic Press).
- Petralia, R.S., Esteban, J.A., Wang, Y.X., Partridge, J.G., Zhao, H.M., Wenthold, R.J., and Malinow, R. (1999). Selective acquisition of AMPA receptors over postnatal development suggests a molecular basis for silent synapses. *Nat Neurosci* *2*, 31-36.
- Pham, T.A., Graham, S.J., Suzuki, S., Barco, A., Kandel, E.R., Gordon, B., and Lickey, M.E. (2004). A semi-persistent adult ocular dominance plasticity in visual cortex is stabilized by activated CREB. *Learn Mem* *11*, 738-747.
- Picconi, B., Gardoni, F., Centonze, D., Mauceri, D., Cenci, M.A., Bernardi, G., Calabresi, P., and Di Luca, M. (2004). Abnormal Ca²⁺-calmodulin-dependent protein kinase II function mediates synaptic and motor deficits in experimental parkinsonism. *J Neurosci* *24*, 5283-5291.
- Pizzorusso, T., Medini, P., Berardi, N., Chierzi, S., Fawcett, J.W., and Maffei, L. (2002). Reactivation of ocular dominance plasticity in the adult visual cortex. *Science* *298*, 1248-1251.
- Pizzorusso, T., Medini, P., Landi, S., Baldini, S., Berardi, N., and Maffei, L. (2006). Structural and functional recovery from early monocular deprivation in adult rats. *Proc Natl Acad Sci U S A* *103*, 8517-8522.
- Prusky, G.T., Alam, N.M., Beekman, S., and Douglas, R.M. (2004). Rapid quantification of adult and developing mouse spatial vision using a virtual optomotor system. *Invest Ophthalmol Vis Sci* *45*, 4611-4616.
- Prusky, G.T., Alam, N.M., and Douglas, R.M. (2006). Enhancement of vision by monocular deprivation in adult mice. *J Neurosci* *26*, 11554-11561.
- Prusky, G.T., and Douglas, R.M. (2004). Characterization of mouse cortical spatial vision. *Vision Res* *44*, 3411-3418.
- Prusky, G.T., West, P.W., and Douglas, R.M. (2000). Behavioral assessment of visual acuity in mice and rats. *Vision Res* *40*, 2201-2209.
- Ranson, A., Cheetham, C.E., Fox, K., and Sengpiel, F. (2012). Homeostatic plasticity mechanisms are required for juvenile, but not adult, ocular dominance plasticity. *Proc Natl Acad Sci U S A* *109*, 1311-1316.
- Rao-Mirotnik, R., Harkins, A.B., Buchsbaum, G., and Sterling, P. (1995). Mammalian rod terminal: architecture of a binary synapse. *Neuron* *14*, 561-569.
- Rao, Y., Fischer, Q.S., Yang, Y., McKnight, G.S., LaRue, A., and Daw, N.W. (2004). Reduced ocular dominance plasticity and long-term potentiation in the developing visual cortex of protein kinase A RII alpha mutant mice. *Eur J Neurosci* *20*, 837-842.
- Richter, K., Langnaese, K., Kreutz, M.R., Olias, G., Zhai, R., Scheich, H., Garner, C.C., and Gundelfinger, E.D. (1999). Presynaptic cytomatrix protein bassoon is localized at both excitatory and inhibitory synapses of rat brain. *J Comp Neurol* *408*, 437-448.
- Roberts, E.B., Meredith, M.A., and Ramoa, A.S. (1998). Suppression of NMDA receptor function using antisense DNA block ocular dominance plasticity while preserving visual responses. *J Neurophysiol* *80*, 1021-1032.

- Rocheffort, N.L., Narushima, M., Grienberger, C., Marandi, N., Hill, D.N., and Konnerth, A. (2011). Development of direction selectivity in mouse cortical neurons. *Neuron* *71*, 425-432.
- Sagi, D., and Hochstein, S. (1985). Lateral inhibition between spatially adjacent spatial-frequency channels? *Perception & psychophysics* *37*, 315-322.
- Sale, A., Berardi, N., Spolidoro, M., Baroncelli, L., and Maffei, L. (2010). GABAergic inhibition in visual cortical plasticity. *Front Cell Neurosci* *4*, 10.
- Sampedro, M.N., Bussineau, C.M., and Cotman, C.W. (1981). Postsynaptic density antigens: preparation and characterization of an antiserum against postsynaptic densities. *J Cell Biol* *90*, 675-686.
- Sato, M., and Stryker, M.P. (2008). Distinctive features of adult ocular dominance plasticity. *J Neurosci* *28*, 10278-10286.
- Sawtell, N.B., Frenkel, M.Y., Philpot, B.D., Nakazawa, K., Tonegawa, S., and Bear, M.F. (2003). NMDA receptor-dependent ocular dominance plasticity in adult visual cortex. *Neuron* *38*, 977-985.
- Schlüter, O.M., Xu, W., and Malenka, R.C. (2006). Alternative N-terminal domains of PSD-95 and SAP97 govern activity-dependent regulation of synaptic AMPA receptor function. *Neuron* *51*, 99-111.
- Schnell, E., Sizemore, M., Karimzadegan, S., Chen, L., Brecht, D.S., and Nicoll, R.A. (2002). Direct interactions between PSD-95 and stargazin control synaptic AMPA receptor number. *Proc Natl Acad Sci U S A* *99*, 13902-13907.
- Sgobio, C., Ghiglieri, V., Costa, C., Bagnetta, V., Siliquini, S., Barone, I., Di Filippo, M., Gardoni, F., Gundelfinger, E.D., Di Luca, M., *et al.* (2010). Hippocampal synaptic plasticity, memory, and epilepsy: effects of long-term valproic acid treatment. *Biol Psychiatry* *67*, 567-574.
- Shapley, R., and Lennie, P. (1985). Spatial frequency analysis in the visual system. *Annu Rev Neurosci* *8*, 547-583.
- Sheng, M., and Sala, C. (2001). PDZ domains and the organization of supramolecular complexes. *Annu Rev Neurosci* *24*, 1-29.
- Sjöstrand, F.S. (1958). Ultrastructure of retinal rod synapses of the guinea pig eye as revealed by three-dimensional reconstructions from serial sections. *J Ultrastruct Res* *2*, 122-170.
- Sloviter, R.S. (1983). "Epileptic" brain damage in rats induced by sustained electrical stimulation of the perforant path. I. Acute electrophysiological and light microscopic studies. *Brain Res Bull* *10*, 675-697.
- Sloviter, R.S. (1996). Hippocampal pathology and pathophysiology in temporal lobe epilepsy. *Neurologia* *11 Suppl 4*, 29-32.
- Song, I., and Huganir, R.L. (2002). Regulation of AMPA receptors during synaptic plasticity. *Trends Neurosci* *25*, 578-588.
- Specht, D., tom Dieck, S., Ammermüller, J., Regus-Leidig, H., Gundelfinger, E.D., and Brandstätter, J.H. (2007). Structural and functional remodeling in the retina of a mouse with a photoreceptor synaptopathy: plasticity in the rod and degeneration in the cone system. *Eur J Neurosci* *26*, 2506-2515.
- Stathakis, D.G., Hoover, K.B., You, Z., and Bryant, P.J. (1997). Human postsynaptic density-95 (PSD95): location of the gene (DLG4) and possible function in nonneural as well as in neural tissues. *Genomics* *44*, 71-82.

- Steinberg, R.H., Frishman, L.J., and Sieving, P.A. (1991). Negative components of the electroretinogram from proximal retina and photoreceptor. In *Retinal Research*, N. Osborne, and G. Chader, eds. (Pergamon, New York: Elsevier), pp. 121-160.
- Steiner, P., Higley, M.J., Xu, W., Czervionke, B.L., Malenka, R.C., and Sabatini, B.L. (2008). Destabilization of the postsynaptic density by PSD-95 serine 73 phosphorylation inhibits spine growth and synaptic plasticity. *Neuron* *60*, 788-802.
- Stellwagen, D., and Malenka, R.C. (2006). Synaptic scaling mediated by glial TNF- α . *Nature* *440*, 1054-1059.
- Steward, O., and Worley, P.F. (2001). Selective targeting of newly synthesized Arc mRNA to active synapses requires NMDA receptor activation. *Neuron* *30*, 227-240.
- Sugiyama, S., Di Nardo, A.A., Aizawa, S., Matsuo, I., Volovitch, M., Prochiantz, A., and Hensch, T.K. (2008). Experience-dependent transfer of Otx2 homeoprotein into the visual cortex activates postnatal plasticity. *Cell* *134*, 508-520.
- Sun, Q., and Turrigiano, G.G. (2011). PSD-95 and PSD-93 play critical but distinct roles in synaptic scaling up and down. *J Neurosci* *31*, 6800-6808.
- Tagawa, Y., Kanold, P.O., Majdan, M., and Shatz, C.J. (2005). Multiple periods of functional ocular dominance plasticity in mouse visual cortex. *Nat Neurosci* *8*, 380-388.
- Taha, S., Hanover, J.L., Silva, A.J., and Stryker, M.P. (2002). Autophosphorylation of alphaCaMKII is required for ocular dominance plasticity. *Neuron* *36*, 483-491.
- tom Dieck, S., Altmann, W.D., Kessels, M.M., Qualmann, B., Regus, H., Brauner, D., Fejtova, A., Bracko, O., Gundelfinger, E.D., and Brandstätter, J.H. (2005). Molecular dissection of the photoreceptor ribbon synapse: physical interaction of Bassoon and RIBEYE is essential for the assembly of the ribbon complex. *J Cell Biol* *168*, 825-836.
- tom Dieck, S., Sanmarti-Vila, L., Langnaese, K., Richter, K., Kindler, S., Soyke, A., Wex, H., Smalla, K.H., Kämpf, U., Fränzer, J.T., *et al.* (1998). Bassoon, a novel zinc-finger CAG/glutamine-repeat protein selectively localized at the active zone of presynaptic nerve terminals. *J Cell Biol* *142*, 499-509.
- Tomita, S., Adesnik, H., Sekiguchi, M., Zhang, W., Wada, K., Howe, J.R., Nicoll, R.A., and Brecht, D.S. (2005). Stargazin modulates AMPA receptor gating and trafficking by distinct domains. *Nature* *435*, 1052-1058.
- Tomita, S., Chen, L., Kawasaki, Y., Petralia, R.S., Wenthold, R.J., Nicoll, R.A., and Brecht, D.S. (2003). Functional studies and distribution define a family of transmembrane AMPA receptor regulatory proteins. *J Cell Biol* *161*, 805-816.
- Tomita, S., Nicoll, R.A., and Brecht, D.S. (2001). PDZ protein interactions regulating glutamate receptor function and plasticity. *J Cell Biol* *153*, F19-24.
- Toro, C., and Deakin, J.F. (2005). NMDA receptor subunit NRI and postsynaptic protein PSD-95 in hippocampus and orbitofrontal cortex in schizophrenia and mood disorder. *Schizophrenia research* *80*, 323-330.
- Tropea, D., Van Wart, A., and Sur, M. (2009). Molecular mechanisms of experience-dependent plasticity in visual cortex. *Philos Trans R Soc Lond B Biol Sci* *364*, 341-355.
- Tschetter, W.W., Douglas, R.M., and Prusky, G.T. (2011). Experience-induced interocular plasticity of vision in infancy. *Front Syst Neurosci* *5*, 44.
- Turrigiano, G.G., and Nelson, S.B. (2004). Homeostatic plasticity in the developing nervous system. *Nat Rev Neurosci* *5*, 97-107.
- Wagor, E., Mangini, N.J., and Pearlman, A.L. (1980). Retinotopic organization of striate and extrastriate visual cortex in the mouse. *J Comp Neurol* *193*, 187-202.
- Wang, B.S., Sarnaik, R., and Cang, J. (2010). Critical period plasticity matches binocular orientation preference in the visual cortex. *Neuron* *65*, 246-256.

- Wässle, H. (2004). Parallel processing in the mammalian retina. *Nat Rev Neurosci* 5, 747-757.
- Wiesel, T.N., and Hubel, D.H. (1963a). Effects of Visual Deprivation on Morphology and Physiology of Cells in the Cats Lateral Geniculate Body. *J Neurophysiol* 26, 978-993.
- Wiesel, T.N., and Hubel, D.H. (1963b). Single-Cell Responses in Striate Cortex of Kittens Deprived of Vision in One Eye. *J Neurophysiol* 26, 1003-1017.
- Wyneken, U., Marengo, J.J., Villanueva, S., Soto, D., Sandoval, R., Gundelfinger, E.D., and Orrego, F. (2003). Epilepsy-induced changes in signaling systems of human and rat postsynaptic densities. *Epilepsia* 44, 243-246.
- Wyneken, U., Smalla, K.H., Marengo, J.J., Soto, D., de la Cerda, A., Tischmeyer, W., Grimm, R., Boeckers, T.M., Wolf, G., Orrego, F., and Gundelfinger, E.D. (2001). Kainate-induced seizures alter protein composition and N-methyl-D-aspartate receptor function of rat forebrain postsynaptic densities. *Neuroscience* 102, 65-74.
- Xu, W., Schlüter, O.M., Steiner, P., Czervionke, B.L., Sabatini, B., and Malenka, R.C. (2008). Molecular dissociation of the role of PSD-95 in regulating synaptic strength and LTD. *Neuron* 57, 248-262.
- Yamaguchi, Y. (2000). Lecticans: organizers of the brain extracellular matrix. *Cell Mol Life Sci* 57, 276-289.
- Yao, H., and Dan, Y. (2005). Synaptic learning rules, cortical circuits, and visual function. *Neuroscientist* 11, 206-216.
- Yao, W.D., Gainetdinov, R.R., Arbuckle, M.I., Sotnikova, T.D., Cyr, M., Beaulieu, J.M., Torres, G.E., Grant, S.G., and Caron, M.G. (2004). Identification of PSD-95 as a regulator of dopamine-mediated synaptic and behavioral plasticity. *Neuron* 41, 625-638.
- Yashiro, K., Corlew, R., and Philpot, B.D. (2005). Visual deprivation modifies both presynaptic glutamate release and the composition of perisynaptic/extrasynaptic NMDA receptors in adult visual cortex. *J Neurosci* 25, 11684-11692.
- Yashiro, K., and Philpot, B.D. (2008). Regulation of NMDA receptor subunit expression and its implications for LTD, LTP, and metaplasticity. *Neuropharmacology* 55, 1081-1094.
- Yazaki-Sugiyama, Y., Kang, S., Cateau, H., Fukai, T., and Hensch, T.K. (2009). Bidirectional plasticity in fast-spiking GABA circuits by visual experience. *Nature* 462, 218-221.
- Yokoi, T., Tokuhara, D., Saito, M., Ichiba, H., and Yamano, T. (2007). Hippocampal BDNF and TrkB expression in young rats after status epilepticus. *Osaka city medical journal* 53, 63-71.
- Yoshida, T., Ozawa, K., and Tanaka, S. (2012). Sensitivity profile for orientation selectivity in the visual cortex of goggle-reared mice. *PLoS One* 7, e40630.
- Yuan, W., Matthews, R.T., Sandy, J.D., and Gottschall, P.E. (2002). Association between protease-specific proteolytic cleavage of brevican and synaptic loss in the dentate gyrus of kainate-treated rats. *Neuroscience* 114, 1091-1101.

6. Abbreviations

%	percent
°	degree
°C	degree Celsius
µg	microgram
µl	microliter
ANOVA	analysis of variance
AMPA	α-amino-3-hydroxy-5-methyl-4-isoxazolepropionic acid receptor
AOS	accessory optic system
BDNF	brain-derived neurotropic factor
Bsn	Bassoon
C/contra	contralateral
CAZ	cytomatrix at the active zone
CCD	charged-coupled- device
cd	candela
cm	centimeter
CNS	central nervous system
Cy2	cyanine dye 2
Cy3	cyanine dye 3
cyc/deg	cycles/degree
d	day
DAPI	4',6-Diamidin-2-phenylindole
DLG4	disks large homolog gene 4
DNA	deoxyribonucleic acid
DZ	diazepam
<i>e.g.</i>	<i>exempli gratia</i>
EEG	electroencephalographic recording
ELISA	enzyme-linked immunosorbent assay

ENI	European Neuroscience Institute
EPSCs	excitatory postsynaptic currents
ERG	electroretinographic recording
ERK	extracellular-signal-regulated kinase
<i>et al.</i>	<i>et alii</i>
g	gram
GABA	γ -amino butter acid
GABA _A R	γ -amino butter acid A receptor
GK	guanylate kinase
h	hour
H ₂ O	water
HZ	heterozygous
<i>i.e.</i>	<i>it est</i>
l/ipsi	ipsilateral
kDa	kilo Dalton
KO	knockout
L x W x H	length x width x height
LGN	lateral geniculate nucleus
LTD	long-term depression
LTP	long-term potentiation
m. r.	maximum response
m ²	square meter
MAGUK	membrane-associated guanylate kinase
MD	monocular deprivation
Mg ²⁺	magnesium
mGluR	metabotropic glutamate receptor
min	minute
ml	milliliter
mm	millimeter

mm ²	square millimeter
mm ³	cubic millimeter
MRT	magnetic resonance imaging
N ₂ O	nitrous oxide
NaCl	sodium chloride
nm	nanometer
NMDAR	N-methyl-D-aspartate receptor
O ₂	oxygen
OD	ocular dominance
ODI	ocular dominance index
P	postnatal day
p	probability-value
PB	phosphate buffer
PDZ	postsynaptic density protein, disc large tumor suppressor, zonula occludens-1 protein
PFA	paraformaldehyde
PKA	cAMP-dependent protein kinase A
PNN	perineuronal net
PSD	postsynaptic density
PSD-95	postsynaptic density protein of 95 kDa
PV	parvalbumin
PV ⁺	parvalbumin positive
s.e.m.	standard error of mean
SAP-90	synapse associated protein of 90 kDa
sec	second
SH3	Src-homology-3
std	standard deviation
SV	synaptic vesicles
TNF α	tumor necrosis factor-alpha

tPA	tissue plasminogen activator
V1	primary visual cortex
VPA	valproic acid
vwt	visual water task
WT	wild-type
α CaMKII	α -calcium/calmodulin-dependent protein kinase II

Acknowledgements

Though only my name appears on the cover of this dissertation, a great many people have contributed to this most scientific challenging to this date. I owe my gratitude to all the people who made this possible.

My deepest gratitude is to my mentor Prof Dr. Siegrid Löwel for the opportunity to study in her lab and for her great supervision.

I am grateful to Prof. Dr. Tobias Moser and Dr. Oliver Schlüter for being part of my thesis committee and their insightful and constructive comments.

It is with immense gratitude that I acknowledge the support of our cooperation partners Dr. Oliver Schlüter who gave me the opportunity to study PSD-95 mutant mice as well as Prof. Dr. Eckart Gundelfinger who gave me the chance to study Bassoon mutant mice.

I am indebted to Prof. Dr. Karl-Friedrich Schmidt for his imperturbable calm during all these years. Thank you for your help with MD and the optomotor setup and for your shoulder to cry on.

I would like to thank my former and current lab members for the nice teamwork and especially Konrad Lehmann, Katja Krempler, Naira Yeritsyan, Verena Orth, and Colin Wenzel for help with some of the experiments.

Most importantly, none of this would have been possible without the immense love, support, and patience of my parents, grandparents, my companion David Bogusch and my whole family. Thank you with all my heart.

I also warmly appreciate the love and support of my friends and flat mates.

Finally, I appreciate the financial support from the HFSP, the DFG, and the BMBF/Bernstein Focus BFNL, BFNT that funded parts of the research discussed in this dissertation.

Curriculum Vitae

Personal Information

Date of Birth	11 th October, 1981; Lichtenstein/Germany
Nationality	German
Gender	Female
Marital Status	Single
Personal Address	Nikolaistr. 28a, D-37073 Göttingen/Germany
Office Address	Systems Neuroscience (Prof. Dr. Siegrid Löwel) Bernstein Focus Neurotechnology (BFNT) and Johann-Friedrich-Blumenbach Institut für Zoologie und Anthropologie, Georg-August-Universität Göttingen Von-Siebold-Str. 4 , D-37075 Göttingen/Germany Phone: +49(0)551-3920163 Fax: +49(0)551-3920162 Email: bianka.goetze@biologie.uni-goettingen.de

Education

09/2010 – present	PhD student at the Göttingen Graduate School for Neurosciences, Biophysics, and Molecular Biosciences (GGNB) Research Group Prof. Dr. Siegrid Löwel, Systems Neuroscience, Bernstein Fokus Neurotechnologie (BFNT) and Johann-Friedrich-Blumenbach Institut für Zoologie und Anthropologie, Georg-August-Universität Göttingen/Germany Research Topic: "Vision, cortical maps and neuronal plasticity in Bassoon and PSD-95 mutant mice."
04/2009 – 08/2010	PhD student in Neurobiology Research Group Prof. Dr. Siegrid Löwel, Institut für Allgemeine Zoologie und Tierphysiologie, Friedrich-Schiller-Universität Jena/Germany Research Topic: "Cortical plasticity and sensory learning in juvenile and adult Bassoon mutant mice."
11/2006 – 04/2009	Diploma thesis, grade 1.7 Research Group Prof. Dr. Siegrid Löwel, Institut für Allgemeine Zoologie und Tierphysiologie, Friedrich-Schiller-Universität Jena/Germany Research Topic: „Vision and visual cortical maps in mice with a photoreceptor synaptopathy: reduced but robust visual capabilities in the absence of synaptic ribbons."
06/2002 – 04/2009	Diploma in Biology (Dipl.-Biol.) at Friedrich-Schiller-Universität Jena/Germany, final grade: 1.2 Major: General Biology and Animal Physiology, Minors: Neurobiology, Genetics

Awards, stipends and selections

- 07/14/2012 – 07/18/2012 Scholarship by German Neuroscience Society for the *8th Forum of European Neuroscience* – in Barcelona/Spain
- 06/05/2011 – 06/11/2011 Awards for most active student as well as best poster and selected as one of 30 PhD students worldwide at the *Development and Plasticity of Cortical Representation* – FENS-IBRO Summer School – in Bertinoro/Italy; poster presentation and talk
- 04/18/2010 – 05/15/2010 Scholarship by *ProChance 2010 – Programm zur Förderung der Chancengleichheit von Frau und Mann in der Wissenschaft* of the Friedrich-Schiller-Universität Jena/Germany as a visiting researcher at the *Laboratory of Neuroanatomy of the Santa Lucia Foundation at the European Center for Brain Research* in Rome/Italy in the lab of Dr. Francesca R. Fusco; Learning of new techniques: brain slicing *via* microtome, immunofluorescence staining, DAB staining, laser scanning microscopy
- 05/18/2009 – 05/19/2009 Scholarship by *ProChance 2009 – Programm zur Förderung der Chancengleichheit von Frau und Mann in der Wissenschaft* of the Friedrich-Schiller-Universität Jena/Germany for the *Organization and Plasticity of the Visual Cortex – Visual Cortex Meeting 2009 of The EuroV1sion Consortium* – in Pisa/Italy
- 09/18/2007 – 09/23/2007 Selected as one of 25 PhD students worldwide for the *5th Fall Course on Computational Neuroscience* – BCCN – in Göttingen/Germany; own talk

Publications in peer-reviewed journals

- Goetze, B.**, Schmidt, K.F., Lehmann, K., Altröck, W.D., Gundelfinger, E.D., and Löwel, S. (2010). Vision and visual cortical maps in mice with a photoreceptor synaptopathy: reduced but robust visual capabilities in the absence of synaptic ribbons. *Neuroimage* 49: 1622–1631.